UNIVERSITÀ DEGLI STUDI DI TRIESTE
e
UNIVERSITÀ CA' FOSCARI DI VENEZIA

XXXI CICLO DEL DOTTORATO DI RICERCA IN

CHIMICA

MECHANOCHEMICAL ACTIVATION OF PRAZIQUANTEL IN A VIBRATIONAL MILL

Settore scientifico-disciplinare: CHIM/09 FARMACEUTICO TECNOLOGICO APPLICATIVO

DOTTORANDA
DEBORA ZANOLLA

Ph.D. student
Debora Zanolla

COORDINATORE
PROF. BARBARA MILANI

Ph.D. program Coordinator
Prof. Barbara Milani

SUPERVISORE DI TESI
PROF. BEATRICE PERISSUTTI

Thesis Supervisor
Prof. Beatrice Perissutti

ANNO ACCADEMICO 2017/2018

Contents

Chapter 1

Introduction

Nowadays, the importance of using sustainable methods and processes in chemistry, avoiding the large use of solvent or toxic substances is well-known and therefore there is an increasing interest in non-traditional synthetic methods based on mechanochemistry. The advantage of the use of this technique relies not only in the greenable chemistry, but also in the practical application especially when performing screening of solid forms, as solvates, polymorphs or cocrystals, and their production in a reliable way, quickly and with a minimal thermal stress of the system. This thesis is focused on the investigation of the mechanochemistry application to one specif drug: praziquantel.

1.1 Mechanochemistry

1.1.1 History pill and generality

The first reported approaches to mechanochemistry were by Michael Faraday in 1820, who reduced AgCl to Ag using a mortar and pestle and various other metals as Zn, Cu, Sn or Fe[1]; then, Carey Lea demonstrated the possibility to obtain different products in mechanochemistry respect to the thermal ones, studying the decomposition of mercury and silver halides[2]. At the beginning, this technique was based on the use of mortar and pestle and also it was mainly adopted in case of inorganic materials, as alloys or metal oxides. Indeed, mechanochemistry was considered part of the chemical disciplines only with Wilhem Ostwald (1853-1932), together with thermochemistry, electrochemistry and photochemistry, divided basing on the different energy input. One of the first mechanochemical reaction can be found around 1920 by Ling and Baker concerning cellulose, but the real clue moment of mechanochemistry was between 1980 and 1990 when mechanosynthesis and cocrystallization were developed,

and went along up to the present days in many different area of organic and metal-organic chemistry, supramolecular chemistry and pharmaceutical chemistry[3]. In particular in the last field, mechanochemistry has been only recently applied, especially in developing methods for the screening of possible polymorphic forms, cocrystals or solvates of various APIs. This application evidenced not only the advantages of reducing time and costs of pharmaceutical research, but also confirmed the possibility to obtain unknown new structure and interactions respect to the traditional methods of synthesis. The mechanochemical process can be performed in two main ways: the first consists in the manual grinding of the system in a mortar with a pestle, which is the easier way, though affected by many issues as the difficulties in maintaining a constant pressure for a long period, the variability of the operator and atmosphere; the automatic grinding is therefore more convenient from every point of view, especially for the great developed instrumentation and materials of the last few years, giving the enclosed environment of the jars and optimized process conditions. Mechanochemistry is usually described as a "solvent-free" process, but the definition "green process" is preferable, since mechanochemistry can involve the use of solvents, but usually in very small quantities (i.e. microliters), as in the case of the Liquid-Asssisted Grinding (LAG, described in the dedicated chapter of this thesis) or as part of the starting materials (hydrates and solvates)[3].

1.1.2 Theoretical hints

The mechanochemical transformation of solids was macroscopically described by Kaupp using a three-stage process: the first step is represented by the activation of the surface of the reactants, followed by the product formation and/or nucleation and the removal of the product for the reactant surface to re-start the cycle, reported in Figure 1.1[4–7]. The mechanism that rules the cycle depends on the system considered: in the case of materials with high vapour pressures the molecular transport across the surface happens via the gas phase, while in the case of reactants with low melting points or forming low-melting eutectics the intermediate phase will be in the liquid state. The third case involves the formation of an amorphous phase, usually as a temporary state before the rapid recrystallization. All these mechanisms share the physical effects of grinding, represented by the micronization of the particles, with exposure of a greater surface area, the closed mixing of the reactants of the system, with the formation of lattice defects and amorphisation, with also local and bulk heating derived from the frictional and impact forces [3, 8].

One of the theories on the mechanochemical energetics deals with the formation of "hot spots" with very high temperatures, and very short duration

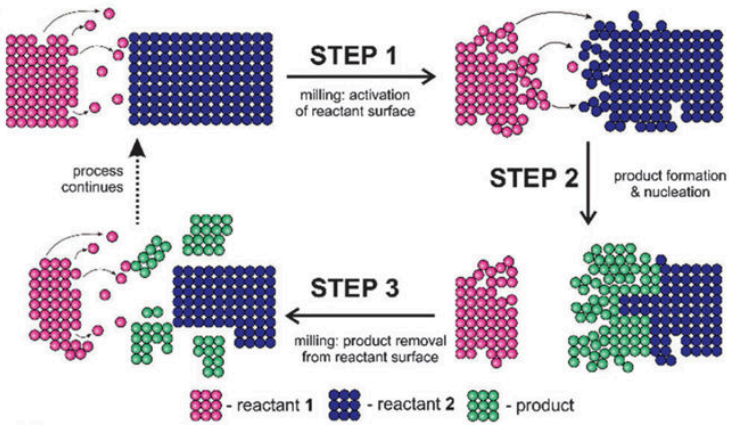

Figure 1.1: Representation of the three-steps mechanism of the mechanochemical reaction from[4–7].

where the high energy created can be converted into usable chemical energy[9, 10]. This approach was considered more appropriate in the case of hard inorganic materials, while in the case of soft matter the most relevant variable of the activation barrier is the temperature of the system, as demonstrated by many works dealing with the variation of the milling frequency, vial temperature and materials. Also, energy distribution in the material will be completely different in system permitting some structural movements than in the highly rigid ones[9, 11]. In particular the energy adsorbed by the system can change the disposition of the atoms, with changes in the bonds lengths, having an higher energy than the starting level. At this point the consequent release of the energy through relaxation processes, lattice disruption and also chemical reactions and bond breaking. The lattice collapse is not an immediate process, but derived from an incremental applied stress, represented by the mechanical energy, starting with an elastic deformation, than plastic till the total lattice disruption[12]. The products, amorphous or nanocrystalline are characterized by an higher energy than the starting one, but with a very short lifetime due to the subsequent crystallization. This is the reason why, especially in the pharmaceutical fields, many efforts are made to stabilized the activated states, for example using different polymers, as it will be described also in this thesis.

1.1.3 Mechanochemical activation of Active Pharmaceutical Ingredients

The reason for the application of the mechanochemical process in the pharmaceutical fields relies on three main advantages:

- the production of pharmaceutical products reducing or even eliminating the use of solvents, avoiding the problem of desolvation, usually difficult, expensive and with the risk of API alteration
- the amelioration of the biopharmaceutical properties of poorly soluble drugs
- the formation of polymorphic form or cocrystals not obtainable using the solution chemistry

The Active Pharmaceutical Ingredients are divided by the biopharmaceutical Classification System (BCS) in four different classes, considering solubility and gastro-intestinal permeability. Actually, more than the 40 % of the new pharmacological entities belong to Class II, having a low solubility that hinders the high permeability [13]. This means that in the case of oral administered drugs, the bioavailability would be low, needing high dosages and high variability. For this reason lots of efforts are being devolved to the amelioration of these properties using different association and production methods, and recently, *via* mechanochemistry. In fact, the reduction of drug crystal size or also its complete disruption of long-range order (i.e. amorphisation) through mechanochemistry lowers the melting temperature and enthalpy, thus increasing drug solubility. Considering the diagram reported in Figure 1.2, the dissolution of a solid phase occurs through different energy barriers: surface interaction, fusion, solvation, mass transfer/diffusion to reach the complete solid dissolution. Mechanochemistry can favour the process by means of the particle size reduction, which helps the generation of new solid-liquids interfaces and the crystal lattice fracture thanks to the partial or complete amorphisation. In particular, it has been reported that when milling is performed below the glass transition temperature (Tg) of the drug the amorphisation is favoured, while when above, the transformations between different polymorphic forms is produced[14].

Also, the study of drug polymorphism is of fundamental importance, since differences in solubility, bioavailability, activity and related effects have been reported. In literature one can find various examples of drug polymorphic transformation upon grinding, with different results while varying the mechanochemical conditions and reactants. An example for this behaviour was reported in the case of barbituric acid, which converts from the commonly observed tri(keto)

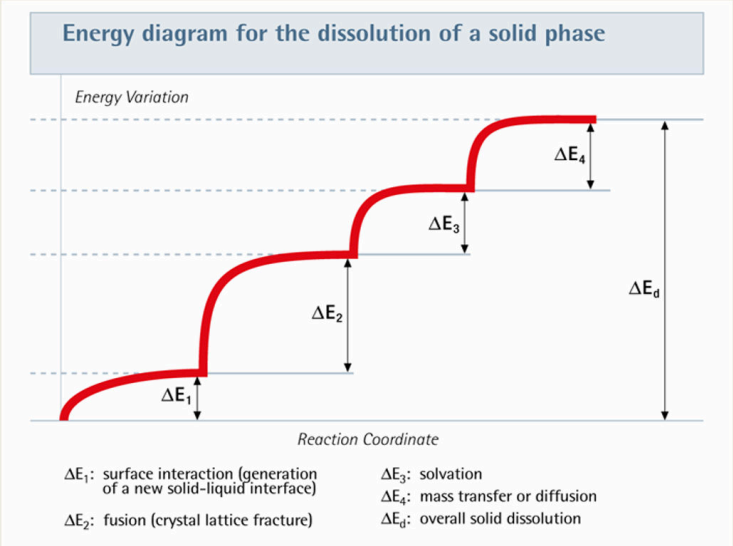

Figure 1.2: Energy diagram for the dissolution of the solid phase[15].

form to the tri(hydroxyl) tautomer, never detected before[8]. In particular the application of the Liquid-Assisted Grinding (LAG), where a very small amount (i.e. microliters) of a solvent is introduced in the milling jar, opened the door for a new and very rapid way of polymorphic/solvated and cocrystal screening. In fact, LAG was reported to accelerate reactions and also to provide products with higher crystallinity than when upon neat grinding. Moreover, the nature of the products varies depending on the liquid selected and its amount[16]. API cocrystals and salts represents the earliest application of mechanochemistry aiming to ameliorate the drug properties, as for solubility, stability, compression properties, avoiding the formation of covalent bonds for its chemical modifications[11]. References on specific examples will be reported in the introduction and related discussion of every specif chapter of the thesis.

1.1.4 Mills and equipment

As previously stated, the common process in the mechanochemical reaction is represented by grinding, usually by means of mills of different types and with various equipment. The two main categories of mills used are the planetary and the shaker/vibrational mills.
In the planetary mill (Figure 1.3, B) at least one jar rotates around its own axis, being in a rotating plate spinning usually in the opposite direction (Figure 1.3, A): in this way the milling media in the jar are subjected to a centrifugal force, increasing the frictional and impact forces and providing high energy to the

system. The frictional mode comes from the jar content sliding along the internal walls of the jar, while the impact mode depends on the content exiting the centrifugal direction and crossing the jar until it hits the opposite wall[17].

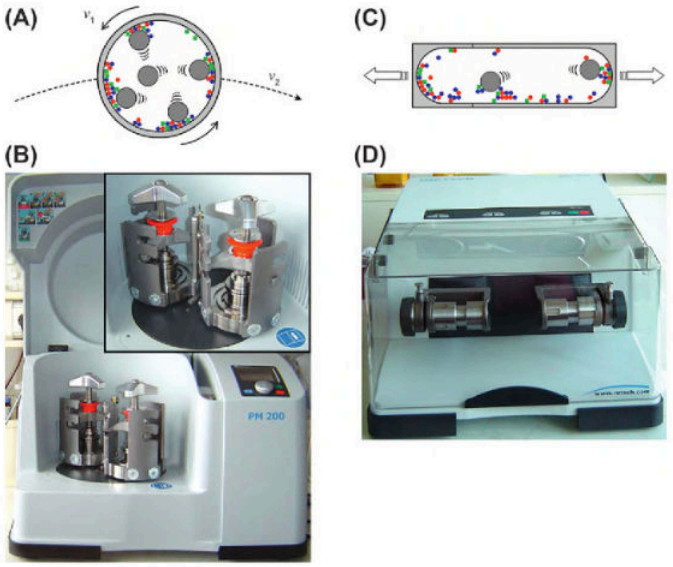

Figure 1.3: Retsch planetary (B) and ball mill (D) with the corresponding representation of the jar motion (A and C) from [17].

The material of the jar can vary among stainless/hardened steel, tungsten carbide, zirconium oxide, polyamide, agate or silicon nitride. Moreover, this mill can come with integrated systems for pressure and temperature measurements, attached to the jars[17] or even the possibility of operating under inert atmosphere (i.e. argon)[18].
The shaker mill, or vibrational (Figure 1.3, D), have recently developed for screening application at the laboratory scale and specifically for mechanochemical processes, due to the possibility of analyzing small quantities of sample. In this mill the jars moves in radial oscillations on the horizontal axis, so that the milling media inside impact with each others, with the jar and the sample, helped by the rounded end of the jars, adding also frictional forces. The milling balls can reach very high speed, causing a high-energy input to the system. Also in this case, the jars and milling media can be of different materials as for example zirconium oxide, stainless steel, tugsten carbide or polytetrafluoroethylene, which are selected depending on the experimental conditions and sample reactivity. Considering the environmental conditions, milling at room temperature represents the most largely used, even though cryogenic milling is possible thanks to integrated apparatus as for example in the Retsch Cryo-mill, where the jar is continuously cooled by liquid nitrogen (Figure 1.4).

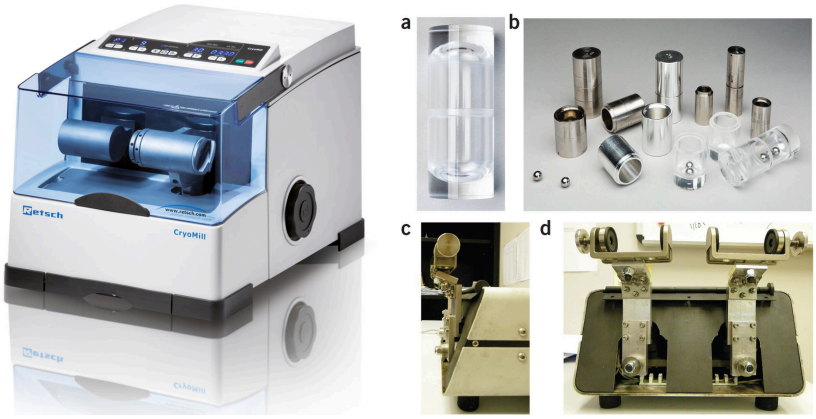

Figure 1.4: Retsch cryogenic mill[19] and modified mill for *in situ* measurements[20] (c, d) with the possible equipment (a, b).

Recently, *in situ* monitoring techniques has been developed, made possible by using transparent poly(methyl)methacrylate (PMMA) jars[21]. In this way a direct insight of the milling process was firstly provided by X-ray powder diffraction reported by Friscic group[20], followed by the contribution of Raman spectroscopy[22] and the combination of both the techniques. These advances helped in understanding the events taking places during milling, a knowledge difficult to derive from *ex situ* characterizations. Nowadays it is possible to buy mills set for X-ray and Raman *in situ* analysis, the latter also included in the system.

1.1.5 The variables of the mechanochemical process

Mechanochemistry can not be represented by a simple grinding of powders: the number of variables affecting this process is high and they strictly affect the result and yield of the processs. Nevertheless, they are not completely independent and the optimal grinding conditions will depend on their effects between each others. The principal grinding variables can be listed as following:

- Type of mill: planetary, vibrational, cryomill and many others: as previously described, different mill design are available, varying in the speed operation, capacity and additional features as the temperature/pression/ambient control[23];

- Size and material of the milling jars and balls: due to the strong forces acting during milling, the material of the milling jars and balls can cause contamination of the system (as in the case of stainless steel) or also act

as a source of catalyst[9], while zirconium oxide and tungsten carbide are usually preferable for a high wear resistance[17]. Also, the high density of the zirconium oxide balls can dramatically reduce the time process of powders and increment the mechanochemical activation. The number and size of the grinding media can vary depending on the milled material and the desidered results[23, 24], while different shapes are available, incrementing the contact area with the jar content;

- Milling intensity, usually expressed as frequency or rotational speed (Hz or rpm): as a general rule, the more is the speed applied, the more would be the energy input. Nevertheless, when above a certain critical speed value, the milling media will be pinned to the jars and not able to fall down and impact to the material. Thus, the speed permitting the maximum collision will be just below the critical value, always keeping in mind the possible jar heating due to the high milling intensity[23];

- Milling time: due to the close correlation with the other variables, as the mill type and milling intensity, the milling time needs to be decided upon considering the other related variables. Nevertheless, as a general precaution, an excessive grinding can led to higher contamination, degradation and overheating effects[23];

- Milling media-to-powder weight ratio (CR, charge ratio): this variable has been applied in large ratios, from 1:1 to 220:1, depending on the milling experiment and apparatus. Considering the mechanochemical activation process, the typical CR used is 30-40:1;

- Total jar fill (volume of the milling media and powder with respect to the total volume of the jar): the milling media and the system particles needs to move freely inside the jar and generally about half of it remains empty[23];

- Milling temperature: the process temperature can be varied by using thermostated jars, as in the case of ranitidine[25], or by using cryogenic milling, as the one reported in Figure 1.4. Nevertheless, the it is worth notice that, due to the energy of the process and/or chemical reaction occurring, the temperature inside the jar can dramatically increase.

Together with the process parameters, the formulation variables represent the other fundamental part of the design of the milling process. In this thesis both the aspects will be deeply analysed when comilling of PZQ with polymers in chapter 2.1, to reach a considerable experience and process knowledge for the later projects.

1.2 Praziquantel and Schistosomiasis

The following paragraphs will firstly give an introduction on Schistosomiasis, then deeply describe Praziquantel, the drug investigated in this thesis, in all its properties as a tool for a detailed understanding of its potentiality and possible challenges.

1.2.1 Schistosomiasis

Among all the helminthic diseases, Schistosomiasis represent a major neglected one, affecting more than 250 million people in the world, especially in the sub-Saharan Africa, where the mortality has estimated to be 280 000 death/year[26] (Figure 1.5). This disease is caused by the infection of worms of the genus *Schistosoma*, of three main species: *S. haematobium*, *S. mansoni* and *S. japonicum*. The infective stage of schistosomes is the "cercaria" one, developed asexually in snails infected by the miracidium larvae, and released in fresh water. The human host infection derives from the penetration of the cercariae into the skin which will migrate through the circulatory system reaching the mesenteric veins (*S. mansoni* and *S. japonicum*) or the venous plexous in the case of *S. haematobium* where they complete the maturation. The subsequent step will re-start the cycle (Figure 1.6), by the laying of eggs after schistosomes mate and the excretion in feces or urine.[27].

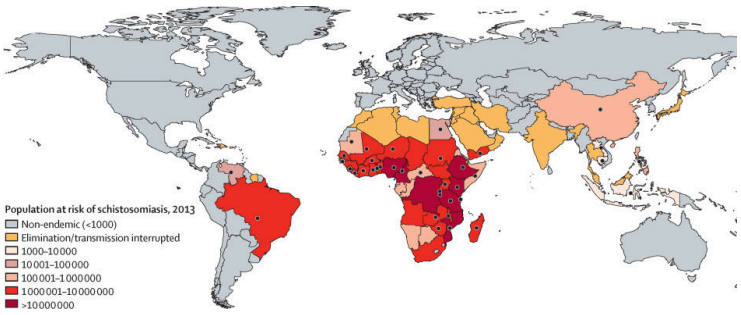

Figure 1.5: Population at risk of Schistosomiasis in 2013[28].

The acute sinthomatology is represented by urticarial rash, fever, fatigue, diarrhea , abdominal pain, dyspnea, weight loss and many others due to the migration of the schistosomulae. Differently, the chronic disease is mainly caused by the eggs that rouse the inflammatory response, with granulomatomas and subsequently fibrotic formations. Other derived bad consequences are represented by bladder cancer, kidney failure, infertility, poor growth and learning difficulties in children[27, 30].

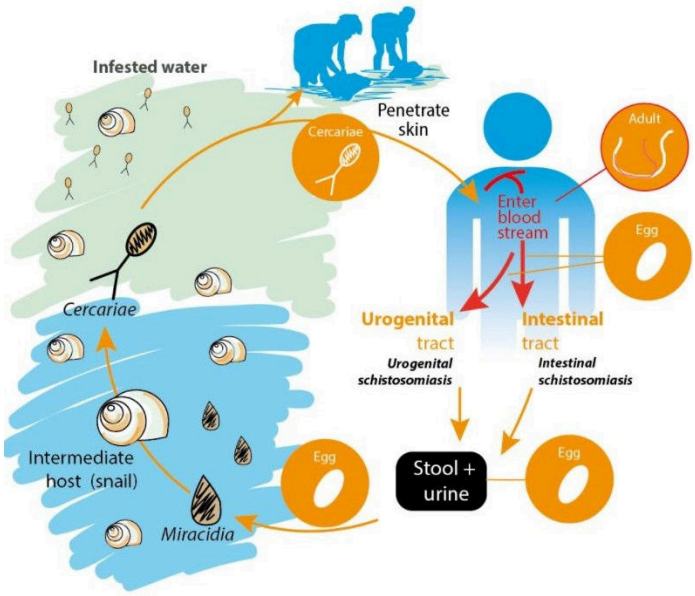

Figure 1.6: Representation of the Schistosomiasis cycle[29].

1.2.2 History

Actually Praziquantel (PZQ) represents the principal therapy against Schistosomiasis and since it is highly effective and with little side effects, it is included in the WHO list of Essential Medicines both for adults and for children. Numerous clinical experiences have been evaluated in the last years confirming the safety of the drug. Also there has been a large use of the drug since 2006, as a preventing therapy in endemic areas; it is estimated a use of 645 million tablets of PZQ in 2018 for the treatment of 235 million people[27]. The development of this drug relies on the common occurrence in the pharmaceutical field where a compound turns out to be effective in many different pathologies; in fact, the research on pyrazino-isoquinolone ring-based systems conducted by Merck (Farmstadt, Germany) was primarily directed to possible new tranquilizer chemical entities, but the discovery of the novel antischistosomal activity gave birth to more than 400 derived compounds, synthesized by Bayer. The activity of all of them was performed both *in vivo*, in mice against S. mansoni and *in vitro*[26, 31]). The selected compound, "EMBAY 8440", later known as Praziquantel, was clinically tested by WHO and Bayer in Brazil, Philippines, Japan and Africa after being previously tested in both in animals and in humans respectively for the antischistosomal activity and for the toxicity and pharmacology. As confirmed by following researches, the drug did not present any serious side effect, becoming the drug of choice against Schistosomiasis[31].

1.2.3 Chemical and Physical properties

Praziquantel is a white crystalline compound, with a bitter taste, but almost odorless and stable under normal conditions[32, 33], chemically a synthetic tetracyclic tetrahydroisoquinoline derivative (2-(cyclohexanecarbonyl)-3,6,7,11b-tetrahydro-1H-pyrazino[2,1-a]isoquinolin-4-one) which sketch is presented in Figure 1.7.

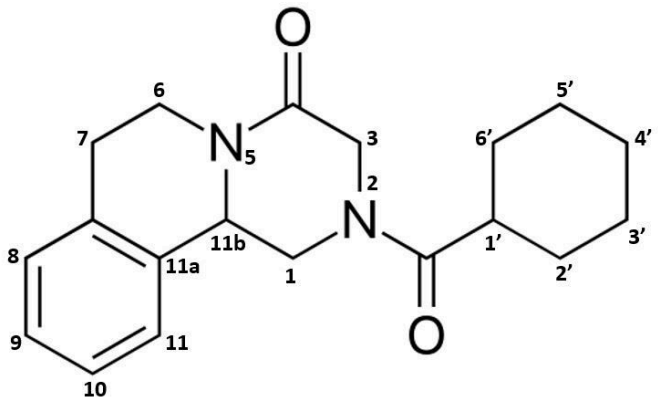

Figure 1.7: Scheme and atom numbering of praziquantel

The structure of the drug is rigid, with one rotable bond and the possible swing of the cycles, while two rotamers could be identified, different in the position of the hexocyclic tertiary amide bond[34]. The structure-activity relationship revealed three important position for the anthelminthic activity, namely:

- the presence of an acyl or thioacyl group in position 2:the reduction of the carbonyl or the increased carbonic chain lead respectively to inactive or less active compounds;
- the oxo group in position 4: if reduced lead to less active derivatives;
- the chiral carbon in 11b: the R-configuration is necessary for the activity.

The possible substitution of other position is not highly influencing the activity, but the unsubstitute analog remains the more active[34–36]. PZQ is actually administered as a racemic compound even though it has been well-documented that the antihelminthic activity is mainly related to the (R-)-enantiomer (Figure 1.8).

This drug has no hydrogen-bond donor group, but the two amides carbonyl groups can act as H-bond acceptor group. It is highly hydrophobic, sparingly

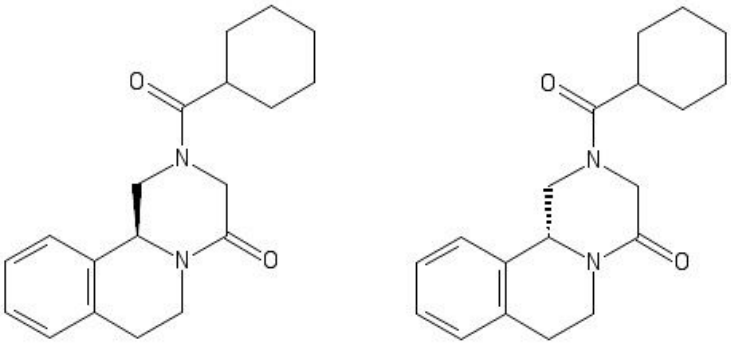

Figure 1.8: Schematic representation of (R)-PZQ and (S)-PZQ.

soluble in water (0.04 mg/mL), but soluble in ethanol (97 mg/mL) and chloroform (567 mg/mL). The melting point is reported in the range 136-142 °C, with a sharp endothermic signal, without any evidence of simultaneous decomposition[33].

Crystal structure of Praziquantel

The crystal structure of PZQ can be found in the Cambridge Structural Database (CSD[37]) with the reference code TELCEU as a racemic compound with a triclinic unit cell (space group P-1), therefore involving two different symmetry operations: identity (x,y,z) and inversion centre at [0,0,0] (-x,-y,-z). Two of the four independent molecules are disordered, but in all of them the carbonyl groups are positioned in the *syn* conformation [38]. The cell parameters are indicated in Table 1.1 and the crystal structure can be seen in Figure 1.9.

Table 1.1: Cell parameter for praziquantel in its raw form (TELCEU)[38].

Parameter	Value
Cell Lenghts (A)	**a** 10.454(3) **b** 15.112(4) **c** 22.963(6)
Cell Angles (°)	α. 99.531(5) β 98.419(5) γ 108.270(5)
Cell volume (A^3)	3320.24
Z, Z'	8, 4

(a) View from a axis.

(b) View from b axis.

(c) View from c axis.

(d) Asymmetric unit.

Figure 1.9: Praziquantel racemic crystal packing (a,b,c) and asymmetric unit(d).

Praziquantel enantiomers

Together with the racemic form, in the CSD database one can find the enantiomers of praziquantel as hemihydrates, with reference code SIGBUG[39] and SIGBUG01. The relative monoclinic cell parameters are reported in Table 1.2. In this case the total number of molecules is four, with one crystallographically independent molecule in a C2 space group and four symmetry operations: identity (x,y,z), rotation axis (-x,y,-z) with direction [0,1,0] at 0,y,0, centring vector (1/2+x,1/2+y,z) [1/2,1/2,0], screw axis (1/2-x,1/2+y,-z) with direction [0,1,0] at 1/4,y,0 with screw component [0,1/2,0].

Table 1.2: Cell parameter for praziquantel in its enatiomeric hemihydrated form (SIGBUG)[39].

Parameter	Value
Cell Lenghts (A)	**a** 27.013(5) **b** 6.0157(12) **c** 11.346(2)
Cell Angles (°)	α. 90.00 β 112.47(3) γ 90.00
Cell volume (A^3)	1703.77
Z, Z'	4, 1

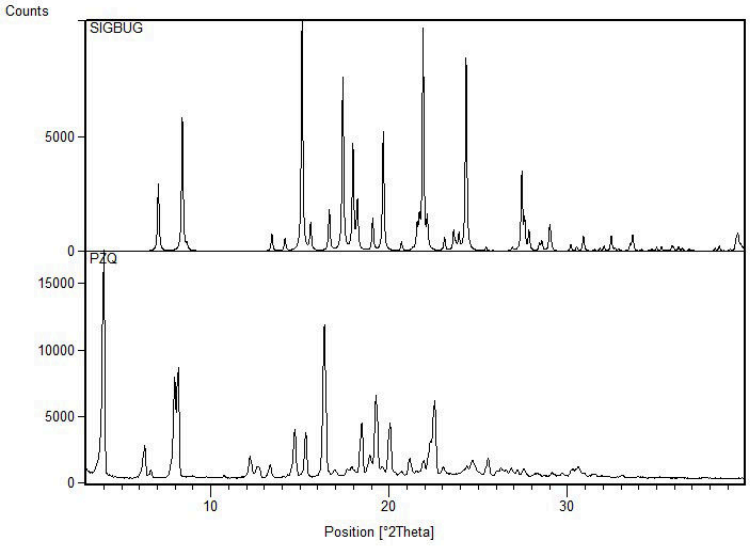

Figure 1.10: PXRD patterns of the calculated enantiomer (top,[39]) and of experimental raw PZQ (bottom).

(a) View from a axis.

(b) View from b axis.

(c) View from c axis.

(d) Asymmetric unit.

Figure 1.11: Praziquantel enantiomeric hemihydrate crystal packing (a,b,c) and asymmetric unit(d).

Interestingly the differences between the racemic mixture and the enantiomers could be evidenced also at the microscope: in fact, the isomer presented a more regular morphology and shorter crystals than the racemic PZQ[40]. The melting point of the enantiomers was recorded at 112.9 °C, of a significantly lower value (about 30 degrees lower) than the racemic drug, thus confirming that PZQ is a racemic compound and not a racemic mixture. Also, the lower melting point could be correlated with the increased solubility as reported by El-Arini and collaborators in 1998. Little differences between the enantiomers and the racemic PZQ were found also in the IR spectra, confirming once again the racemic compound nature of the drug[40]. Figure 1.10 reports the PXRD patterns of raw PZQ (experimental) and the enantiomer (calculated from CSD database[39]): the peak distribution is completely different and in particular the range 4-10 of 2θ, where PZQ is characterized by an intense signal at 4.00 and two nearly overlapped peaks at 8.00 and 8.20, while SIGBUG presents 2 intense signal at 7.08 and 8.42 of 2θ. Unfortunately, the PXRD patterns of the anhydrous enantiomers are not available.

In literature one can find various methods for PZQ resolution, involving chromatography and crystallization[41–43] or hydrolysis and resolution with tartaric acid[44]. Interestingly one approach included the formation via mechanochemistry of a diastereomeric cocrystal pair formation with L-Malic Acid: R-PZQ:L-Ma could be separated from S-PZQ:L-Ma due to differences in their solubilities, and L-PZQ was obtained in the hemihydrated form by stirring in water[45]. Unluckily, even if the switch to an enantiomerically pure product can represent an enormous advantage in drug administration with a reduction in dosage and tablet dimension, the difference in terms of production costs is still significative, preventing the attempts of new global formulations. The only contribution is given by the Pediatric Praziquantel consortium[46], which includes experts of praziquantel formulation and Schistosomiasis, working on a new praziquantel formulation for pediatric patients, the main involved population in the helminthic disease. As shown in Figure 1.12, the new formulation is much more smaller than the old one, thanks to the use of the only active PZQ eutomer. For 2018, the clinical phase III is expected.

Figure 1.12: Comparison between the old and the new praziquantel formulation[46].

1.2.4 Efficacy

As previously mentioned, PZQ is actually administered as a racemic mixture, even though the activity reseals only in the (R)-enantiomer.In fact the administration of a single dose of 400 mg/Kg of PZQ was as effective as 200 mg/Kg of the (R)-PZQ, whilst by using a double dose of (S)-PZQ (800 mg/Kg) none of the mice were cured and the worm burden reduction was not significative[47]. Also, it was reported that the bitter and disgusting taste of the drug are correlated with the inactive distomer ((S)-enantiomer) which also contributes to the massive size of the tablets[48]. In order to evaluate the efficacy of an antischistosomal drug, a practical method is represented by analyzing the differences in the pattern of schistosome egg excretion. In this way it is possible to evaluate the cure rate, by counting the cured patients as a percentage of the infected ones before the treatment, and the egg reduction rate, as the percentage reduction of the excreted eggs after drug administration. In the case of *S. Mansoni*, a biphasic sensitivity was found: in fact, schistosomes are susceptibile in the early stages after infection, followed by a decrease in weeks 3-4; then, the susceptibility increases again to a maximum after 6-7 weeks[26, 49]. Other schistosomas species (i.e. *japonicum* and *haematobium*) in the immature stages demonstrated to have a similar insensitivity to praziquantel[50]. In general, PZQ can reach a very high cure rate (between 60 and 90%) with a reduction of the excreted eggs of 80-95% (average) when considering four weeks after the treatment with a dose of 40 mg/Kg[26]. In fact, as already reported, PZQ lacks in efficacy against the juvenile forms of *Schistosoma*[51]. In the case of an intense infection, as in the case of patients from very high transmission areas, a higher cure rate could be observed when administrating two doses of praziquantel at a distance of 2-4 weeks, giving time to the immature stages to become susceptible. On the contrary, by increasing the dose to 60 mg/Kg no significant variations were observed[26]. Actually, PZQ is produced by about 30 different generic brands, that dramatically reduced the price. Botros and colleagues reported a study on the efficacy and bioavailability of different praziquantel brands: Distocide (EIPICO), Epiquantel (syrup, EIPICO), Biltricide (Alexandria Pharmaceutical Company/Bayer), Bilharzid (Pharco Pharmaceuticals Company) and Praziquantel (T3A Pharmaceuticals Company); they concluded with the suggestion of including a biological test (i.e. bioavilability and efficacy) when evaluating an possible equivalent PZQ formulation, since significative variations where found and only Biltricide and Distoicide could compete with the pure drug[52]. Moreover, since praziquantel demonstrated to be effective against other trematodes and cestodes, its administration is very convenient in areas affected by polyparasitism[26]. Finally, praziquantel is being used for a long period and few drug

resistance cases were reported: the first was a low efficacy of Senegal isolate of *S. mansoni*[53], then a extraordinary multiple dosage needing in Egyptian Villagers affected by the same schistosomas type[54] and also, when treating laboratory schistosomes with repeated praziquantel doses became partly insensitive to the API[55]. Nevertheless, the rare reported cases of low drug sensitivity were often explained by alternative considerations, instead of an effective insurgence of PZQ resistance[26].

1.2.5 Safety

The extensive use of praziquantel in the last decades permitted to have great amounts of data available to study the immediate ad delayed effects of the drug, in many different patients, from various geographical areas and with sundry characteristics, condition and ages and also infected with different species of parasites; the overall consideration attests its safety. Concerning the side-effects of praziquantel, the most reported were nausea, vomiting, abdominal pain, dizziness, while the most severe were colic and bloody diarrhoea; furthermore the more severe was the infection, the more these consequences were intense, due to the massive schistosomes death, movement and excretion. Also, it was reported that in case of infected pregnant and lactating women the use of praziquantel is recommended, since the possible risks connected to the use of the drug are of a little importance when compared to the cure benefit[26, 30].

1.2.6 Mechanisms of action

Despite praziquantel has been used nowadays for more than 30 years, the mechanism of its action has been not completely understood. The majority of the works in literature suggest the central role of Ca^{2+} voltage-gated channels, involving the Ca^{2+} influx into the schistosome and the consequent muscle contraction with changes in the tegument surface as vacuolation and blebbing; this is possibly followed by the exposure of parasite antigens on the sufarfaces being therefore recognised by the host immmune system, increasing the parasite clearence[26, 49, 56]. Also, the β sub-unit of these channels was reported as a potential molecular target. However, other additional hypothesis were reported as the possible reduction in glutathione schistosomal concentration, the action on actin (i.e. binding) which favours the tegument disruption and the interference with the uptake of adenosine[57].

1.2.7 ADME and Pharmacokinetics

Similarly to the previous paragraph, PZQ pharmacokinetics is still not well defined and there has not been reported any studies on the target population, that is the paediatric patients affected by schistosomiasis. There are a few works evaluating PZQ pharmacokinetic in healthy volunteers, using different dosages (5-50 mg/Kg) and in adults patients (25-40 mg/Kg)[58–60]. Praziquantel is a BCS Class II drug, characterized by low solubility and high permeability; as it is typical for oral drugs, there would be a great variability on drug pharmacokinetics dictated by different blood flow at the absorption site, by the transit time and the food uptake (dietary). The absolute bioavailability of praziquantel in humans is not know, since there is not any parenteral formulation to be studied; in animals, the absolute oral bioavailability is around 36%. Finally, not to forget the already mentioned effect of different brands and formulations, which were demonstrated to have different dissolution profiles and bioavailability. Figure 1.13 reports a schematic view of PZQ ADME.

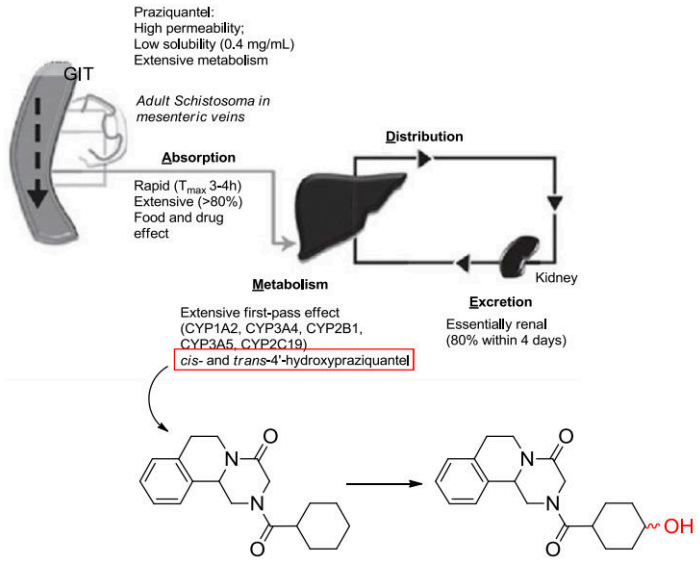

Figure 1.13: Scheme of praziquantel ADME(Adsorption, Distribution, Metabolism and Elimination[36]

Absorption After administration, praziquantel is highly adsorbed, mainly with a transcellular transport [36], reaching an adsorption value of 80% of the dose[33], with a maximum concentration of the drug in the serum in 2.0-2.6 hours[27, 61, 62]. Also, it was reported that the administration of praziquantel in healthy adults following a carbohydrate-enriched diet (50%) produced an

increment of 2.7 times the bioavailability of the drug, that can reach even higher value by augmenting the percentage of carbohydrates to 75 %. The same trend was evidenced in Sudanese adult males eating cooked beans, cotton seed oil (%) or bread and in neurocysticercosis patients with high carbohydrate diet[58]. Therefore the food effect in praziquantel pharmacokinetics plays a great role, significantly increasing its absorption and plasma concentration, especially when composed of lipids (two times increased value) and carbohydrates (five times increased value)[36]. Furthermore, it was noticed that when analyzing healthy volunteers versus patients, the latter had higher AUC and t1/2 [58].

Distribution As reported before, praziquantel is characterized by a high permeability, since the apparent permeability coefficient measured in Caco-2 cells is 4.4 x $10^(-5)$ cm/s [36]. The drug is distributed in all the body, concentrating in kidneys and liver, and also crossing the blood-brain barrier. Other sites of higher concentration are represented by lungs, pancreas and certain glands (adrenal, pituitary and salivary)[27]. The drug is highly bound with plasma proteins, especially albumin (about 80%), meaning a significative difference depending on nutrition and inflammation of the patient and a higher free drug fraction in infants due to the lower amount of plasma proteins. The peak in plasma concentration is observed in human after 1.3 hours from the administration[58, 61, 62].

Metabolism The drug is highly metabolized by the liver, in particular by cYP1A2, CYP3A4, CYP2B1, CYP3A5 and CYP2C19, with a dose-dependent mechanism. The activity of these enzyme depends on individual characteristics and differences in pharmacogenetics, interactions with other substances as drugs or food and the conditions of the liver. Despite the differences in the metabolites between rats, mouses and humans, the main metabolic route is the hydroxylation; in particular the 4'-hydroxypraziquantel is the main metabolite, respectively in the *cis* conformation in rats and in the *trans* conformation in humans. The latter had a comparable activity against *S. mansoni in vitro* to the active PZQ eutomer (R-PZQ), but was less effective against *S. japonicum*, therefore not further investigated as a potential substitute.

Elimination The 80% of Praziquantel is eliminated by the kidneys in four days, but the majority of the dose is excreted in the first 24 hours. Also, when administered in lactating women, it is excreted in breast milk[33, 58]. The effective half-life of praziquantel was reported to be 1.5 hours[58, 63, 64].

1.2.8 Research and state of the art

In this part, the main research topics involving praziquantel will be described, starting from the derivatives and possible association with various excipients to ameliorate its biopharmaceutical properties, to the formation of associations as a starting point to develop new advantageous cocrystals.

Praziquantel association with various excipients In the pharmaceutical fields, the use of excipients to enhance the biopharmaceutical properties of poorly soluble drug is still an actual topic. Among all the techniques, the preparation of solid dispersion proved to be highly effective for enhancing the dissolution, absorption and therapeutic efficacy of different drugs. In fact in this way the drug can be finely dispersed into the polymer, entrapped in the coil structure as amorphous, adsorbed on the polymer chain, or reduced in its particle size[65, 66]. In the case of Praziquantel, various methods have been applied, as the association with polyvinylpyrroldone (PVP), sodium starch glycolate[67], sodium alginate abd carboxymethylcellulose[68], cyclodextrines of different grades, liposomal, nanoparticles systems and flexible and dispersible granules for paediatric oral administration[69]. In the case of PZQ various solid dispersions with PVP were obtained by solvent evaporation (ethanol) with different drug-polymer weight ratios and using many different molecular weight PVP[66, 70]. The drug in the coprecipitate systems based on ethanol was in the amorphous form (as reported by SEM images and PXRD patterns) and when using at least a 1:5 drug to polymer ratio the dissolution rate was highly increased. Also, the use of smaller molecular weight PVP favoured a better solubility of the drug[70]. The solid dispersions with PVP proved also to be more effective *in vivo* against *S. mansoni* than the raw drug even when using reduced dosages[65]. Recently, Costa and coworkers studied the influence of the solvent used for the binary PZQ:PVP solid dispersion preparation on PZQ crystallinity, showing that a higher ethanol content favoured the amorphisation of the drug, while in presence of water a major crystallinity of PZQ was observed[71]
Another trial was conducted using α-, β- and γ- cyclodextrins, commonly known for the hydrophobic cavity that can include poorly water-soluble drugs as PZQ, forming hydrogen bonds and other weak interactions as hydrophbic, van der Walls', electrostatic or charge-transfer. The inclusion complexes obtained by Becket and coworkers showed an enhanced PZQ dissolution comparing to the raw drug and the β inclusions were the favoured for the higher complex constant[72]. The interaction between PZQ and the βcyclodextrins and derivatives was deeply investigated later by other authors[73, 74] and also by high resolution solid-state NMR spectroscopy where the PZQ tendency to adopt the *anti*

conformation in complexes, mainly formed when using a guest:host molar ratio of 1:2, was highlighted[75].
Other strategies investigated in the past were the formation of nanoparticles based on polymers of poly(L-lactic-acid) and their copolymers with glycolic acid[76], lipid nanoparticles[77–79], poly (methyl methacrylate) nanoparticles[80], nanoemulsion hydrogels[81] or also liposomal systems, which had an improved efficacy in preclinical assay against *S. mansoni*[82].

Praziquantel cocrystals Recently there has been an increasing interest in Praziquantel propensity to cocrystal formation due to the huge contributions in literature on this new solid-state approach. A very deep and complete study was performed by Espinosa-Lara and coworkers in 2012 combining Praziquantel with various dicarboxylic acids, i.e. Oxalic, Succinic, Maleic, Fumaric, Glutaric, Adipic and Pimelic acids using Liquid-Assisted Grinding as the production technique. The crystal structures obtained were characterized and studied also in the intermolecular hydrogen bonding interaction and short contacts, finding homo and heterodimeric hydrogen bonds motifs of the supramolecular organization of the cocrystals. The structure of Praziquantel in act does not contain any hydrogen bond donor group, but can accept bonding in different sites and its flexibility relies on two rotational coformers, which differs for the carbonyl groups configuration, *syn* or *anti*. In all the proposed cocrystals, except for the one with Malonic Acid, PZQ was in the *anti* conformation, which better favours the formation of hydrogen bonds with the coformers due to the larger space between the two carbonyl regions. This work put in light the possibility of new praziquantel cocrystals with hydrogen bond donor coformers[38]. Moreover, as already reported in the paragraph 1.2.3, the cocrystallization process was used by Sanchez-Guadarrama and coworkers to achieve a chiral resolution of Praziquantel via the formation of a cocrystal diastereomeric pair with L-Malic Acid (L-MA)[45]. Finally, Cugovcan and coworkers recently reported PZQ cocrystal obtained with with citric, malic, salicylic and tartaric acid by Liquid-Assisted grinding, which solubility and dissolution rate were pH dependent. In the same work, cyclodextrins complexes were prepared by neat grinding with amorphous hydroxypropylβcyclodextrin and randomly methylatedβcyclodextrin, improving drug solubility and dissolution rate[83].

Aim of the research

The research project focuses on the investigation of Praziquantel (PZQ) behavior when subjected to a solvent-free process as the mechanochemical activation using a vibrational mill. PZQ is and antihelmintic drug used worldwide against Schistosomiasis, which is a parasitic diseases affecting more than 200.000 people, especially in the sub-saharian area. Despite being highly effective and safe, this drug has 2 major drawbacks: the first one is the low biopharmaceutical profile (i.e. solubility and bioavailability) and therefore the high dosage needed. The second one is the very bitter and disgusting taste, which makes even more difficult its administration, in particular in pediatric patients, the main involved. The literature reports just a few works envolving PZQ and mechanochimistry, mainly focused on the formation of PZQ cocrystals or solid dispersions, but there is a wide range of applications still unexplored. In fact, the cogrinding with pharmaceutical excipients has been limited to cyclodextrines[83], while in the case of co-crystals, the approach was mainly focused on the chemical field, with little indications of possible therapeutic relevances[38, 45]. In this context, the research presented in this thesis aims to combine both the mechanochemical approaches: from one side the PZQ chemical structure and related products, from the other the possibility of alternative formulations which can improve its poor biopharmaceutical and taste properties. The first step that will be studied is the evaluation of the variables affecting the mechanochemical process, including not only the time and frequency of grinding, but also the type/quantity of the milling media, the drug-to-excipient ratio, the jar filling and the grinding temperature when working with different polymers and excipients largely used for pharmaceutical formulations. In particular povidone and copovidone will be deeply investigated, followed by mesoporous silica, natural/synthetic sweeteners and sucrose esters. The products obtained will be deeply studied in their solid state/biopharmaceutical properties, including the evaluation of the *in vitro* activity against *S. mansoni* in selected samples. Subsequentely, together with the neat grinding, other techniques, as the Liquid-Assisted Grinding (LAG), the Neat-LAG and the Neat-Neat grinding will be investigated to search for

the formation of PZQ polymorphs, solvates or hydrated forms having improved biopharmaceutical properties. At the end, PZQ microparticles will be formed combining the mechanochemically obtained products with the spray-congealing technique. Also in these cases, the most promising samples will be tested to check the maintainance of the *in vitro* and *in vivo* activity against *S. mansoni*.

Chapter 2

Milling of praziquantel with polymers

One of the most widespread challenge in the pharmaceutical research is the enhancement of drug solubility of poor water soluble API, since it represents the main requirement for a suitable drug oral bioavailability and therefore activity. Different techniques can be applied to enhance the drug solubility as the reduction of the particle size, cocrystal and nanocrystallization, cyclodextrines complexations, or the creation of lipid dispersion or amorphous solid dispersions. Despite the crystalline state of an API provides a highly pure and stable form, the amorphous phase is generally preferred due to the higher free energy which enhances drug apparent solubility, dissolution and oral bioavailability. Nevertheless, the amorphous phase lacks in physical and chemical stability, with the high probability of new crystallization or degradation processes. In this context, the formation of amorphous solid dispersion using a polymeric carrier demonstrated to be effective in drug stabilization and maintanance of the enhanced biopharmaceutical properties. This effect is based on different polymer abilities as for example the crystallization inhibition (retarding the nucleation rate), the antiplaticization (increasing the free energy necessary for the transition to the crystalline form), the creation of intermolecular interactions (by means of H-bonds, van der Waals or hydrophobic forces) and the reduction of the API molecular mobility. The properties of the obtained solid dispersion depend on the selected polymer which can be synthetic, as polyvinylpyrorolidone or polyethilene glycols, or natural as cellulose and derivatives[84, 85]. The polymeric amorphous dispersion can be formed using different techniques as the fusion, solvent or supercritic methods or by means of the mechanochemical activation[85]: in this case, called co-grinding, the components are intimately

mixed, in a process that comprehends several variables like time and frequency of milling, the ratio between the drug and the polymer, the type of polymer and also other milling variables (choice of the grinding media, in material, number and ratio with the powder). In literature few works reported the analysis of different grinding variables, like the milling time, milling media material and dimensions in Al_2O_3 crystal size[86], or in the organic synthesis[17]. Concerning praziquantel, many works can be found about the characterization of solid dispersion using different polymers as cyclodextrines[75] or polyvinylpyrrolidone [66, 69–71], as already reported in paragraph 1.2.8; conversely, this chapter focuses firstly on the explorative analysis of all the formulation and process variables of grinding praziquantel with different polymers. To optimize the number of the trials and identify the most relevant variables, an experimental design is applied, and in particular a screening design with the details below described. After this part, the system with the best properties will be further characterized at the solid state and also in its efficacy *in vitro*. The last part of the chapter is dedicated to the identification of PZQ degradation products formed upon co-milling.

2.1 Evaluation of the formulation and process variables during comilling of praziquantel

2.1.1 Introduction

In this project different excipients were selected for the cogrinding with PZQ, as reported in the material section, while others were discarded during preliminary analysis, as in the case of Soluplus (polyvinylcaprolattame vinylacetate-polyethilen-glycol-graftcopolymer) which exhibited bad technological properties (i.e. rubbery consistence) or Ac-di-sol (sodium cros caramellose), because of the poor increase in drug solubility. Differently, the use of different carriers as Sodium Starch Glycolate (SSG) and hydrophilic polymers as polyvinylpyrrolidone (PVP) and related derivatives (crosslinked PVP, CROSPVP, polyvinylpyrrolidone vinyl-acetate, PVP-VA) led to very interesting products.

Considering the huge number of variables in a grinding process, the risk of performing useless experiments without a clear objective is quite common. For this reason the application of a Design Of Experiment (DOE) can facilitate and even improve the laboratory trials[87]. The DOE approach is based on the definitions of the variables and the responses to be considered: the experimental variables are independent factors involved in the considered process (i.e. drug-to-polymer wt ratio, milling frequency or time, etc.) while the reponses are the

experimental results, measured depending on the project aim. The variables, which can be qualitative (as for the selection of one reagent instead of another) or quantitative need to be defined in an experimental domain by considering a minimum and a maximum value. The planification of the trials depends on the project and on the previous knowledge of the process. When starting a new experiment, the preferable way is represented by the screening design, which allows the determination of the significative variables of the process[88]; in this way, the subsequent optimization design leads to the definition of the experimental conditions necessary to achieve the best responses[89]. Many experimental design can be applied depending on the specific project: in this chapter the application of a full-factorial design will be applied in the comilling of PZQ with different polymers, as a screening design, considering drug residual crystallinity, recovery and solubility enhancement as the experimental reponses and many formulation and process variables later described.

2.1.2 Materials and Methods

Materials

Praziquantel (PZQ, (11bRS)-2-(Cyclohexylcarbonyl)-1,2,3,6,7,11b-hexahydro -4-H-pyrazino[2,1-a]isoquinolin-4-one)) was of Ph. Eur. grade and kindly donated by Fatro S.p.a. (Bologna, Italy). Povidone (PVP, Kollidon K30) was purchased from Fluka Chemie-Buchs, Germany) while micronized crospovidone (CROSPVP, Kollidon CL-M) was from BASF-Ludwihshafen, Germany). Sodium Starch Glycolate (SSG) was from Explotab (Milano, Italy) and copovidone -1-vinylpyrrolidove-co-vinyl acetate (PVPVA) was purchased from Sigma Aldrich Chemie (USA). The impurity A (2-Benzoyl-1,2,3,6,7,11b-hexahydro-4-H-pyrazino[2,1-a]isoquinolin-4-one) and B (2-Cyclohexanecarbonyl-2,3,6,7-tetrahydro-pyrazino[2,1-a]isoquinolin-4-one) of PZQ, purchased from Endotherm Gmbh (Saarbruecken, Germany) were both of Ph. Eur. grade. The HiPersolv Chromanorm methanol used for the HPLC analysis was of Ph. Eur. grade and purchased from VWR Chemicals (BHD PROLABO®Milano, Italy).

Methods

Design of the experiments: screening design By using the software NEMRODW[90], a screening design was prepared with the aim of identify the most significant variables in the comilling process of PZQ with the selected excipients. The variables and the responses selected for this plan were chosen basing on previous experiences on the drug and the milling process. The variables selected and the corresponding levels were the following:

- (X1) - drug/polymer weight ratio: 1:1 and 1:2
- (X2) - grinding media: one large (ϕ=25 mm) and 3 small (15 mm) spheres
- (X3) - milling time: 1 and 4 hours
- (X4) - frequency: 20 and 30 Hz
- (X5) - type of polymer: CROSPVP, PVPVA, SSG and PVP

while as the responses, PZQ residual crystallinity, recovery and solubility enhancement were selected as reported in Figure 2.1.

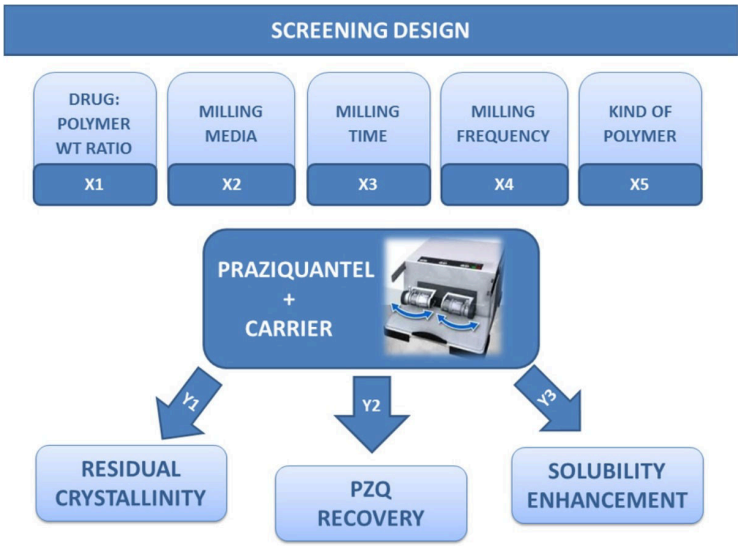

Figure 2.1: Schematic view of the planned experimental design.

Y1 (PZQ residual crystallinity) was selected to analyze the structural changes derived form the milling process that can affect drug solubility and physical stability and was assayed by DSC as the PZQ heat of fusion (J/g) in the coground samples compared to raw PZQ value (96.15 $\pm$ 0.75 J/g).
Y2 represents drug recovery, since there have been few examples in literature about the formation of impurities or drug degradation due to the grinding process, which was investigated by HPLC.
The last response, the enhancement of drug solubility (Y3) was calculated by subtracting solubility of the drug in the coground system with that of the corresponding physical mixture. In this way the carrier was studied in its influence upon milling in certain conditions and not in its intrinsic effect. Further details on the responses evaluation will be reported in the corresponding method section.

As reported, the variables X1, X2, X3 and X4 were considered at two levels, while X5 had five different levels: the resulted factorial design consisted in 16 trials, reported in Table 2.1, corresponding to 8 different conditions carried out in double.

Table 2.1: Experimental plan of the screening design. X1: drug/polymer wt ratio, X2: milling media (3s: 3 small spheres, 1ls: one large sphere), X3: milling time, X4: milling frequency, X5: type of polymer.

Exp number	X1 wt ratio	X2 mill. media	X3 h	X4 Hz	X5 polymer
1	1:1	3s	4	20	CROSPVP
2	1:1	3s	4	20	CROSPVP
3	1:1	1ls	4	30	PVPVA
4	1:1	1ls	4	30	PVPVA
5	1:1	3s	1	30	SSG
6	1:1	3s	1	30	SSG
7	1:1	1ls	1	20	PVP
8	1:1	1ls	1	20	PVP
9	1:2	1ls	1	30	CROSPVP
10	1:2	1ls	1	30	CROSPVP
11	1:2	3s	1	20	PVPVA
12	1:2	3s	1	20	PVPVA
13	1:2	1ls	4	20	SSG
14	1:2	1ls	4	20	SSG
15	1:2	3s	4	30	PVP
16	1:2	3s	4	30	PVP

Preparation of the physical mixture For each drug/polymer system a binary mixture was prepared by mixing the weighted powders in an agate mortar for 3 minutes. The same procedure was used to prepare the powders to be inserted in the jars for co-milling. The batch size was of 1.072 g or 0.843 g depending on the experiment considered.

Milling conditions A Retsch MM400 vibrational mill (Retsch GmbH, Hann, Germany) and zirconium oxide jars and balls were chosen for the comilling process. On the basis of previous experiences, a 1:30 wt ratio between the powder and the milling media was selected; therefore, each jar was filled with 1.072 g

of powder when using three small grinding balls (ϕ=15 mm) or with 0.843 g of powder when using one large ball (ϕ=20 mm). The ratio between the drug and the polymer depended on the experiment and was preventively prepared, as described for the physical mixtures, to achieve a good homogeneity of the system. The milling experiment was then conducted following the conditions reported in Table 2.1 and the ground samples were collected and stored in a desiccator in the dark at RT. All the samples were subjcted to the characterization at least the day after the preparation.

Determination of drug residual crystallinity Each sample was analyzed using a Mettler DSC TA 4000 (Greifensee, Switzerland) connected to a calorimetric cell Mettler DSC20 and using STARE software version 9.30 for data analysis. Prior to analysis the instrument was calibrated with Indium, Zinc and Lead for the temperature and with Indium for the enthalpy quantification; each sample, containing about 2 mg of PZQ exactly weighted, was placed in a 40 μm aluminum pan with perforated lid and heated from 30 to 160 °C (10 °C/min) under air atmosphere. The PZQ enthalpy of fusion was determined by integrating the area of the corresponding endothermic peak and calculated as the percentage of drug residual crystallinity (response Y1) by comparing with the raw drug value (96.15±0.75 J/g). This method was supported by the linearity of the calorimetric response of the binary systems, previously assessed as reported in the appendix A (paragraph 2.4.1).

Determination of PZQ recovery The content of PZQ was assayed by means of a reverse-phase HPLC[1], adapting a method already reported in literature[91]; the system had two delivery pumps (LC-10 ADVP, Shimadzu, Japan), an autosampler (SIL-20A, Shimadzu, Japan) a UV-vis detector (SPD-10Avp, Shimadzu, Japan) and the data were acquired at a fixed wavelength of 220nm using an interface SCL-10Avp (Shimadzu, Japan) and analyzed with Ez-Star software; the column used was a Kinetex 5 μm C18 (150 x 4.60mmm, Phenomenex, Bologna). The mobile phase used was composed of methanol:water (65:35 v/v), purged at 1 mL/min. PZQ retention time was 5.5 min while the total run time for each sample was set at 12 min. Prior to analysis, a linear calibration curve with r^2=0.99996 was obtained for PZQ under the described conditions using different concentrations of the drug from 0.3 to 10 mg/mL. Each day, a standard solution (with a concentration of 2.5 mg/L) was prepared by dissolving about 10 mg of PZQ accurately weighted in methanol of HPLC grade (20 mL) and diluting the solution 1:200 with the mobile phase. Moreover,

[1]In collaboration with N. Passerini and B. Albertini, from the Department of Pharmacy and Biotechnology, University of Bologna (Italy) as well as for the solubility analyses.

two additional calibration curves were obtained respectively for the relative impurities indicated in the Eur. Ph. (Ed. 8.0)[32], impurity A (r^2=0.9993) and impurity B (r^2=0.9994), which were identified at the retention time of 3.45 min and 11.2 min. The reference solution did not report any of these impurities. For the analysis, 20-30 mg of the coground sample were accurately weighted, dissolved in 20 ml of methanol, diluted 1:200 with the mobile phase and injected in the HPLC system. Each sample was analyzed three times and the retention time of PZQ was at about 5.4-5.5 min in every coground system. The average of the sum of the PZQ peaks was compared to the sum of all the peaks (of PZQ, impurities and other products) and expressed as the percentage of drug recovery (Y2).

Water solubility test For the determination of the drug solubility enhancement, saturated solution of each coground sample in distilled water were prepared and kept under agitation in the dark for 48 hours at 20 °C; on the basis of previous experiences and according also to literature[92], a longer time would favour PZQ degradation. Then, the solutions were filtered using a 0.20 μm membrane and diluted 1:200 with the mobile phase (65:35 v/v methanol:water) for the subsequent HPLC analysis, following the previous mentioned HPLC method. The Y3 value, representing the enhancement of drug solubility, was obtained by subtracting the solubility of the drug in the coground system with the one of the corresponding physical mixture.

Scanning Electron Microscopy For the acquisition of the SEM images a Leica Stereoscan 430i (Leica Cambridge LTd, Cambridge, UK) was used on sample metallized with a S150A Sputter Coater (Edwards High Vacuum Crawley, West Sussex, UK).

ATR-FT-IR spectroscopy The sample were analyzed at the solid state without preparing any dilution using a PerkinElmer Spectrum 100 FT-IR (Beaconsfield, England) with a Universal ATR sampling and software PE version 6.3.4 copyright 2008. The spectra were collected between 650 and 4000 $cm^(-1)$ using a scan number of 4.

Powder X-Ray Diffraction The sample were analyzed by powder X-ray diffraction (PXRD) using a Siemens D500 (Siemens, Munich, Germany) diffractometer (Cu Kα radiation with wavelength: 1.5418 A), using a secondary flat graphite crystal as the monochromator. The preparation of the samples consisted in pressing about 20-30 mg of powder over a glass slide to have a flat surface. The data were collected in a 2θ range of 3-35 degree with steps of 0.05

° every 5 seconds. The apparatus was set at a current of 20 mA and a voltage of 40 kV for all the analyses.

Evaluation of the *in vitro* activity against *S. mansoni* [2] The efficacy of the coground samples was test against adult *S. mansoni* obtained from infected mice and incubated with different concentrations (0.33-0.021 μg/mL) for up to 72h. By inverse microscope observation (Carl Zeiss, Germany, 80x magnification) parasites morphological alteration, motility and viability were checked in treated and not treated worms. The results were then averaged and the IC_{50} was calculated using CompuSyn Software.

Physical stability The stability of the sample was checked by PXRD and DSC as well as in drug recovery and solubility by HPLC, over a total period of 6 months.

2.1.3 Results and Discussion (1)

The screening design prepared for this research project aimed to identify the significative formulation and process variables that affect three fundamental aspects for the amelioration of PZQ properties: its recovery, residual crystallinity and solubility enhancement upon grinding with different polymers. In fact, as reported in many literature works, one of the possible ways to increase the solubility of poor soluble drugs and hence their dissolution is represented by the production of amorphous systems, especially in combination with polymeric excipients[84, 85, 93], possibly able also to stabilize the system. Conversely, the evaluation of drug degradation is quite neglected in the field of the mechanochemical activation and only few samples were reported in literature[94–96]. In the case of PZQ, this aspect needs to be investigated, due to its degradation tendency already reported[92, 97, 98]. The total number of experiments was 8, conducted in double following a random order, to reduce the sistematic error; nevertheless, even when operating at the same conditions, slight differences were noticed as shown in Table 2.2, but were considered of little significance since they did not affect the trend and were also found in previous experiences as well as in literature[95].

The peculiarity of the selected design of experience (screening design) is the capability to highlight the more significant factors among the all considered by comparing the levels of each factor one at a time[87, 88]. In this case the least square method was applied, comparing each level weight to the reference level (the upper level weight). Figure 2.2 shows the effect of the factors variation (X1,

[2] Study conducted at the Swiss Tropical and Public Health Institue of Basel, in collaboration with prof. Jennifer Keiser

Table 2.2: Responses observed for each trial of the experimental plan.

Exp number	X1 wt ratio	X2 mill. media	X3 h	X4 Hz	X5 polymer	Y1 %	Y2 %	Y3 mg/L
1	1:1	3s	4	20	CROSPVP	9.61	87.22	436.77
2	1:1	3s	4	20	CROSPVP	11.99	89.93	448.26
3	1:1	1ls	4	30	PVPVA	21.36	96.64	282.08
4	1:1	1ls	4	30	PVPVA	37.39	94.12	220.01
5	1:1	3s	1	30	SSG	69.37	100.00	285.59
6	1:1	3s	1	30	SSG	73.45	100.00	282.05
7	1:1	1ls	1	20	PVP	42.54	94.60	229.49
8	1:1	1ls	1	20	PVP	25.66	96.51	290.68
9	1:2	1ls	1	30	CROSPVP	0.00	88.63	210.71
10	1:2	1ls	1	30	CROSPVP	0.00	91.65	200.71
11	1:2	3s	1	20	PVPVA	0.00	90.47	113.35
12	1:2	3s	1	20	PVPVA	1.49	92.09	93.56
13	1:2	1ls	4	20	SSG	0.00	90.32	127.48
14	1:2	1ls	4	20	SSG	0.00	91.24	135.51
15	1:2	3s	4	30	PVP	0.00	94.13	110.11
16	1:2	3s	4	30	PVP	10.85	94.84	140.29

X2, X3, X4, X5) on the three different responses (Y1, Y2, Y3). For a better understanding, the reference level (the upper for each factor) is drawn as a red bar with the same dimension in every factor set: in this way the influence of the variation of the factor level on the responses can be easily visualized. The significance values (α): ***p=.001, **p=.01, *p=.05 were used to highlight the most significant factors.

In this screening design the first thing to be noticed (Figure 2.2) was that the variation of the considered factors influenced drug residual crystallinity and recovery in a very similar way, and the presence of the polymer (X1) seamed to favour PZQ amorphisation and degradation. This means that the high drug degradation found in certain samples could not be interpreted as a consequence of grinding, but more interestingly as a results of drug destructuration towards an amorphous system with a higher chemical reactivity. Also, the presence of the polymer in the coground system seamed to favour this destructuration trend, since when using a 1:2 wt ratio between PZQ and the polymer, drug degradation and amorphisation were much higher than when using the 1:1 ratio. This was confirmed by literature reports, as for example in the case of the coground systems of PVP with sulphathiazole: during drug neat grinding the mechanochemical activation favoured the transition of the drug from form III to form I, while when ground in presence of the polymer, the amorphisation degree was proportional to the polymer content[99]. Likewise, the cogrinding

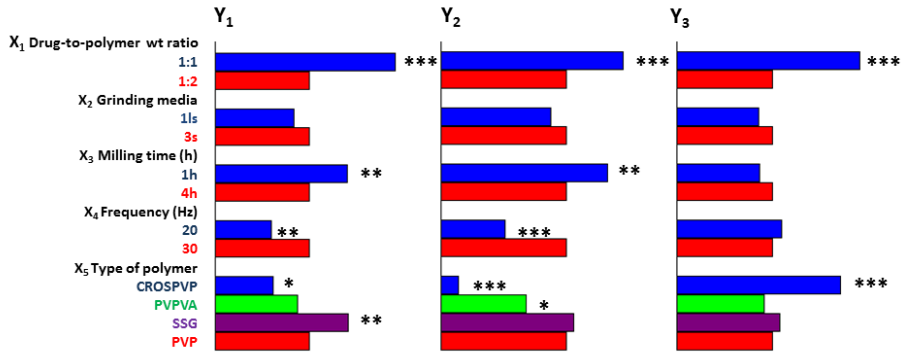

Figure 2.2: Graphical representation of the results: the red bars indicate the reference level for each factor and have the same dimension in every set of response. (The significance codes are the following (α): ***p=.001, **p=.01, *p=.05).

of Raloxifene Hydrochloride with CROSPVP was reported to reduce drug crystallinity[100]. A high polymer content was also reported to be reponsible for a more effective energy transfer creating a higher amorphisation of the powders[101–103]. Additionally, the presence of the polymer may change the glass transition temperature (Tg) of the considered milling system, playing an important role in the grinding outcome, since amorphisation was reported to be favoured when milling is performed at a lower temperature than the system Tg[104, 105] (this aspect will be further investigated in chapter 3.1, involving the cryo-milling process).

While the amorphisation of the drug in presence of polymers was highly reported in literature, as previously described, the formation of degradation products is a novel observation: in fact, as for PZQ amorphisation, when using a 1:2 wt ratio with the polymers, drug degradation increased, and this was not directly related to any chemical interaction between the components, but to the increased chemical reactivity of the amorphous state induced by milling, since no degradation was found in the corresponding physical mixtures.

Analyzing the other variables, the selection of the grinding media was not significative in any of the experiments. However, in this case it is worth of notice that the change of the grinding media did not affect the ratio between the powder and the milling balls (which is a highly relevant factor of the process) since the powder weight was varied when using one large ball or three medium balls, as reported in paragraph 2.1.2. Differences on drug recovery and on drug residual crystallinity were also noticed when varying the excipient, in particular when using CROSPVP higher degradation (p=.02) and amorphisation (p=1.38) were found, comparing to the other polymers implied. Interestingly, SSG seamed

to act as a protector towards drug degradation and destructuration (p=.167). The evaluation of the milling process factors (frequency and time) led to the following observations: drug recovery was significantly lower when grinding for less time and at higher frequency, while grinding for a prolonged time enhanced its amorphisation. Drug degradation seamed to be therefore not directly dependent from the mechanical stress, but more likely from its destructuration, favoured by the presence of the polymer and resulting in different related products, analyzed and described in the last part of this chapter (paragraph 2.3). Finally, analyzing the enhancement of drug solubility, the preparation of these coground systems was certainly advantageous since all the samples had an augmented solubility compared to the physical mixtures, as visible from the largely positive values of Y3 and also with respect to the pure drug (140.30 mg/L). This response (Y3) was affected more significantly by the formulation variables, as the drug to polymer wt ratio and the type of the polymer used, than the process parameters: in fact, when using a 1:1 wt ratio between the components, the solubility enhacement was significantly better (p=.01) and in particular when using CROSPVP the highest Y3 values were found (p=.01).

2.1.4 Conclusions (1)

Trying to summarize the results, the de-structuration of PZQ due to the milling process in presence of the polymer had a parallel trend as drug degradation, both when varying the formulation and the process variables, meaning that the greater mobility achieved by the system in its amorphous form favoured PZQ degradation. In fact, Y1 (drug amorphisation) and Y2 (drug degradation) were significatively affected by all the variables except for the choice of the grinding media. Conversely, even though the enhancement of drug solubility was achieved in each sample, since it was from 1.5 to 4.6 folds higher than raw PZQ (140.30 mg/L), this increase was not closely related to the amorphisation degree, but to the ratio and kind of polymer used, the only variables significatively affecting this response. The best results for Y3 were obtained using CROSPVP, confirming its optimal ability to increase drug solubility as already reported in literature[106], thanks to its cross-linked and amphiphilic structure. However, this polymer was also responsible for a higher drug degradation.

2.2 Additional characterization of selected samples

2.2.1 Results and Discussion (2)

In the previous part, the screening of the formulation and process variables of milling PZQ with different polymers led to the identification of the significative variables affecting drug crystallinity, degradation and solubility enhancement. Since the further objective of this study is the amelioration of PZQ oral formulation, the best products obtained were chosen for further investigation at the solid state and in their activity *in vitro* against *S. mansoni*:

- PZQ:CROSPVP in a 1:1 wt ratio ground for 4 hours at 20 Hz (3 small balls, ϕ= 15 mm)
- PZQ:PVP in a 1:1 wt ratio ground one hour at 20 Hz (1 large ball, ϕ= 20 mm)

The system with SSG was discarded for the high crystallinity of PZQ and low drug solubility enhancement, while PVPVA systems were very similar to PVP ones. The selected PZQ:CROSPVP sample had a water solubility at 20 °C of 642.54 mg/L, 3.3 fold greater then the physical mixture (194.28 mg/L) and 4.6 fold then the raw drug (140.30 mg/L), with a residual crystallinity of 11.99% and a recovery ranging about 90%. The selected PZQ:PVP sample had a solubility of 442.46 mg/L, PZQ residual crystallinity 25.66% and a recovery ranging about 96%.

The high amorphisation degree of the coground samples was noticed in all the characterizations, starting from the DSC and then in the ATR-FTIR and PXRD analyses. The thermograms in Figure 2.3 and 2.4 shows that while in the physical mixture the presence of the drug is still clear by means of the endothermic peak around 142 °C, in the coground system the corresponding PZQ peak is nearly disappeared and the small signal that remains (9.61%) can be found at a lower temperature comparing to the melting point of the drug (141.98±0.03 °C). This was in agreement with the already reported behaviour of nanocrystalline size powder to have a lower melting temperature and enthalpy[107]. A similar set of curves were found in the system based on PVP, with a residual crystallinity of about 20-30% in the coground samples.

In the PXRD analyses the amorphisation demonstrated by DSC traces was highlighted even more: the coground samples exhibited an halo-pattern in which none of the PZQ characteristic peaks could be identified, differently from the

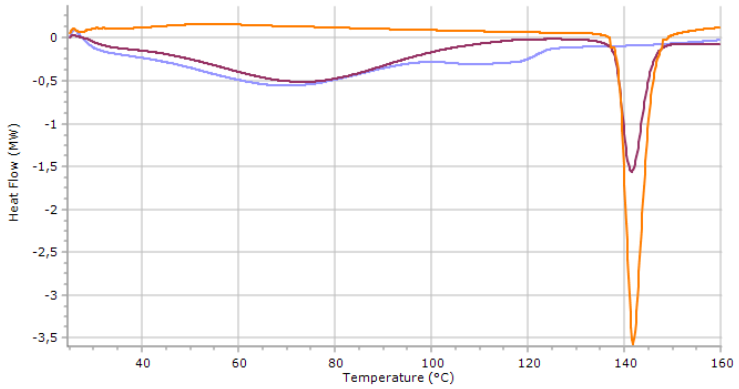

Figure 2.3: DSC thermograms of the coground sample with PVP: in blue the coground sample, in red the corresponding physical mixture, in orange raw PZQ.

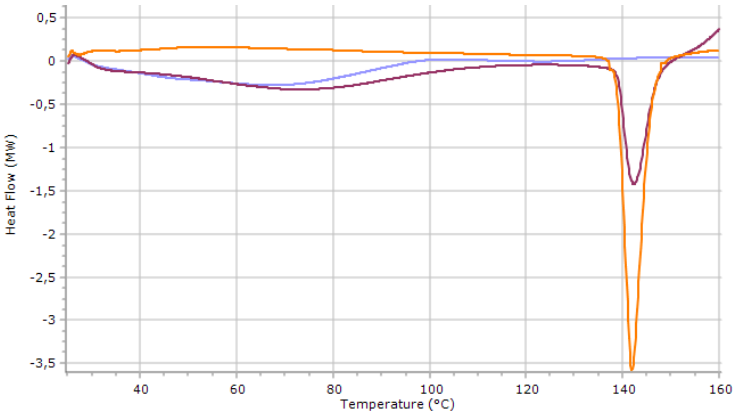

Figure 2.4: DSC thermograms of the coground sample with CROSPVP: in blue the coground sample, in red the corresponding physical mixture, in orange raw PZQ.

physical mixtures, where PZQ peaks were evidenced, though with a reduced intensity due to the dilution effect of the polymer (Figure 2.5). Similar results were observed for the samples with PVP, even though a higher residual crystallinity was noticed by low intensity peaks as reported in Figure 2.6.

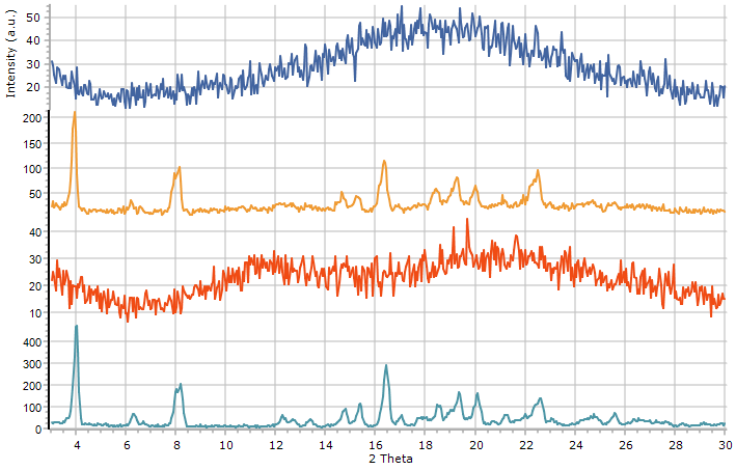

Figure 2.5: PXRD patterns of (up to down) PZQ:CROSPVP coground sample, the corresponding physical mixture, raw CROSPVP and PZQ.

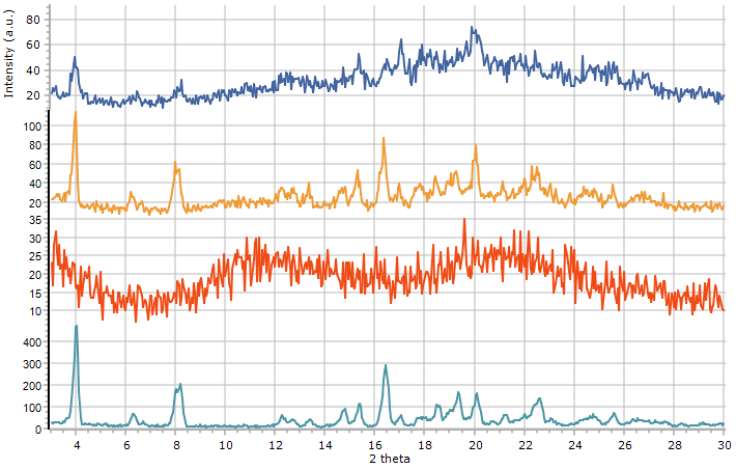

Figure 2.6: PXRD patterns of (up to down) PZQ:PVP coground sample, the corresponding physical mixture, raw PVP and PZQ.

The ATR-FTIR spectra of the selected coground samples are reported in Figure 2.7: the amorphisation of the system is indicated by the general broad traces and especially in the carbonyl stretching region, where the split band of raw PZQ become a large and very broad signal, particularly evident in the case of PZQ:CROSPVP (red spectrum in Figure 2.7). The reduction in intensity of the coground system with respect to the raw drug could be attributed both to the amorphisation and to the dilution made by the polymer. As in the DSC traces, the PXRD and ATR-FTIR spectra did not evidence any formation of new solid entities or chemical interaction between the drug and the polymers.

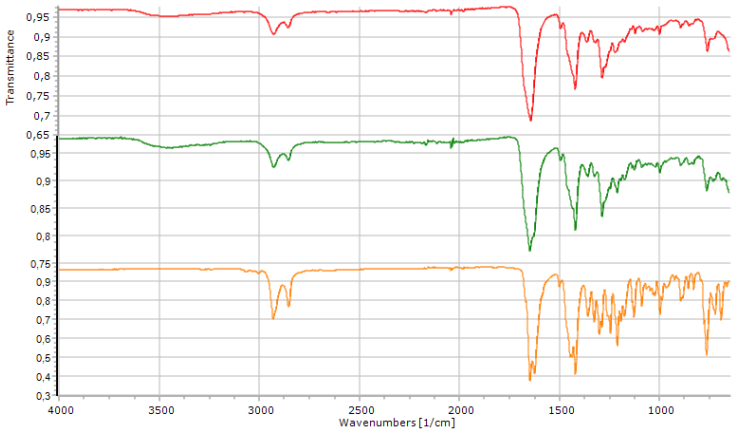

Figure 2.7: ATR-FTIR spectra of the selected coground samples PZQ:CROSPVP (red), PZQ:PVP (green) and raw PZQ (orange).

Regarding the morphology of the samples, Figure 2.8 reports the images collected by SEM for raw PZQ, characterized by an acicular shape of the particles with a smooth surface. In the coground sample with PVP, the polymer spherical particles are replaced by irregular aggregates, while PZQ is visible as very small whiskers in the most magnified image. Differently, in the case of the coground sample with CROSPVP, aggregates of cubic-pyramid particles were evidenced on larger particles, changing the almost spherical shape of the polymer and without any evidence of PZQ crystallinity (Figure 2.9). For comparison, the SEM images of the raw materials are reported in Appendix A (section 2.4.2).

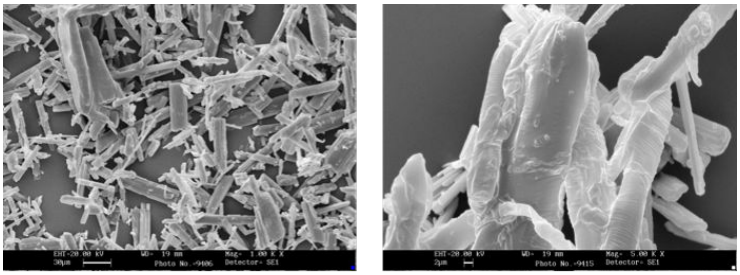

Figure 2.8: SEM images of raw PZQ, magnification of 1000x and 5000x.

The selected samples were also checked in their physical, chemical and solubility properties after 6 months storage by means of DSC, HPLC, solubility and PXRD analyses. All the techniques attested the capacity of the polymer to stabilize the coground samples (reported for CROSPVP in Figure 2.10) since there were no evidence of recrystallization or significant changes over time, even

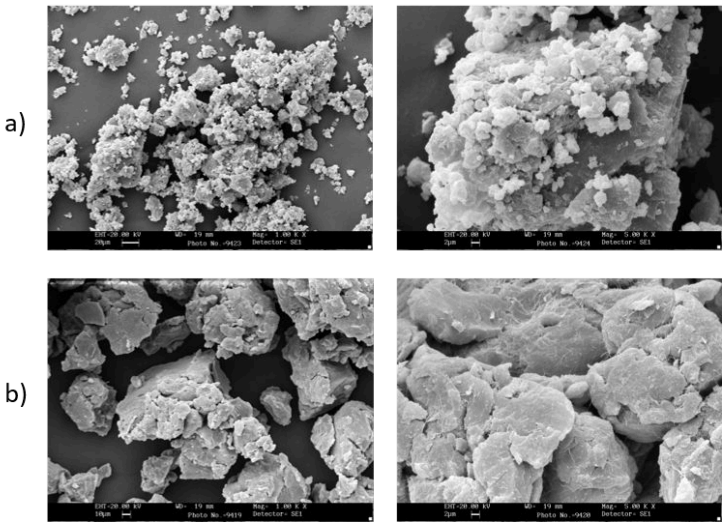

Figure 2.9: SEM images of PZQ:CROSPVP (a) and PZQ:PVP (b), each one with a magnification of 1000x and 5000x.

in the drug solubility enhancement, which was stable.

Despite the high degree of drug amorphisation and low recovery of the system composed of PZQ and CROSPVP, the *in vitro* activity against *S. mansoni* was maintained and even slightly enhanced, since a IC_{50} of 0.102 μg/mL was found comparing to the IC_{50} of the raw drug (0.165 μg/mL).

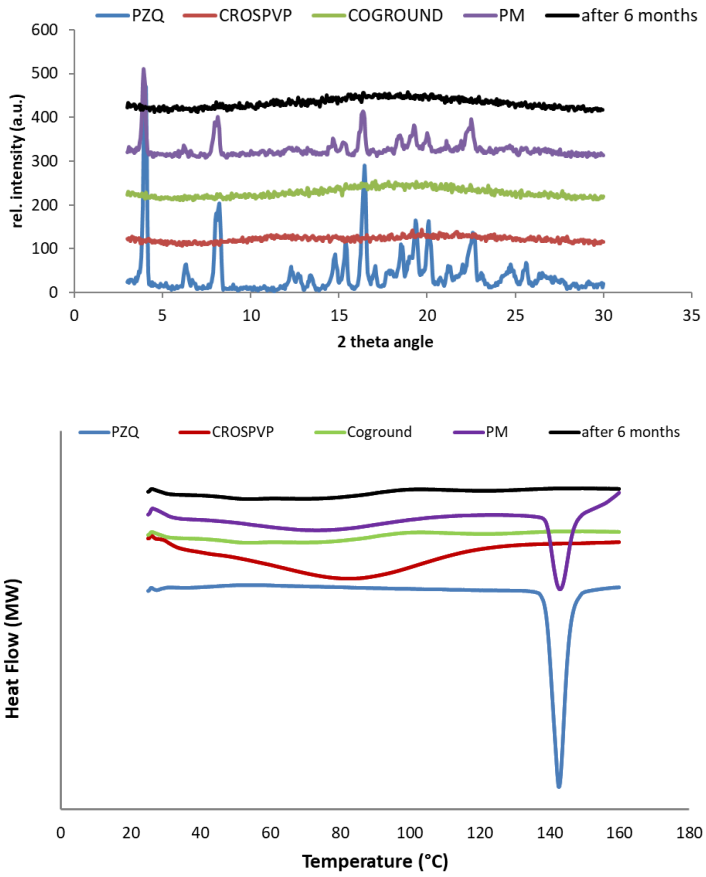

Figure 2.10: PXRD and DSC traces of the PZQ:CROSPVP selected system after 6 months storage.

2.2.2 Conclusions (2)

The selected samples composed of PZQ:CROSPVP and PZQ:PVP (1:1 w/w) demonstrated to have very interesting properties, with an high amorphous degree and a high solubility enhancement which was up to 4.6 fold grater than the raw drug. The amorphous nature of the samples was confirmed by solid-state analysis, as DSC, PXRD and ATR-FT-IR, while the content of PZQ remained high (around 90 %). The polymers were successful also in stabilizing the amorphous state of the drug for at least 6 months without affecting drug activity against *S. mansoni*. These facts confirmed the optimal characteristic of the two selected polymers for the production of advantageous samples, providing a possible alternative of the poor soluble PZQ oral formulation.

2.3 Identification of the PZQ degradation products upon cogrinding

When considering the mechanochemical effect of grinding an API, the majority of the works reported in literature are focused on the evaluation of the amorphisation degree reached after grinding, particularly emphasized when grinding is performed at cryogenic temperatures, as reported for example in the case of indomethacin[108], ketoconazole and griseofulvin[109]. Nevertheless, drug degradation as the effect of chemical changes of the system, is an important effect that is often underestimated; Kaminska and collaborators reported an investigation on the degradation products of furosemide ground with inulin or PVP[94, 96]. Another example comes from the presence of water in the excipients, favouring hydrolysis reaction as in the case of 4-methylphenylamino acetate hydrochloride upon grinding with lactose hydrate[110].The degradation of PZQ has been reported by Čizmić and collaborators[98] upon direct photolytic and photocatalytic processes, or after prolonged heating [92], while the effect after grinding was studied in coground samples with cyclodextrines and cocrystals with citric, malic, salicylic and tartaric acids by Cugovcan and coworkers[83]. The authors reported accelerated stability and photostability tests: PZQ degradation over time was remarkable in all the coground samples with also a significant photodegradation comparing to raw PZQ. The authors concluded that the lack of the stability effect, highly reported in literature and in particular in cyclodextrines application, was due to the non-inclusion in the cyclodextrine cavity of the pyrazino-4-one group, reported to be involved in PZQ thermal and photochemical degradation[98, 111]. Nevertheless, no other examples where found in literature on investigation and identification of PZQ degradation products upon technological processes.
As previously reported (2.1.3), when PZQ was ground in presence of PVP and CROSPVP two unknown related compounds were found by HPLC analysis, different depending on the excipient considered. This section presents the analysis of the mentioned coground samples performed in collaboration with I. Sagud and I. Škorić[3] towards the identification of the PZQ degradation products.

2.3.1 Materials and Methods

Materials

Praziquantel (PZQ, (11bRS)-2-(Cyclohexylcarbonyl)-1,2,3,6,7,11b-hexahydro -4-H-pyrazino[2,1-a]isoquinolin-4-one)) was of Ph. Eur. grade and kindly do-

[3]Department of Organic Chemistry, Faculty of Chemical Engineering and Technology, University of Zagreb (Croatia).

nated by Fatro S.p.a. (Bologna, Italy). Povidone (PVP, Kollidon K30) was purchased from Fluka Chemie- Buchs, Germany) while micronized crospovidone (CROSPVP, Kollidon CL-M) was from BASF-Ludwihshafen, Germany). The impurity A (2-Benzoyl-1,2,3,6,7,11b-hexahydro-4-H-pyrazino[2,1-a]isoquinolin-4-one) and B (2-Cyclohexanecarbonyl-2,3,6,7 -tetrahydro-pyrazino[2,1-a]isoquinolin-4-one) of PZQ, purchased from Endotherm Gmbh (Saarbruecken, Germany) were both of Ph. Eur. grade. Deuterated chloroform ($CD(Cl)_3$, 99.80% with TMS as standard) was purchased from Euriso-Top (St. Aubin, Cedex). As solvent, redistilled dichloromethane of technical grade was used. The acetonitrile used for the HPLC analysis was ultra gradient (J.T.Baker), the water was filtered by a MilliQ system and a 10 mM solution of NH_4HCO_3 was added with ammonia to reach pH=10.

Preparation of the samples

The samples selected for the in-depth analyses were the following:

- Sample 1: PZQ:PVP, 1:1 wt ratio, ground for 4 hours at 20 Hz;
- Sample 2: PZQ:CROSPVP, 1:1 wt ratio, ground for 4 hours at 20 Hz;
- Sample 3: PZQ:PVP, 1:1 wt ratio, ground for 90 minutes at 25 Hz;
- Sample 4: PZQ:CROSPVP, 1:1 wt ratio, ground for 90 minutes at 25 Hz.

The mill used for their preparation was a Retsch MM400 vibrational mill (Retsch, Germany), using 2 zirconium oxide jars of 35 mL with three milling balls (ϕ=15mm) and inserting 1.072 g of powders previously weighted and mixed in an agate mortar for 3 minutes. After milling the samples were collected and stored in a desiccator at room temperature in the dark.

GC-MS The gas chromatograph used was a Varian CP-3800 system with a Varian Saturn 2200 mass spectrometer. The column used was a Factor Four Capillary one, VF-5 ms (50 m x 0.2 mm). The method used was the following: firstly the oven was kept at 110 °C for 1 minute, then heated to 300 °C (33.1 °C/min) and maintained at the same temperature for 10 min. The injection volume was 1 μl and Helium was purged 1 mL/min as the carrier gas. The temperature of the injector and MS source was 350 °C. For sample ionization, the electron impact mode was used at 70 eV.

UPLC-MS An Acquity UPLC-DQD mass spectrometer system was used for the UPLC-MS conditions, with a Acquity UPLC BEH C18 column (50 mm x 2.1 mm i.d. with a packing diameter of 1.7 μm) maintained at 40 °C. The solvent

used were acetonitrile and a NH_4HCO_3 solution (pH=10). The injection volume applied was 2μL and the flow rate was 0.9 mL/min. An alternate electrospray (ES+/ES-) was used as the ionization mode of the mass spectrometer.

NMR spectroscopy The ^1H and ^{13}C spectra were recorded on a spectrometer at 300 MHz in $CDCl_3$, using tetremethylsilane as the reference. The signals were referred as singlet (s), doublet (d), triplet (t), quartet (q), doublet of doublets (dd), multiplet (m) and broad (b).

2.3.2 Results and Discussion

The first analysis to be conducted was a GC-MS, which highlighted the presence, in all the coground samples and in raw PZQ, of a molecular mass of 310 g/mol, corresponding to PZQ impurity B[32], as shown in the comparison of the GC-MS spectra of Figure 2.12.

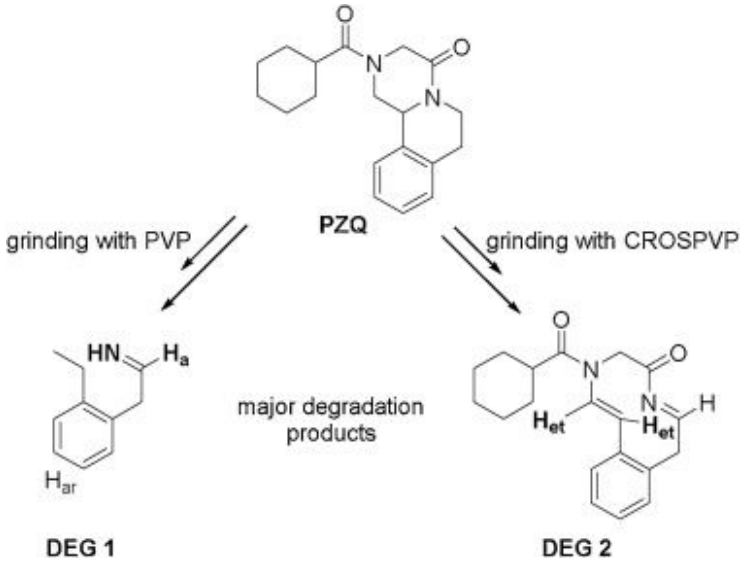

Figure 2.11: Scheme of the different degradation pathways of PZQ upon milling with PVP (top) and CROSPVP (bottom).

The UPLC-MS spectra permitted to better highlight the additional degraded products of the samples, reported completely in the Appendix A, paragraph 2.4.3. The results suggested that the nature of the degradation pathway depended mainly on the excipient used (Figure 2.11), since the UPLC spectra of samples 1, 3 (with PVP) and 2, 4 (with CROSPVP) were very similar as shown in Figure 2.13. The two related products found had m/z 147 (PZQ:PVP - DEG1) and m/z 311 (PZQ:CROSPVP - DEG2).

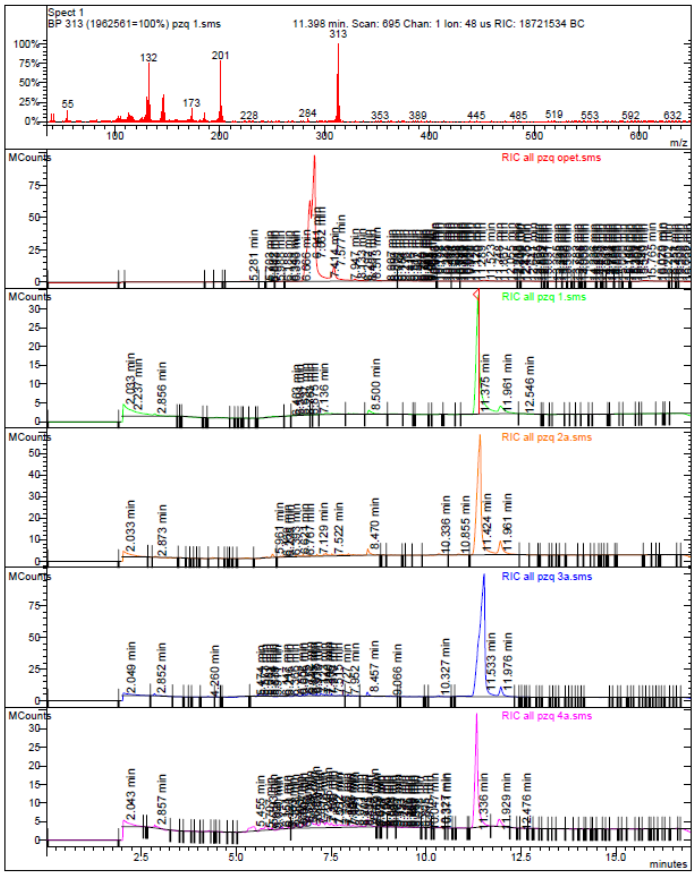

Figure 2.12: Comparison of the GC-MS spectra of the coground samples and raw PZQ. Impurity B was found at a retention time of 7.5 min for PZQ and 11.96 min for the coground samples, while PZQ peak was at 7.5 and 11.4 min respectively. From top: PZQ, sample 1, sample 2, sample 3 and sample 4.

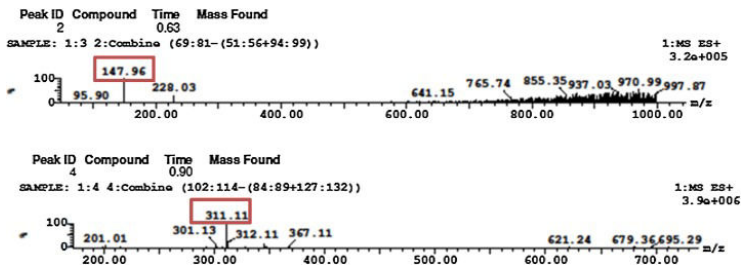

Figure 2.13: MS spectra obtained with a UPLC-MS system of the main PZQ degradation products.

DEG1 and DEG2 were found in all the samples, but DEG1 was the main product of samples 1 and 3, while DEG2 of samples 2 and 4. Also, some minor degradation products were found with m/z 313 and 327, but their identification was not possible because of the very small quantity in the sample, even not detectable in GC-MS and ^{1}HNMR analyses.

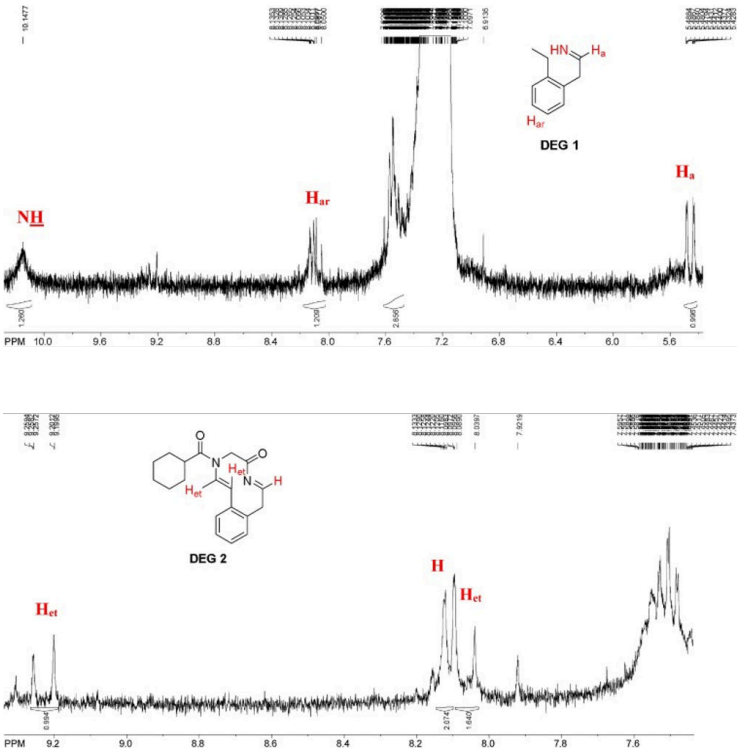

Figure 2.14: ^{1}HNMR spectra of sample 1 (up) and sample 2 (down).

The ^{1}HNMR spectra of sample 1 is reported in Figure 2.14: the ion m/z 147 showed a signal for the NH group on a double bond, differently from another degradation product found in the study of photolytic and photocatalytic oxidation of praziquantel[98]. The chemical shift of the NH proton was of 10.15 ppm, coupled with the Ha proton on the double bond (chemical shift: 5.50 ppm and coupling constant JNH,Ha:14.6 Hz). The signal at 8.1 ppm is of the proton in the aromatic ring, while the other are represented by the multiplet at 7.6-7.5 ppm. The only signals that could not be observed were the ones of the ethyl and methylene group of the aliphatic region, because of the overshadowing of the polymer signals in this region.

Similarly, Figure 2.14 reports the main degradation product observed in samples 2 (the same as sample 4). The identification was made possible thanks to the dramatic shift of two signals for the ethylenic protons to lower field, only explicable by a chemical de-shielding environment. This role could be played by the nitrogen and the benzene

ring, while the *trans* conformation was the only plausible for the coupling constant found.

2.3.3 Conclusion

The in-depth analysis of selected coground samples led to the identification of two main PZQ degradation products formed by grinding with PVP and CROSPVP, with m/z of 147 and 311 respectively. The GC-MS, UPLC-MS and ^{1}HNMR analyses were fundamental for their identification and the chemical pathway for the formation of the related compounds was explicable with the breaking of a C-N bond to form two conjugated double bonds.

2.4 Appendix A

2.4.1 Assessment of the linearity of the calorimetric reponse for the binary systems

The response Y1 (PZQ residual crystallinity) could be determinated as the PZQ heat of fusion (J/g) in the coground samples compared to raw PZQ value (96.15 ± 0.75 J/g) after verifying the linearity of the calorimetric reponse for binary systems: physical mixtures with different drug-to-polymer wt ratios (1:0, 1:1, 1:2 and 1:4) were prepared in an agate mortar and subsequentely analyzed using the same method described in paragraph 2.1.2. PZQ heat of fusion, recovered as the area of the endothermic peak, was plotted versus the composition of the mixture (i.e. % PZQ) and the linear regression was calculated. As reported in Figure 2.15, the linearity was confirmed (r^2=0.998) in both cases.

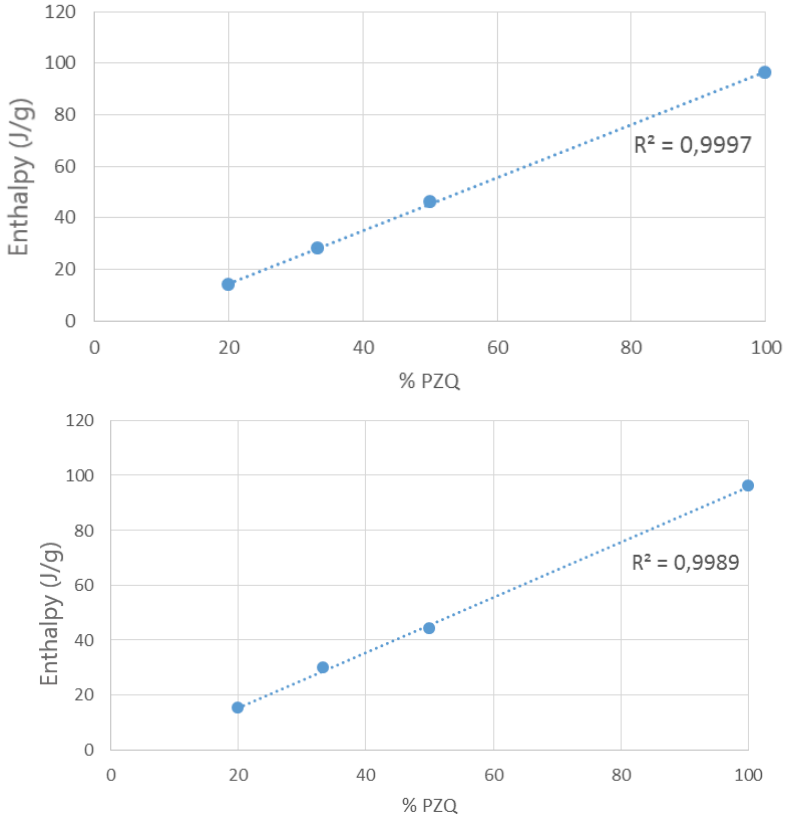

Figure 2.15: DSC response for the system PZQ:PVP (top) and PZQ:CROSPVP (bottom).

2.4.2 SEM images of the raw polymers

As a comparison with the physical mixtures and the coground samples, Figure 2.16 reports the SEM images of raw PVP[112] and CROSPVP[113]. PVP is characterized by regular and almost spherical particles with a smooth surface, different from the rough one of CROSPVP, mostly similar to aggregates of filiform particles.

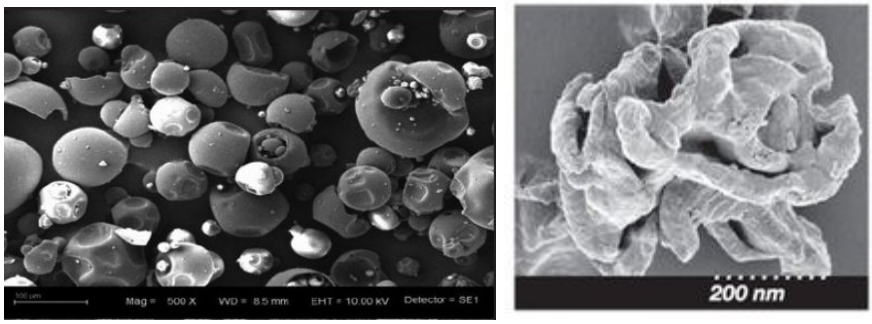

Figure 2.16: SEM images for raw PVP (left)[112] and raw CROSPVP (right)[113].

2.4.3 Identification of PZQ degradation products

The following images report the complete analyses perfomed on the coground samples to identify PZQ degradation products. The samples are referred as:

- Sample 1: PZQ:PVP, 1:1 wt ratio, ground for 4 hours at 20 Hz;
- Sample 2: PZQ:CROSPVP, 1:1 wt ratio, ground for 4 hours at 20 Hz;
- Sample 3: PZQ:PVP, 1:1 wt ratio, ground for 90 minutes at 25 Hz;
- Sample 4: PZQ:CROSPVP, 1:1 wt ratio, ground for 90 minutes at 25 Hz.

In particular Figure 2.17 shows a comparison of the GC-MS chromatograms for PZQ and the coground samples. It is worth of notice that, in PZQ sample, the retention time for PZQ was of 6.8 min and for impurity B of 7.5, while in the coground samples they were 11.4 and 11.96 respectively.

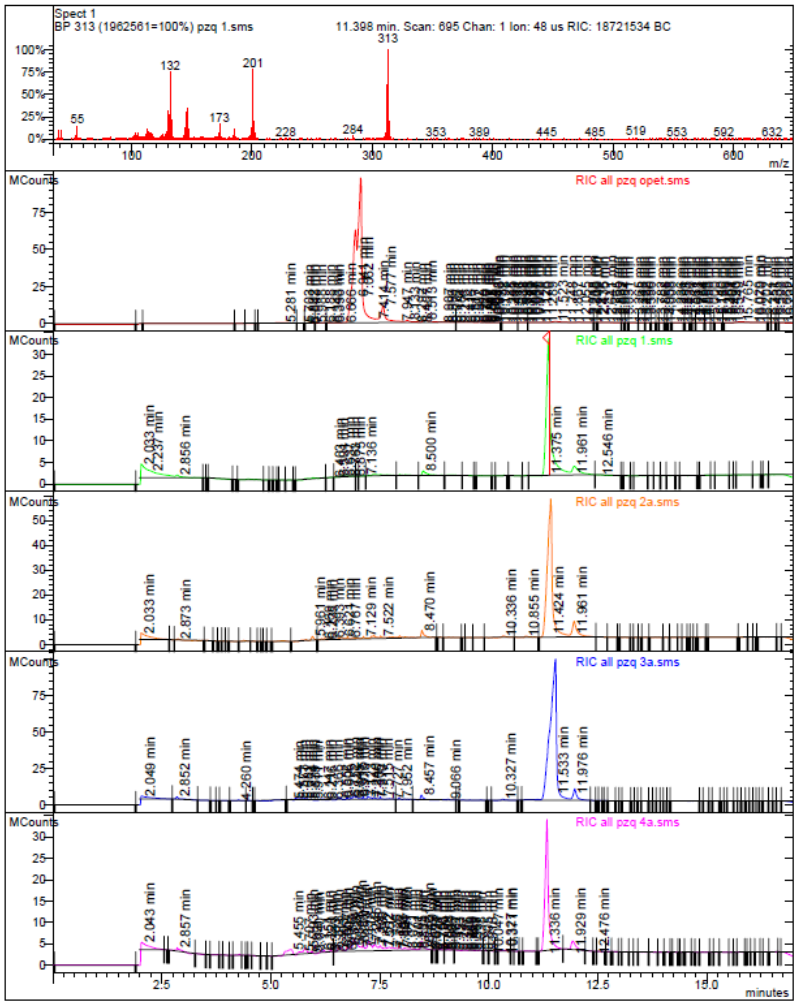

Figure 2.17: Comparison of the GC-MS chromatograms.

From Figure 2.18 to Figure 2.22 the UPLC-MS chromatograms for PZQ and for all the coground samples are reported.

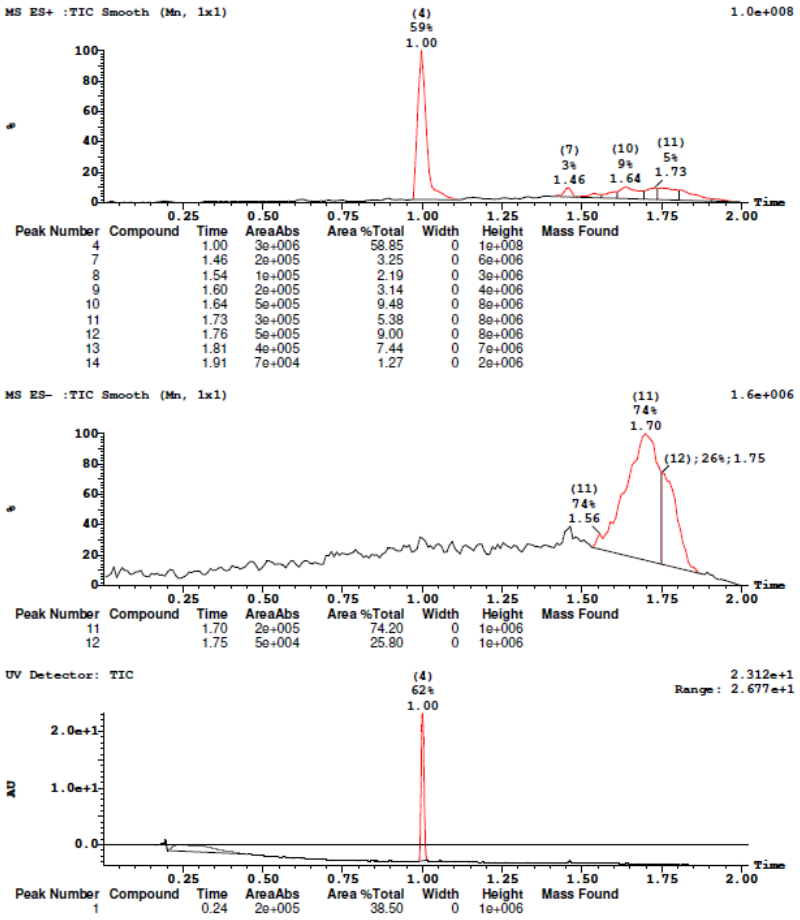

Figure 2.18: UPLC-MS Chromatograms for PZQ.

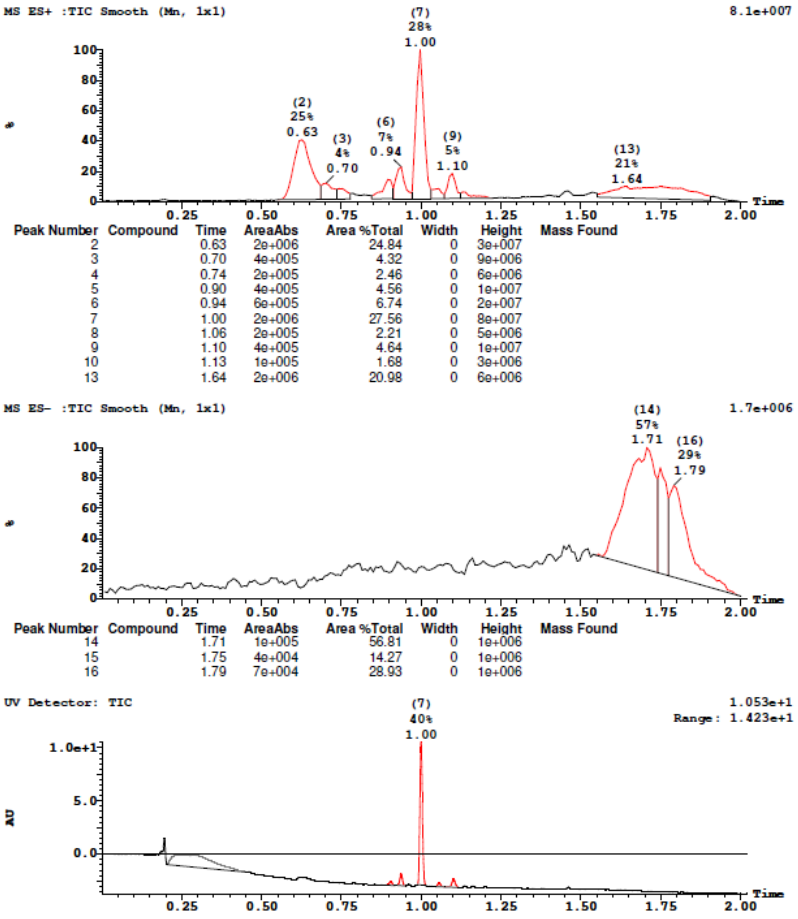

Figure 2.19: UPLC-MS Chromatograms for PZQ 1.

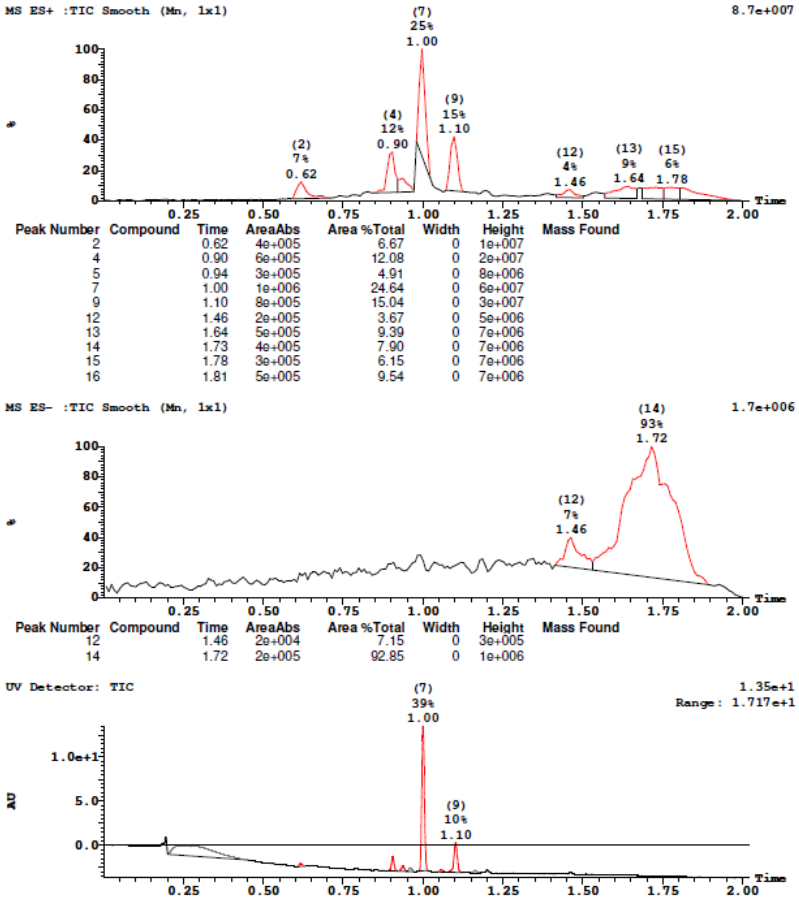

Figure 2.20: UPLC-MS Chromatograms for PZQ 2.

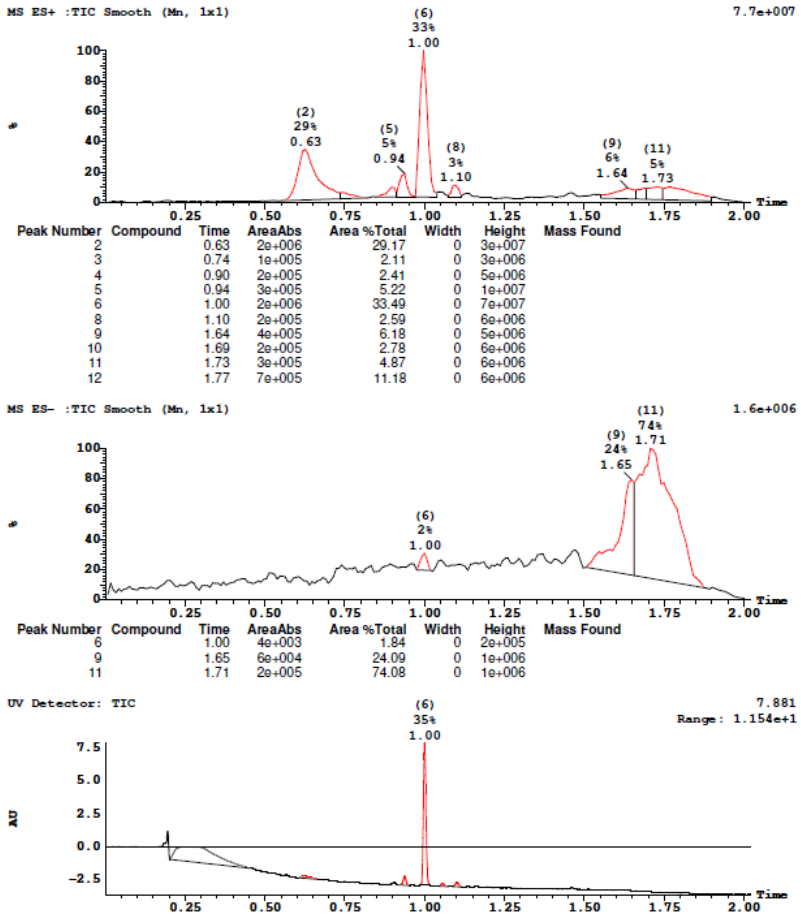

Figure 2.21: UPLC-MS Chromatograms for PZQ 3.

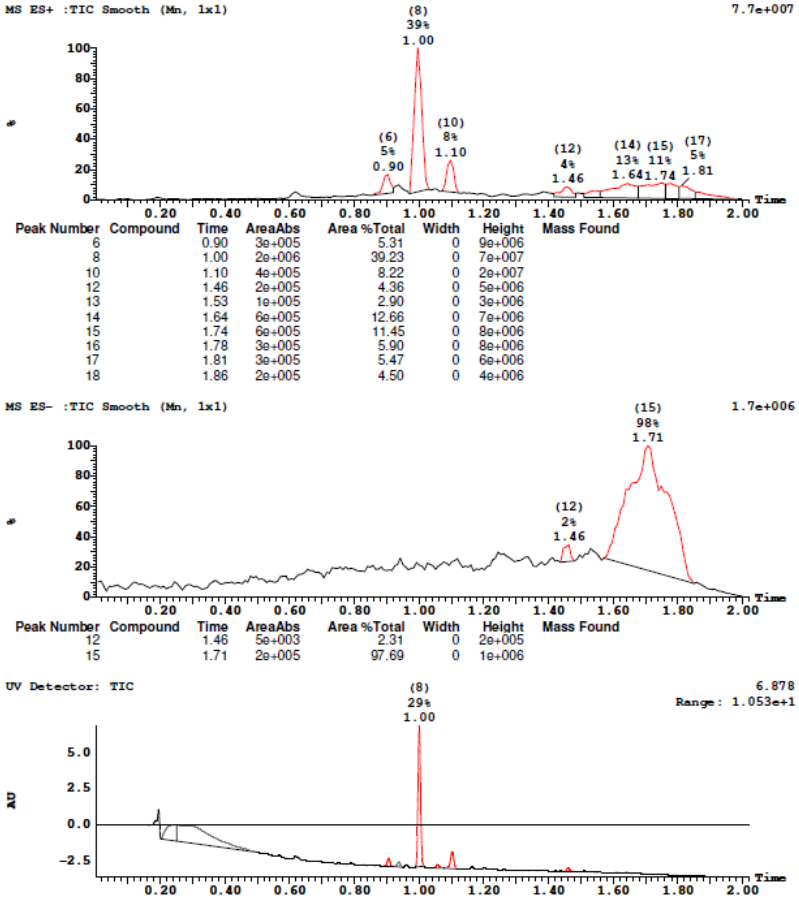

Figure 2.22: UPLC-MS Chromatograms for PZQ 4.

From Figure 2.23 to Figure 2.31 the related ^{1}H NMR spectra are reported.

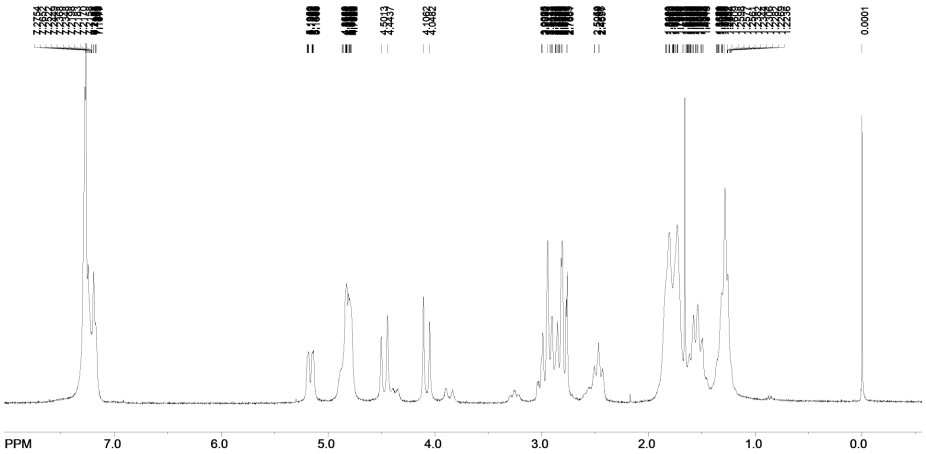

Figure 2.23: ^{1}H NMR spectrum for raw PZQ (CDCl3, 300 MHz).

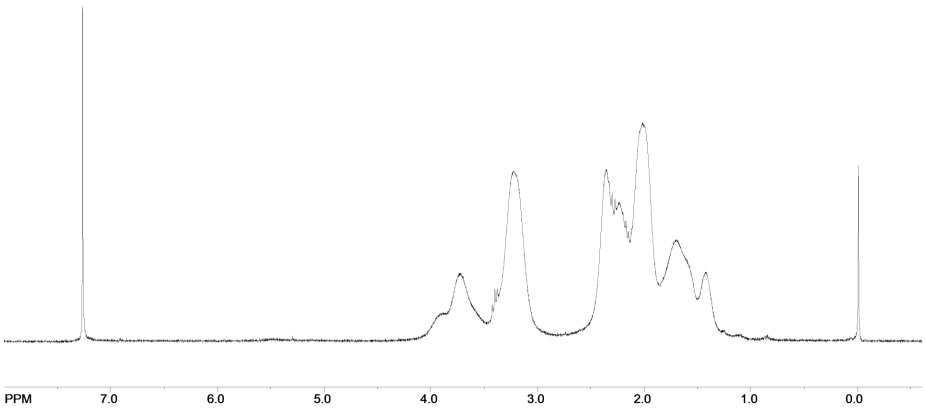

Figure 2.24: ^{1}H NMR spectrum for raw PVP (CDCl3, 300 MHz).

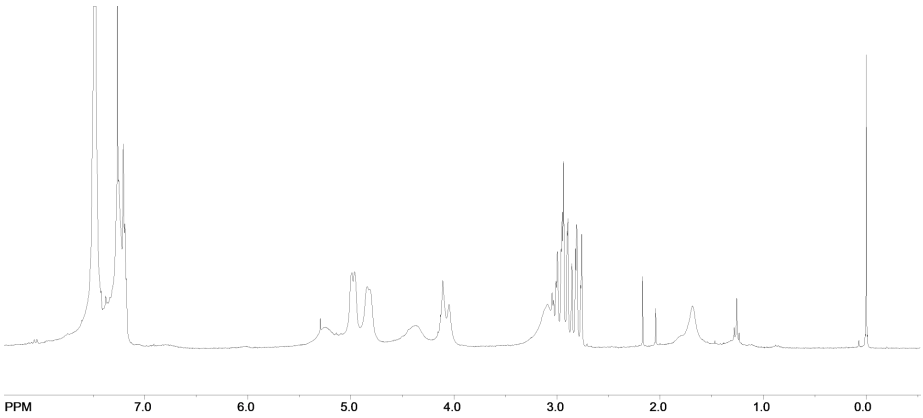

Figure 2.25: ^{1}H NMR spectrum for IMP A (by European Pharmacopoeia 7.0)[32] (CDCl3, 300 MHz).

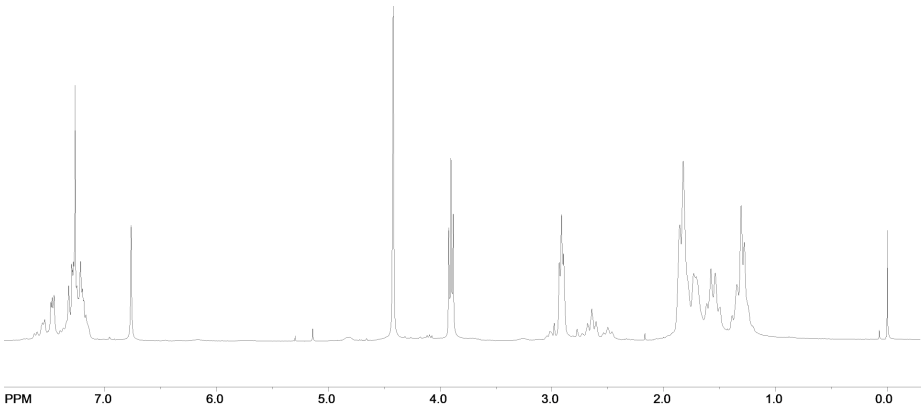

Figure 2.26: ^{1}H NMR spectrum for IMP B (by European Pharmacopoeia 7.0)[32] (CDCl3, 300 MHz).

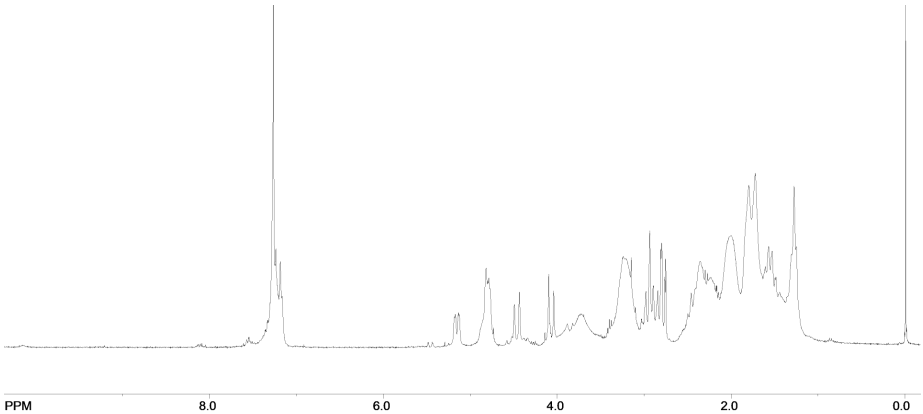

Figure 2.27: ^{1}H NMR spectrum for PZQ 1. (CDCl3, 300 MHz).

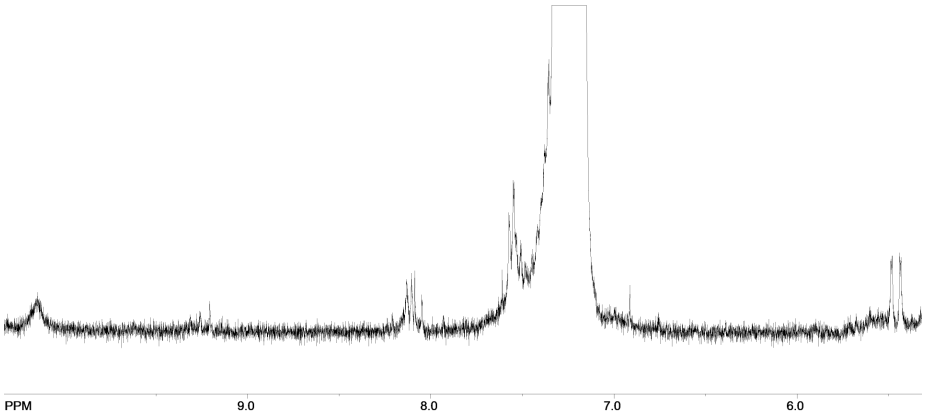

Figure 2.28: ^{1}H NMR spectrum for PZQ 1 - DEG 1 (CDCl3, 300 MHz).

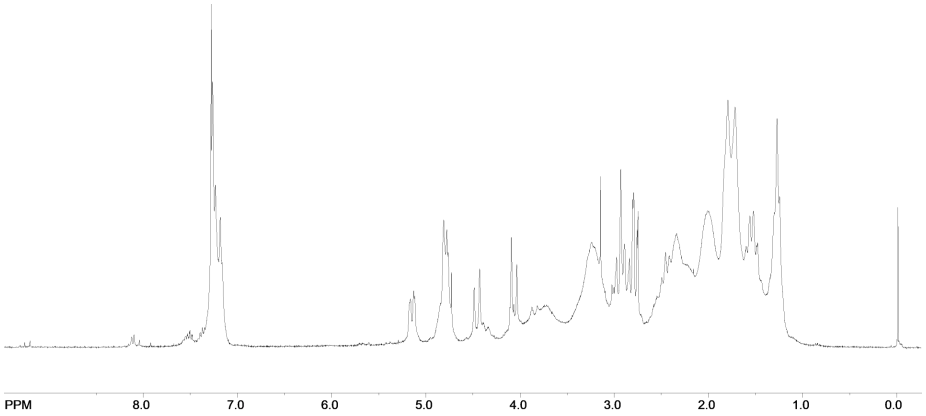

Figure 2.29: ^{1}H NMR spectrum for PZQ 2 (CDCl3, 300 MHz).

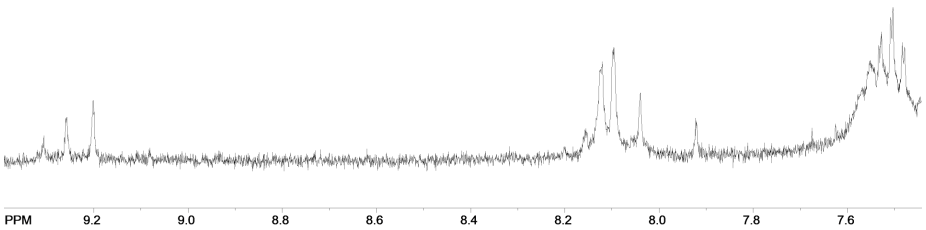

Figure 2.30: ^{1}H NMR spectrum for PZQ 2 - DEG 2 (CDCl3, 300 MHz).

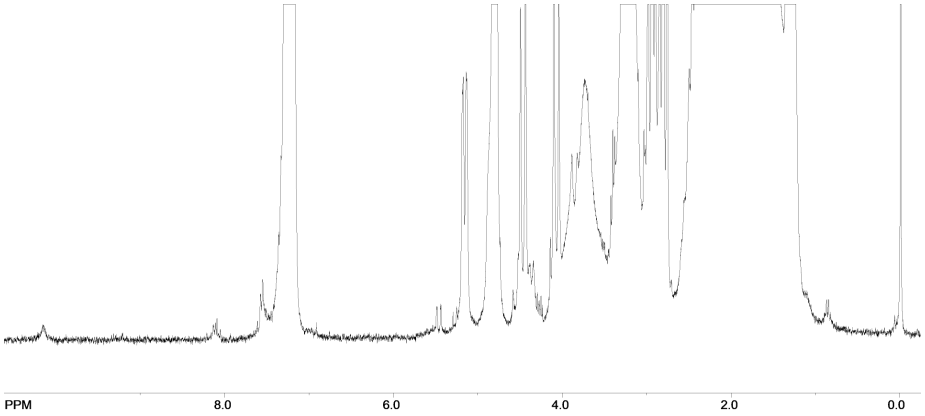

Figure 2.31: ^{1}H NMR spectrum for PZQ 3 (CDCl3, 300 MHz).

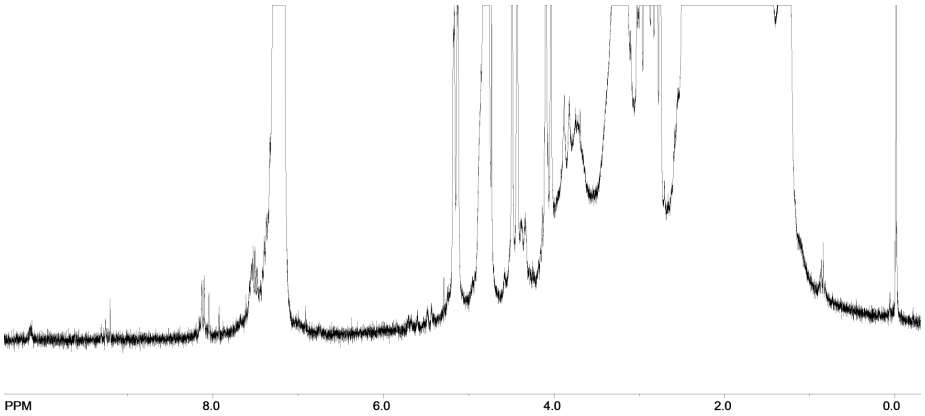

Figure 2.32: ^{1}H NMR spectrum for PZQ 4 (CDCl3, 300 MHz).

Chapter 3

Milling and comilling at cryogenic temperatures

3.1 Comparison between the process-induced effects on PZQ by milling at RT and under cryogenic conditions

3.1.1 Introduction

As previously stated, the application of the mechanical energy to pharmaceutical compounds is not a new process in the manufacturing industries, since it is commonly used to reduce the particle size. Indeed, the mechanochemical process can led to various API modifications including polymorphic transition, crystal lattice disruption and amorphisation or chemical complexations, which can modify its efficacy. The cryomilling, milling at cryogenic temperature using liquid nitrogen, can bring some advantages on the product outcome by preventing the overheating of the system, which can led to chemical reaction between the phases or thermal damages/decomposition[114], as well as reducing the recrystallization of amorphous material[115]. Recently the group of Descamps investigated the role of the glass transition temperature (Tg) during milling and cryomilling, reporting the following: when the milling process is conducted at temperature lower than the Tg of the system, as during cryomilling, the amorphisation is favoured, while crystal-to-crystal transformations, as the polymorphic transitions, are more likely to happen when working above the Tg. In the case of milling in the glass transition range, the results depend on the milling intensity[14]. The work was based on compounds with different Tg, as trehalose, lactose, budesonide, sorbitol and mannitol, but other systems were investigated in their behaviour upon cryogenic processes as for indomethacin amorphisation/polymorphic transition[116, 117], complexation ability of ursodeoxycholic acid[118], carbamazepine and ranitidine polymorphism[25, 119],

pharmaceutical nanocrystals by ultra cryomill[120]. Regarding the cryo-comilling of polymeric systems, the works in literature were mainly focused on achieving the amorphous phase[117, 121, 122]. In addition, the use of the cryogenic ambient can make the system brittle, descreasing the energy necessary for milling, reducing also particle aggregation[12]. Nevertheless, cryogenic milling was also reported to be able to start the mechanically induced decomposition of furosemide[123]. In this chapter, the influence of the frequency, time, temperature of milling (ambient or cryogenic) and type of the polymer on drug recovery and residual crystallinity will be statistically evaluated, further investigating the systems presented in paragraph 2.

3.1.2 Materials and Methods

Materials

Praziquantel (PZQ, (11bRS)-2-(Cyclohexylcarbonyl)-1,2,3,6,7,11b-hexahydro-4-H -(pyrazino[2,1-a]isoquinolin-4-one)) was of Ph. Eur. grade and kindly donated by Fatro S.p.a. (Bologna, Italy). Povidone (PVP, Kollidon K30) was purchased from Fluka Chemie- Buchs, Germany) while micronized crospovidone (CROSPVP, Kollidon CL-M) was from BASF-Ludwihshafen, Germany). The impurity A (2-Benzoyl-1,2,3,6,7,11b-hexahydro-4-H- pyrazino[2,1-a]isoquinolin-4-one) and B (2-Cyclohexanecarbonyl-2,3,6,7-tetrahydro-pyrazino[2,1- a]isoquinolin-4-one) of PZQ, purchased from Endotherm Gmbh (Saarbruecken, Germany) were both of Ph. Eur. grade. The HiPersolv Chromanorm methanol used for the HPLC analysis was of Ph. Eur. grade and purchased from VWR Chemicals (BHD PROLABO® Milano, Italy).

Methods

Design of experiment and statistical analysis As in the previous chapter, a design of experiments was used to plan the grinding trials. The factorial design planned with JMP software (SAS Institute, Inc.[124]) consisted of 3 process and 1 formulation variables. The considered process variables were time, frequency and temperature of milling each one in two levels: 30 or 90 minutes, 15 or 25 Hz and room (RT) or cryogenic (CC) temperature conditions. Otherwise, the formulation variables had three levels: raw PZQ, PZQ:PVP and PZQ:CROSPVP, which were selected following the previous experiences of PZQ comilling. The drug-to-polymer weight ratio was 1:1 and the experiments were performed in double, resulting in 48 total trials. The responses considered in this experimental plan were drug residual crystallinity (Y1) and recovery (Y2), by means of DSC and HPLC analyses respectively with the method reported below. The experimental plan of the factorial matrix used is reported in Figure 3.1: the yellow circles represent the tested points reported also in Table 3.1 and the same matrix was applied to each formulation system and at room temperature (RT) and under Cryogenic conditions (CC), as reported in Table 3.2 with all the trials details.

The statistical analysis was performed also using JMP software[124]: time and frequency were considered as continuous-numerical variables and the effects were eval-

Table 3.1: Factorial matrix and experimental plan used for all the formulations and process conditions (RT and CC).

Levels X1	Levels X2	X1:Time	X2:Frequency
		Min	Hz
+1	+1	90	25
-1	+1	30	25
0	0	60	20
+1	-1	90	15
-1	+1	30	25

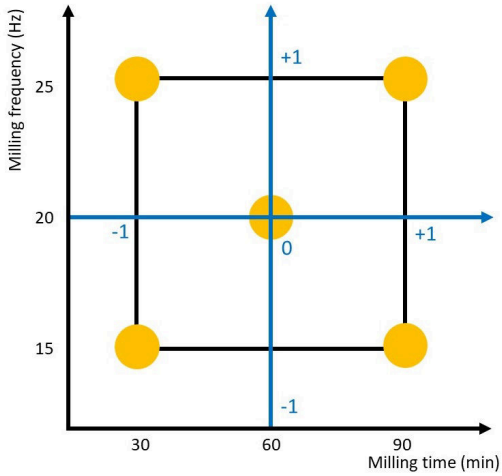

Figure 3.1: Graphical representation of the experimental plan using the factorial matrix.

uated by means of the Dunnett's test (i.e. multiple comparison of each level against a control level).

Grinding experiments The grinding was conducted using a Retsch MM400 vibrational mill (Retsch GmbH, Haan, Germany) and 2 zirconium oxide jars (volume=35 mL) and three balls (ϕ= 15 mm). The total amount of powder inserted in each jars was 1.072 g, derived from previous experiences, previously mixed in an agate mortar for three minutes. The milling conditions, regarding time and frequency, were varied depending on the different trials. When working at RT temperature, no variation were made during grinding, while when milling at cryogenic temperature the procedure was the following: once the jars were filled with powder and milling media, they were sealed and immersed in liquid nitrogen for 1 minute. Subsequently, the grinding process was started. Recooling of the jars was performed every 15 minutes grinding till the end of the trial using the same method (Figure 3.2). After grinding, the samples were collected and stored in a desiccator.

Figure 3.2: Refrigerated grinding jars.

Determination of drug residual crystallinity Each sample was analyzed using a Mettler DSC TA 4000 (Greifensee, Switzerland) connected to a calorimetric cell Mettler DSC20 and using STARE software version 9.30 for data analysis. Prior to analysis the instrument was calibrated with Indium, Zinc and Lead for the temperature and with Indium for the enthalpy quantification; each sample, containing about 2 mg of PZQ exactly weighted, was placed in a 40 μm aluminum pan with perforated lid and heated from 30 to 160 °C (10 °C/min) under air atmosphere. The PZQ enthalpy of fusion was determined by integrating the area of the endothermic peak and subsequentely compared to raw PZQ to calculate the percentage of drug residual crystallinity (response Y1).

Determination of PZQ recovery The content of PZQ was assayed by means of a reverse-phase HPLC[1] by adapting a method already reported in literature[91]; the system had two delivery pumps (LC-10 ADVP, Shimadzu, Japan), an autosampler (SIL-20A, Shimadzu, Japan) a UV-vis detector (SPD-10Avp, Shimadzu, Japan) and the data were acquired at a fixed wavelength of 220nm using an interface (SCL-10Avp, Shimadzu, Japan) and analyzed with Ez-Star software; the column used was a Kinetex 5 um C18 (150 x 4.60mm, Phenomenex, Bologna). The mobile phase used was a mixture of methanol:water (65:35 v/v), purged at 1 ml/min. PZQ retention time was 5.5 min while the total run time for each sample was set at 12 min. Prior to analysis, a linear calibration curve with r^2=0.99996 was obtained for PZQ under these conditions using different concentrations of the drug from 0.3 to 10 mg/mL. Each day, a standard solution (with a concentration of 2.5 mg/L) was prepared by dissolving about 10 mg of PZQ accurately weighted in methanol of HPLC grade (20 mL) and diluting the solution 1:200 with the mobile phase. Moreover, two additional calibration curve were obtained respectively for the relative impurity indicated in the Eur. Ph. (Ed. 8.0)[32], impurity A (r^2=0.9993) and impurity B (r^2=0.9994), which were identified at the retention time of 3.45 min and 11.2 min. The reference solution did not report any of these impurities. For the analysis 20-30 mg of the coground sample were accurately weighted, dissolved in 20 ml of methanol, diluted 1:200 with the mobile phase and injected in the HPLC system. Each sample was analyzed three times and the retention time of PZQ was at about 5.4-5.5 in every coground system. The average of the sum of the PZQ peaks was compared to the sum of all the peaks (of PZQ, impurities and other products) and expressed as the percentage of drug recovery (Y2).

Measurement of the sample temperature during milling The temperature of the samples was recorded using a 35XP-A Amprobe K-type thermocouple (Amprobe Test Tools Europe, Glottertal, Germany). Every 15 minutes of grinding the jars were opened and the temperature was measured by placing the K-type bead in contact with the powder. The temperature was measured in all the formulation systems and both at RT or cryogenic conditions. The final values were averages of three different measurements.

Modulated Differential Scanning Calorimetry Part of the samples were analyzed under modulated differential scanning calorimetry[2] using a DSC1 Stare System (Mettler Toledo, CH) with a refrigerator cooling system (RCS). The samples were accurately weighted and placed in an aluminum pan with holed-pin and subjected to the analysis. The method used was the following: heating from 10 to 180/200 °C at 1K/min with a period of 90 s and an amplitude of 0.5 °C. during the analysis dry nitrogen was purged in the DSC cell and in the RCS at 80 and 120 mL/min respectively. To obtain amorphous PZQ, the powder was heated at 10 K/min from 25 to 160 °C,

[1] In collaboration with proff. N. Passerini and B. Albertini of the Department of Pharmacy and Biotechnology of the University of Bologna (Italy).

[2] In collaboration with proff. F. Cilurzo and F. Selmi of the Department of Pharmaceutical Science of the University of Milan (Italy).

cooled to 0 °C (20 K/min) and then heated again to 100 °C (20 K/min).

3.1.3 Results

Reponses of the experimental design The experimental design used in this section comprised 24 trials conducted in double which details are reported in Table 3.2. The variables considered were formulation and grinding time, frequency and temperature, while as the response drug recovery and residual crystallinity were evaluated. The following equation was used to calculate the drug residual crystallinity of the samples: drug residual crystallinity (%)=ΔH sample*100/ ΔH PZQ. In the case of drug recovery, the indicated value is expressed as the percentage of PZQ recovered with respect to the sum of all the peaks (corresponding to PZQ and its related impurities and/or products).

Table 3.2: Results of the experimental plan for milling and comilling at room (RT) and cryogenic (CC) temperatures.

Experimental number	Experimental variables				Experimental responses (%)	
	Time (min)	Frequency (Hz)	Conditions	Formulation	PZQ recovery	PZQ res. crystallinity
1	30	15	RT	PZQ	100.00,100.00	79.89, 86.89
2	90	15	RT	PZQ	100.00,100.00	86.41, 71.34
3	30	25	RT	PZQ	100.00, 100.00	74.09, 72.69
4	90	25	RT	PZQ	99.97,100.00	81.82, 80.84
5	30	15	CC	PZQ	100.00, 100.00	72.31, 75.52
6	90	15	CC	PZQ	100.00, 100.00	44.93, 47.97
7	30	25	CC	PZQ	100.00, 100.00	22.48, 23.08
8	90	25	CC	PZQ	100.00, 100.00	2.37, 2.52
9	30	15	RT	PZQ:PVP	100.00,100.00	48.47, 45.20
10	90	15	RT	PZQ:PVP	97.25, 96.84	5.66, 5.26
11	30	25	RT	PZQ:PVP	97.07, 95.88	29.66, 12.85
12	90	25	RT	PZQ:PVP	94.74, 95.35	36.76, 44.47
13	30	15	CC	PZQ:PVP	98.92, 98.79	47.18, 48.02
14	90	15	CC	PZQ:PVP	98.03, 97.76	10.29, 12.78
15	30	25	CC	PZQ:PVP	97.00, 96.82	7.29, 3.19
16	90	25	CC	PZQ:PVP	95.19, 95.79	0.00, 0.00
17	30	15	RT	PZQ:CROSPVP	100.00,97.67	45.89, 47.68
18	90	15	RT	PZQ:CROSPVP	96.30, 96.48	16.14, 11.15
19	30	25	RT	PZQ:CROSPVP	96.32, 95.81	24.25, 11.05
20	90	25	RT	PZQ:CROSPVP	94.35, 95.18	12.31, 18.58
21	30	15	CC	PZQ:CROSPVP	98.91, 99.04	555.79, 53.70
22	90	15	CC	PZQ:CROSPVP	98.04, 97.96	7.82, 11.46
23	30	25	CC	PZQ:CROSPVP	96.32, 95.81	0.00, 0.00
24	90	25	CC	PZQ:CROSPVP	94.28, 94.18	4.05, 5.98

Determination of the glass transition temperature The Tg of the mixtures, PZQ and the polymers is shown in Table 3.3. As reported, the Tg observed for the pure components were in accordance with the respective theoretical values. In the case of the majority of the mixtures analyzed, only one Tg was found, evidencing the homogeneity of the dispersion: the temperature of this Tg was intermediate between that of the raw materials in the coground samples as well as in the cryo-coground samples. Differently, in the samples ground for less time and at low frequencies, together with the Tg of the glassy mixture (at about 112 °C), other 3 Tg were found, corresponding to the drug (37.70 °C) and the polymers, 141.92 °C for PVP and 146.37 °C for CROSPVP, which were at lower temperature values due to the co-presence of other phases. This behaviour indicated the separation of part of the amorphous drug phase from the polymer.

Table 3.3: Glass transition temperatures of the raw materials and comilled samples.

Sample	Tg Exp.
PZQ	37.70 °C
PVP	160.70°C
CROSPVP	181.23 °C
PZQ:PVP	118.60 °C
PZQ:CROS	118.59 °C
PZQ:PVP CCRIO	112.8 °C
PZQ:CROS CC	112.23 °C

Measurement of the sample temperature during grinding During the grinding process, the impact and friction of the milling media with each others and the jars can induce an increase of the temperature inside the system. In order to understand this process and its trend, the temperature of the milled powder was measured using a thermocouple every 15 minutes grinding from 0 to 90 minutes, at every frequency and with each formulatio used in the experimental design. As reported in Figure 3.3, the trend was the same in each formulation tested, and in all the frequency set the temperature rapidly increased in the first 30 minutes grinding, reaching slowly a plateau which remained constant, even when milling for four hours.

When milling was performed at the higher frequency, the temperature reached the maximum values of 46.9 °C after 90 minutes, while when grinding at 15 Hz the temperature never went beyond 30-33 °C. Also, the effect of jars refrigeration was studied and reported in Figure 3.3: by using cryo-milling the temperature was maintained always below 20 °C, since the maximum temperature was 18.8 °C, that means about 25-30 °C below comparing to the RT conditions. In fact, the controlled cooling every 15 minutes prevented the increase of temperature with grinding. Additional investigation on the grinding temperature were performed using specific thermo jars with integrated measuring system, reported in the Appendix B (paragraph 3.2.1).

Presence of impurities The presence of PZQ related compound, indicated in the European Pharmacopoeia[32], was evaluated in all the ground systems. In fact PZQ impurities, photo-thermal stability and the ways of photolytic and photocatalytic oxidation has been already reported in literature[92, 97, 98], and the evaluation of the impurities formed upon grinding have been already discussed in the previous chapter (paragraph 2.3). In the samples analyzed the quantity of the related impurity A was never beyond 0.2%, which represent the maximum limit for the USP 36-NF 31, while impurity B was never detected. Also in this study, the above described related degradation compounds of PZQ:PVP and PZQ:CROSPVP samples (paragraph 2.3) were identified (Figure 3.4).

Statistical assessment of the results The statistical analysis of the results was conducted in two parts: in the first, shown in Table 3.4, the influence of the variation of the milling conditions (time, frequency and temperature conditions) on the experimental responses (drug recovery and residual crystallinity) was evaluated for all the composition systems (PZQ, PZQ:PVP and PZQ:CROSPVP). Then the influence of varying the milling parameters and the composition of the system on the same experimental responses was analyzed in both temperature conditions (RT and CC), visible in Table 3.5. When grinding PZQ by itself, the variation of time, frequency or temperature did non significantly influence drug recovery, while the residual crystallinity was dramatically reduced when grinding at cryogenic temperature (***p=.001) and also when increasing the milling frequency (**p=.0058). PZQ recovery in both systems with the polymers was significantly reduced by increasing time and frequency of milling, but not by changes in the environmental conditions. The residual crystallinity, however, was uninfluenced by any of the variables in the case of PZQ:PVP, while when grinding with CROSPVP, the increase of time and frequency were poorly (*p=.015) and medium significant (**p=.0069) respectively. As reported in Table 3.5, the presence of the polymers was highly significant on the experimental responses both at RT and under cryogenic conditions. The difference of the effect of using PVP or CROSPVP could only be observed at cryogenic temperature regarding drug recovery, where the variable "choice of the polymer" was of little significance (*p=.037).

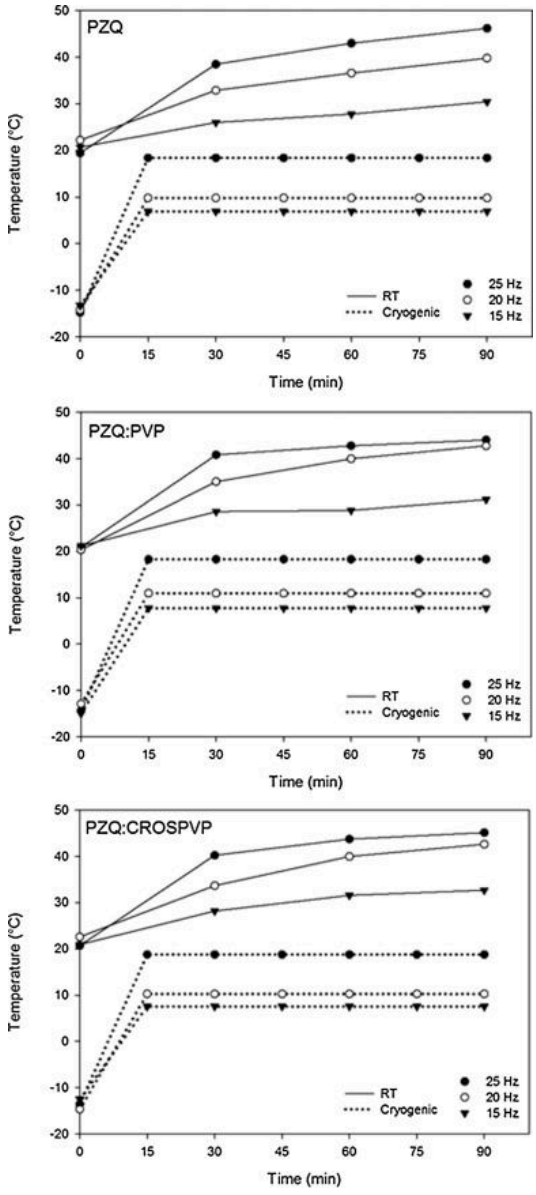

Figure 3.3: Temperature trend during the milling process, at different frequencies, powder compositions and grinding conditions (solid lines: RT, dashed lines: CC).

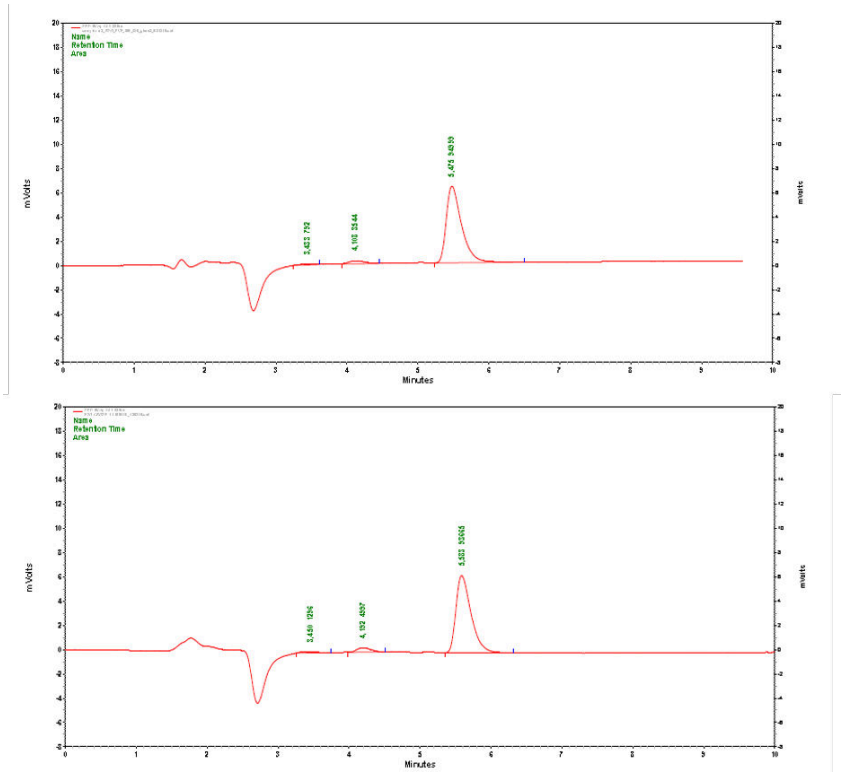

Figure 3.4: HPLC chromatograms of the PZQ:PVP and PZQ:CROSPVP coground samples, processed for 90 minutes at 25 Hz.

Table 3.4: Effect of increasing of time/frequency of milling on the selected experimental responses in the three different sample compositions. Each level was compared to the control level indicated in brackets (significative levels: n.s.: not significative, *p<.05, **p<.01, ***p<.001).

Drug recovery

	PZQ			PZQ:PVP			PZQ:CROSPVP		
Milling parameters	Difference	p-value	95%CI	Difference	p-value	95%CI	Difference	p-value	95%CI
Time (30)	0.00	n.s.	-0.012 to 0.004	-1.69	***p< .001	-2.30 to -1.07	-1.94	***p< .001	-2.61 t -1.29
Frequency (15)	0.00	n.s.	-0.012 to 0.004	-2.47	***p< .001	-3.08 to -1.85	-2.96	***p< .001	-3.62 to -2.30
Temperature conditions (RT)	0.00	n.s.	-0.004 to 0.012	0.14	n.s.	-0.47 to 0.76	0.00	n.s.	-0.66 to 0.66

Drug residual crystallinity

	PZQ			PZQ:PVP			PZQ:CROSPVP		
Milling parameters	Difference	p-value	95%CI	Difference	p-value	95%CI	Difference	p-value	95%CI
Time (30)	-11.09	n.s.	-27.81 to 5.62	-15.83	n.s.	-34.72 to3.06	-18.86	*p=.015	-33.37 to -4.35
Frequency (15)	-25.46	***p=.006	-42.39 to -8.95	-11.08	n.s.	-29.97 to 7.81	-21.68	**p=.007	-36.18 to -7.17
Temperature conditions (RT)	-42.85	***p<.001	-59.57 to 26.13	-12.45	n.s.	-31.34 to 6.44	-6.03	n.s.	-20.54 to 8.48

Table 3.5: Effect of the increasing of time/frequency of milling on the selected experimental responses in the different temperature conditions. Each level was compared to the control level indicated in brackets, significative levels: n.s.: not significative, *p<.05, **p<.01, ***p<.001.

Drug recovery

	Room Temperature			Cryogenic Conditions		
Milling parameters	Difference	p-value	95%CI	Difference	p-value	95%CI
Time (30)	-1.10	n.s.	-2.30 to 0.10	-0.60	n.s.	-1.40 to 0.21
Frequency (15)	-1.39	*p=.027	-2.58 to -0.19	-1.09	*p=.12	-1.89 to -0.29
Presence of PVP (PZQ)	-2.86	***p<.001	-4.05 to -1.66	-2.71	***p<.001	-3.51 to -1.91
Time (30)	-1.22	n.s.	-2.45 to 0.01	-0.73	n.s.	-1.88 to 0.42
Frequency (15)	-1.32	*p=.038	-2.55 to -0.09	-1.64	**p=.009	-2.80 to -0.49
Presence of CROSPVP (PZQ)	-3.20	***p<.001	-4.43 to -1.97	-3.21	***p<.001	-4.36 to -2.06
Time (30)	-2.32	***p<.001	-3.00 to -1.63	-1.32	***p<.001	-1.78 to -0.86
Frequency (15)	-2.70	***p<.001	-3.38 to -2.01	-2.73	***p<.001	-3.19 to -2.27
Choice of the polymer (PVP)	-0.35	n.s.	-1.03 to -0.34	-0.5	*p=.037	-0.95 to -0.04

Drug residual crystallinity

	Room temperature			Cryogenic conditions		
Milling parameters	Difference	p-value	95%CI	Difference	p-value	95%CI
Time (30)	-4.65	n.s.	-20-29 to 10.99	-22.28	***p<.001	-32.01 to -12.54
Frequency (15)	0.51	n.s.	-15.31 to 16.15	-37.26	***p<.001	-47.00 to 27.52
Presence of PVP (PZQ)	-50.51	***p<.001	-66.34 to 35.07	-20.31	***p<.001	-30.04 to -10.57
Time (30)	-7.98	n.s.	-19.28 to 3.32	-21.97	**p=.003	-34.70 to -9.25
Frequency (15)	-8.72	*n.s.	-20.02 to 2.58	-38.63	***p<.001	-51.35 to 25.90
Presence of CROSPVP (PZQ)	-55.87	***p<.001	-67.16 to -44.57	-19.05	**.007	-31.77 to -6.32
Time (30)	-14.34	n.s.	-31.58 to 2.90	-20.35	**p=.006	-33.55 to -7.15
Frequency (15)	-4.44	n.s.	-21.68 to 12.80	-28.32	***p<.001	-41.52 to -15.12
Choice of the polymer (PVP)	-5.16	n.s.	-22.4 to 12.08	1.26	n.s.	-11.94 to 14.46

Stability of the samples The well-known capacity of polymer to stabilize other compound was confirmed in this study, since the coground samples were physically stable for at least 6 months, without any evidence of drug recrystallization, as shown in Figure 3.5 reporting the DSC traces over time of the cryo comilled samples. Moreover, drug recovery did not change over time, as the impurity were the same as the fresh samples, meaning that their formation is more probably due to the grinding process rather than a simple interaction between the components.

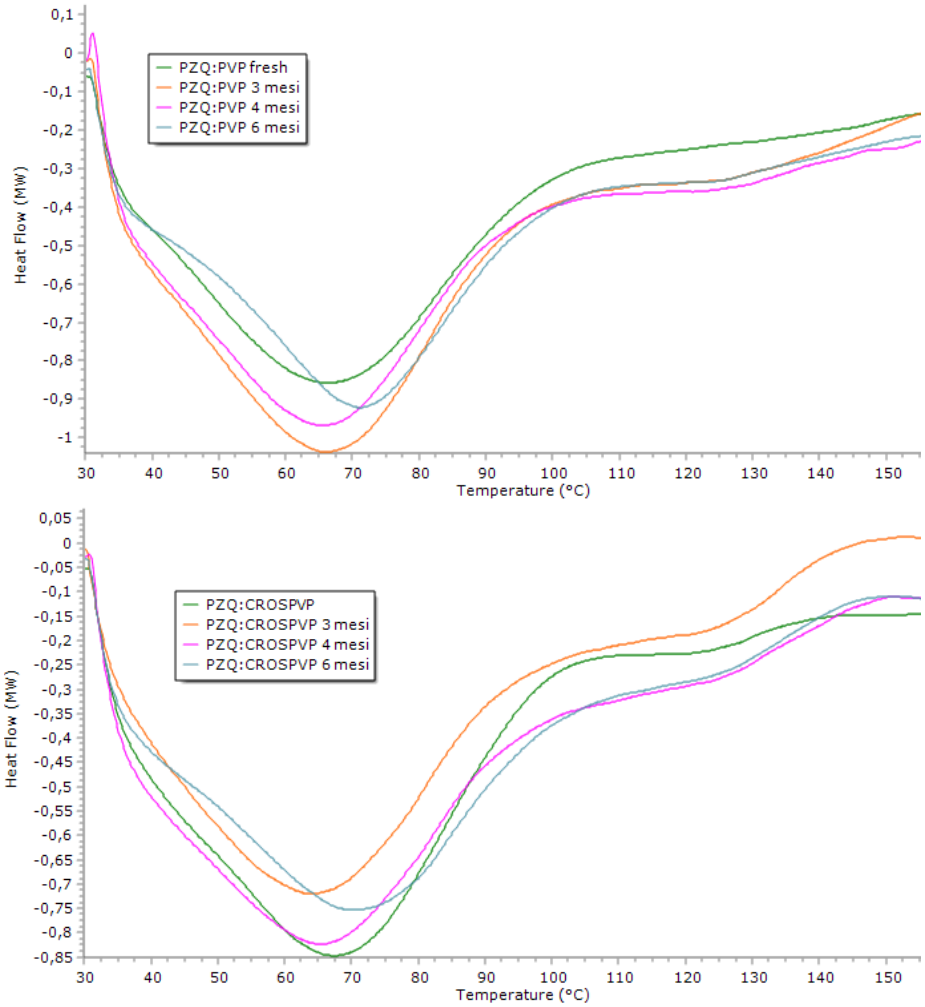

Figure 3.5: DSC traces over time of the cryo comilled samples with PVP (top) and CROSPVP (bottom).

3.1.4 Discussion

PZQ demonstrated to maintain its integrity upon grinding by its own, even at the most stressful conditions of 90 minutes at 25 Hz, while, as previously noticed, when in

presence of the polymers, drug degradation was significantly augmented and the more the energy transmitted by grinding, the more PZQ degraded. Thus, the polymers did not act like protectors by coating/dilution, but as promoters of drug degradation in the same way, since no difference in this behaviour was found when using PVP or CROSPVP. As previously stated, PZQ degradation seamed to be not depending on drug interaction with the polymers, but on the input of mechanical energy during the grinding process. In fact, no evidence of chemical interaction were found in the physical mixture or in the coground samples (paragraph 2.1). Also, the increase of temperature inside the jars in unlikely to be responsible for drug degradation since no significative variation in the powder temperatures were found between the powder composition, as reported in Figure 3.3, and PZQ did not degrade when ground by itself. Moreover, there have been few studies on PZQ stability towards thermal decomposition[92, 97], where PZQ was found to be stable when heated at 60 °C for 4 hours. In the presented experimental design the powder reached a maximum of 46.9 °C after 90 minutes grinding, well below the temperature studied by Hashem and collaborators. One interesting difference between the composition studied is represented by the water content: in fact, the polymers used contain a certain amount of water due to their hygroscopic nature, differently from the pure anhydrated drug. Thus, drug degradation could be also be promoted by the included water in the coground mixtures. Concerning drug amorphisation, the presence of the polymers favoured also PZQ destructuration that was almost complete in the coground samples, while when grinding the lone drug, its crystallinity remains around 72%. This was in accordance with Huttenrauch and collaborators who suggested the dependency of drug degradation from a previous drug destructuration, as a subordinate step[125]; in fact, in this design the more degrade products (i.e. binary mixtures) were also the more amorphous ones. Interestingly, the contribution to drug amorphisation in the coground systems was similar between the two polymers, without any statistical differences, as also demonstrated at the MT-DSC analysis by the the formation of two homogeneous systems. Recent studies reported similar behaviour of polymers to favor chemical reactions[126] or physical transformations of a drug to, for example, the amorphous phase, polymorphs and dispersed state inside the polymer[127, 128]. This is one of the case in which the catalytic effect of the polymer is highly effective on drug amorphisation, though favor also it degradation. Similarly, the amorphisation of piroxicam was achieved in less cryo-cogrinding time by incrementing the content of PVP [121]. When time and frequency of milling were increased, the experimental responses tended to increase, but this was not the general rule for all the conditions, since it was mainly verify when using cryogenic conditions and observing drug residual crystallinity. It is well known from the literature[104, 108] that when the grinding temperature is below the glass transition point the powder is more prone to amorphisation/destructuration while when staying beyond this point there can be physical transition to polymorphic forms. In this case the use of the cryogenic conditions when grinding PZQ by itself permitted to maintain the temperature well below PZQ glass transition point (37.70 °C), thus favouring drug amorphisation and the repeated cooling avoid any increase

of temperature, that was conversely very pronounced when working at RT conditions. In fact, the effect of the grinding temperature was very significative in the case of the lone drug. Differently, when grinding PZQ with the polymers the grinding temperature was far below the glass transition point of the mixtures, both at RT and under cryogenic conditions, therefore the same temperature effect was not statistically significative. As the last observation, the switch to the cryogenic condition seamed to make the experimental responses more predictable upon the variation of the milling parameters (i.e. time and frequency).

3.1.5 Conclusions

The experimental design implied in this part of the thesis permitted to study the effect of grinding at RT and under cryogenic conditions different systems: the drug by it self and in combination with linear and cross-linked polyvinylpyrrolidone. As previously reported, PZQ did not degrade when ground by itself, but in presence of the polymers, both at RT and cryogenic conditions. Also, this degradation matched with a more pronounced drug amorphisation in the binary systems. The switch to cryogenic condition permitted to dramatically reduce the crystallinity of PZQ when ground by itself, due to the grinding temperature maintained below it glass transition point. Between the two polymers, the effects were very similar both at RT and under cryogenic conditions, promoting drug amorphisation and degradation, but also stabilizing the PZQ amorphous phase for at least 6 months storage.

3.2 Appendix B

3.2.1 Evaluation of the milling temperature by using thermojar system

The evaluation of the temperature during the milling process was further evaluated by using a specific system of InSolidoTechnology reported in Figure 3.6: it is composed by a PMMA jar with an integrated temperature sensor and a IR transmitter, which is received and trasmitted to the dedicated PC software.

Figure 3.6: Thermojar system by InSolidoTechnology.

In this way, the temperature measurements is specifically referred to the innert part of the jar, giving a more detailed description of its progress during time.

Figure 3.7 reportes the graph of the temperature progress during PZQ grinding in the thermojar at 25 Hz. If the process was not interrupted, the temperature reaches about 40 °C after 50 minutes grinding, which was in good agreement with the measurements performed with the thermocouple (figurename 3.3). When interrupted for different grinding experiments, as in the blue line with the addition of water, the maximum temperature reached was slightly lower, due to the partial cooling when opening the jar.

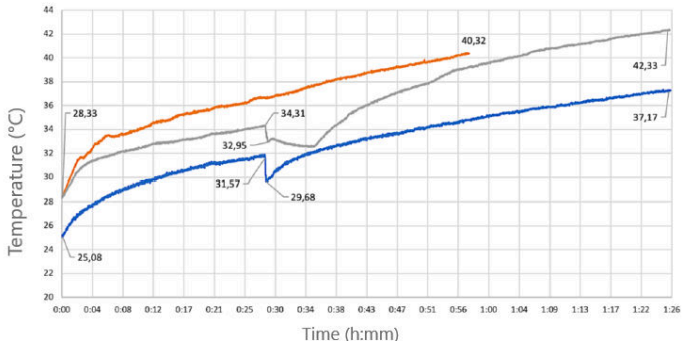

Figure 3.7: Example of temperature measurement using the thermojars at 25 Hz.

Chapter 4

Neat Grinding of praziquantel

The pharmaceutical industry is one of the fields in which the deep study of the solid-state and modification propensities of an API upon technological processes is of great importance to ensure the security and efficacy of the drug. In fact, the different crystal packing of a compound determines differences also in the physicochemical and biopharmaceutical properties, as for example the melting point or its solubility and dissolution rate. Thus the preference of one polymorph instead of another would allow the optimization of the willing properties. The classical methods for polymorph screening comprehend different crystallizations methods in various conditions, changing fundamental parameters as the selected solvent, temperature, pressure and overall process. Recently, grinding has been used to study the solid-state changes induced by the mechanochemical energy, including amorphisation and polymorphic transitions[129]and in particular liquid-assisted grinding (LAG) demonstrated to be effective in changing the polymorphic outcomes by the simply inclusion of a small quantity of a specific solvent[129–131]. For example the polymorphic conversion of different API by grinding was reported in literature for aspartame form II which transforms to form I upon milling [132], carbamazepine transitions [133] and many others examples[134–136].Moreover, even the amount of the liquid was reported to be significatively involved in the polymorphism of the products, as reported by Hasa and collaborators[16]: in fact, the caffeine-anthranilic acid system they presented was subjected to LAG using different solvents in different quantities, confirming the selectivity of certain polymorphs and also demonstrating the possibility to change the outcome by varying the amount liquid inserted. Additionally, the same author reported also polymer-assisted grinding as a useful method for polymorphs screening in a mechanochemical cocrystal synthesis[128].

This chapter will start from the preparation and deep characterization of Form B, the only ever-known polymorph of PZQ. Then, a design of experiment will be employed to study the optimal grinding conditions for Form B formation, resulting in the discovery of another polymorph, Form C, which characterization will be presented in the last part of the chapter.

4.1 Polymorph B

4.1.1 Materials and Methods

Materials

Praziquantel (PZQ, (11bRS)-2-(Cyclohexylcarbonyl)-1,2,3,6,7,11b-hexahydro-4-H -(pyrazino[2,1-a]isoquinolin-4-one)) was of Ph. Eur. grade and kindly donated by Fatro S.p.a. (Bologna, Italy). The HiPersolv Chromanorm methanol used for the HPLC analysis was of Ph. Eur. grade and purchased from VWR Chemicals (BHD PROLABO® Milano, Italy).

Methods

Preparation of Form B PZQ was ground in a Retsch MM400 vibrational mill using two zirconium oxide jars of 35 mL, each one containing three grinding balls (ϕ=15 mm). The powder to be inserted in the jar was 1.072 g on the basis of previous experiences and the grinding process was performed at 20 Hz for 4 hours. In order to ensure Form B formation the milling should not be stopped at anytime, on pain of product outcome. Form B was then stored in a desiccator in the dark at room temperature.

Differential Scanning Calorimetry Each sample was analyzed using a Mettler DSC TA 4000 (Greifensee, Switzerland) connected to a calorimetric cell Mettler DSC20 and using STARE software version 9.30 for data analysis. Prior to analysis the instrument was calibrated with Indium, Zinc and Lead for the temperature and with Indium for the enthalpy quantification. For each analysis, about 2 mg of the sample accurately weighted were placed in a 40 μm aluminum pan with perforated lid and heated 10 °C/min from 30 to 160 °C under air atmosphere. The PZQ enthalpy of fusion was determined by integrating the area of the endothermic peak.

Thermogravimetrical Analysis Thermogravimetrical analyses were performed in selected samples using a Mettler Toledo TGA/SDTA851e: about 10-15 mg of the sample accurately weighted were placed in aluminum crucible (100μL); then, the heating was performed from 25 to 220 °C, at 10 °C/min under nitrogen atmosphere. The software used to calculate the weight loss from the weight-temperature diagram was STARe software 11.00.

Powder X-Ray Diffraction - PXRD The sample were analyzed by powder X-ray diffraction using a Panalytical X'Pert Pro Diffractometer with Ni-filtered Cu Kα radiation (wavelength=1.5418 A), the detector was a RTMS X'celerator. The preparation of the samples consisted in pressing about 20.30 mg of powder over a glass slide to have a flat surface. The data were collected in a 2θ range of 3-40 degree.

Synchrotron X-ray powder diffraction Thanks to the collaboration with Dr. N. Demitri and Dr. L. Gigli of Elettra Sincrotrone in Trieste, Form B was analyzed using the X-ray diffraction beam line XRD1[137] in order to obtain a diffraction powder suitable for the crystal structure solution due to the improved resolution and signal to noise ratio comparing with the data from the conventional laboratory source. Form B was packed in a borosilicate capillary with a diameter of 300 μm and the pattern was collected at RT temperature using a monochromatic wavelength of 0.700A (17.71 KeV), 200*2000 μm2 spot size and as the hybrid-pixel area detector a Dectris Pilatus 2M. The pattern was then integrated using Fit2D program[138], after calibrating the hardware setup with LaB6 standard reference powder (NIST 660a).

Solid-state NMR analyses Solid-state NMR measurements of PZQ and Form B were collected using a Bruker Avance II 400 instrument[1]. The spectra were obtained at 100.65 and 40.55 MHz for ^{13}C and ^{15}N respectively. Cylindrical zirconia rotors (4 mm o.d) were used with a sample volume of 80 μl and spun at 12 and 9 kHz respectively for ^{13}C and ^{15}. In all the analyses a RAMP-CP pulse sequence (^{1}H 90° pulse = 3.05 us), TPPM ^{1}H decoupling with an rf field of 75 kHz were used during the acquisition. The number of transients acquired was 124 for both raw PZQ and Form B with 3.5 ms of contact time and a relaxation delay different between the two: 20 s for raw PZQ and 30 s for Form B. As the reference, the resonance of hexamethylbenzene was used for ^{13}C (17.4 ppm for the methyl signal) and $(NH_4)_2SO_4$ for ^{15}N (-355.8 ppm, respect to CH_3NO_2).

DTF calculations The crystal structure proposed for Form B was validated by performing periodic lattice calculations using the density functional theory (DFT-D). All the details of this part, performed by Dr. P. Cerreia Vioglio of the Aix-Marseille Université (France) are reported in the Appendix C (paragraph 4.6.1.)

Determination of PZQ degradation The content of PZQ was assayed by means of a reverse-phase HPLC-UV, adapting a method already reported in literature[91]; the system had two delivery pumps (LC-10 ADVP, Shimadzu, Japan), an autosampler (SIL-20A, Shimadzu, Japan) a UV-vis detector (SPD-10Avp, Shimadzu, Japan) and the data were acquired at a fixed wavelength of 220 nm using an interface (SCL-10Avp, Shimadzu, Japan) and analyzed with Ez-Star software; the column used was a Kinetex 5 μm c18 (150 x 4.60mmm, Phenomenex, Bologna). The mobile phase used was a mixture of methanol:water (65:35 v/v), purged at 1 ml/min. PZQ retention time was 5.5 min while the total run time for each sample was set at 12 min. Prior to analysis, a linear calibration curve with r^2=0.99996 was obtained for PZQ under these conditions using different concentrations of the drug from 0.3 to 10 mg/mL. Each day, a standard solution (with a concentration of 2.5 mg/L) was prepared by dissolving about 10 mg of PZQ accurately weighted in methanol of HPLC grade (20 mL) and diluting the solution 1:200 with the mobile phase. Moreover, two additional

[1] In collaboration with prof. M. R. Chierotti of the Department of Chemistry, University of Turin (Italy)

calibration curve were obtained respectively for the relative impurity indicated in the Eur. Ph. (Ed. 8.0)[32], impurity A (r^2=0.9993) and impurity B (r^2=0.9994), which were identified at the retention time of 3.45 min and 11.2 min. The reference solution did not report any of these impurities.

Scanning Electron Microscopy For the acquisition of the SEM images a Leica Stereoscan 430i (Leica Cambridge LTd, Cambridge, UK) was used on sample metallized with a S150A Sputter Coater (Edwards High Vacuum Crawley, West Sussex, UK).

ATR-FTIR spectroscopy The sample were analyzed at the solid state without preparing any dilution using a PerkinElmer Spectrum 100 FT-IR (Beaconsfield, England) with a Universal ATR sampling and software PE version 6.3.4 copyright 2008. The spectra were collected between 650 and 4000 cm^{-1} using a scan number of 4.

FT-IR spectroscopy Additional FT-IR analyses were performed using a Perkin Elmer System 2000 FT-IR on raw PZQ and Form B. The samples were mixed with KBr in an agate mortar and then pressed with an hydraulic press for 2 minutes at 10 Ton to obtain homogeneous and transparent discs. The analyses were conducted form 400 to 4000 cm^{-1} with a resolution of 2 cm^{-1} and total scan number of 10.

Solubility measurements To analyze the water solubility of Form B and raw PZQ[2], saturated solution of the corresponding samples were prepared in distilled water and kept under agitation in the dark for 48 hours. Subsequently the solutions were filtered with a membrane of 0.2 nm pore size, diluted 1:200 with the mobile phase (65 % MeOH-35 % H_2O) and injected in the HPLC instrument using the method previously described in the degradation measurement paragraph. For each sample, three different analyses were conducted and the average was taken as the final data.

Determination of the intrinsic dissolution rate For the intrinsic dissolution studies about 150 mg of the samples were compressed into a disc using an hydraulic press (PerkinElmer, Norwalk, USA) for 1 min at 1 Ton; the sample holder was a stainless steel cylinder which permitted to obtain tablets with a flat surface area of 0.785 cm^2 and a diameter of 1 cm. The system (comprised of the sample holder and the tablet) was inserted in 1L of distilled water kept at 37 °C, with a paddle rotating at 100 rm and placed 3.5 cm from the tablet surface. 2 ml of aliquots were withdrawn every 10 minutes till 1 hour and replaced each time with 2 mL of the same dissolution medium. These aliquots were subsequentely analyzed by HPLC-UV following the method previously described. For each sample, three test were conducted and the SD and RSD (%) were calculated at each time step. The amount of drug dissolved per unit area over time, indicated by the slope of the curve, was compared between the samples using linear regression.

[2]In collaboration with proff. N. Passerini and B. Albertini of the Department of Pharmacy and Biotechnology, University of Bologna (Italy), as well as for the intrinsic dissolution studies.

Efficacy in *in vitro* and *in vivo*. The *in vitro* and *in vivo* tests were performed at the Swiss Tropical and Public Health Insitute (Basel, Switzerland, prof. Jennifer Keiser). For the *in vitro* studies the samples were tested in their efficacy by preparing different concentrations, ranging from 0.021 to 0.33 μg/L in which adult Schistosomes were incubated for up to 72 hours. By using an inverse microscope (Carl Zeiss, Germany, magnification 80x) all the alterations of morphology, motility and viability were observed and the IC_{50} value was calculated with CompuSyn software. For the *in vivo* studies, the 4 NMRI mice used were infected 49 days before the treatment with *S. mansoni*, while 9 mice served as controls. The samples tested were administered using single oral doses (400 mg/Kg). The animals were sacrified by the CO_2 method and dissected to permit the count of the worms[139] and the interpretation of the results as worm burden reduction. Moreover, many different dosages of Form B were tested and also an in-depth side by side comparison of PZQ and Form B pharmacokinetics was performed; in particular the pharmacokinetic (PK) parameters of R- and S-PZQ following treatment with both the forms in mice were determined using a validated liquid chromatography (LC) tandem mass spectrometry (MS-MS) method. The details of the study and results are reported in Appendix C (4.6.3).

Physical stability All the samples were kept in a desiccator at RT temperature and tested over 12 months by PXRD and DSC analyses to evaluate possible changes in the solid state. Also, the stability upon additional grinding for 30 minutes at 25 Hz was tried. Moreover, PXRD patterns were collected upon *in situ* heating from 60 °C to 80 °C, at heating rate of 10 °C/min and stopping after each step for 1 hour using the same difractometer described in the PXRD paragraph.

Hot Stage Microscopy Raw PZQ and part of the samples were observed using a Reichert Biovar microscope with micro ocular MD-300 and using the software Webcam Companion for data collection. For the analysis, some grain of powder were positioned in the apposite sample holder and then observed upon heating from RT to about 150 °C.

Polarimetric analyses A Jasco P-2000 (Lecco, Italy) was used to evaluate the optical rotation of Form B and of raw PZQ using λ=589 nm and ethanol as the solvent, since when using $CHCl_3$, as suggested by Espinosa-Lara and coworkers[140] a high number of air bubbles were formed in the sample holder. The concentration of the sample solution was 1 g/100 ml.

4.1.2 Results and Discussion

As previously anticipated, the neat grinding of Praziquantel using the method described above, a polymorph was found, being, surprisingly, also the first anhydrous polymorph of the racemic drug. The powder recovered from the jars was firstly investigated towards the identification of possibile chemical modifications due to the grinding process using ^{1}H NMR, HPLC and polarimetric analysis. The NMR spectrum of raw

PZQ (in agreement with the reported one of Cedillo-Cruz and collaborators[140] was the same as Form B suggesting that no chemical changes were induced by grinding, except for the very poor amount of impurity found by HPLC (0.42 %) that was not found in raw PZQ. Nevertheless, the recovery of PZQ was of 99.52 %, completely acceptable and not exceeding the USP/FDA regulamentation. As for PZQ, in the polarimetric analysis no enantiomeric excesses were found since the [α] derived from the mean of three trials, near to zero, attested the racemic nature of both the compounds. In particular [α] of 0.5 $\pm$ 2.9 and 0.1 $\pm$ 1.6 were found respectively for raw PZQ and the polymorphic form. From there on the analysis confirmed the differences between the two solid forms, showing the singularity of the just discovered Form B.

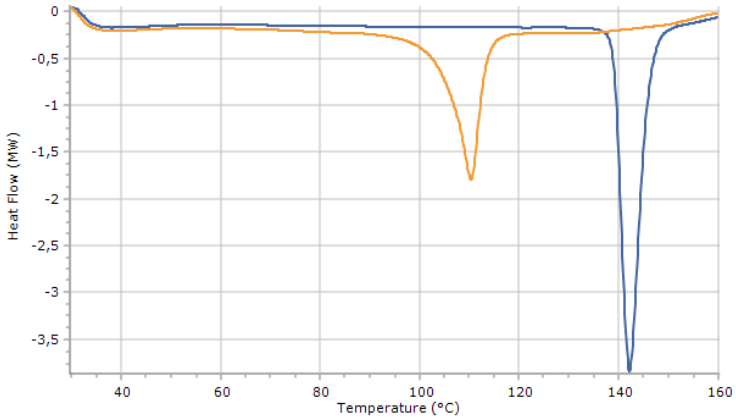

Figure 4.1: DSC traces of raw PZQ (blue) and Form B (orange).

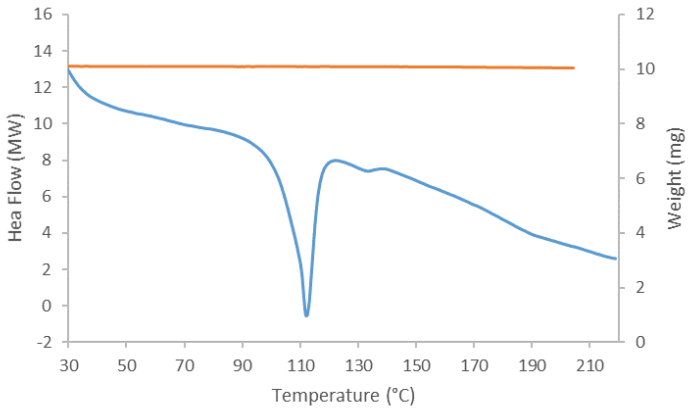

Figure 4.2: TGA analysis of Form B showing no weight loss (orange line).

At the calorimetric analysis Form B showed one endothermic event at 110.28 °C, corresponding to its melting point (61.50 J/g) almost 30 degrees below raw PZQ (142.17 °C, 103.29 J/g) as reported in Figure 4.1. Due to the high difference be-

tween the melting points of the native and polymorphic form, the behaviour of Form B could not be attributed to the melting of very small crystals via a Gibbs-Thompson effect[107], but more specifically to the difference between the lattice energies of the two forms. Additionally, to verify the absence of any dehydration events, a TGA analysis was conducted on Form B, which confirmed its anhydrous nature (Figure 4.2).

The PXRD pattern of Form B was completely different from PZQ, as reported in Figure 4.3. PZQ is characterized by a very intense peak at 4.01 of 2θ, followed by reflections at 6.32, 8.00-8.19, 14.73, 15.74, 16.40, 18.48, 19.30, 20.07 and 22.57 ° of 2θ. Differently, the first reflections of Form B can be found at 6.7 and 8.4, followed by others at 13.6, 15.7, 16.2, 16.4, 18.2, 19.6, 20.3, 21.6, 25.5 ° of 2θ. The central part of the pattern shows a partial peak broadening as typical of a powder obtained by grinding.

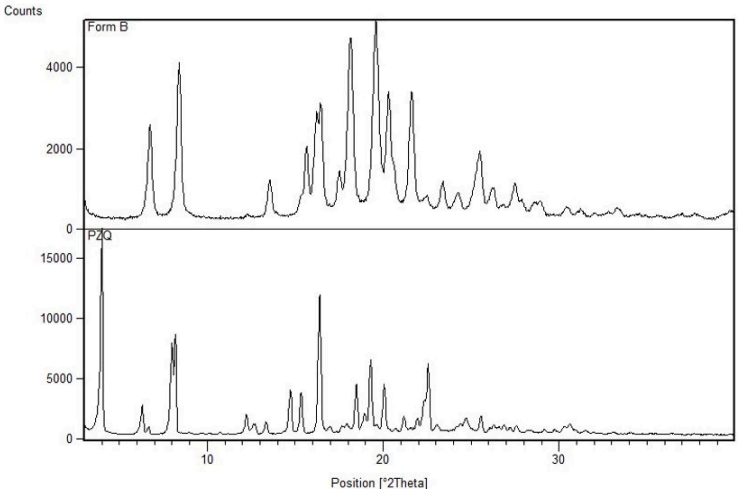

Figure 4.3: PXRD pattern of Form B (top) and raw PZQ (bottom).

To better understand the transition pathways of raw PZQ to Form B, subsequent PXRD analysis were performed on PZQ samples ground for 30 minutes, 1, 2, 3 and 4 hours, reported in Figure 4.4: the main PZQ peak at 4 of 2 θ gradually disappeared, while the reflections of Form B started to grow till completion after 4 hours. This behaviour was in agreement with previous DSC analysis on samples ground for 1, 2, 3 and 4 hours, reported in Figure 4.5, showing a gradual shift of the melting point from raw PZQ to Form B. This means that the grinding of PZQ led to the formation of a nanocrystalline phase of PZQ, then to a nearly amorphous state which subsequentely crystallized as Form B, in agreement to the mechanism of polymorph transition by neat grinding *via* amorphous transient phase as also attested, for wxample in the case of sulphathiazole[141].

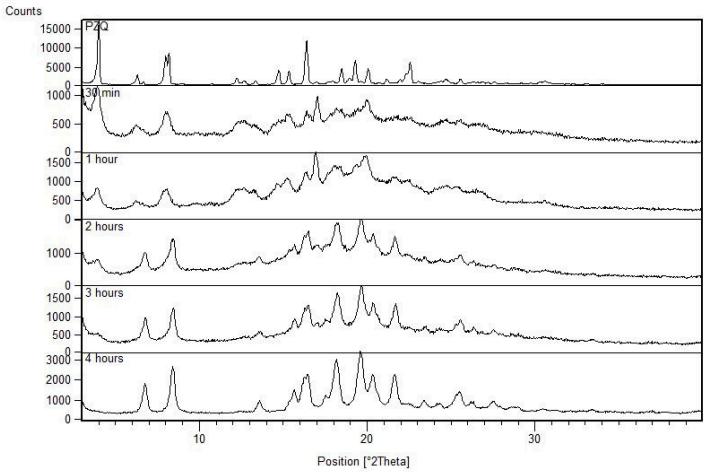

Figure 4.4: Subsequent PXRD patterns collected after grinding for different times at 25 Hz. From the top: raw PZQ, sample ground for 30 minutes, 1, 2, 3 and 4 hours.

The next step encompassed the crystal cell determination of Form B from the PXRD pattern. Due to the central nearly overlapped part of the pattern the identification of the crystal cell was very difficult and requested the collection of other PXRD data using more intense radiation. The pattern collected using the synchrotron radiation could be indexed using EXPO software[142], finding different plausible cells, of which the most reliable was a monoclinic C2/c cell with a volume of 3369.97 $A\hat{3}$. The first fitting of the pattern was made by Pawley refinement with a Rwp[3] of 1.52% obtaining a cell with the following parameters: a=21.991(1) A, b=5.8884(3) A, c=27.331(1) A, α=γ=90 °, β=107.787(5)° and density=1.232 gcm^3. Subsequentely, a simulated annealing process was performed using TOPAS software[143] and SIGBUG structure[39] (paragraph 1.2.3) as the molecular model, after removing the water molecule. The obtained asymmetric unit of Form B contained one PZQ independent molecule, with

[3]Rwp represents the weighted profile R-factor

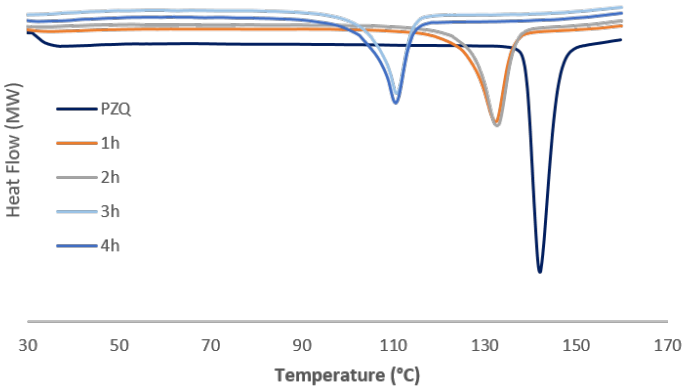

Figure 4.5: DSC traces of PZQ ground for 1, 2, 3 and 4 hours.

8 different symmetries. The Rietveld refinement (shown in Figure 4.6) had a R-Bragg factor of 1.96 % that represents quite a good fit between the calculated and the experimental pattern, also with a meaningful density of 66.6 % compared to the one of raw PZQ (67 %), calculated with PLATON VOID[144] routine. The obtained crystal structure was deposited in the Cambridge Structural Database[37] with reference name TELCEU01.

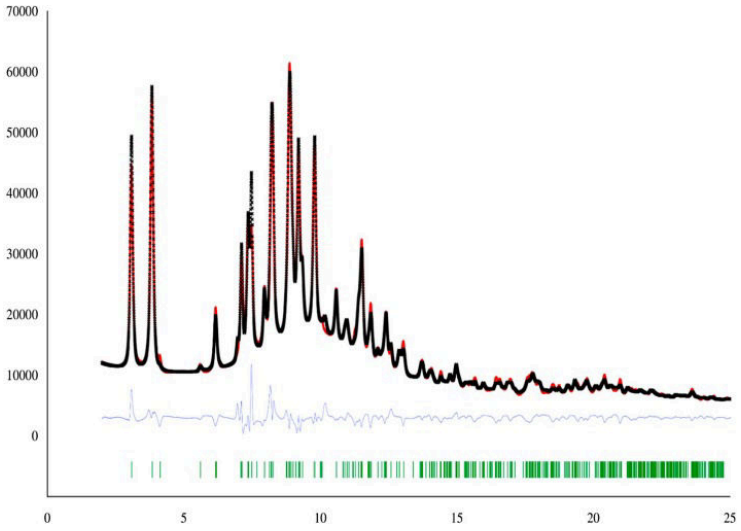

Figure 4.6: Rietveld refinement profile fit of Form B. The black curve is the experimental pattern collected at 0.700 A, in red the calculated one, in grey the residuals and the green ticks represent the reflections.

The unit cell of Form B is reported in Figure 4.7: as previously anticipated, the monoclinic C2/c cell hosts 8 PZQ molecules, one of which is crystallographically independent. The packing is therefore completely different from raw PZQ, where the

cell is triclinic with 4 independent molecules (paragraph 1.2.3). The obtained crystal structure was deposited in the Cambridge Structural Database[37] with deposition number: 1557658.

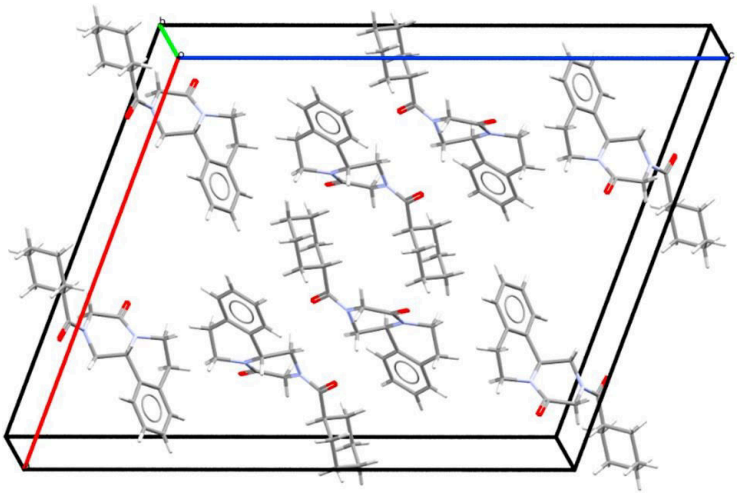

Figure 4.7: Capped stick representation of Form B monoclinic cell.

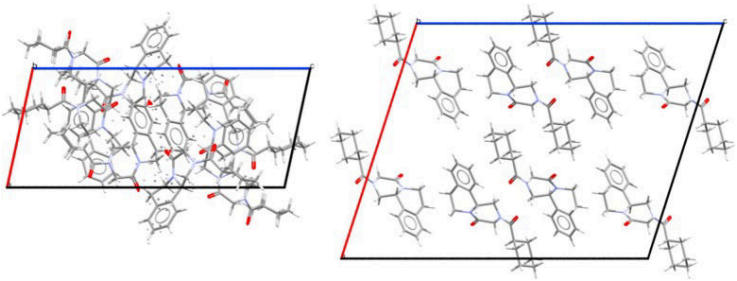

Figure 4.8: On the left the crystal packing of PZQ, on the right of Form B. These crystal packing images are from b axis, the complete packing visualization is reported in Appendix C, paragraph 4.6.2

The Solid-State NMR analysis of Form B was very useful for many reasons: firstly, the changes in the crystal packing were identified as shift of peaks position due to the different chemical and magnetic environment; then the shape of the peaks was related to the crystallinity of the sample and also indicated the number of molecules in the Asymmetric Unit (ASU). Both the spectra collected, ^{15}N and ^{13}C (Figure 4.9 and Figure 4.10) presented sharper (FWHM 100 Hz) and shifted peaks of about 0.2-3 ppm in Form B comparing to raw PZQ, thus indicating the high crystallinity and the different crystal packing. In the ^{13}C spectrum of Form B a single set of resonances was observed, confirming the single molecule in the ASU, differently from raw PZQ, which was characterized by splitted signals due to the 4 molecules in the ASU. Also, Form B was "polymorphically" pure since no signals of raw PZQ were found in the spectrum.

Finally, the the ^{13}C chemical shift observed for Form B were similar to the reported one for amorphous raw PZQ[75], suggesting the *anti* conformation of the drug when in the polymorphic form, which will be further investigated in the ATR-IR analyses.

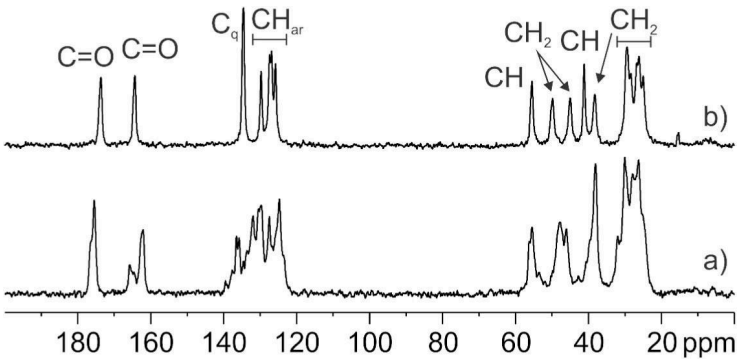

Figure 4.9: ^{13}C (100.656 MHz) spectra of raw PZQ (a) and Form B (b).

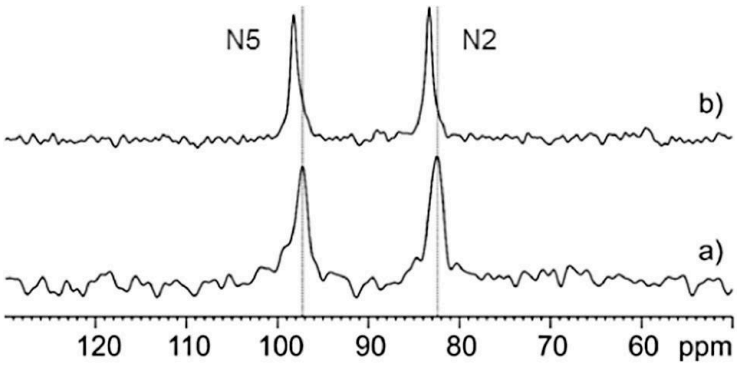

Figure 4.10: ^{13}N (40.55 MHz) spectra of raw PZQ (a) and Form B (b).

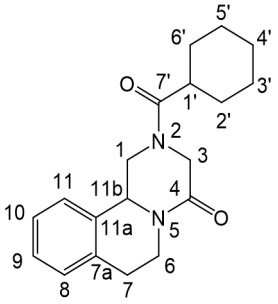

Figure 4.11: PZQ chemical structure and atoms numbering.

Another confirmation of the crystal structure proposed was obtained by DFT-D calculations on the atomic positions in the unit cell and the calculated SSNMR

chemical shift in good agreement with the experimental data, as reported in Table 4.1 (The details of the DFT-D calculations are reported in the Appendix C, section 4.6.1).

Table 4.1: Experimental and calculated chemical shift for SSNMR analyses of Form B compared to raw PZQ. The last column reports the chemical shift for SSNMR analysis of amorphous PZQ[75]. Atoms numbering refers to Figure 4.11.

Atom	Group	PZQ exp	Form B exp	Form B calc	PZQ[75] amorphous
		^{13}C			
7'	C=O	175.4, 176.2 sh	173.6	172.6	174.1
4	C=O	165.8, 164.6, 162.1	164.3	164.3	164.3
7a	Cq	137.7, 136.5	134.6	135.7	134.2
11a	Cq	135.7, 134.6	134.6	136.4	134.2
8	CH	129.7, 127.5, 123.8	129.8	130.5	127.0
11	CH	133.7, 132.0, 130.5	127.5	128.2	134.2
10	CH		126.9	127.0	127.0
9	CH		125.8	126.1	127.0
11b	CH	56.3, 55.5	55.5	54.6	55
3	CH_2	46.1	49.8	47.8	
1	CH_2	47.9	45.0	41.6	39.9
1'	CH	39.7	41.2	38.5	39.9
6	CH_2	38.1	38.3	35.1	39.9
6'	CH_2	32.0, 30.1, 27.9, 26.3, 25.3	29.4	26.1	
2'	CH_2		29.4	26.1	
7	CH_2		28.4	25.0	
4'	CH_2		26.7	24.0	
3'	CH_2		26.1	22.4	
5'	CH_2		25.0	21.6	
		^{15}N			
5	N	97.2	98.2	101.8	
2	N	82.4	83.3	86.7	

The Figure 4.12 shows the ATR-IR spectra of Form B compared to raw PZQ. The vibration observed for raw PZQ were in agreement with the data reported in literature by many authors[33, 67, 145–147], here resumed in Table 4.2. The vibrational frequencies of Form B were in general of little shifted with respect to raw PZQ, but the main interesting difference is in the carbonyl region between 1700 and 1600 cm^{-1}: raw PZQ had two bands at 1647 and 1624 cm^{-1} that become 1641 and 1633 cm^{-1} in Form B. These frequencies represent the symmetric stretching of the heterocyclic carbonyl and of the carbonyl near to the cyclohexyl group, as was also reported in literature[147]. The difference between the frequencies of the carbonyl groups was reported to be index of their spatial disposition: when in the *syn* conformation, the difference is higher, as in the case of raw PZQ, while in Form B is lower, indicating the presence of *anti* conformers, as it was also reported in literature[146], confirming once again the differences in the crystal packing between the two forms and the model proposed for Form B.

Table 4.2: Vibrational frequencies (cm^{-1}) of raw PZQ.

Frequency (cm^{-1})	Group assignment
3000-2900	stretching CH_2 and CH
1650-1720	stretching carbonyl groups, bending aromaticCH
1500-1400	stretching aromatic C, bending CH_2
760	bending aromatic CH

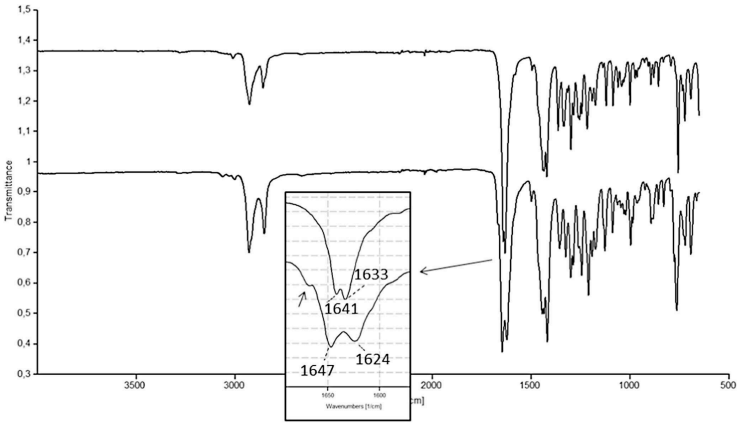

Figure 4.12: ATR-IR spectra of Form B (top) and raw PZQ (bottom).

Additional FT-IR spectra were collected with a resolution of 2 cm^{-1}, which confirmed the ATR-IR data and are reported in Figure 4.13.

Interestingly, also the morphology of PZQ changed after grinding and transition

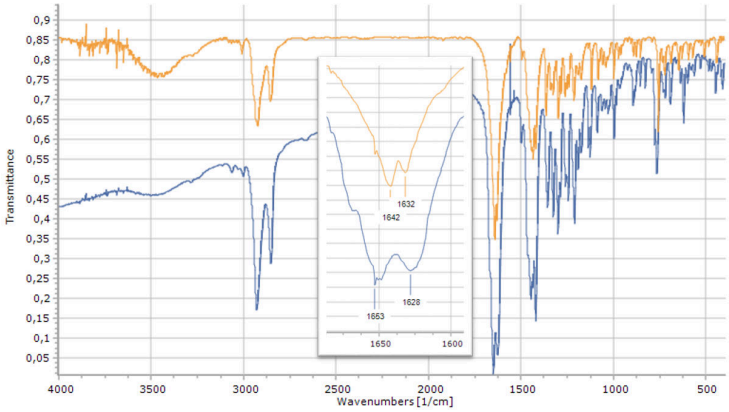

Figure 4.13: FT-IR spectra of raw PZQ (blue) and Form B (orange).

to Form B, both in habit and in size: agglomerates of very thin whiskers replaced the needle/acicular shape of native PZQ crystals as it is shown in Figure 4.14.

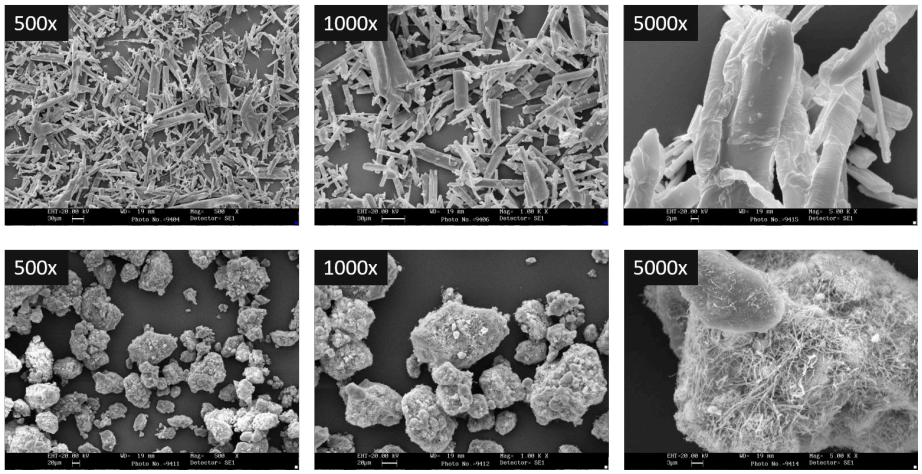

Figure 4.14: SEM images of raw PZQ (top) and of Form B (bottom).

The final part of the characterization was focused on the biopharmaceutical properties of Form B, i.e. solubility, intrinsic dissolution rate and *in vitro/in vivo* tests, to evaluate its suitability as a new PZQ formulation. First of all, the solubility of Form B at 20 °C was very high, comparing to raw PZQ, with a value of 281.31 ± 8.32 mg/L, double than the native phase (140.30 ± 9.26 mg/L). This effect was probably due to the different packing of the polymorphic form; anyway, to exclude any secondary effect, due to the powder fundamental properties, the intrinsic dissolution rate (IDR) was evaluated for raw PZQ and Form B, therefore operating with a costant solid surface. The IDR in water at 37 ∘C was significantly different between the two polymorphs (Figure 4.15)[4], confirming the distinction between the two phases: for

[4] $p<.0004$ Student's t test.

Form B a value of 62.2 ± 1.3 $\mu g/cm^2 min$ was found, while was 31.2 ± 0.6 in raw PZQ (each reported value is a mean of 3 tests).

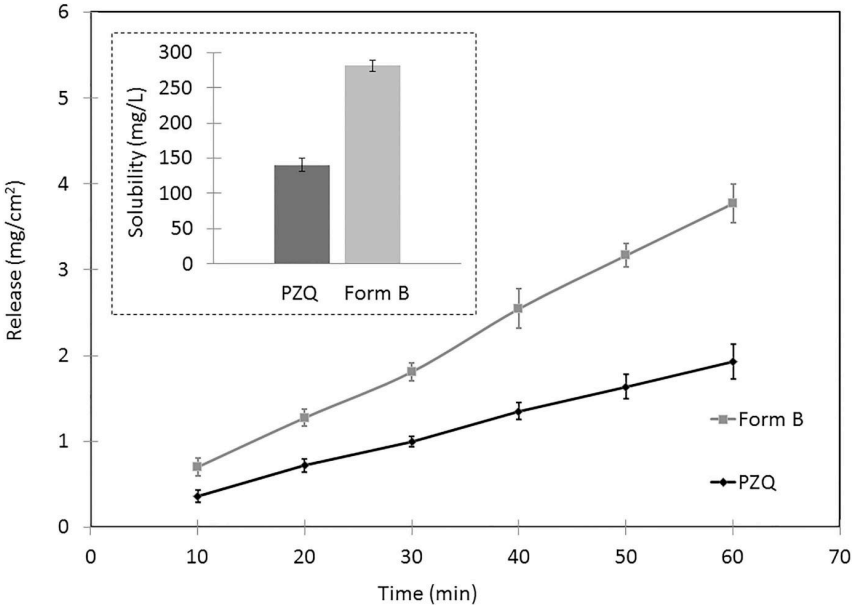

Figure 4.15: Solubility (frame) at 20°C and intrinsic dissolution rate (37 °C) of raw PZQ and Form B in water.

The activity of Form B was tested *in vitro* against adult *S. mansoni* and compared to the native drug. The IC_{50} of 0.165 μg/ml of starting PZQ was exceeded by Form B with a value of 0.135 μg/ml. Indeed, the efficacy of Form B was also tested *in vivo*: the polymorph and the raw drug were administered *per os* in 4 infected mice with a dose of 400 mg/kg and the pharmacological effect was evaluated after 49 days as the worm burden reduction. In the case of Form B the worms were totally knock-out, while in the case of raw PZQ about 2% of the parasites was left.
The polymorph demonstrated to be highly stable at room temperature in a desiccator for at least one year, as proved by DSC (Figure 4.17) and PXRD (Figure 4.16) traces with no significative differences over time.

Moreover, the high stability of the polymorphic form was confirmed also by performing *in situ* PXRD upon heating from 60 °C to 80 °C, where no changes were evidenced for all the duration of the analysis. Finally, when Form B was further ground for other 30 minutes at 25 Hz, no modifications of the solid-state were observed by PXRD traces, as reported in Figure 4.18.

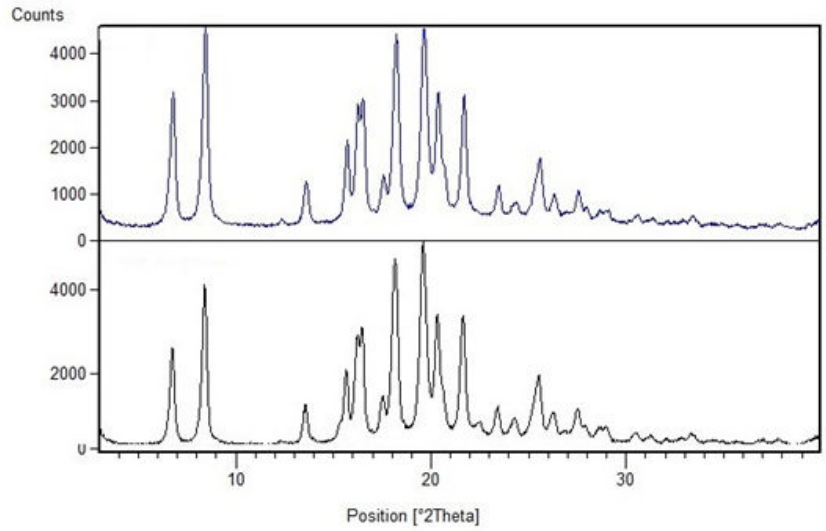

Figure 4.16: PXRD patterns of fresh Form B (top) and after one year storage (bottom).

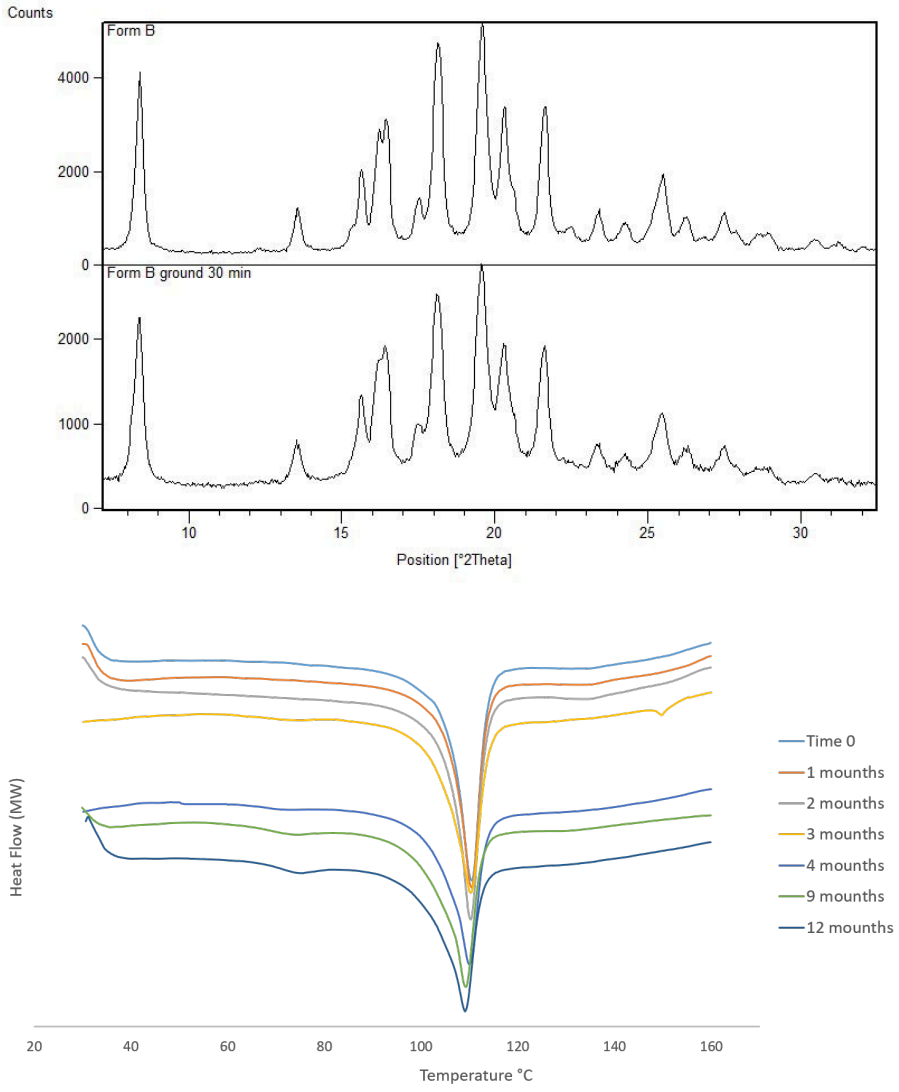

Figure 4.17: PXRD patterns of Form B ground for 30 minutes at 25 Hz compared to fresh sample and DSC traces of Form B in multiple analysis over time.

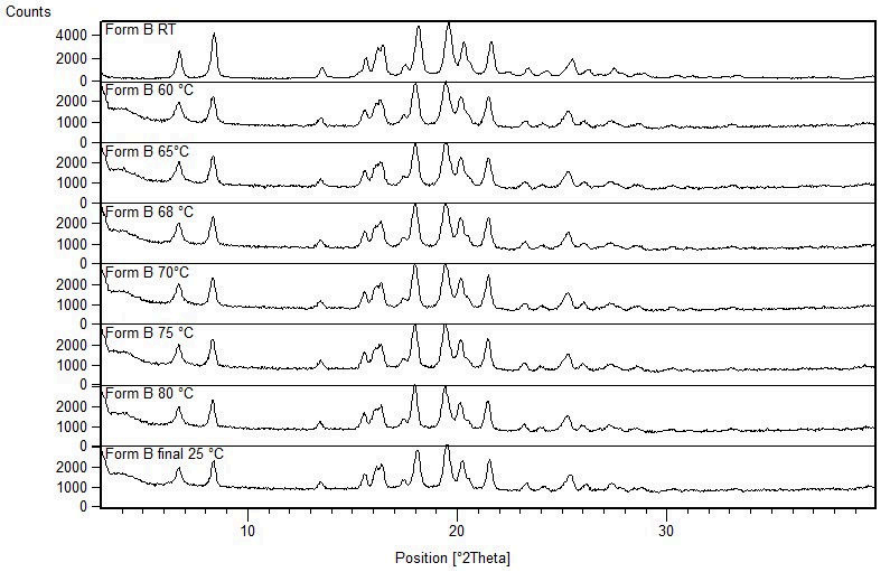

Figure 4.18: Physical stability of Form B upon heating by *in situ* PXRD from 60 to 80 °C.

4.1.3 Conclusions

The polymorphic Form B of PZQ was obtained after 4 hours neat grinding in a vibrational mill, with a quantitative conversion as demonstrated in the whole characterization of its solid-state comparing to native PZQ. The crystal structure was solved from the synchrotron X-ray powder diffraction pattern, resulting in a C2/c monoclinic cell completely different from the triclinic P-1 of raw PZQ. The solution proposed was validated by DFT-D calculations that also showed a perfect correlation between the calculated and the experimental ^{13}C SSNMR chemical shift. Apart from the structural characterization, the biopharmaceutical properties of Form B were really impressive: it had a double solubility and intrinsic dissolution rate comparing to raw PZQ, thus maintaining the *in vitro* and the *in vivo* activity, which was also slightly augmented. Thanks also to its physical stability, this polymorph represents an interesting alternative to commercial PZQ and therefore further studies are needed, from one side to evaluate the possible reduction in the dosage (due to the advantageous properties) and also to find a faster method of production and scale-up. For the moment the last updated tests on Form B activity and pharmacokinetics are reported in Appendix C (paragraph 4.6.3).

4.2 Exploring polymorph B formation: use of a Doehlert design

Polymorph B was produced by neat grinding for 4 hours in a vibrational mill, as reported in the previous section. In the following one, the nearby milling conditions of Form B production will be deeply investigated by using a design of experiments, and in particular a Doehlert design was chosen. This design, derived from the simplex optimization, has been frequently used in the optimization processes of many fields because of the uniformity of the points in the experimental region that permits to identify a response surface by means of a minimum of experiments[87, 89]. In this case it will be applied to explore the experimental domain of Form B milling conditions, defined by 2 process variables: time and frequency of milling. Generally, the Doehlert design can be proposed in the classical hexagonal form or in its rotated form, where each point is characterized by different values of the selected variables (Table 4.3), that is also the design chosen for this chapter.

Table 4.3: Classical and rotate Doehlert design for two variables[89, 148]

Classical		Rotated	
X1	X2	X1	X2
0.000	0.000	0.966	0.259
-1.000	0.000	-0.966	-0.259
-0.500	-0.866	0.258	0.966
1.000	0.000	-0.259	-0.966
0.500	0.866	0.707	-0.707
-0.500	0.866	-0.707	0.707
0.500	0.866	0.00	0.00

This design permitted not only to identify the optimal condition for the production of Form B, but also to discover other two phase groups, one corresponding to another anhydrous PZQ polymorph, Form C, and the other to a miscellaneous of various forms.

4.2.1 Materials and Methods

Materials

Praziquantel (PZQ, (11bRS)-2-(Cyclohexylcarbonyl)-1,2,3,6,7,11b-hexahydro-4-H -(pyrazino[2,1-a]isoquinolin-4-one)) was of Ph. Eur. grade and kindly donated by Fatro S.p.a. (Bologna, Italy). The HiPersolv Chromanorm methanol used for the HPLC analysis was of Ph. Eur. grade and purchased from VWR Chemicals (BHD PROLABO® Milano, Italy).

Methods

Design of the experiments: Doelhert design As previously anticipated, the experimental design comprehended two process variables: milling frequency (X_1) and time (X_2). The conditions of polymorph B formation (4 h grinding at 20 Hz) were chosen as the central point of the Doehlert matrix, while the experimental plan, prepared with NEMRODW software[90], varied from 3 to 5 hours and from 15 to 25 Hz. The rotated design was selected in order to maximize the differences between the variables levels[87]. The resulted matrix is reported in Table 4.4 and graphically in Figure 4.19, composed of 10 different experimental points, which were executed in double, and, to reduce the sistematic error, the trials were conducted in a random order, as reported in Table 4.4 (2^{nd} column).

Table 4.4: Doehlert matrix applied for the exploration of Form B nearby milling conditions.

Experimental number	Randomization	Variables	
		Time of milling (X_1)	Frequency of milling (X_2)
1	6	298	21
2	2	182	19
3	10	256	25
4	3	224	15
5	9	282	16
6	4	198	24
7	1	240	20
8	5	214	19
9	7	266	19
10	8	240	23

Preparation of the samples The sample were prepared in a Retsch mill MM400 using zirconium oxide jars and balls following the random order and the milling conditions reported in Table 4.4. In each jar the total amount of powder was 0.800 g and the number of grinding media was 3 with a diameter of 15 mm (Figure 4.20). After grinding the samples were removed and kept in closed vials in a desiccator at ambient temperature.

Powder X-Ray Diffraction The sample were analyzed by powder X-ray diffraction using a Panalytical X'Pert Pro Diffractometer with Ni-filtered Cu K(α) radiation (λ=1.5418 A), the detector was a RTMS X'celerator. The preparation of the samples

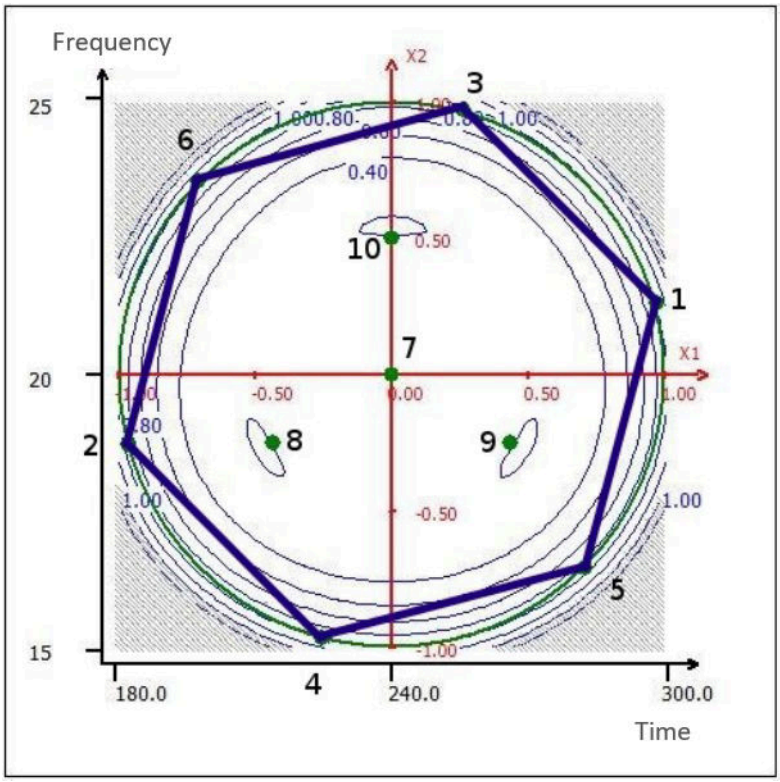

Figure 4.19: Graphical representation of the Doelhert matrix used.

Figure 4.20: Example of the jar partially filled with the powder to be ground and with the milling media.

consisted in pressing about 20-30 mg of the powder over a glass slide to have a flat surface. The data were collected in a 2θ range of 3-40 degree.

Differential Scanning Calorimetry Each sample was analyzed using a Mettler DSC TA 4000 (Greifensee, Switzerland) connected to a calorimetric cell Mettler DSC20 and using STARe software version 9.30 for data analysis. Prior to analysis the instrument was calibrated with Indium, Zinc and Lead for the temperature and with Indium for the enthalpy quantification; for each analysis, about 2 mg of the sample accurately weighted were placed in a 40 μm aluminum pan with perforated lid and heated at 10 °C/min from 30 to 160 °C under air atmosphere. The PZQ enthalpy of fusion was determined by integrating the area of the endothermic peak.

Thermogravimetrical Analysis Certain samples were analyzed by TGA using a Mettler Toledo TGA/SDTA851e: about 10-15 mg of the sample accurately weighted were placed in aluminum crucible (40 μl); then the heating was performed from 30 to 200 °C, with a heating rate of 10 °C/min.

Laser Light Scattering Analysis The analysis of the particle size were conducted using a Mastersizer 2000 laser light scattering (Malvern Instrument, Malvern United Kingdom). The samples were dispersed in distilled water plus 0.5 % w/w polysorbate 80 (Sigma Aldrich, Milan, Italy), sonicated for one minute and analyzed. This analysis was conducted thanks to the collaboration with Dr. E. Franceschinis of the Department of harmaceutical and Pharmacological Sciences of the University of Padova, Italy.

4.2.2 Results and Discussion

The experiments were performed following the randomized order proposed in Table 4.4 in double, since the mills allows the set-up of two jars at the same time. Interestingly, the presence of Form B as the exclusive phase was found only in EXP1, EXP2 and EXP7, with the characteristic endothermic peak at about 110 °C, while in experiments 3, 6, 8 and 10 the unique melting peak was found at about 106-107 °C, suggesting the presence of another phase, later referred as Form C; finally in experiment 4, 5 and 9 a mixture of polymorphic and raw forms was found. A graphical representation of these results is presented in Figure 4.21, while the DSC traces can be summarized in Figure 4.22

The characterization of the samples obtained will be now presented in details, but the complete investigation of Form C is reported to the dedicated section in last part of the chapter (paragraph 4.3).

In the thermal analysis (shown in Figure 4.22) raw PZQ is characterized by one single endothermic peak corresponding to its melting point at 142.56°C (103.29 J/g). The already described polymorph B has a melting point of 110.28 °C (61.50 J/g) which was encounted also in the experiment 1 and 2 of the design, but in the latter

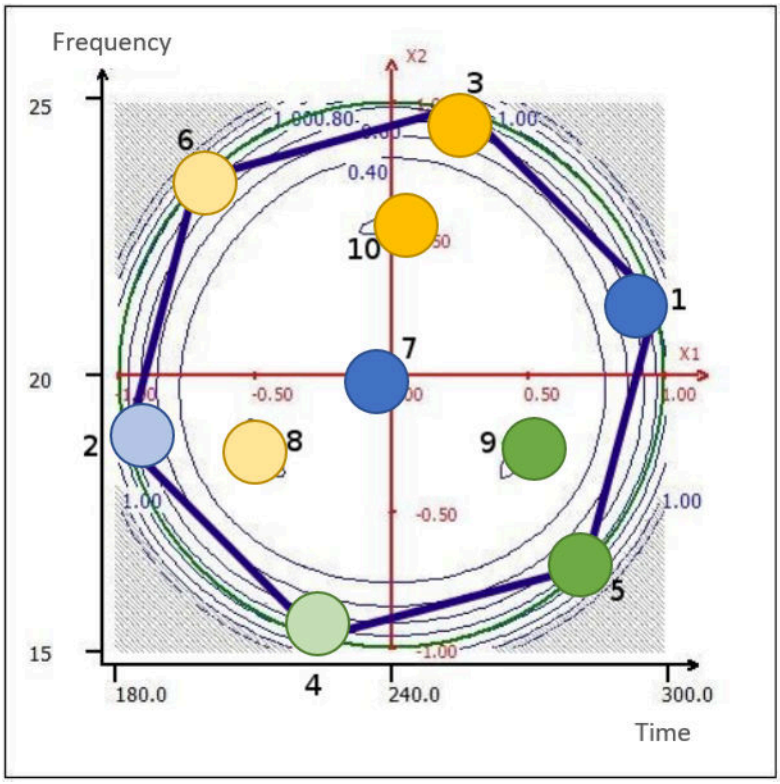

Figure 4.21: Graphical representation of the results obtained: in blue the polymorphic Form B, in yellow the polymorphic Form C and in green the mixture of different forms. The light colors refers to a poor yield of the experiments.

the ripetibility and the melting enthalpy were not as good as in points 7 and 1. Interestingly, experiments 3, 6, 8 and 10 evidenced the presence of an unknown polymorph, called Form C, that had a melting point of about 106-107 °C (about 65-70 J/g). As in point 2, experiment 6 and 8 did not reproduce a constant result, evidencing the high variability in the process outcome when grinding at temperature near to the Tg of the system. In fact, as previously mentioned in this thesis (paragraph 3.1) and reported by other authors[14], in this condition the behavior of the system highly depends on the milling conditions. In this case, the experiments with lighter colors in Figure 4.21 were performed using lower frequency and/or milling time, therefore the temperature reached inside the jar was expected to be in the PZQ Tg range, basing on the previous temperature measurements reported in paragraph 3.1. This fact increased the uncertainty of the milling outcome, extremely variable in that temperature range.

Experiments 4,5 and 9, located in the bottom part of the scheme (Figure 4.21) presented thermograms with various endotherms: PZQ was found at 132.81 °C, due to the nanocrystalline form after to the grinding process, therefore a shift in the melting point respect to the raw material was expected via Gibbs-Thompson effect[107].

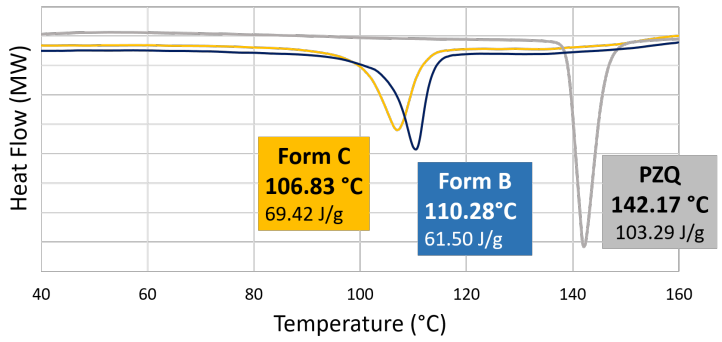

Figure 4.22: DSC thermograms for polymorph B, C and raw PZQ.

Then, other two weak events were frequently evidenced at around 60-70 °C and around 98 °C; in particular the first of them could be attributed to the presence of a certain humidity in the sample, as demonstrated by the TGA analysis where a weight loss of 1.35 % was found around 70 °C (shown in Figure 4.23 and Table 4.5), which was not evidenced in the analysis of the polymorphic forms (experiment 7 and 10), thus confirming that they are anhydrous solid forms. Due to the presence of multiple solid forms of praziquantel, a correct stechiometry was not found. The presence of water could be attributed to the high higroscopicity of PZQ[32, 149] and, once againg, to the fact that when grinding at low frequency the temperature reached inside the jars is not as high as when working at 20 or 25 degrees (probably not exceeding 30 degrees, as it was measured and reported in paragraph 3.1.3), thus not permitting a certain evaporation of water. This fact was further confirmed by literature, where even the water present as moisture can favour the crystallization of an amorphous solid[11]. Unfortunately, do to the very low enthalpy of the event correlated to water, no changes could be observed using a hot-stage microscopy.

Table 4.5: Summary of the TGA analyses of selected samples.

Sample	Weight loss (%)	Temperature (°C)
EXP 7	0.00	-
EXP 10	0.00	-
EXP 5	1.35	70
EXP 9	1.35	70

The PXRD analyses were fundamental to confirm the above suggestions about the division of three behaviors. The groups are reported separately in Figure 4.24 for Form

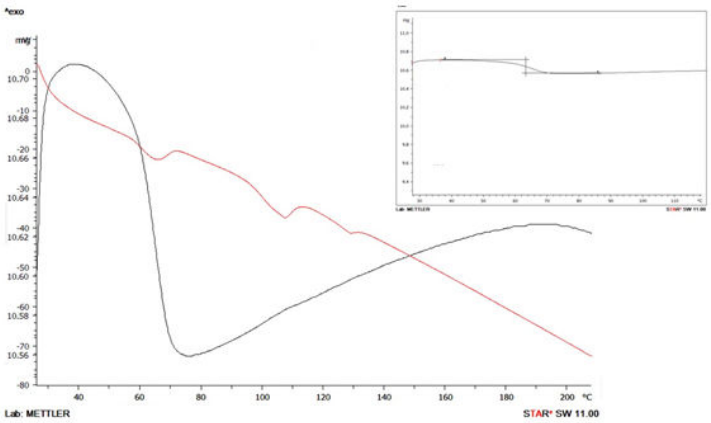

Figure 4.23: TGA thermogram of the miscellaneous group: in red the heat flow, in black the weight loss.

B, Figure 4.25 for Form C and Figure 4.26 for the mixture. Moreover PXRD analysis were useful to compare the results obtained with the already known structures of PZQ, in particular of the two enantiomeric hemihydrate. The dramatic difference that permitted the immediate identification of the presence or not of PZQ was represented by the very intense diffraction peak at about 4° of 2θ, which completely disappeared in the groups of Form B and Form C. In these patterns, the PXRD traces showed the crystallinity of the samples, while in the miscellaneous samples (4, 5 and 9), the patterns were characterized by a partial broadening of the signals. Experiments 1 and 2 were completely superimposable with experiment 7, as shown in Figure 4.24, and the reflections observed corresponded to polymorph B. In the case of experiments 3, 6, 8 and 10 the PXRD spectra were very similar to polymorph B, but a deep analysis highlighted some peculiar differences that permitted to identify the new polymorphic form, namely Form C. The main different peak were found at 6.98, 8.55, 15.42, 19.82, 22.56 with also the absence of the peak at 20.37 ° of 2θ, found in Form B.

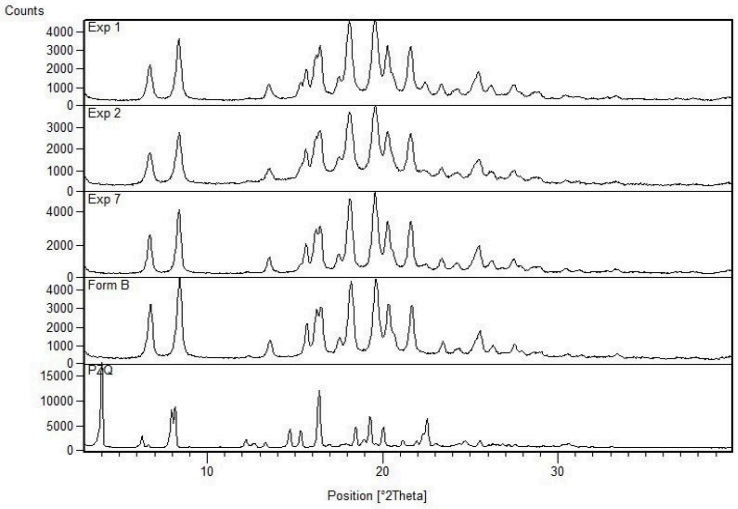

Figure 4.24: PXRD patterns of the samples of the Doehlert matrix, from the top: Exp 1, 2, 7, Form B and raw PZQ.

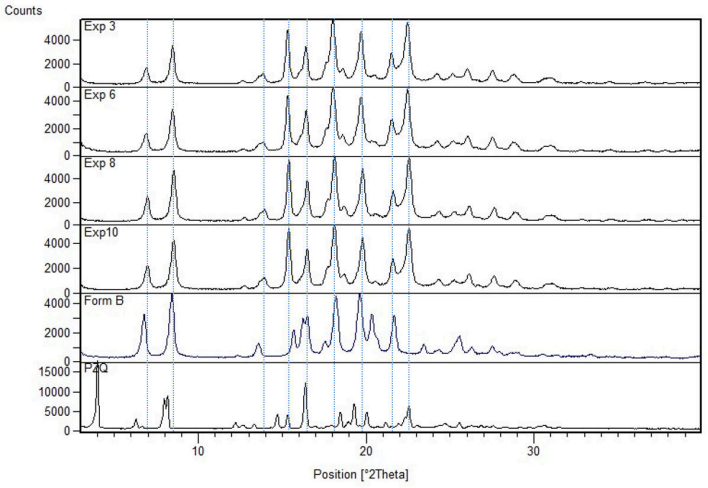

Figure 4.25: PXRD patterns of the samples of the Doehlert matrix, from the top: Exp 3, 6, 8, 10 and raw PZQ.

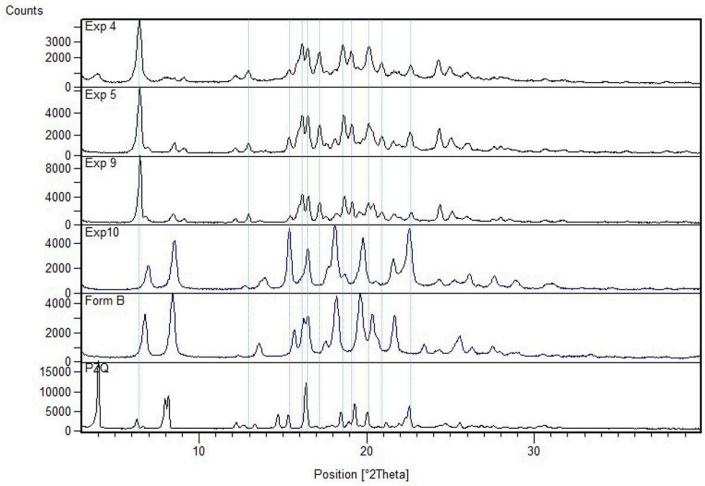

Figure 4.26: PXRD patterns of the samples of the Doehlert matrix, from the top: Exp 4, 5, 9, Form B, Form C and raw PZQ.

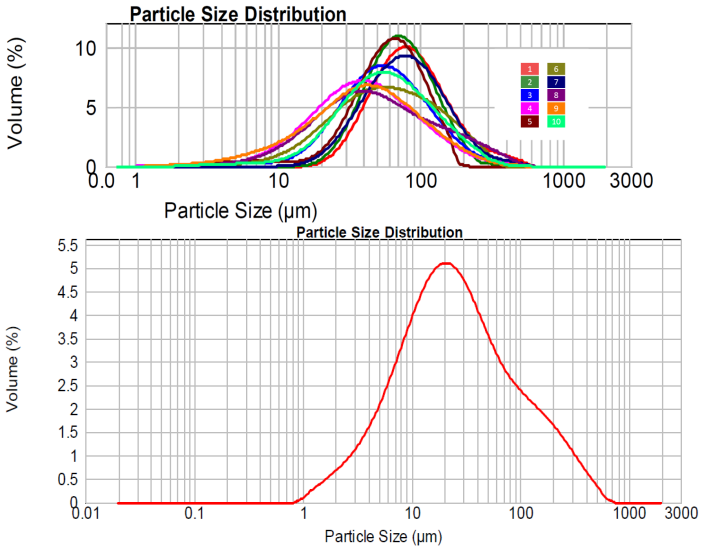

Figure 4.27: Particle size distribution of the Doelhert matrix experiments (top) and of raw PZQ (bottom).

With the aim of searching for a possible correlation between the different forms and the particle size as reported by Belenguer and collaborators[95], a laser light scattering analysis was performed for each sample of the Doehlert matrix. The superimposition of the curves found is reported in Figure 4.27.

The distribution of the samples particle size was lightly different between the three groups. Praziquantel raw has a median of 23.989 μm (Figure 4.27, down) with a slightly hinted bimodal shape. Even though a precise division could not be based on the particle size distibution, a certain trands among the samples could be identified as the following: Form B presented the higher values, ranging around a d(0.5) of 70-75 μm while in the case of polymorph C the d(0.5) was smaller (around 55 μm). The lowest values for d(0.5) were found in the case of the mixtures (around 40 μm). This analysis suggested a certain difference between the polymorphic outcome and the particle size of the samples and, looking at the shapes of the curves, a higher uniformity of the particles resulted in a polymorphic form, while in the case of the mixture the presence of different solid forms was confirmed by the larger particle size distribution.

4.2.3 Conclusions

The use of the Doehlert matrix for the experimental design was successful in identifying the favorable conditions to form PZQ polymorph B, found in experiments 1, 2 and in 7, the central point of the design. Due to the low repetibility of point 2 and to the higher milling time of point 1, the milling conditions of experiments 7 were confirmed to be optimal ones to achieve the formation of Form B. Interestingly, this study permitted to discover another polymorphic form, named Form C, in the nearby milling conditions of Form B that will be fully described in the next paragraph. Additionally, the other experimental points were characterized by the formation of a mixture of different forms including a possibile hydrated form, further investigated in the next chapter. This part of the study represents a further confirm of the incredible advantages of using a DOE to plan the experiments in a laboratory, avoiding the waste of money, time and substances and achieving interesting results in very short times.

4.3 Praziquantel polymorph C

In the previous part of this chapter the experimental design permitted to identify a new PZQ polymorph, hereby called Form C, very similar to the Form B described in paragraph 4.1. This section will focus on the in-depth solid-state characterization of the polymorph C, including the crystal structure solution and the analysis of the biopharmaceutical properties.

4.3.1 Materials and Methods

Materials

Praziquantel (PZQ, (11bRS)-2-(Cyclohexylcarbonyl)-1,2,3,6,7,11b-hexahydro-4-H -(pyrazino[2,1-a]isoquinolin-4-one)) was of Ph. Eur. grade and kindly donated by Fatro S.p.a. (Bologna, Italy). The HiPersolv Chromanorm methanol used for the HPLC analysis was of Ph. Eur. grade and purchased from VWR Chemicals (BHD PROLABO® Milano, Italy). Ethanol (96%, Sigma-Aldrich, Milan, Italy).

Methods

Preparation of Form C Form C was obtained by neat grinding of PZQ in a Retsch MM400 vibrational mill (Retsch, Germany) for 4 hours at 23 Hz, using zirconium oxide jars of 35 mL and three balls (ϕ=15 mm). After milling, the samples were collected and stored in a desiccator in the dark at room temperature.

Differential Scanning Calorimetry Each sample was analyzed using a Mettler DSC TA 4000 (Greifensee, Switzerland) connected to a calorimetric cell Mettler DSC20 and using STARE software version 9.30 for data analysis. Prior to analysis the instrument was calibrated with Indium, Zinc and Lead for the temperature and with Indium for the enthalpy quantification. In each analysis, about 2 mg of the sample was accurately weighted, placed in a 40 μm aluminum pan with perforated lid and heated 10 °C/min from 30 to 160 °C under air atmosphere. Form C enthalpy of fusion was determined by integrating the area of the endothermic peak.

Thermogravimetrical Analysis The thermogravimetric analysis was conducted using a Mettler Toledo TGA/SDTA851e: about 10-15 mg of the sample accurately weighted were placed in aluminum crucible (100 μL); then the heating was performed from 25 to 220 °C, with a heating rate of 10 °C/min under nitrogen atmosphere. To calculate the weight loss from the weight-temperature diagram, STARe software 11.00 was used.

Powder X-Ray Diffraction The sample were analyzed by powder X-ray diffraction using a Panalytical X'Pert Pro Diffractometer with Ni-filtered Cu Kα radiation (λ=1.5418 A), the detector was a RTMS X'celerator. The preparation of the samples consisted in pressing about 20.30 mg of powder over a glass slide to have a flat surface. The data were collected in a 2θ range of 3-40 degree.

Synchrotron X-ray powder diffraction Thanks to the collaboration with Dr. N. Demitri and Dr. L. Gigli of Elettra Sincrotrone in Trieste, Form C was also analyzed using the X-ray diffraction beam line XRD1[137] in order to obtain a diffraction powder suitable for the crystal structure solution due to the improved resolution and signal to noise ratio comparing with the data from the conventional laboratory source. Form C was packed in a borosilicate capillary with a diameter of 300 μm and the pattern was collected at RT temperature using a monochromatic wavelength of 0.700A (17.71 KeV), 200*2000 μm^2 spot size and a Dectris Pilatus 2M as the hybrid-pixel area detector. The pattern was then integrated using Fit2D program[138], after calibrating the hardware setup with LaB6 standard reference powder (NIST 660a).

Solid-state NMR analyses Solid-state NMR measurements were performed[5] on a Bruker Avance II 400 instrument operating at 100.65 and 40.55 MHz for ^{13}C and ^{15}N nuclei, respectively. Cylindrical 4 mm o.d. zirconia rotors with a sample volume of 80 μL were employed and spun at 12 (^{13}C) and 9 (^{15}N) kHz. All experiments employed the RAMP-CP pulse sequence (^{1}H 90° pulse=3.05 μs) with the TPPM ^{1}H decoupling with a rf field of 75 kHz during the acquisition period. 124 (^{13}C) or 5700 (^{15}N) transients were acquired with 3 (^{13}C) or 4 (^{15}N) ms of contact time and a relaxation delays of 20 s. ^{13}C and ^{15}N chemical shifts were referenced with the resonance of hexamethylbenzene (^{13}C methyl signal at 17.4 ppm) and ($NH_4)_2SO_4$ (^{15}N signal at -355.8 ppm with respect to CH_3NO_2).

DTF calculations The crystal structure proposed for Form C was validated by performing periodic lattice calculations using the density functional theory (DFT). All the details of this part, performed by Dr. P. Cerreia Vioglio of the Aix-Marseille Université (France) are reported in the appendix C (section 4.6.4).

Determination of drug recovery after milling The content of PZQ was assayed by means of a reverse-phase HPLC-UV[6] by adapting a method already reported in literature[91]; the system had two delivery pumps (LC-10 ADVP, Shimadzu, Japan), an autosampler (SIL-20A, Shimadzu, Japan) a UV-vis detector (SPD-10Avp, Shimadzu, Japan) and the data were acquired at a fixed wavelength of 220nm using an interface (SCL-10Avp, Shimadzu, Japan) and analyzed with Ez-Star software; the column used was a Kinetex 5 um c18 (150 x 4.60mmm, Phenomenex, Bologna). The mobile phase used was a mixture of methanol:water (65:35 v/v), purged at 1 ml/min. PZQ retention time was 5.5 min while the total run time for each sample was set at 12 min. Prior to analysis, a linear calibration curve with r^2=0.99996 was obtained for PZQ under these conditions using different concentrations of the drug from 0.3 to 10 mg/mL. Each day, a standard solution (with a concentration of 2.5 mg/L) was prepared by dissolving about 10 mg of PZQ accurately weighted in Methanol of HPLC grade (20

[5] In collaboration with prof. M.R. Chierotti of the Department of Chemistry, University of Turin (Italy).

[6] In collaboration with proff. N. Passerini and B. Albertini of the Department of Pharmacy and Biotechnology of the University of Bologna (Italy) as well as for the water solubility studies.

mL) and diluting the solution 1:200 with the mobile phase. Moreover, two additional calibration curve were obtained respectively for the relative impurity indicated in the Eur. Ph. (Ed. 8.0)[32], impurity A (r^2=0.9993) and impurity B (r^2=0.9994), which were identified at the retention time of 3.45 min and 11.2 min. The reference solution did not report any of these impurities.

FT-IR spectroscopy FT-IR spectroscopy was performed using a Perkin Elmer System 2000 FT-IR (Perkin-Elmer, Monza, Italy). The samples were mixed with anhydrous KBr (Anhydrous potassium bromide UVASOL, Sigma-Aldrich, Milan, Italy) in an agate mortar and then pressed with an hydraulic press for 2 minutes at 10 Ton to obtain homogeneous and transparent discs. The analysis was conducted form 400 to 4000 $cm^(-1)$ with a resolution of 2 cm^{-1} and total scan number of 10.

Environmental Scanning Electron microscopy The morphology of Form C was studied by E.S.E.M. (Quanta 200 FEI-XRF embedded).

Solubility measurements To analyze the water solubility of Form C and compare it with raw PZQ, saturated solution of the corresponding samples were prepared in distilled water and kept under agitation in the dark for 48 hours at 20 °C. Subsequently the solutions were filtered with a membrane of 0.2 μm pore size, diluted 1:200 with the mobile phase (65 % MeOH-35 % H_2O) and injected in the HPLC instrument using the method previously described. For each sample, three different analyses were conducted and the average was taken as the corresponding data.

Dissolution studies For the dissolution tests of Form C, 900 ml of distilled water kept at 37 ±1 °C were used as dissolution medium and uniformity conditions were ensured by an impeller (stirring rate 100 rpm). The determination of PZQ concentration was performed by using a fiber optic apparatus (HELLMA, Milano, Italy) connected to a UV-spectrophotometer (ZEISS, Germany) and managed with an user interface (Aspect Plus, Carl-Zeiss, Oberkochen, Germany). Prior to analysis, the peak of the UV-wavelength absorbance of PZQ was identified at 217.10 nm. The quantity of the sample to be introduced was calculated in order to achieve the sink conditions (with a total concentration ≤0.20 Cs), resulting in 20 mg and the quantity of PZQ dissolved was assayed in continuum for 60 minutes (one scan for minute). The calibration curve (R^2=0.9762) was prepared as follows: 10 mg of PZQ were well dissolved in ethanol corresponding to a concentration of 1g/1L; then, subsequent dilutions with distilled water were prepared in the range of 1-30 mg/L, in each case not exceeding the 5% of ethanol. Each sample was analyzed in triplicate and the resulted mean±SD was considered as the final value.

Efficacy in *in vitro* The *in vitro* tests were performed at the Swiss Tropical and Public Health Insitute (Switzerland, thanks to the collaboration with J. Keiser). The samples were tested in their efficacy against adult *S. mansoni* by preparing different

concentrations, ranging from 0.021 to 0.33 μg/L in which adult Schisosomes were incubated for up to 72 hours. By using an inverse microscope (Carl Zeiss, Germany, magnification 80x) all the alterations of morphology, motility and viability were observed and the IC_{50} value was calculated with CompuSyn software.

Physical stability All the samples were kept in a desiccator at RT temperature and tested over 12 months by DSC analyses to evaluate possible changes in the solid state. Also, the stability of Form C was tested by PXRD upon grinding for additional 60 minutes at 25 Hz.

Polarimetric analyses A Jasco P-2000 (Lecco, Italy) was used to evaluate the optical rotation of Form C and of raw PZQ using λ=589 nm and ethanol as the solvent (1g/100 ml), according to the method proposed by Cedillo-Cruz and coworkers[140], slightly modified by using ethanol instead of $CHCl_3$ to avoid air bubbles formation in the sample holder.

4.4 Results and Discussion

As previously reported, PZQ tendency to polymorphic formation was discovered by milling the drug by itself for long periods (i.e. 3-4 hours) and the Doehlert design described in 4.2 revealed the formation of another anhydrous polymorph of PZQ, Form C. This polymorph could be achieved in the conditions of EXP 3 and 10 of the design in the same paragraph 4.2, corresponding respectively to 256 minutes grinding at 25 Hz and 4 hours at 23 Hz. Nevertheless, the conditions of EXP 10 were taken as the standard ones, due to a minor grinding time and frequency and a higher crystallinity. Similarly to Form B, the long milling time of the drug itself did not favour any API degradation, since the recovery was of 100.00%, as assessed by HPLC analysis. The thermal analysis evidenced the melting point, found at 106.83 °C (69.42 J/g), as reported in Figure 4.22, well recognizable even if closed to polymorph B. Also, its anhydrated nature was confirmed in the TGA analysis without any sign of weight loss (reported in Table 4.5). The PXRD pattern of Form C, even if very similar to Form B, was characterized by reflections at 6.98, 8.55, 12.76, 13.96, 15.42, 16.52, 18.12, 19.82, 21.62, 22.57, 26.15, 27.65 and 28.92 ° of 2θ as reported in Figure 4.28, which highlight the differences between the forms.

As for Form B, the crystal structure of Form C was solved from the synchrotron powder X-ray diffraction pattern collected at Elettra synchrotron in Trieste. The cell was indexed using EXPO2014[142] and TOPAS V5[143] was used for the simulated annealing process, but being much more easier using Form B as the model. The process led to a Rietveld refinement with Rwp of 0.025, shown in Figure 4.29. The resulted monoclinic cell (reported in Figure 4.30) has space group C2/c and the following parameters: a=28.477(7) A, b=5.9100(10) A, c=26.980(2) A, α=γ=90 °, β=107.87(5)°, density =1.26 g/cm^3 and volume 3304.6 A^3.

The cell has one crystallographically independent molecule in the asymmetric unit,

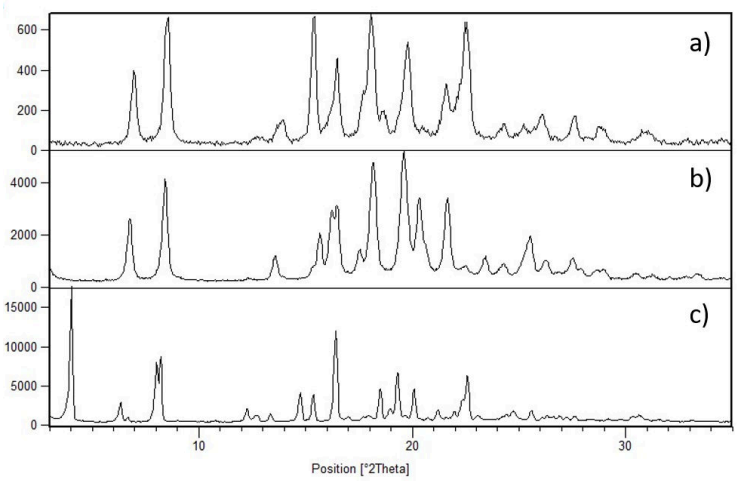

Figure 4.28: PXRD patterns of Form C (a), Form B (b) and raw PZQ (c).

as also confirmed in the SS-NMR (Figure 4.31) in which the differences between the packing of Form B and C were clearly visible and very different form raw PZQ. In fact, similarly to Form B, in Form C only one set of resonance is visible, while raw PZQ is characterized by splitted signals, clearly evident in particular for the heterocyclic carbonyl at 164 ppm. The powder was also highly crystalline, since the peaks were sharp, and also they were shifted from the ones of raw PZQ. GIPAW-DFT calculations were performed on the proposed crystal structure of Form C (reported in Appendix C (paragraph 4.6.4) which confirmed the structure proposed showing a perfect superimposition of the crystal cell obtained from the Rietveld refinement and the DFT-calculated one. Also, the calculated chemical shift were in excellent agreement with the experimental data, as reported in Table 4.6.

The crystal structure suggested a racemic nature for Form C, which was confirmed by polarimetric analysis, presenting a [α] of 0.0144±0.0295 (n=3).

The FT-IR spectroscopy of Form C, even if collected at 2 cm^{-}1 (Figure 4.32 was about the same as Form B, highlighting the close relationship between the polymorphs found and the differences with raw PZQ, as previously reported, in particular for the region corresponding to the stretching of the carbonyl group. Also in the case of Form C, the conformers were in the *anti* position, as demonstrated by the lower frequency difference in the carbonyl groups (1642.3 and 1631.8 cm^{-1}), comparing to starting PZQ (1651.2 and 1627.7 cm^{-1}), presenting the *syn* conformation[146], indicated in the frame of Figure 4.32.

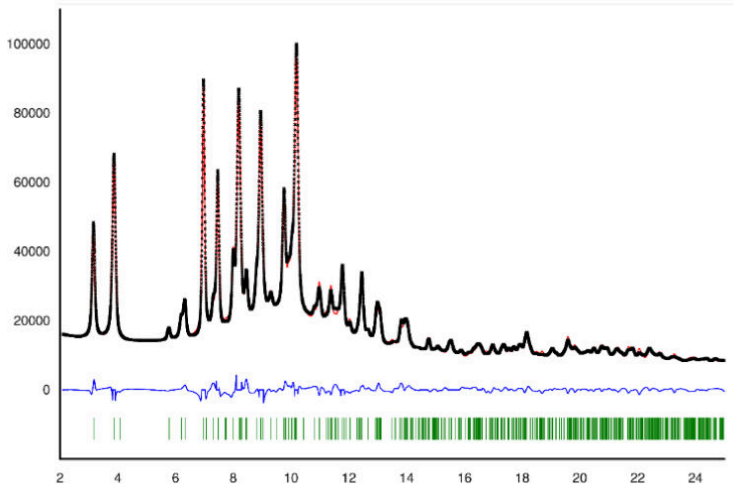

Figure 4.29: Rietveld refinement of Form C: in red the calculated pattern, in black the experimental one. The residues are shown in blue and the reflections in green.

Figure 4.30: Capped-stick representation of Form C unit cell.

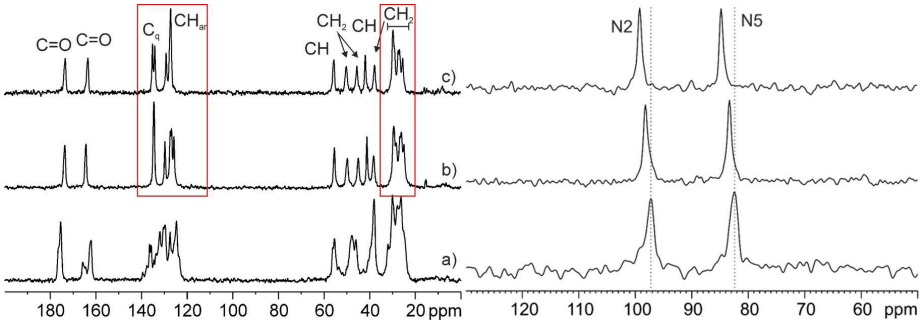

Figure 4.31: ^{13}C 100.65 MHz CPMAS spectra of Form C (c), Form B (b) and raw PZQ (a) recorded at 12 KHz with principal groups assignments and relative ^{15}N 40.55 MHz CPMAS spectra recorded at 9 KHz.

Table 4.6: Experimental and calculated chemical shift for SSNMR analyses of Form C compared to raw PZQ and Form B. Atoms numbering refers to Figure 4.11.

Atom	Group	PZQ exp	Form B exp	Form C exp	Form C calc
		^{13}C			
7'	C=O	175.4, 176.2 sh	173.6	173.3	173.8
4	C=O	165.8, 164.6, 162.1	164.3	163.4	163.2
7a	Cq	137.7, 136.5	134.6	135.1	137.8
11a	Cq	135.7, 134.6	134.6	134.0	136.9
8	CH	129.7, 127.5, 123.8	129.8	129.1	131.1
11	CH	133.7, 132.0, 130.5	127.5	127.5	129.3
10	CH		126.9	127.1	128.5
9	CH		125.8		128.1
11b	CH	56.3, 55.5	55.5	55.5	56.0
3	CH_2	46.1	49.8	50.1	49.3
1	CH_2	47.9	45.0	45.5	43.7
1'	CH	39.7	41.2	41.8	40.7
6	CH_2	38.1	38.3	37.7	35.3
6'	CH_2	32.0, 30.1, 27.9, 26.3, 25.3	29.4	27.4	27.2
2'	CH_2		29.4	29.6	28.2
7	CH_2		28.4	29.1	27.4
4'	CH_2		26.7	25.4	24.5
3'	CH_2		26.1	26.8	25.4
5'	CH_2		25.0		23.5
		^{15}N			
5	N	97.2	98.2	99.2	99.5
2	N	82.4	83.3	84.8	84.6

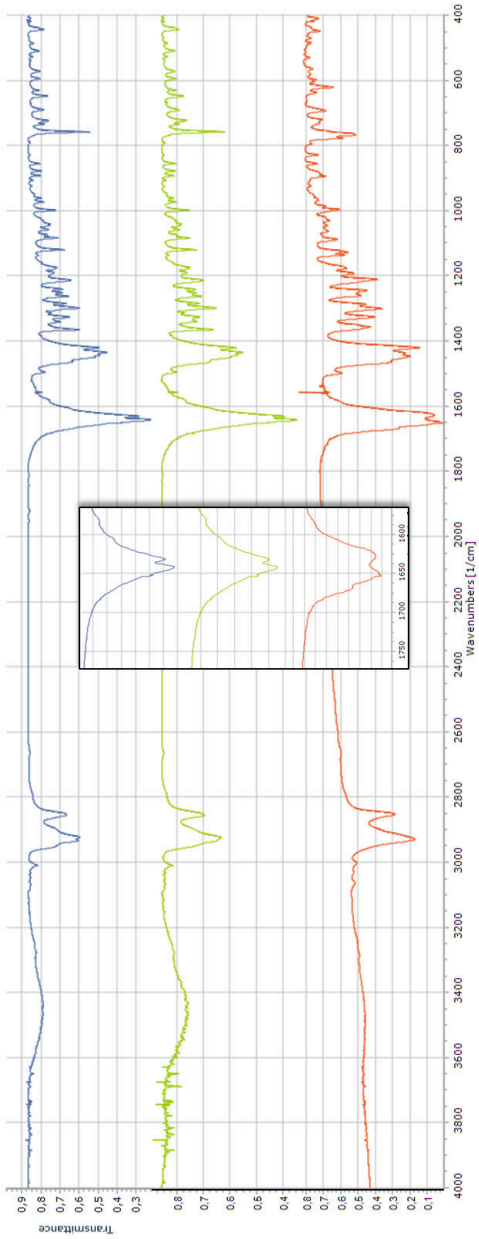

Figure 4.32: FT-IR spectra collected with resolution 2 cm^{-1}: Form C in blue, Form B in green and raw PZQ in red.

Form C exhibited some differences in the habitus morphology comparing to Form B and raw PZQ: the particles were agglomerated in groups, without any sign of the needle-shape like of raw PZQ or little whiskers of Form B (Figure 4.33).

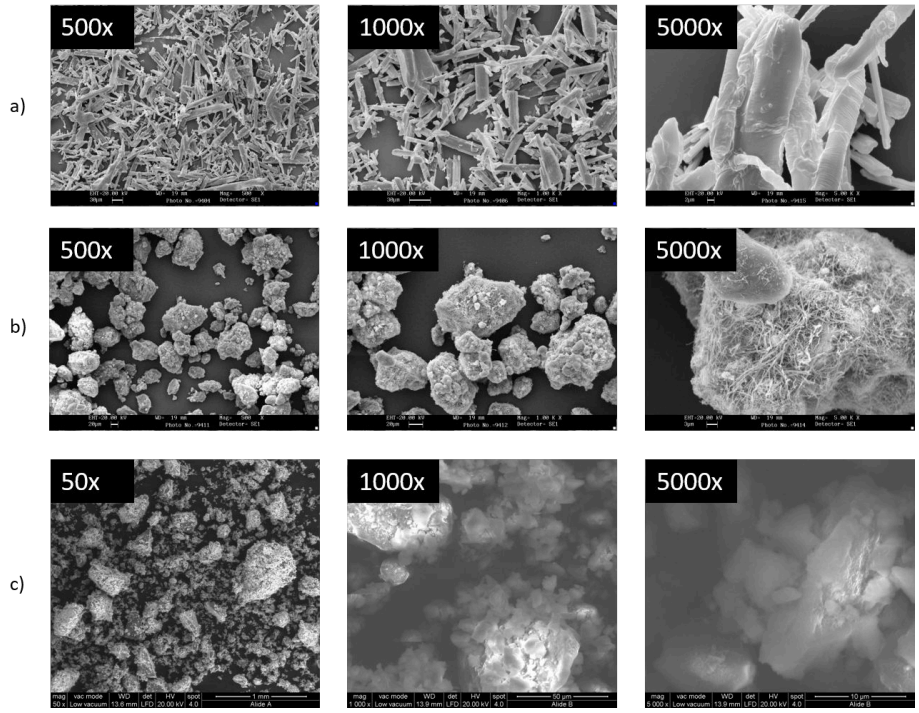

Figure 4.33: ESEM images of PZQ (a), Form B (b) and Form C (c).

The water solubility at 20 °C of Form C was analyzed by HPLC and compared to raw PZQ and Form B, resulting in the more soluble form with 382.69 ± 9.26 mg/L, while raw PZQ was 140.30 ± 9.26 and Form B 281.31 ± 8.32 mg/L (Figure 4.34). Also, Form C maintained the *in vitro* antischistosomal activity with an IC_{50} of 0.067 μg/ml similar to PZQ one (0.165 μg/ml).

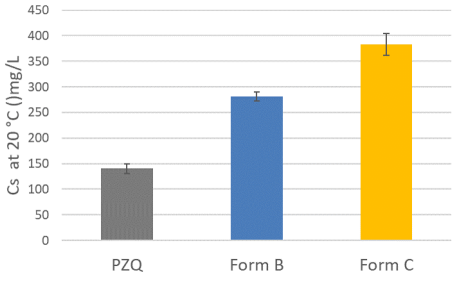

Figure 4.34: Water solubility at 20 °C of the anhydrous forms of PZQ.

Similarly, the dissolution rate of Form C at 37 °C was 2.6 fold greater than raw PZQ, as reported in Figure 4.35.

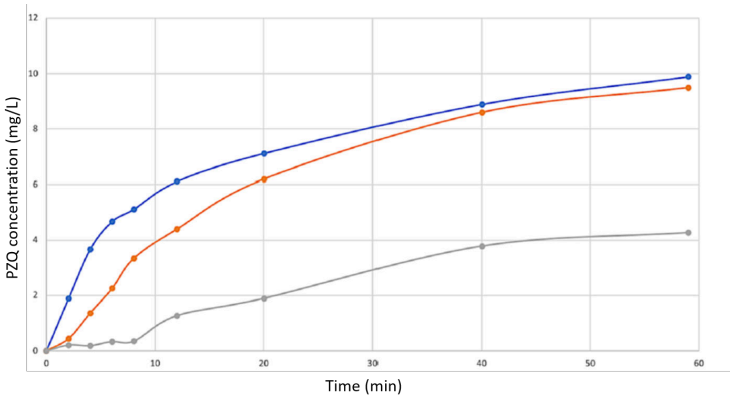

Figure 4.35: Dissolution of Form C (orange), Form B (blue) and raw PZQ (grey) in water at 37 °C.

Till this point, Form C seamed to be the most favourable form of PZQ, due to its highly solubility and dissolution rate, but unfortunately its physical stability resulted to be poor. In fact, DSC analyses repeated over a period of 4 months after its preparation showed a progressive recrystallization in the original PZQ form, starting from 2 months (Figure 4.36). These results were also confirmed by PXRD analyses, not reported for the sake of brevity. Also, the additional grinding of Form C for 60 min at 25 Hz confirmed its tendency to recrystallize, as evident from a very slight endotherm identified as raw PZQ at 135.81 °C, though this was not visible in the PXRD analyses (Figure 4.37).

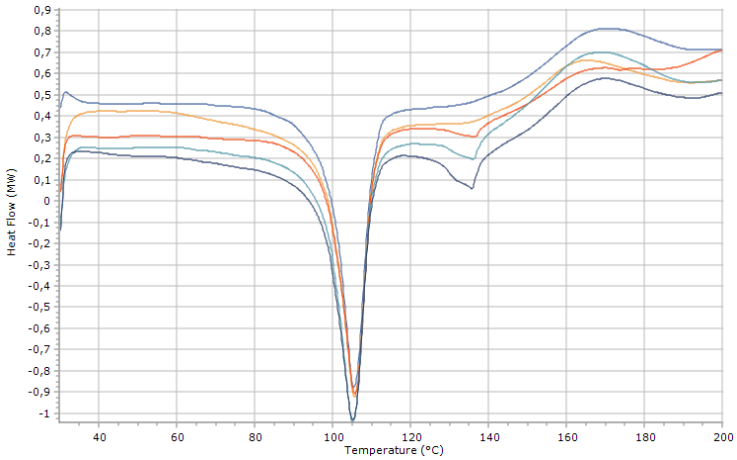

Figure 4.36: DSC traces of Form C over time, from up to down: fresh sample, after 1, 2, 3 and 4 months.

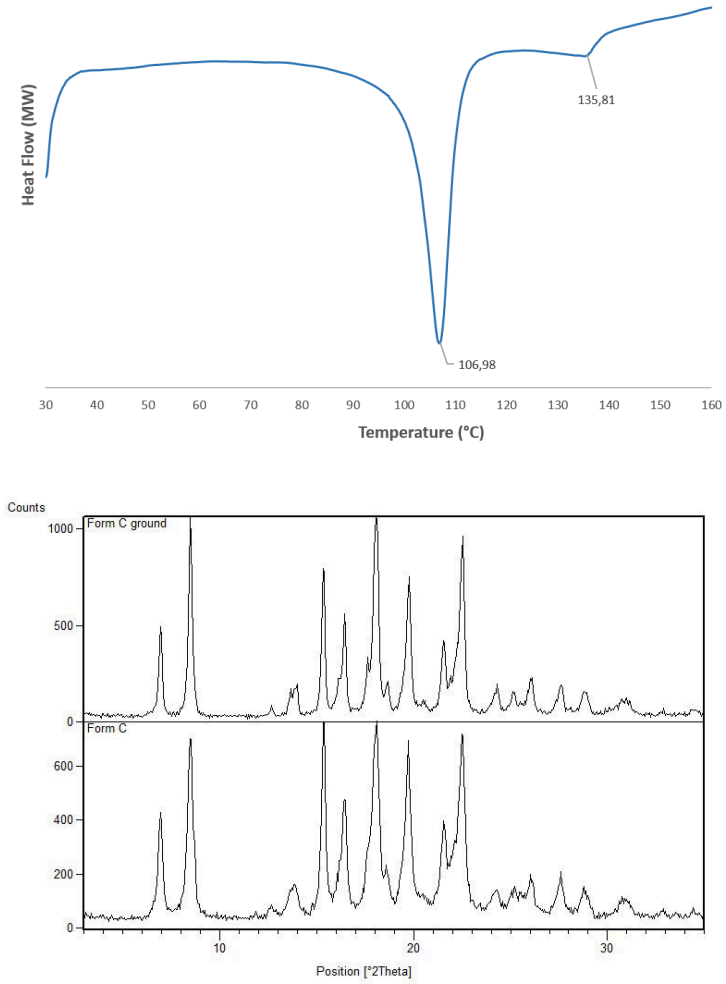

Figure 4.37: Stability upon grinding of Form C: DSC and PXRD traces of Form C additionally ground.

4.5 Conclusions

The third anhydrous polymorph of PZQ has been completely characterized at the solid state and also in its solubility and dissolution rate. Even though the PXRD pattern of From C was very similar to the one of Form B, the two forms were distinguishable for specific reflections and, as for Form B, the crystal structure could be solved from the synchtrone PXRD. The structure proposed was validated by DFT calculations and the simulated SSNMR chemical shift were in perfect agreement with the experimental ones. The solubility and the dissolution of this new form were highly augmented comparing to raw PZQ, but unfortunately its stability was poor and after only 3 months it started to recrystallize in its native form. Considering all the researches presented so far, PZQ demonstrated a certain capacity to transform upon appropriate mechanochemical activation, spreading the possibilty of new interactions with other coformers, towards the formation of solvated forms, cocrystals or binary systems that will be the focus of the next chapters.

4.6 Appendix C

4.6.1 DFT-D calculations for Form B

Periodic lattice calculations were performed using CASTEP[150] Academic Release version 17.2 which exploits a plane-wave and pseudopotential approach within density functional theory (DFT) [150]. Magnetic shieldings were calculated with GIPAW algorithm[151] as implemented in the CASTEP code. The geometry optimization and the NMR chemical shift calculations were performed using a generalized gradient approximation (GGA) PBE exchange-correlation functional[152] with the semi-empirical dispersion scheme[153] TS [153] and ultrasoft pseudopotentials, generated on the fly. The geometry optimization was performed starting from the Form B crystal structure determined from PXRD data. The planewave cut-off energy was set equal to 700 eV. The Brillouin zone was automatically sampled using a Monkhorst-Pack grid with a k-point spacing of 0.05 A^{-1}. The geometry optimization was done with fixed unit cell parameters. For the subsequent magnetic shielding calculation, the refined structure was used with the same cut-off energy as above. The theoretical absolute ^{13}C and ^{15}N isotropic magnetic shielding (σiso) values were converted in the corresponding isotropic chemical shifts (δiso) relative to the absolute magnetic shielding of the reference substance glycine computed at the same level. The following equation was used: (δiso = σref - σiso, where σref is the reference shielding of glycine, 170.1 ppm (^{13}C) and 192.9 ppm (^{15}N).

4.6.2 Complete packing of Form B

For completeness, the packing view from axis a, b and c for both PZQ and Form B are reported in Figure 4.38, while Figure 4.39 reports the crystal packing for the DFT-D optimized Form B.

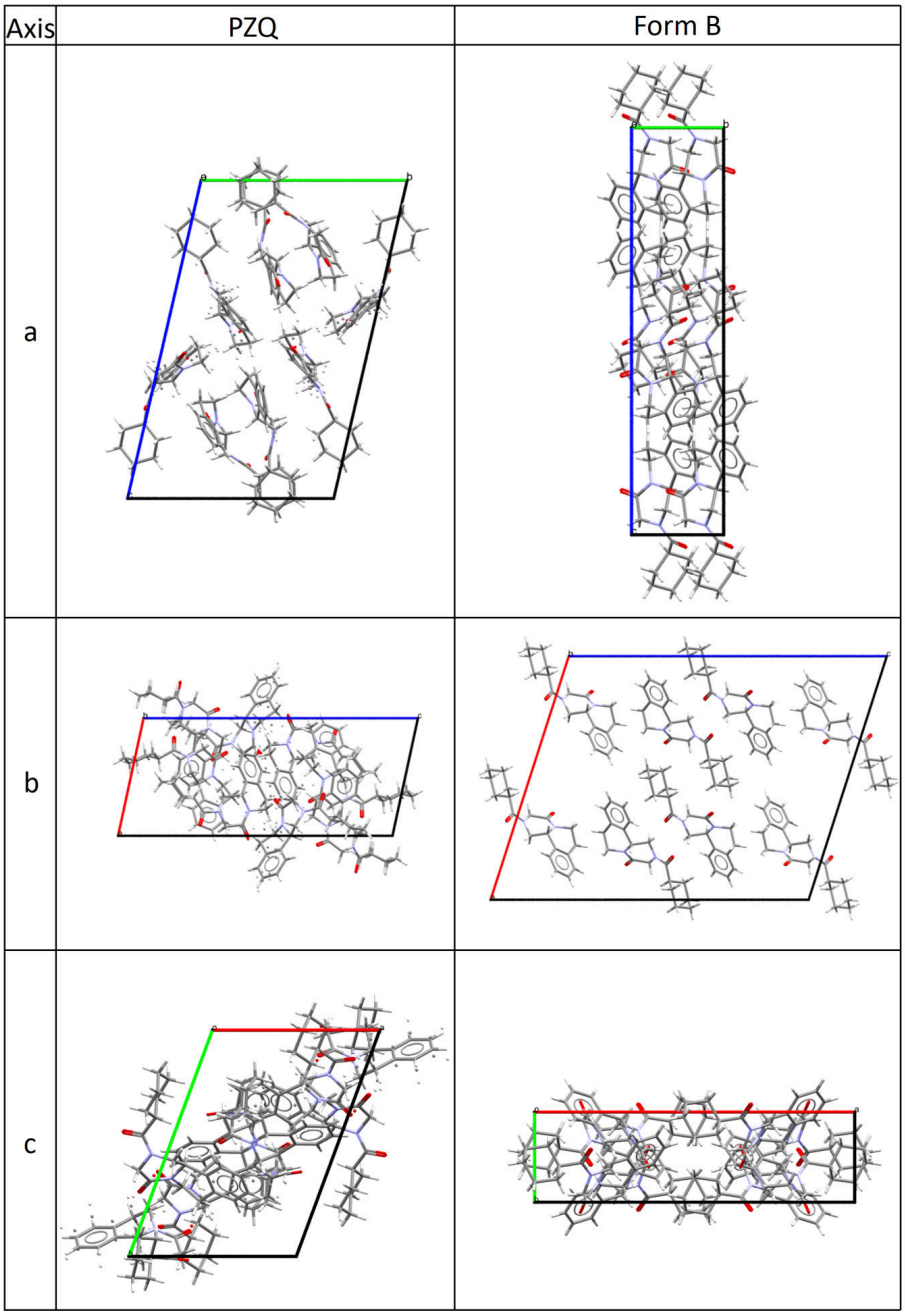

Figure 4.38: Complete packing of Form B and raw PZQ.

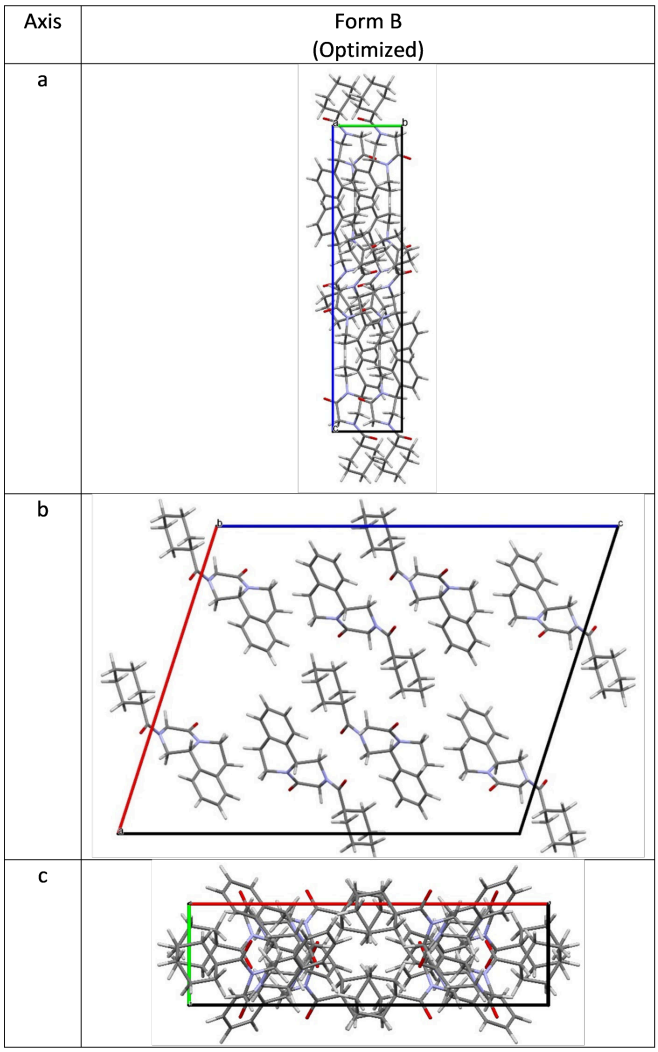

Figure 4.39: Crystal packing for the DFT-D optimized Form B.

4.6.3 Form B *in vivo* studies and pharmacokinetic evaluation

Given initial promising *in vitro* and *in vivo* findings on TELCEU01, an in-depth side by side comparison of PZQ and the polymorph B has been conducted by the group of Prof. Jennifer Keiser, at Department of Medical Parasitology, Swiss Tropical and Public Health Institute, Basel, Switzerland. In particular, in vitro studies were conducted on the larval and adult stages of *S. mansoni*. ED 50 values were determined in mice harbouring a chronic *S. mansoni* infection. In the second part of the reseach, the pharmacokinetic (PK) parameters of R- and S-PZQ following treatment with both PZQ and Form B in mice using a validated liquid chromatography (LC) tandem mass spectrometry (MS-MS) method were determined. The results, based on *in vitro* and *in vivo* studies using the *S. mansoni* mouse model, show that the novel formulation has no benefit over the current formulation. No significant differences were observed in the *in vitro* and *in vivo*, in contrary to preliminary *in vitro* and *in vivo* results which showed higher efficacy of the formulation derivative compared to the standard PZQ. The ED50 value of 90.90 mg/kg for the standard PZQ calculated in this study is in line with previously reported values for susceptible *S. mansoni* strains ranging from 70-100 mg/mL but slightly lower than the one previously determined in our laboratory (246.5 µg/mL). While a slightly higher ED50 of 137.40 mg/kg was calculated for the polymorph derivative no significant difference was observed between the two treatments (as aqueous suspensions) at the individual dosages. The pharmacokinetic analysis was based on non-compartmental analysis using a trapezoidal linear model, given the small number of time points used in the study (30, 60, 240 minutes and 24 hours). The data here presented show that, surprisingly, the polymorph has an overall lower exposure profile for both R- and S- enantiomers, indicating a lower bioavailability of the drug, in comparison with the standard PZQ. The PZQ polymorph shows lower plasma peak concentrations of the R and S enantiomers (mean of overall R-polymorph Cmax = 0.76 µg/mL and 0.32 µg/mL for the S-polymorph) compared to the standard PZQ formulation (mean of overall R-PZQ Cmax = 1.4 µg/mL and 0.81 µg/mL for the S-PZQ). This observation of the lower plasma exposure of the drug seems to be in accordance with the overall lower WBR observed with the polymorph administration. Perhaps the polymorph lost its stability, undergoing a solution-mediated polymorphic transformation, during the dispersion in water or the oral administration. This could have altered the dissolution rate of the compound in the gastro-intestinal (GI) tract, subsequently reducing the compound's bioavailability and dissolution rate. Another possibility is that the metastable form of the crystalline PZQ polymorph was absorbed faster in the GI. The polymorph PZQ has previously been shown to have a faster dissolution rate compared to the standard PZQ. The faster dissolution rate, combined with the very fast first pass metabolism typical of PZQ (P450 cytochrome family), might concur to achieve lower distribution profiles of the drug over time, especially in the mesenteric veins. This theory would be in accordance with the higher Cl/F, lower Cmax, and similar Tmax that we observed in the polymorph PZQ pharmacokinetics profiles. On the other hand, the two crystal forms have a similar Tmax of a mean

value of 0.58 h for PZQ and 0.54 h for the polymorph. In addition, the observed half-life for both the drugs was spanning between median values of the R-PZQ 5.93 h (50; 300 mg/kg dose) to 2.64 h (100 mg/kg), whilst the R-polymorph ranged from median values of 10.56 h (100 mg/kg dose) to 3.08 h (200 mg/kg dose). The new polymorph shows an increased overall average half-life ($t1/2 = 5.67$ h), while the standard formulation exhibits a lower average half-life ($t1/2 = 4.21$ h). Notably, the AUC was 40% lower for the polymorph compared to the standard formulation, but the WBR was differing between the two drugs for about 15-18%. Therefore, despite the differing exposure profiles, the in vivo effect was similar indicating that the portal vein drug concentration is the main responsible for the activity of PZQ. A limitation of the pharmacokinetic study was the rather small sample size for each treatment arm (four mice) which could influence the error rate in the study. To limit this experimental error, the test and the control mice were chosen randomly within the same infection batch. A possible additional limitation was the comparison of the two crystalline form as water suspension: Once the drugs were suspended in water for the oral administration, this might have altered the conformation of the polymorph, thereby possibly altering its properties. Instead, it might have been advantageous to use the two crystalline polymorphs as powders in mini gelatin capsules suitable for oral administration in mice or loaded in microparticles. This research, entitled "Activity and pharmacokinetics of a PZQ crystalline polymorph in the *S. mansoni* mouse model", authored by Flavio C. Lombardo, Beatrice Perissutti, Jennifer Keiser is currently under submission at the Antimicrobial Agents and Chemotherapy.

4.6.4 GIPAW-DFT study on Form C

Periodic lattice calculations were performed using CASTEP[150] Academic Release version 17.2 which exploits a plane-wave and pseudopotential approach within density functional theory (DFT)[154]. The absolute chemical shieldings were calculated using the GIPAW algorithm[151], implemented in the CASTEP code. The geometry optimization was initiated from the structure determined from the PXRD pattern (376 atoms) and the refined structure was used for the chemical shift calculation. As reported in Figure 4.40 the geometriy-optimized structure was almost completely superimposable with the one form the PXRD data and the simulated PXRD were identical (Figure 4.41). The geometry optimization and the NMR chemical shielding calculations were carried out employing the generalized gradient approximation (GGA) PBE exchange-correlation functional[155] with the semi-empirical dispersion scheme[152] TS[156] and ultrasoft pseudopotentials which were generated on the fly. The plane-wave cut-off energy was set equal to 700 eV, and the Brillouin zone was automatically sampled using a Monkhorst-Pack grid with a k-point spacing of 0.05 A^{-1}. The geometry optimization was performed starting from the structure of Form C determined from synchrotron PXRD data (376 atoms in the unit cell, space group C2/c, Z' = 1). The unit cell parameters were kept during the optimization, as they were considered to be of acceptable quality from the experimental data. The convergence tolerances for the total energies, forces and displacements were set to 0.2 10^{-4} eV $atom^{-1}$, 0.05 eV A^{-1}, and 0.001A, respectively. The refined structure was used in the subsequent chemical shielding calculation. The absolute ^{13}C and ^{15}N isotropic chemical shieldings (σiso) were converted into the corresponding isotropic chemical shifts, δiso(calc), using the following conversion: δiso(calc) = σref - δiso. Here, σref is the reference shielding, obtained by plotting the experimental chemical shifts δiso(exp) against the GIPAW-calculated chemical shieldings. A linear regression model with slope constrained to (-1) was applied to find the best fit to the data. The value of σref is determined by the intercept with the y axis[157, 158]. The obtained values of σref are 170.1 ppm and 190.9 ppm for ^{13}C and ^{15}N, respectively.

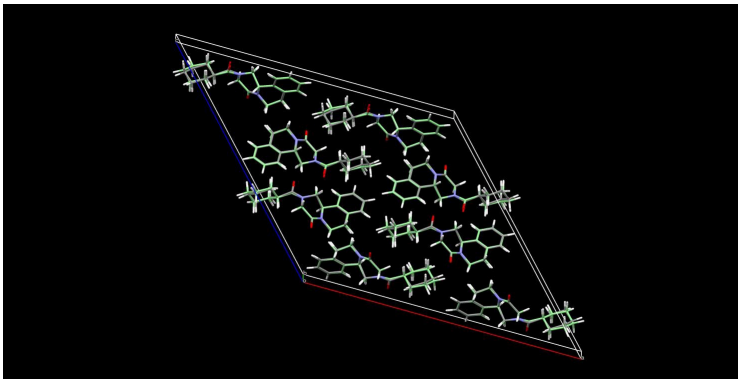

Figure 4.40: Overlay of the crystal structure of Form C from PXRD data and its geometry-optimized crystal structure by DFT calculations (in green). Images prepared with Mercury[159]

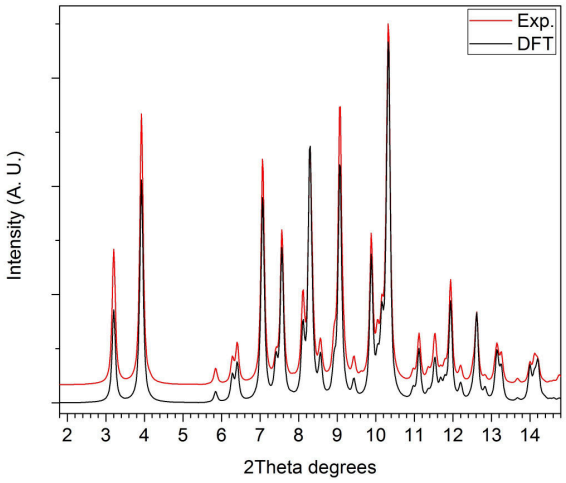

Figure 4.41: Calculated PXRD pattern of Form C from the DFT-optimized structure (black) and the simulated from the crystal structure solved (red). Both simulations were performed with Mercury[159] setting λ=0.7094A (Mo kα).

Chapter 5

Liquid-Assisted Grinding

The term Liquid-Assisted Grinding (LAG), also reported as solvent-drop grinding, is a particular grinding technique in which a very small amount of liquid (i.e. microliters) is added to the system, usually composed of powders, which was firstly reported in the study of the cocrystal[1] formation kinetics by the group of prof. W. Jones[160]. The ratio of the solvent volume to the sample weight has been expressed by the parameter η, which was further investigated to predict the cocrystal outcome basing on approximate solubilities of the cocrystal coformers[161]. Subsequentely, a huge amount of works were reported from all over the word regarding the application of LAG not only as a method to accelerate known reactions/interactions, but also as a valuable process for polymorph or cocrystal selective formation and screening, achieving results sometimes not possible using classical methods[129, 162–164]. In fact, the insertion of the solvent was reported to drammatically change the product outcome, even accelerating cocrystal reactions and increasing the crystallinity, respect to neat grinding[3]. Also, not only the nature of the liquid used, but also its amount can selectively determine the formation of different products, as verified by Hasa and coworkers, who studied the polymorphisms of the caffeine-anthranilic acid system[16]. The advantages of LAG are even improved when considering the pharmaceutical field: in fact, the general connection in the pharmaceutical co-crystal is represented by hydrogen bonds, that is usually broken when in contact with solvents. Therefore, the solution-based method lacks in efficiency in the co-crystal screening comparing to LAG (especially when using API with low solubility), because the API will separate from the solution containing the most soluble coformer[3]. Finally, not to forget, the possiblity of working with very little amount of liquid classifies LAG in the list of the *green* methodologies. Among all the deposited structure of PZQ, the only entries for PZQ solvates/hydrates are represented by the enantiomeric hemihydrates[39]. This section will present the study of PZQ behaviour upon the application of LAG, starting with water for the research of possible hydrated forms and then with the application of the main solvents used in the

[1] A co-crystal is multicomponent crystalline system formed by two or more different chemical entities, comprehending also hydrates and solvates.

classical polymorphs/solvates screening procedures. The research studies presented in this chapter were performed at the Department of Chemistry of the University of Cambridge under the supervision of prof. William Jones, during the Erasmus+ Traineeship program.

5.1 PZQ hemihydrate

5.1.1 Introduction

When seraching a definition for an API hydrated form, one can consider it as a particular solvated form in which the solvent is represented by water. Comparing to the other possible solvates, the hydrates of API are the most common due to specific properties of the water molecule, as its no toxicity, its small size, the presence as atmospheric humidity and the ability of acting both as a donor and as an acceptor of hydrogen bonds, thus linking with itself and other compounds and creating also other connections, as coordinated covalent bonds and van der Waals interactions[165]. The presence of water in a pharmaceutical compound determines changes in the internal energy and enthalpy of the system, as well as in the degree of crystalline disorder, causing different physical-chemical and biopharmaceutical properties of the API [165, 166]. It was estimated that one-third of the API could exist in the hydrated form[167], while the hydrated forms actually known represent the 11% of the structures included in the Cambridge Structural Database (CSD[37]). There can be different levels of hydrates, depending of how many water molecules are present in the the crystal unit cell, creating monohydrate, hemihydrate, dihydrate, etc. The most common scenario is represented by one molecule for each one of host (the monohydrate), while the hemihydrated cathegory is represented by only the 8 % of the total[168]. Considering PZQ, the CSD reports only the hemihydrated form of the enantiomers (refcode SIGBUG[39] and SIGBUG01) while other possible hydrated form are still unknown. In this context the LAG technique was applied to investigate the existence of any PZQ hydrate, using, as the starting material, both raw PZQ and the previously described PZQ polymorph, Form B (see Section 4.1).

5.1.2 Materials and Methods

Materials

Praziquantel (PZQ, (11bRS)-2-(Cyclohexylcarbonyl)-1,2,3,6,7,11b-hexahydro-4-H -pyrazino[2,1-a]isoquinolin-4-one)) was of Ph. Eur. grade and kindly donated by Fatro S.p.a. (Bologna, Italy). The HiPersolv Chromanorm methanol used for the HPLC analysis was of Ph. Eur. grade and purchased from VWR Chemicals (BHD PROLABO® Milano, Italy).

Methods

Grinding experiments The grinding experiments were performed using a Retsch vibrational mill MM200 (Retsch, Germany) and 2 stainless steel jars of 25 mL, each one containing 2 stainless steel balls with ϕ=7 mm. The powders were accurately weighted (200 mg) and placed in the jars with the grinding media. Depending on the experiment, a certain amount of water was inserted in the jar (ranging between 10 and 100 μL) and the grinding process was started. Additionally, in certain cases the liquid was added after a preliminary neat grinding of the powders, using a method that we called Neat-LAG. For the further characterization, the samples were prepared *via* Neat-LAG (Retsch MM400, Retsch, Germany) using 436 mg of PZQ and 24.6 μL of water in 35 mL zirconium oxide jars, each one containing 2 balls (ϕ= 10mm), corresponding to an equimolar ratio between the drug and the water.

Slurry experiments To perform the slurry experiments PZQ and Form B were added in excess to 1 ml of distilled water and kept under stirring at room temperature for 7 and 3 days respectively. The obtained slurry was filtered and the solid excess was immediately analyzed by PXRD.

Thermal analyses Differential scanning calorimetry was conducted using a Mettler Toledo DSC822e system; about 2 mg of the samples were accurately weighted and put in a 40 μL aluminum perforated crucible and analyzed heating from 30 to 200 °C at 10 °C/min under nitrogen atmosphere. When using the Mettler Toledo TGA/SDTA851e for TGA analyses, the amount of sample was about 10-15 mg, exactly weighted in a 100 μL (?) aluminum crucible. The method used was the same of the above mentioned DSC procedure.

FT-Infrared Spectroscopy The samples were analysed using a Perkin-Elmer System 2000 FT-IR instrument on compressed KBr discs, which were prepared by gently grinding the sample in an agate mortar with anhydrous KBr (in a 1:15 ratio by wt) and pressing with and hydraulic press. The range observed was from 400 to 4000 cm^{-1}, the resolution used was 4 cm^{-1} with a step of 1 cm^{-1} and scan number of 3.

Polarimetry The polarimeter used was a Jasco P2000 Polarimeter (Lecco, Italy) set at 25 °C and λ=589 nm. The solutions were prepared in ethanol with a concentration of 1g/100 mL, instead of $CHCl_3$[140] to avoid the formation of air bubbles in the sample holder.

Hot Stage Microscopy A hot stage microscopy apparatus (Mettler-Toledo Ltd, Leicester, United Kingdom) was used for the observation of the samples by taking movies during heating from 25 to 150 °C using a dedicated ocular and software.

Powder X-Ray Diffraction-PXRD Powder X-Ray Diffraction analyses were conducted by means of a Panalytical X'Pert Pro Diffractometer, with a RTMS X'celerator

detector and Cu Kα radiation (wavelength=1.5418 A). About 20 mg of the sample was prepared on a sample holder by gently press with a glass slide.

Scanning -Electron Microscopy A JEOL JSM-5510LV Scanning Electron Microscope (city) was used for imaging on metallized sample (Suppetr Coater,???).

Environmental Scanning Electron Microscopy Selected samples were observed using a Quanta 200 FEI-XRF embedded instrument.

SS-NMR Solid-state NMR measurements of PZQ and Form B were collected using a Bruker Avance II 400 instrument[2]. The spectra were obtained at 100.65 MHzfor ^{13}C. Cylindrical zirconia rotors (4 mm o.d) were used with a sample volume of 80 μl and spun at 12 kHz (^{13}C). In all the analyses a RAMP-CP pulse sequence (^{1}H 90° pulse = 3.05 us), TPPM ^{1}H decoupling with an rf field of 75 kHz were used during the acquisition. The number of transients acquired was 124 with 3 ms of contact time and a relaxation delay of 20 s. As the reference, the resonance of hexamethylbenzene was used (^{13}C methyl signal at 17.4 ppm).

Crystal structure determination from powder X-ray diffraction data, Periodic DFT calculations and SSNMR modelling All these computational analyses were performed thanks to the collaboration with Dr. M. Arhangelskis of the Department of Chemistry of the MCGill University in Montral (Canada), and are reported in the Appendix D (paragraph 5.3, 5.3 and 5.3).

Saturation Solubility and intrinsic dissolution rate The solubility of the samples was analyzed by preparing 10 ml of saturated solutions of each samples in deionized water, kept under agitation in the dark for 48 hours. Then, the solutions were filtered using a membrane (pore size=0.45 μm) and diluted 1:200 with the mobile phase prior injection in the HPLC system. The HPLC used was an Agilent HPLC-UV 1260 Infinity II with a EC-C18 Poroshell 120 A column of 4 μm and dimensions of 4.6 x 10 mm. The mobile phase was composed of 65% methanol and 35% of deionized water (MilliQ filtered) and the flux used was of 0.750 mL/min. The instrument was set at 25 °C and with a fixed wavelength of 220 nm for recording the absorbances. The external standardization method was used for the quantification of the integrated peaks. The PZQ retention peak was found at 7.7 minutes in a total run time of 10 minutes and the calibration curve obtained in the range of 0.5-10 mg/L had r^2=0.9988. Each analysis was conducted in triplicate and the average was reported. For the intrinsic dissolution rate determination, about 150 mg of the samples were inserted in the sample holder and pressed using an hydraulic press (PerkinElmer, Norwalk, USA) for 1 min at 1 ton. The sample surface area obtained was of 0.785 cm^2 and the entire sample holder with the compressed powder was immersed in a vessel containing 1 L of distilled water kept at 37 °C. The system used was a Hanson Research SR8 Plus dissolution test station

[2]In collaboration with prof. M. R. Chierotti of the Department of Chemistry, University of Turin (Italy)

and the paddle were positioned at 3.5 cm from the tablet surface, with a rotation speed of 100 rpm. About 2 ml of the dissolution medium were withdrawn every ten minutes till 60 min and immediately replaced with an equal amount of thermo-stated distilled water. The aliquots were then diluted 1:20 with the mobile phase and analyzed using the same above mentioned method. The analyses were performed in triplicate and for each point the mean, with SD (%) and RSD (%) were calculated. The amount of the dissolved drug per unit area over time was indicated by the slope of the curves, obtained through a linear regression method. For the comparison of the different curve the one-way ANOVA test was used and the data were considered statistically different when having a p value $< .05$.

Physical stability Several samples were kept in a desiccator, in the dark and at room temperature for long time and analyzed using DSC and PXRD. In addition, the hemihydrated form was also analyzed by PXRD upon heating in the range of 30-80 $^{\circ}$C.

***In vitro* activity** The hemihydrated form was also tested in its *in vitro* activity against adult *S. Mansoni* thanks to the collaboration with the Swiss Tropical and Public Health Institute of Basel (Switzerland), in particular prof. Jennifer Keiser. For the *in vitro* studies the samples were tested in their efficacy by preparing different concentrations, ranging from 0.021 to 0.33 μg/L in which adult Schisosomes were incubated for up to 72 hours. By using an inverse microscope (Carl Zeiss, Germany, magnification 80x) all the alterations of morphology, motility and viability were observed and the IC_{50} value was calculated with CompuSyn software.

5.1.3 Results and Discussion

In these years, an increasing amount of literature work were focused on PZQ, in particular on the formation of possible cocrystal to ameliorate the biopharmaceutical properties of the drug. In this context the liquid-assisted grinding (LAG) has been already applied in combination with various coformers, but not exclusively with water, which is the focus of this chapter. The first attempt were conducted using raw PZQ as the milling powder and varying the quantity of water introduced prior to grinding; in fact, it has been reported that the product outcome can vary depending not only on the different liquid, but also on its amount[16]. In this case the grinding of raw PZQ for 30 minutes at 25 Hz with water did not lead to any new solid form, neither when varying the amount of water (10, 40, 60 and 100 μL), since no changes at all were noticed, as reported in Figure 5.1. Surprisingly, when using Form B as the milling powder a new solid form was found, specifically a racemic hemihydrate, that will be later described and characterized. If the grinding was performed for 30 minutes, the formation of the hemihydrate was incomplete, so 60 minutes were considered the suitable grinding time. Nevertheless, it is worth notice that, also in this case, every change in the quantity of water inserted led to the same outcome.

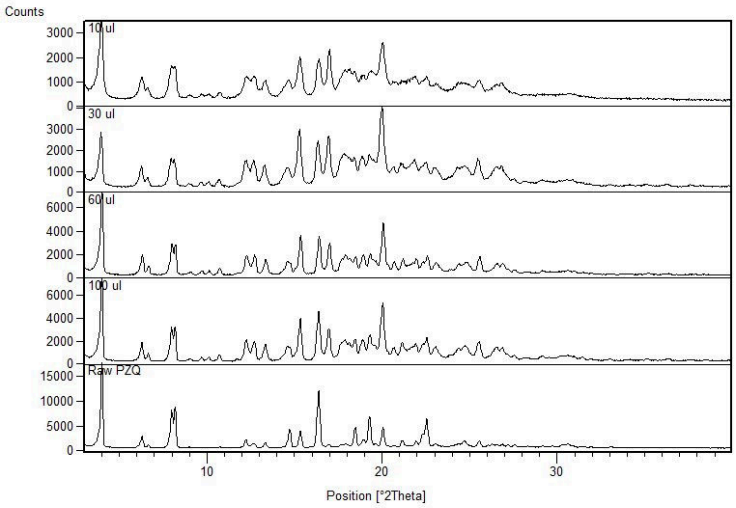

Figure 5.1: LAG experiments (30 min, 25 Hz) on raw PZQ with different amounts of deionized water.

The same new solid form could be also obtained in another very peculiar way: raw PZQ was ground by itself for 30 minutes at 25 Hz and water was subsequently introduced, then the milling was carried-on for other 60 minutes at 25 Hz. This fact means that the formation of the hemihydrate required a partial de-structuration of the raw drug to permit the insertion of the water molecule, in particular the switch to a different conformer, where the carbonylic groups are in the *anti* position, which is typical of the amorphous PZQ, as reported by Arruà and coworkers[75]. A further confirmation of this hypotesis was given by the possibility to obtain PZQ hemihydrate also when grinding Form B with water, since the same polymorphic entity is characterized by the same *anti* conformation, illustrated in paragraph 4.1. The PXRD pattern of the new solid form is presented in Figure 5.2 and will be further described later.

The slurry experiments led to very similar results, since after only 3 day slurring of Form B the hemihydrate was formed, while in the case of raw PZQ, even after one week the only phase found in the sample corresponded to the starting phase (Figure 5.3). This trial confirmed the previous hypothesis, since during the slurry experiment raw PZQ did not change its conformation, thus the formation of the hemihydrated could not be favoured. Differently, the *anti* spatial disposition of Form B permitted the interaction and the formation of the new phase.

To ensure the racemic nature of the hemihydrate, polarimetric analyses were performed on different samples and compared to raw PZQ: the mean $[\alpha]\lambda$ value registered for RacH-PZQ was 0.02±0.06, perfectly corresponding to a racemic compound, as in the case of raw PZQ ($[\alpha]$ of 0.5 ± 2.9).

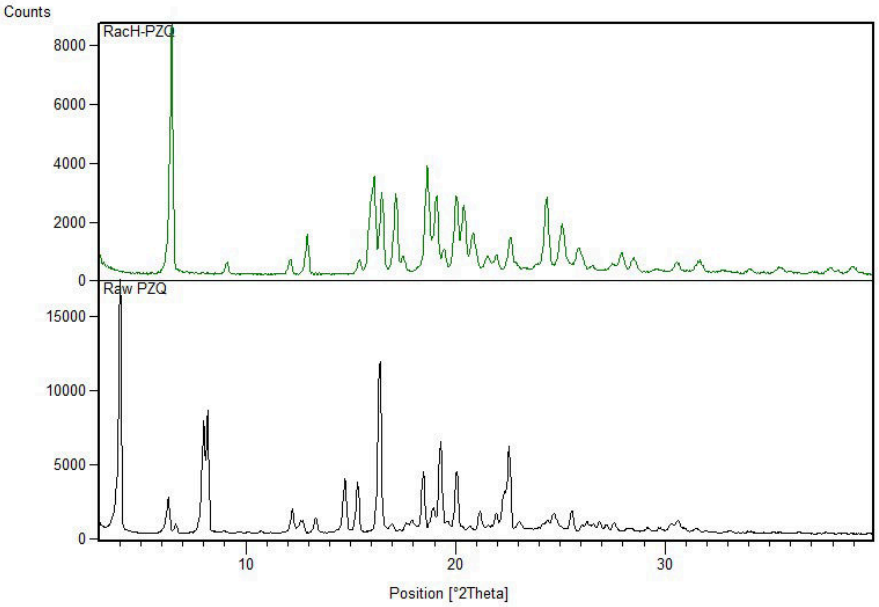

Figure 5.2: Rac-HPZQ (top) and the raw drug (bottom).

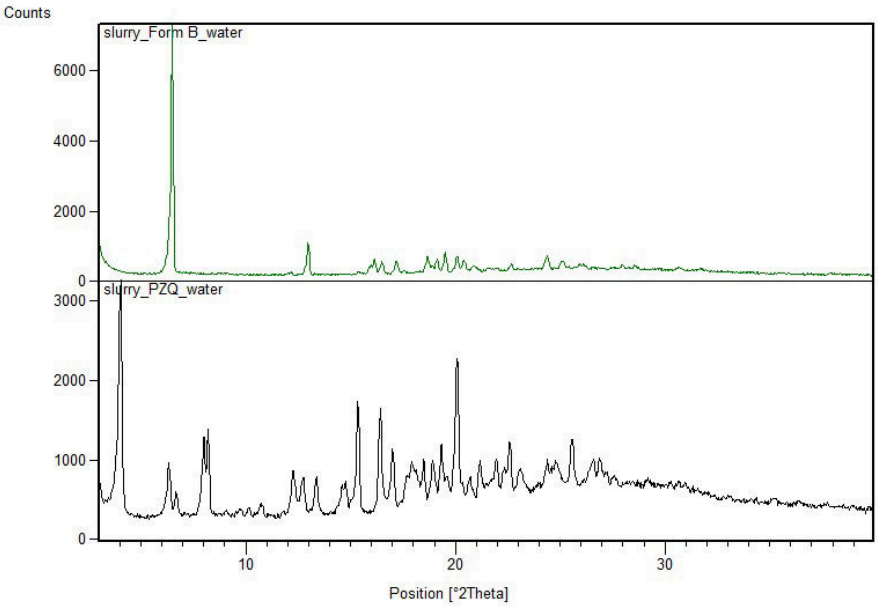

Figure 5.3: PXRD patterns of the solid residues after one week slurry in water of Form B for 3days (green) and of raw PZQ for 7 days (black).

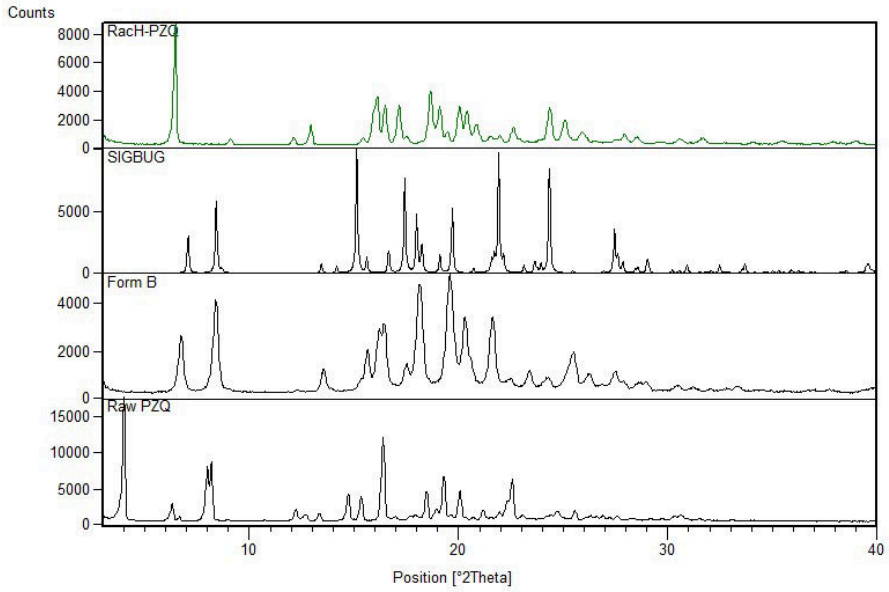

Figure 5.4: From up to down: PXRD patterns of Rac-HPZQ (green), calculated enantiomeric hemihydrate (SIGBUG[39]), Form B and raw PZQ.

The PXRD pattern of Rac-HPZQ was completely different from the already known PZQ structures, as shown in Figure 5.4 and Figure 5.2, in which the reader can found also the calculated pattern of the enantiomeric hemihydrate (CSD ref. code SIGBUG[39]), Form B and raw PZQ; the characteristic reflections of RacH-PZQ were found at 6.28, 16.14, 16.50, 17.18, 18.67, 19.12, 20.05, 20.41 and 24.37 °of 2θ. The crystal structure of Rac-HPZQ was solved from the capillary powder X-ray diffraction pattern following the method described in the appendix D (paragraph 5.3): the space group P-1 of Rac-HPZQ was the same as raw PZQ, but with just one molecule in the asymmetric unit, instead of 4, where every water molecule is connected with two PZQ entities, one R- and one S-, through hydrogen bonds, as reported in Figure 5.6. The Rietveld refinement fit of the experimental pattern with the calculated one is reported in Figure 5.5. PZQ does not have any H-bond donor group, thus these connections are possible thanks to the presence of the oxygen atoms acting as acceptor, since the nitrogen electron pair is occupied in the πelectron delocalization, as it was also reported in literature[38].

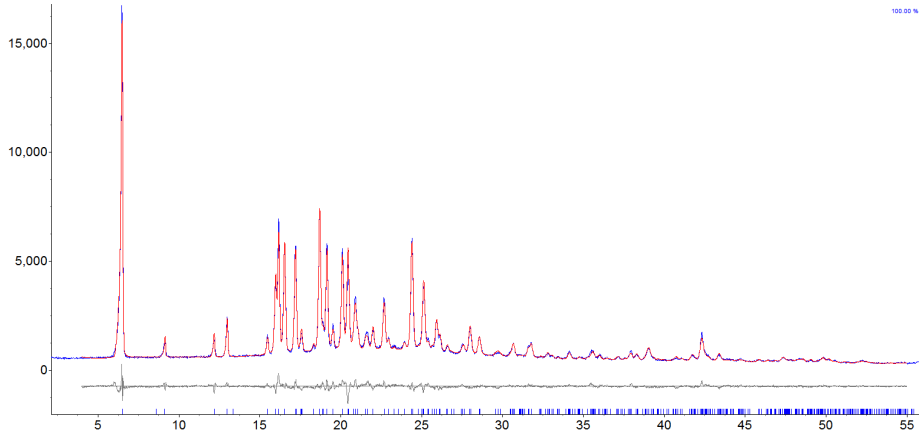

Figure 5.5: Rietveld refinement fit of the experimental pattern (red) and the calculated one (blue). In grey the corresponding residuals.

The refined unit cell had the following parameters:

- Space group: P-1
- Cell lengths (A): a=5.857, b=10.921, c=14.299;
- Cell angles (°): α= 105.755, β=94.622, γ=99.564;
- Volume (A^3): 860.342;
- Density: 1.24.

These oxygen atoms can be referred as the one in the eterocycle (Oet) and the one linked with the cyclohexyl group (Ocy). Observing the packing of the unit cell of the new hemihydrate and the enantiomeric one (Figure 5.6), in both cases the PZQ molecule are inversely positioned and linked to the water molecule between them. The difference is in the oxygen involved in these bonds: in RacH-PZQ the molecules are

Figure 5.6: Capped stick representation of the unit cell of RacH-PZQ (left) compared with the enantiomeric hemihydrate one (SIGBUG[39] right).

linked *via* a Ow-H ..O=Cet hydrogen bond, while in the enantiomeric hemihydrate the oxygen bonded to the water is the cyclohexylic one, creating a Ow-H...O=Ccy. Concerning the PZQ conformation, in the Rac-HPZQ the same *anti* conformation of Form B and of amorphous PZQ[75] was observed, while the raw drug has the *syn* one. It has been already noted in literature that the *anti* conformation creates a larger space between the molecules favouring the accomodation of other entities[38]. This new form is another confirmation PZQ propensity to hydrogen bonds links when in *anti* conformation.

Moreover, the water molecules are not linked between each other, but connected with the drug and the thermal analysis (Figure 5.9) presented a sharp dehydration endotherm in a narrow weight loss range: according to literature these means that the new RacH-PZQ belongs to the isolated site class of pharmaceutical hydrates[169]. In particular, the endothermic event at about 68 °C (61.38 J/g) represents the dehydration, confirmed also by the weight loss in the TGA, which was of 2.19 % in good agreement with the theoretical value of 2.73 %. The other endothermic events were recorded at 109.05 °C and 133.95 °C with an enthalpy of fusion of 10.25 J/g and 32.49 J/g respectively, which were identified as the melting of Form B and raw PZQ. Different DSC traces of Rac-HPZQ were collected in different samples, but the amount of the other forms observed was not consistent, due to the variability of the dehydration. Nevertheless, the overall behavior was confirmed by the hot stage microscopy analysis: around 68-75°C the hydrate melting, followed by a melting at 110 °C, a partial recrystallization and a melting around 135-138 °C, as reported in Figure 5.8.

Figure 5.7: Packing representation of RacH-PZQ (left) compared with the enantiomeric hemihydrate (SIGBUG[39] right).

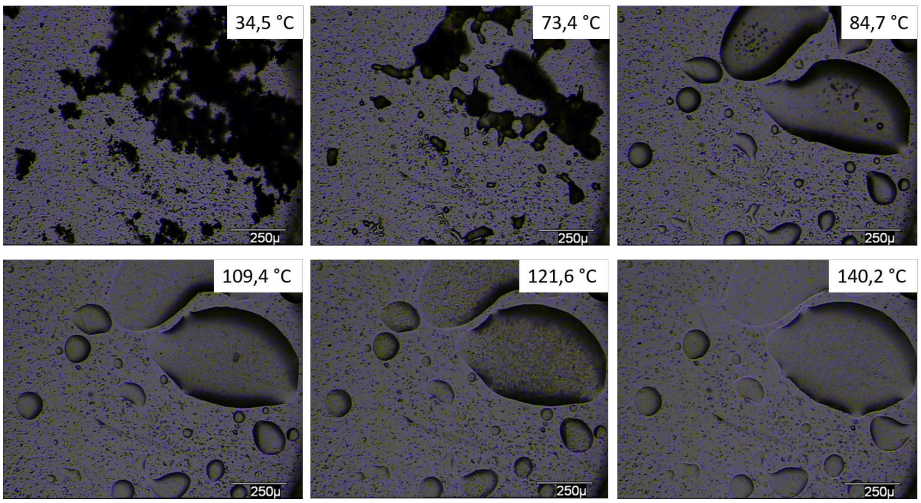

Figure 5.8: Hot-stage microscopy images for RacH-PZQ.

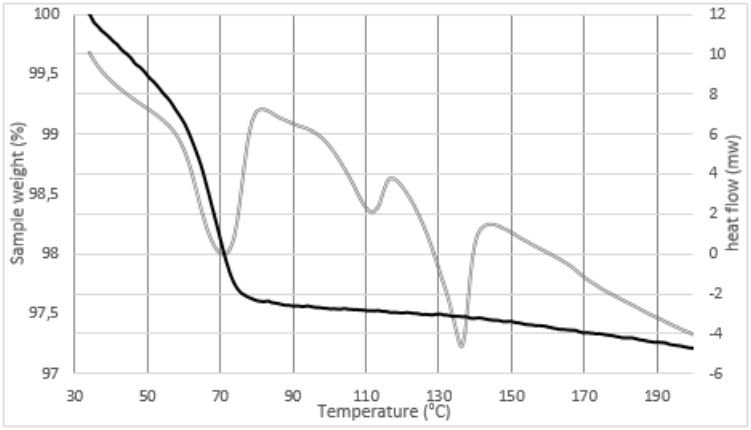

Figure 5.9: DSC-TGA traces of Rac-HPZQ.

The ^{13}SS-NMR spectrum of RacH-PZQ was compared to the already know anhydrous polymorphs, reported in Figure 5.10: the analysis confirmed not only the differences between the phases, but also the presence of just one molecule in the asymmetric unit (due to the single set of signals compared to the multiple one of PZQ) and the crystallinity of the sample, represented by very well defined and intense peaks. Also, the experimental data were in agreement with the calculated one, as reported in Table 5.1, which method details are reported in Appendix D (paragraph 5.3).

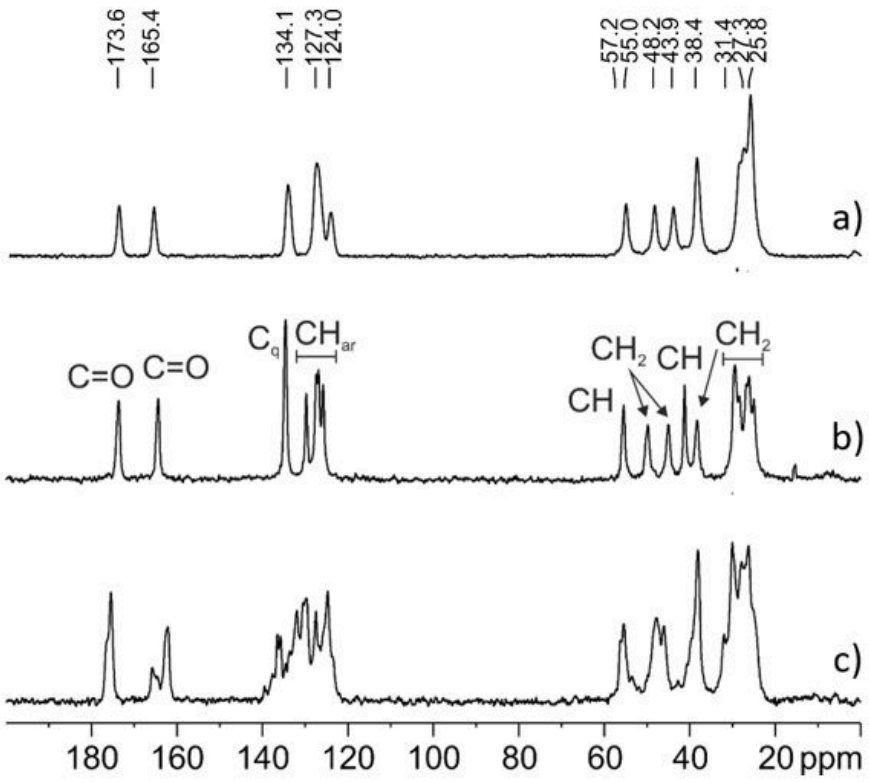

Figure 5.10: 100.65 MHz ^{13}SS-NMR spectra of RacH-PZQ (a), Form B (b) and raw PZQ (c).

Table 5.1: Experimental and calculated chemical shift for ^{13}C SSNMR analyses of RacH-PZQ, compared to raw PZQ, Form B and amorphous PZQ[75]. Atoms numbering refers to Figure 4.11.

Atom	Group	PZQ	Form B	RacH-PZQ	RacH-PZQ	PZQ[75]
		exp	exp	exp	calc	amorphous
		^{13}C				
7'	C=O	175.4, 176.2 sh	173.6	173.6	173.8	174.1
4	C=O	165.8, 164.6	164.3	165.4	165.4	164.3
		162.1				
7a	Cq	137.7, 136.5	134.6	134.1	136.3	134.2
11a	Cq	135.7, 134.6	134.6	134.1	136.2	134.2
8	CH	129.7, 127.5	129.8	127.3	129.4	127.0
		123.8	124.0			
11	CH	133.7, 132.0	127.5		129.9	134.2
		130.5				
10	CH		126.9		128.4	127.0
9	CH		125.8		124.7	127.0
11b	CH	56.3, 55.5	55.5	57.2	55.1	55.0
			55.0			
3	CH_2	46.1	49.8	48.2	46.70	-
1	CH_2	47.9	45.0	43.9	41.4	39.9
1'	CH	39.7	41.2	38.4	36.8	39.9
6	CH_2	38.1	38.3		35.8	39.9
6'	CH_2	32.0, 30.1, 27.9	29.4	31.4, 27.3	24.5	-
		26.3, 25.3	25.8			
2'	CH_2		29.4		24.0	-
7	CH_2		28.4		26.2	-
4'	CH_2		26.7		23.5	-
3'	CH_2		26.1		24.0	-
5'	CH_2		25.0		25.3	-

The FT-IR spectrum of RacH-PZQ, compared to Form B and raw PZQ, is shown in Figure 5.11. The characteristic bands of PZQ, already reported in previous chapters, were found in all spectra, as the stretching of C-H and C-H_2 bonds (3000-2854 cm^{-1}), the stretching of aromatic C and bending of -CH_2 (1500-1400 cm^{-1}). In particular in the spectrum of RacH-PZQ a broad band was found in the range 3650-3200 cm^{-1}, corresponding to the stretching of the O-H bonds (see frame in Figure 5.11). In the typical range of the stretching of the carbonyl group, a single broad band was found at 1629 cm^{-1}, confirming not only the intermolecular interaction between the drug and the water, but also its specificity, since the C=Oet is shifted of about 22 cm^{-1} in comparison to raw PZQ, while the C=Ocy, involved in the hydrogen bond, is missing. The signal at 758 cm^{-1} is superimposable to that of Form B, corresponding to the bending of the aromatic -CH, which was at 765 cm^{-1} for raw PZQ.

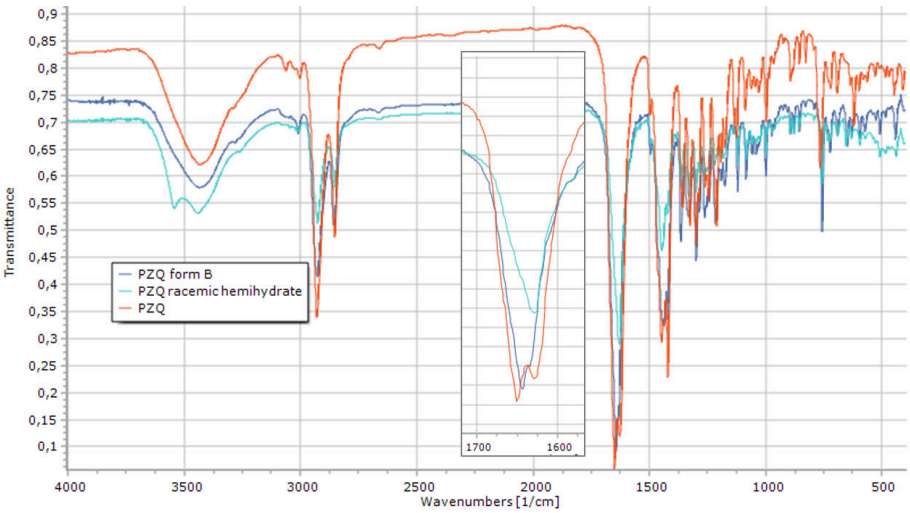

Figure 5.11: FT-IR spectra of Rac-HPZQ (green), Form B (blue) and raw PZQ (orange), zoom detail in the box.

The needle-shape like morphologies of raw PZQ (Figure 5.13, top) and the whiskers-like of Form B (Figure 5.13, bottom) were very different comparing to the new solid form: agglomerates of large plates were observed, probably favoured by the binding effect of the water.

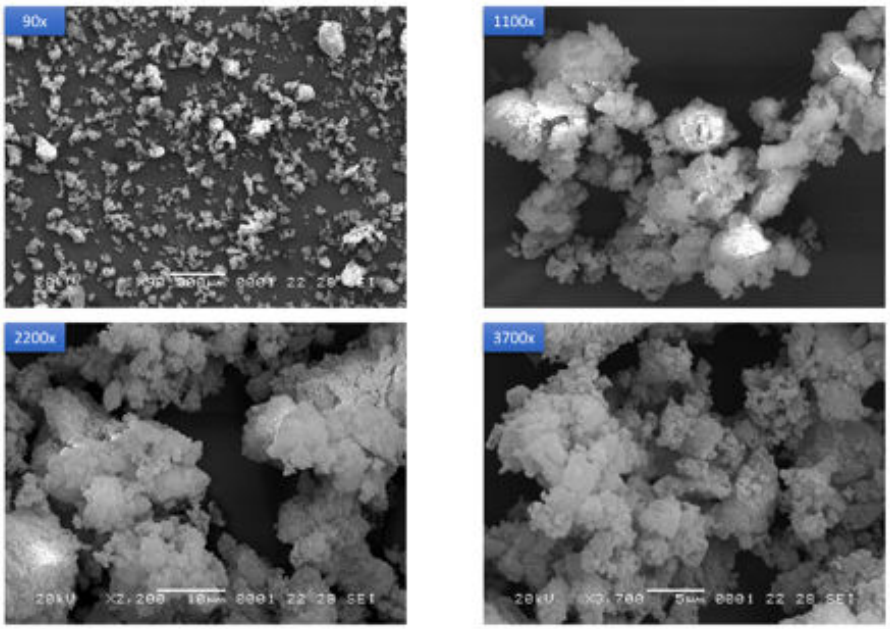

Figure 5.12: SEM images of RacH-PZQ.

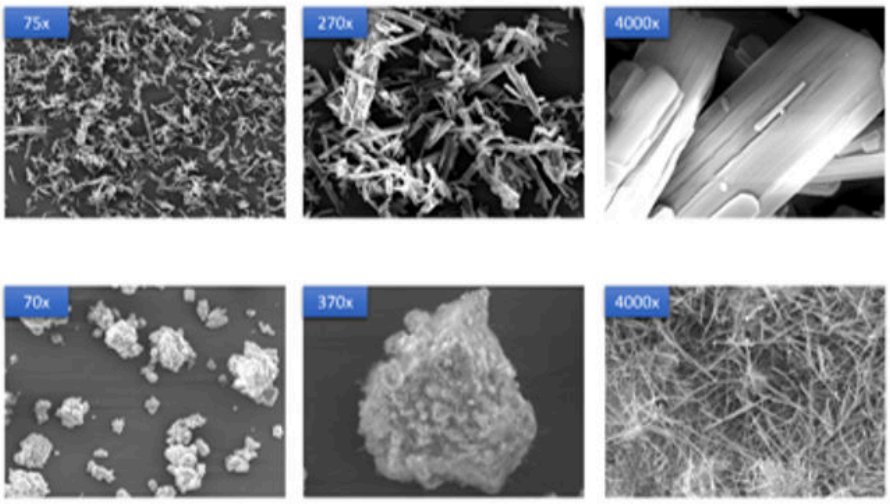

Figure 5.13: SEM images of raw PZQ (top) and Form B (bottom).

RacH-PZQ demonstrated excellent biopharmaceutical properties, since the saturation solubility (after 48 hours at 25 °C) was of 310.89 ±3.07 mg/L, while for raw PZQ was 217±10.33 mg/L. The intrinsinc dissolution rate, as reported in Figure 5.14 was double than the raw drug, in fact a value of 0.0673±0.0057 mg/cm^2/min was found for RacH-PZQ, while for the raw drug it was 0.0299±0.031 mg/cm^2/min. A similar enhancement was reached for Form B, as previously reported, and the statistical comparison between the polymorphic form and the new hemihydrate did not reveal any significant difference.

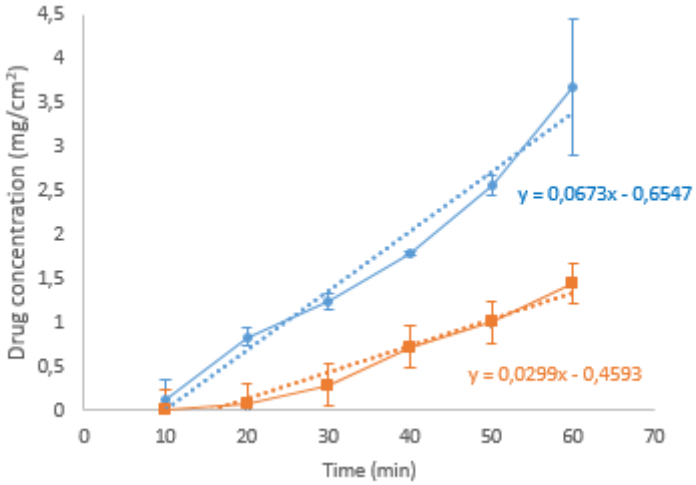

Figure 5.14: Intrinsic dissolution rate curve (in water at 37 °C) for RacH-PZQ (blue) and raw PZQ (orange).

The enhancement in drug solubility and intrinsic dissolution rate of PZQ when in the hemihydrated form can be explained by the much weaker structure created by the insertion of the water molecule, acting as a wedge pushing the PZQ molecules apart, hindering their interaction in the crystal lattice and weakening the structure. This fact counteract the general rule that an anhydrous form is usually more soluble than the hydrated form, even though some other examples were reported in literature, as in the case of erythromycin dehydrate[170]. Other two reasons for this behaviour of RacH-PZQ can be supposed, starting from the *anti* conformation that proved to favour the solubility enhancement as reported for Form B (section 4.1), and also one can expect a conversion to the polymorphic form when in contact with water: in fact, the saturation solubility and dissolution profiles were almost identical between the two forms, suggesting a possible very rapid conversion. These facts were confirmed by the observation of the same conversion of RacH-PZQ upon heating under vacuum and even spontaneously during storage, that will be now described. When RacH-PZQ was left at 50 °C, under vacuum (35 mmHg) overnight, Form B was obained as demonstrated by DSC (data not shown) and PXRD analyses (Figure 5.15). Moreover, the morphology of the desolvated sample was very similar to Form B, showing agglomerates of whiskers

as reported in the ESEM of Figure 5.16.

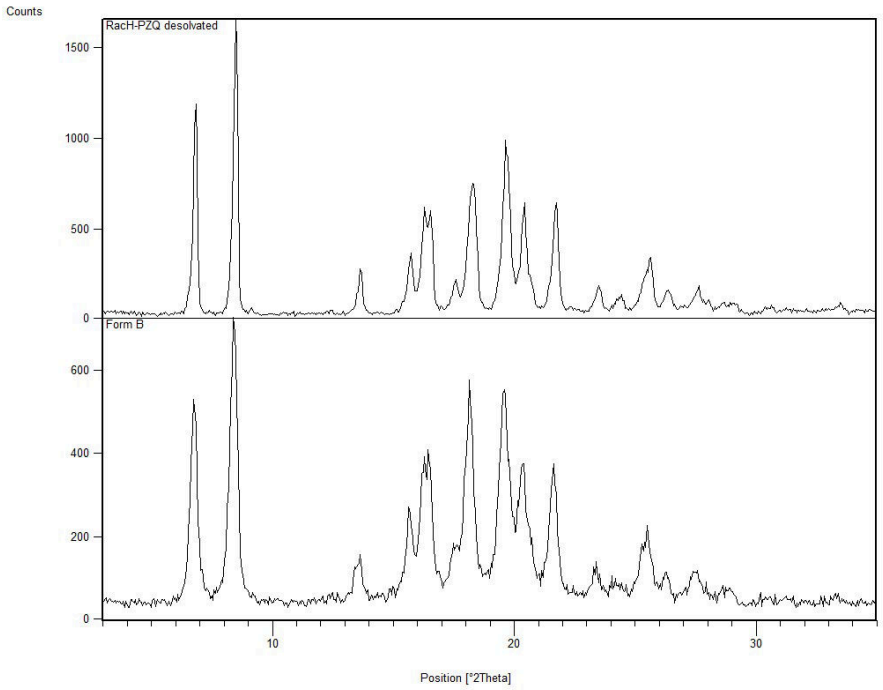

Figure 5.15: PXRD patterns of the desolvated Rac-HPZQ (top, heated over night at 50 °C, 35 mmHg) corresponding to Form B (bottom).

The physical stability of RacH-PZQ was maintained only for 3-4 months, since after this time the main reflections of Form B were noticed in the PXRD pattern, while there were no signals referable to raw ZQ (Figure 5.17).

These facts underlined the close relationship between Form B and Rac-HPZQ, despite of raw PZQ, and also when Rac-HPZQ was ground for other 60 minutes at 25 Hz the reflections of PZQ polymorph B appeared, as shown in Figure 5.18.

RacH-PZQ stability was finally tested upon heating by by *in situ* PXRD, reported in Figure 5.19: the transition to Form B was already complete at 60 °C, which remained stable until 80 °C. This analysis confirmed not only the transition from one phase to the other, but also the stability of Form B when kept at high temperatures. Concluding, the hemihydrated form maintaned also the *in vitro* activity as proved by tests performed against *S. Mansoni* exhibiting a IC_{50} of 0.048 μM, not significantly different form raw PZQ (IC_{50} of 0.165 μg/ml).

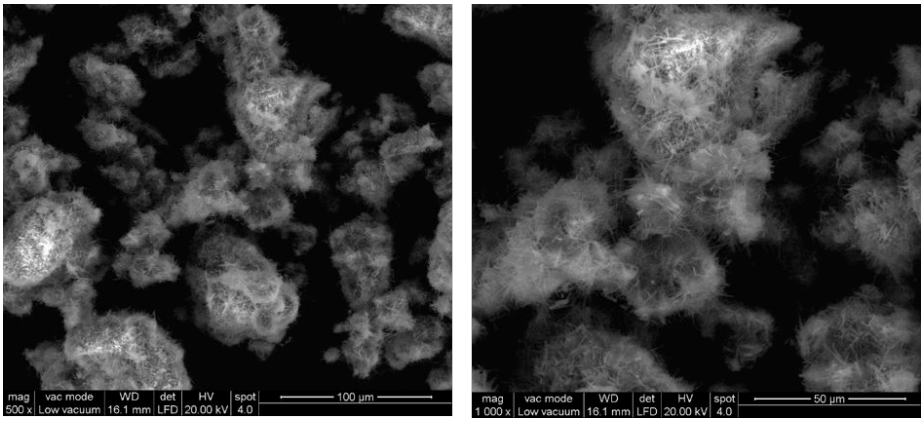

Figure 5.16: ESEM of the desolvated samples: magnification is 500x on the left, 1000x on the right.

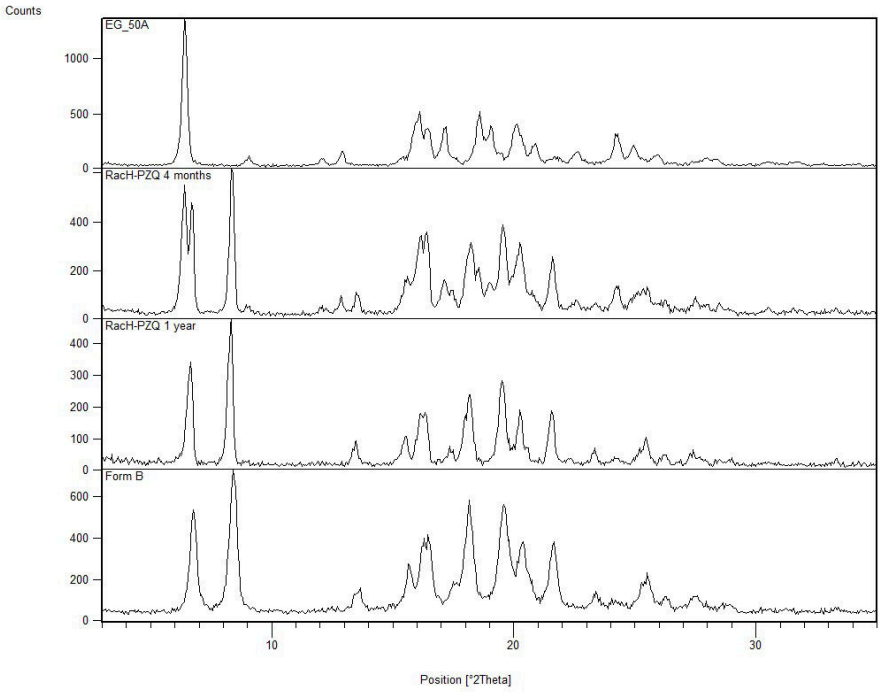

Figure 5.17: PXRD patterns of Rac-HPZQ fresh, after 4 months, one year storage and Form B.

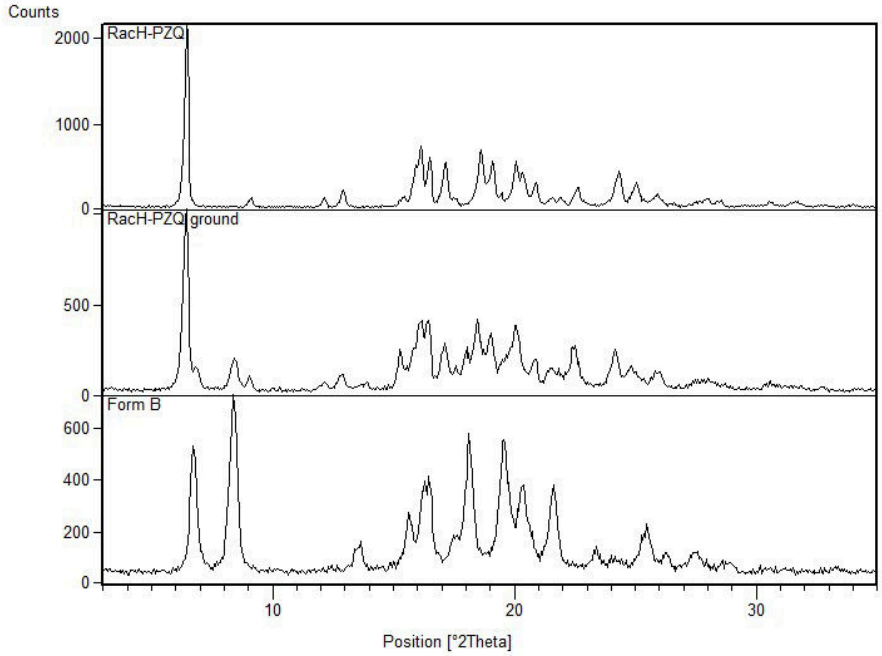

Figure 5.18: PXRD pattern of RacH-PZQ (top), RacH-PZQ ground for 30 minutes at 25 Hz (middle) and raw PZQ (bottom).

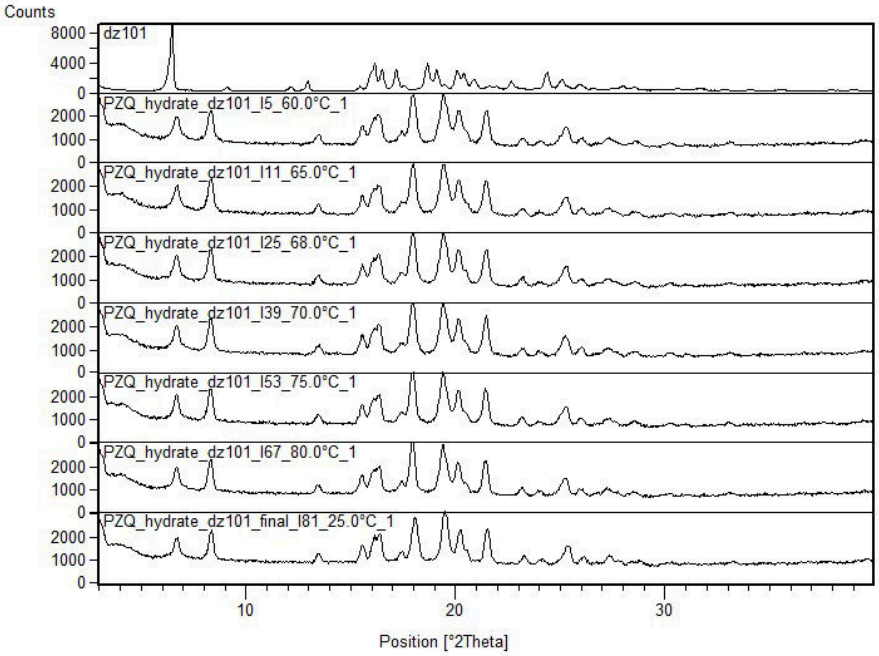

Figure 5.19: PXRD pattern of RacH-PZQ upon heating from 60 to 80 °C from up to down and after cooling (bottom).

5.1.4 Conclusions

The results reported in this chapter reached of several important goals: on one hand, a further investigation on PZQ crystal structure and its propensity to intermolecular interactions, documenting for the first time the possibility of water solvation of the racemic compound. RacH-PZQ was obtained by LAG from Form B or by neat-LAG of PZQ with water in a vibrational mill and the fundamental condition for its formation seemed to be the *anti* conformation of PZQ, which better allows the insertion of the water molecule. The crystal structure was solved from the powder X-ray diffraction pattern, confirmed by DFT calculations, resulting in a triclinic P-1 unit cell as well as PZQ, with one crystallographic independent molecule. RacH-PZQ was completely characterized at the solid state, showing an enhanced water solubility and a double IDR value comparing to raw PZQ. Moreover, a peculiar behavior upon heating and during storage was noticed, i.e. the transition to Form B. This fact, despite being a lack of stability can be seen as an advantageous behavior, since Form B was previously reported as a very interesting PZQ phase with optimal biopharmaceutical properties and activity, until now obtainable only after long neat grinding. Passing through RacH-PZQ, Form B can be easily obtained, without the use of any solvent except of water and in a very minor production time. Finally, the recent test on RacH-PZQ attested its activity *in vitro* against *S. Mansoni*, once again pointing out the properties of this interesting PZQ phase.

5.2 PZQ solvates

In the pharmaceutical field, solvates (referring to the multicomponent system not based on water) can fulfill multiple approaches: from one side they can be consider as valid alternatives to anhydrous drugs, but unfortunately, the majority of the solvents is harmful and therefore the permitted by pharmacopea are just a very small part of the total. From the other side, they can be used as precursor of other solid phases, obtained through a process of purification and separation. The so-obtained products were proved to have high chemical and physical purity and interestingly, the product outcome can be varied in terms of particle size, morphology and defects concentration depending on the desolvation conditions[171]. This method was succesfully used to produce polymorphs of drugs, comprehending also forms which were difficult to obtain by direct crystallization from solution[172–174]. Nevertheless, it is worth notice that at the moment it is not possible to perfectly predict the desolvation products, since the difference in structural and molecular interactions can not give any information on the different or identical desolvation outcome[175, 176]. Considering the solvated drugs, the solvent insertion in a crystal lattice, even though it can sometimes bring some disorder in the structure, can also favour the formation of hydrogen bonds and strong interactions that improve the stability of the system. Also, not to forget the possibility of the solvent to act as a "space filler" in the crystal lattice[165]. The following part of the chapter deals with the research of possible solvated forms of PZQ formed by LAG; it is worth notice that the purpose of the project was more focused on PZQ crystal investigation rather than on possible new pharmaceutical formulations, therefore the solvents used were not selected among the GRAS permitted list. Indeed, only with acetic acid and 2-pyrrolidone two new solid forms were discovered, which were also partially characterized, as presented below. The crystal structure solution of these new phases is still and on-going process due to the failed attempt to single crystal formation and the very challenging powder X-ray pattern.

Materials

Praziquantel (PZQ, (11bRS)-2-(Cyclohexylcarbonyl)-1,2,3,6,7,11b-hexahydro-4-H -pyrazino[2,1-a]isoquinolin-4-one)) was of Ph. Eur. grade and kindly donated by Fatro S.p.a. (Bologna, Italy). Nitromethane, acetonitrile, 1,4-dioxane, ethyl acetate, L-ethyl lactate, methanol, 2-pyrrolidone and Acetic Acid were from SIGMA-Aldrich. The HiPersolv Chromanorm methanol used for the HPLC analysis was of Ph. Eur. grade and purchased from VWR Chemicals (BHD PROLABO® Milano, Italy).

Methods

Grinding experiments The grinding experiments were performed using a Retsch vibrational mill MM200 (Retsch, Germany) and stainless steel jars of 25 mL with 2 stainless steel balls with ϕ= 7 mm. PZQ was accurately weighted (200 mg) and placed in the jars with the milling media. Depending on the experiment, a certain amount of liquid was inserted in the jar (ranging between 10 and 100 μL) and the grinding

process was performed for 30 minutes at 25 Hz. For the further characterization the samples were prepared *via* LAG (Retsch MM400, Retsch, Germany) using 436 mg of PZQ and an equimolar amount of the solvent, using two zirconium oxide jars (35 mL), each one containing 2 balls (ϕ= 10mm).

Thermal analyses Differential scanning Calorimetry was conducted using a Mettler Toledo DSC822e system; about 2 mg of the samples were accurately weighted, put in a 40 μL aluminum perforated crucible and analyzed heating from 30 to 200 °C at 10 °C/min under nitrogen atmosphere. When using the Mettler Toledo TGA/SDTA851e for TGA analyses, the amount of powder was about 10-15 mg of the sample, exactly weighted in a 100 μL aluminum crucible. The method used was the same of the above mentioned DSC procedure.

FT-Infrared Spectroscopy The samples were analyzed using a Perkin-Elmer System 2000 FT-IR instrument on compressed disc prepared by gently grinding the sample in an agate mortar with anhydrous KBr (in a 1:15 ratio by wt) and pressing with and hydraulic press. The range observed was from 400 to 4000 cm^{-1}, the resolution used was 4 cm^{-1} with a step of 1 cm^{-1} and scan number of 3.

Powder X-Ray Diffraction Powder X-Ray Diffraction analyses were conducted by means of a Panalytical X'Pert Pro Diffractometer, with a RTMS X'celerator detector and Cu Kα radiation (wavelength=1.5418 A). About 20 mg of the sample were prepared on a sample holder by gently press with a glass slide.

Scanning electron microscopy A JEOL JSM-5510LV Scanning Electron Microscope was used for imaging on gold metallized sample.

SS-NMR analyses Solid-state NMR measurements were collected using a Bruker Avance II 400 instrument[3]. The spectra were obtained at 100.65 MHzfor ^{13}C. Cylindrical zirconia rotors (4 mm o.d) were used with a sample volume of 80 μl and spun at 12 kHz (^{13}C). In all the analyses a RAMP-CP pulse sequence (^{1}H 90° pulse = 3.05 us), TPPM ^{1}H decoupling with an rf field of 75 kHz were used during the acquisition. The number of transients acquired was 124 with 3 ms of contact time and a relaxation delay of 20 s. As the reference, the resonance of hexamethylbenzene was used (^{13}C methyl signal at 17.4 ppm).

Saturation Solubility and intrinsic dissolution rate The solubility of the samples was analyzed by preparing 10 ml of saturated solutions of each samples in deionized water, kept under agitation in the dark for 48 hours. Then, the solutions were filtered using a membrane (pore size 0.45 μm) and diluted 1:200 with the mobile phase prior injection. The method used was the same as the above described HPLC method. Each analysis was conducted in triplicate and the average was reported.

[3]In collaboration with prof. M. R. Chierotti of the Department of Chemistry, University of Turin (Italy)

For the intrinsic dissolution rate determinations, about 150 mg of the samples were inserted in the sample holder and pressed using an hydraulic press (PerkinElmer, Norwalk, USA) for 1 min at 1 ton. The sample surface area obtained was of 0.785 cm^2 and the entire sample holder with the compressed powder was immersed in a vessel containing 1 L of distilled water kept at 37 °. The system used was a Hanson Research SR8 Plus dissolution test station and the paddle used were positioned at 3.5 cm from the tablet surface, with a rotation speed of 100 rpm. About 2 ml of the dissolution medium were withdrawn every ten minutes till 60 min and immediately replaced with an equal amount of thermo-stated distilled water. The aliquots were then diluted 1:20 with the mobile phase and analyzed using the same above mentioned method. The analyses were performed in triplicate and for each point the mean, with SD (%) and RSD (%) were calculated. The amount of the dissolved drug per unit area over time was indicated by the slope of the curves, obtained through a linear regression method. For the comparison of the different curves the one-way ANOVA test was used, and the data were considered statistically different when having a p value $< .05$.

Physical stability Several samples were kept in a desiccator at room temperature in the dark and analyzed over time using DSC and PXRD.

5.2.1 Results and Discussion

Also in this case, the first part of the study of PZQ propensity to solvate formation was performed during the Erasmus+ traineeship at the Department of Chemistry of the University of Cambridge (United Kingdom) under the supervision of prof. William Jones, while the further characterization was developed at the University of Trieste and by means of a large network of collaborators. The application of LAG to PZQ was done using different solvents generally applied for the search of possible solvated forms: nitromethane, acetonitrile, 1,4-dioxane, ethyl acetate, L-ethyl lactate and methanol. Different quantities were tried (10, 30, 60 and 100 μL), but none of the experiments led to new solid forms, since the PXRD pattern of the products reflected exactly the raw drug. Differently, when using acetic acid and 2-pyrrolidone 2 new solid forms were found, named PZQ-AA (with acetic acid) and PZQ-2P (with 2-pyrrolidone). Similarly to the case of RacH-PZQ, the quantity of liquid added was not significant, since the same patterns were collected in all the experiments. Therefore, to simplify the preparation of the sample and the relative comparison, an equimolar ratio between the component was selected as the main production method. Also, the same solid forms could be obtained when performing LAG with Form B, even improving the crystallinity of the samples. The PXRD pattern of PZQ-AA and PZQ-2P were completely different than the already known crystal structures, but quite similar each others, as reported in Figure 5.20. the main reflections of PZQ-AA were at 6.21, 9.17, 14.90, 15.49, 17.69, 19.20, 20.85, 21.20, 22.57, 23.08 and 28.57 ° of 2θ. For PZQ-2P the main peaks were the following: 6.19, 9.11, 10.09, 14.85, 17.47, 17.83, 19.23, 20.30, 22.23, 22.87, 23.23 and 28.48 ° of 2θ.

Morerover, the formation of the new phases was complete, since no evidence of

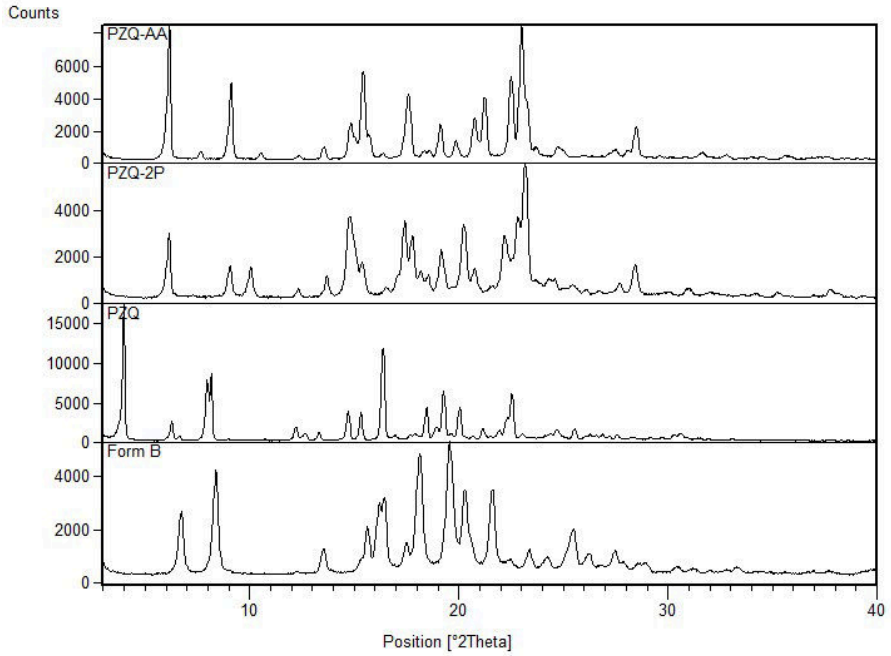

Figure 5.20: PXRD patterns of PZQ-AA (top), PZQ-2p (middle), Form B (use for LAG) and raw PZQ (bottom).

the starting material was found, neither when performing LAG of Form B, nor raw PZQ. To confirm the solvate nature of PZQ-AA and PZQ-2P, different samples were subjected to DSC-TGA analysis, reported in Figure 5.21: each new phase was characterized by one single endothermic event, corresponding to the melting point at 72.26 °C (-74.15 J/g) for PZQ-AA and at 85.69 (-74.48 J/g) °C for PZQ-2P. The other two lines on the graph report the weight loss profile: the experimental weight loss, considering the whole profile[4], was in good agreement with the theoretical monosolvated loss.

For PZQ-AA a theoretical weight loss was of about 16% versus an experimental one of about 13%; in the case of PZQ-2P the experimental data reports a weight loss of about 17% versus a calculated of about 21%. Nevertheless, the final confirmation of the solvated form, together with the correct stoichiometry can be defined only after the crystal structure solution, which is actually a work-in-progress.

[4]The thermogravimetric analysis of PZQ using the same method resulted in an horizontal line till the maximum temperature reached, meaning the absence of any weight lost

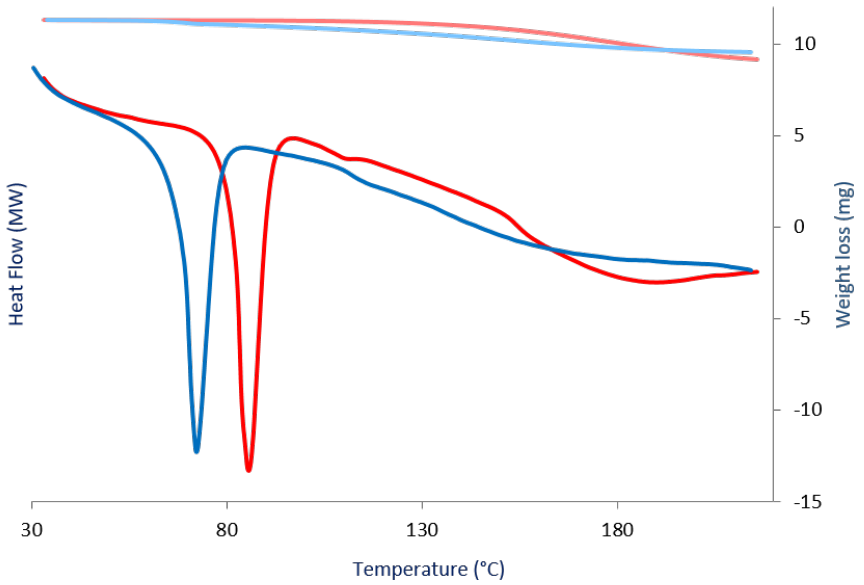

Figure 5.21: DSC-TGA traces of PZQ solvate with acetic acid (blue) and with 2-pyrrolidone (red).

The SS-NMR highlighted the differences between PZQ-AA and PZQ-2P, and with raw PZQ: in particular, Figure 5.22 reports also the chemical shift assigned to the corresponding peaks. In the case of PZQ-AA, one of the C=O signal is not visible, due to the overlapping with the COOH signal of the acetic acid, while in the case of PZQ-2P the additional C=O is easily recognized. Both spectra confirmed the high crystallinity of the samples with very well defined and intense peaks.

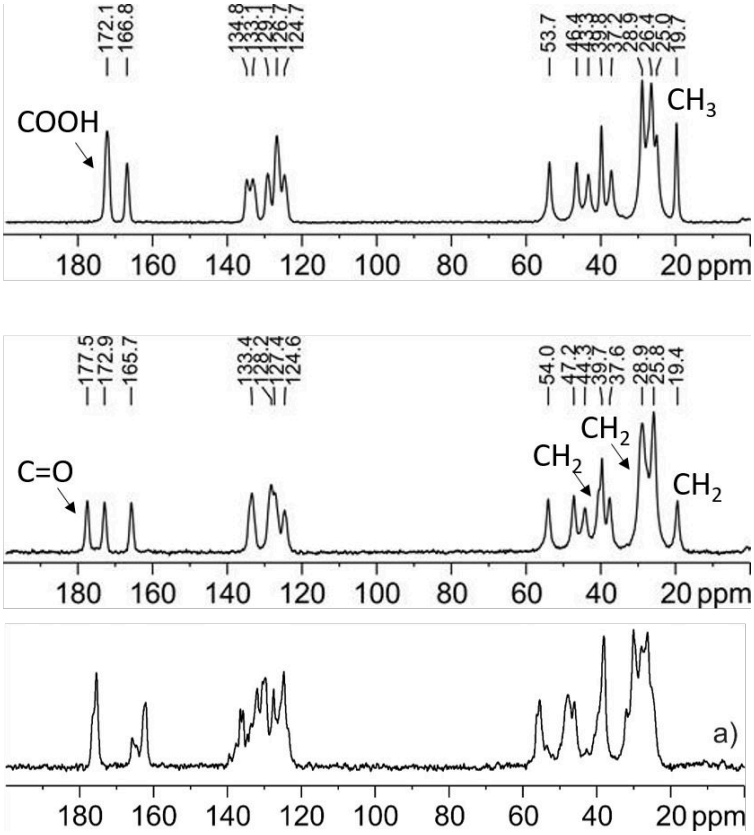

Figure 5.22: $_{13}$C SS-NMR traces of PZQ-AA (up), and PZQ-2P (middle) and raw PZQ (down).

The FT-IR of PZQ-AA and PZQ-2P are reported in Figure 5.23: the presence of intermolecular interactions between PZQ and the solvent molecules were represented by the shift of various bands, as for the carbonyl stretching vibrations of the carbonyl groups of PZQ (recorded at 1651 and 1628 cm^{-1}) found respectively at 1638 and 1611-1601 cm^{-1} for PZQ-AA, 1638 and 1626 cm^{-1} for PZQ-2P, and the characteristic bands of the solvent which were shifted. Figure 5.24 (bottom) reports the corresponding for PZQ-AA: the signal of acetic acid in the range of 1800-1700 cm^{-1} is visibly shifted to lower wavenumbers in PZQ-AA. Similarly (on the top) the set for PZQ-2P is presented: in the solvate form, the intense 2-pyrrolidone peak at 1761 cm^{-1} is shifted to 1687 cm^{-1} and this assignment was confirmed by subsequentely FT-IR analysis on samples obtained in different molar ratio between PZQ and 2-pyrrolidone.

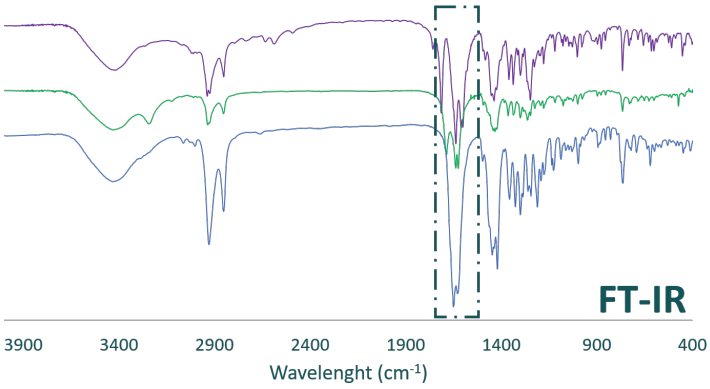

Figure 5.23: FT-IR spectra of PZQ-AA (violet), PZQ-2P (green) ad raw PZQ (blue).

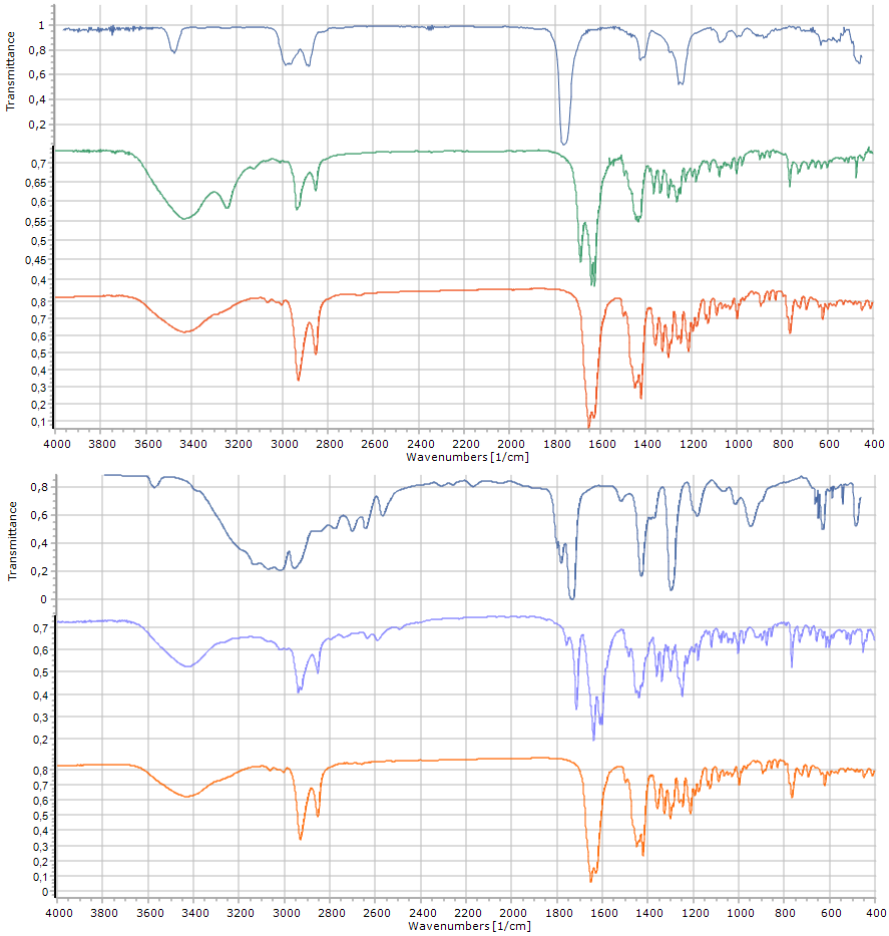

Figure 5.24: On the top: FT-IR spectra of 2-pyrrolidone (database, blue), PZQ-2P (green), raw PZQ (orange). On the bottom: FT-IR spectra of acetic acid (database, blue), PZQ-AA (violet), raw PZQ (orange).

The SEM images of the new solid forms revealed some interesting differences in their morphologies: in the case of PZQ-AA layered blocks with almost flat particles were found, with a rough surface presenting some holes while the needle-shape like aspect of raw PZQ is completely missing. Differently, in PZQ-2P the flat surface of the agglomerates are almost covered by very thin needles (Figure 5.25) somehow remembering the habitus of raw PZQ.

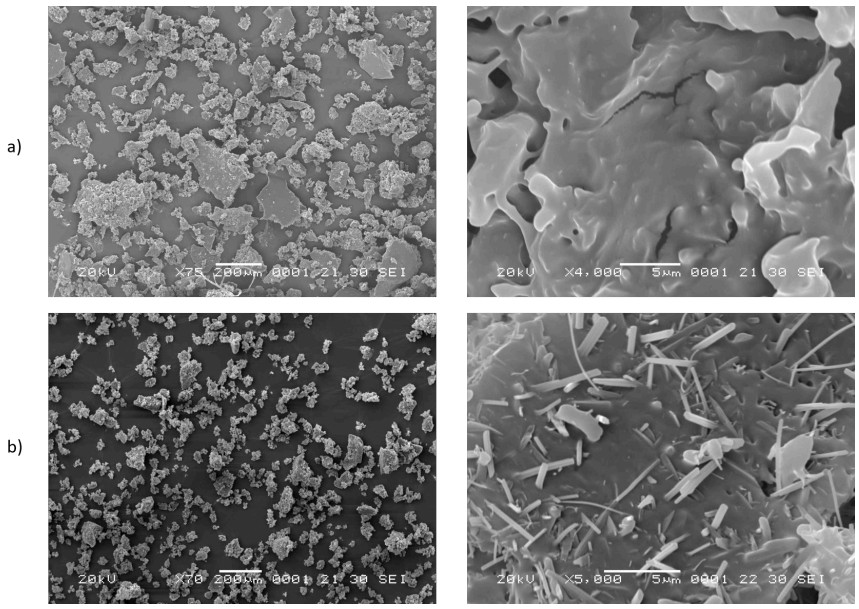

Figure 5.25: SEM images of PZQ-AA (a, 75x and 4000x) and PZQ-2P (b, 70x and 5000x).

The water saturation solubility and the intrinsic dissolution rate were analyzed for the new solid forms and compared to raw PZQ. The solubility at 25 °C for PZQ-AA was 311.91±15.22 mg/L and for PZQ-2P was 340.27±23.18 mg/L, both higher than the raw drug (217.15±10.33 mg/L). Similarly, the intrinsic dissolution rate in water at 37 °C was enhanced in the new forms as reported in Figure 5.26: values of 0.0628±0.0655 and 0.0563 ±0.4745 were recorded respectively for PZQ-2P and PZQ-AA, about double than raw PZQ (0.0341±0.6526). This was in agreeement with the common reported behaviour of the solvated form to be more soluble than the corresponding anhydrous form[177].

Finally, the obtained monosolvate were stable for at least 4 months as demonstrated in Figure 5.27.

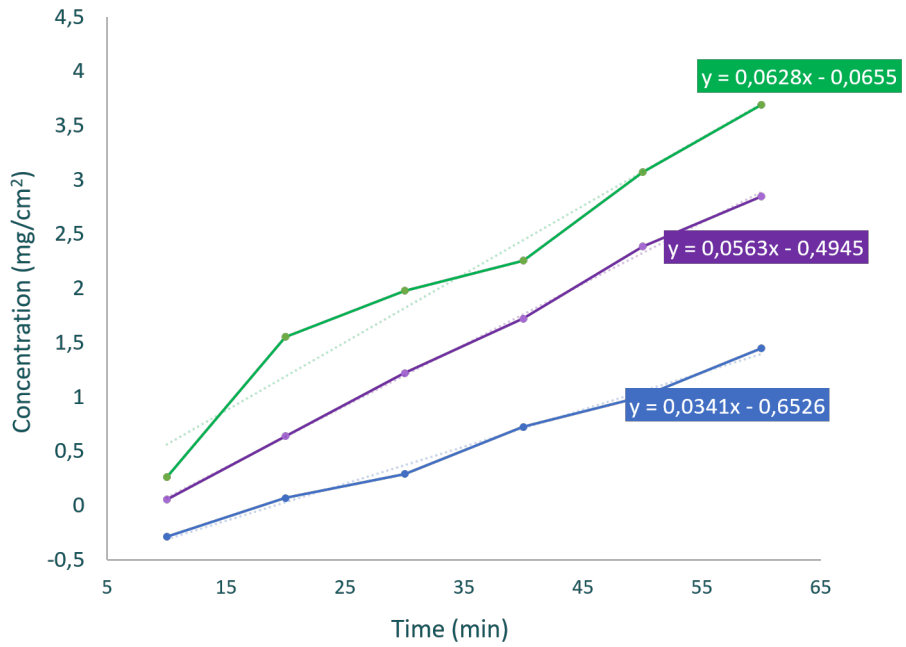

Figure 5.26: Intrinsic dissolution profiles of PZQ-AA (violet), PZQ-2P (green) and raw PZQ (blue).

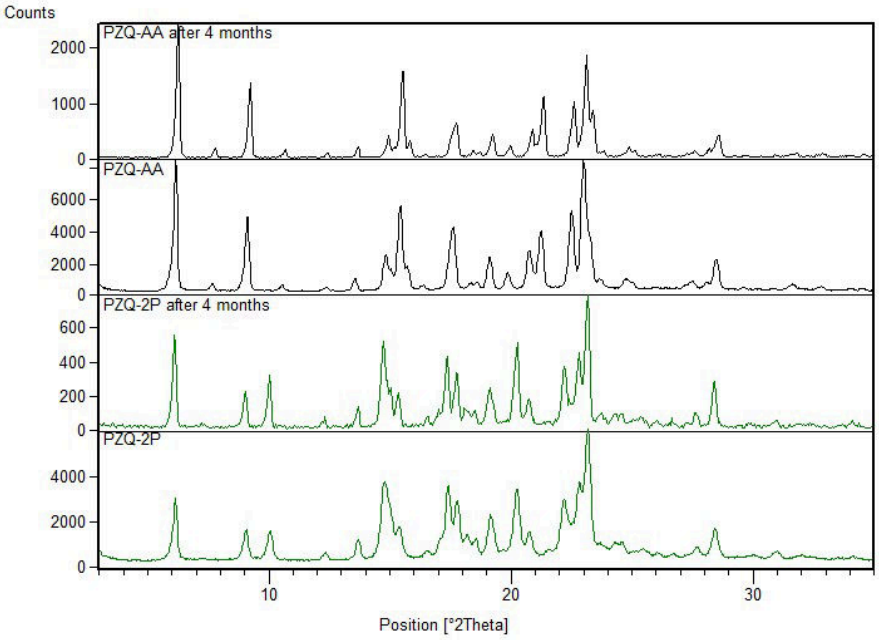

Figure 5.27: Comparison between the PXRD patterns of PZQ-AA (black) and PZQ-2P after 4 months storage and fresh.

5.2.2 Conclusions

The LAG of PZQ, either in its raw and polymorphic form, was successful in creating two completely new monosolvates using acetic acid and 2-pyrrolidone. The new solid forms were characterized at the solid state and also in their solubilities and intrinsic dissolution rates, which were enhanced comparing to raw PZQ. Unfortunately, the crystal structure solution of PZQ-AA and PZQ-2P is at the moment very challenging and still a work-in-progress and the attempts to single crystal formation failed. Anyhow, these findings put in light once again the propensity of PZQ to form different phases not only when in its amorphous or polymorphic form, but also in its raw state. Certainly the chemical nature of the solvent used seems to be a highly significant variable of the LAG process, as it was reported by Trask and collaborators[129], but also the starting phase was demonstrated to be important in the final product outcome, as reported in the case of RacH-PZQ. Therefore further studies in this direction are needed to deeply investigate the significative variables of PZQ solvate formation and, subsequentely, the possible obtainable products upon their desolvation in different conditions.

5.3 Appendix D

Crystal structure determination from powder X-ray diffraction data The PXRD pattern of PZQ hemihydrate material was indexed using N-TREOR algorithm via an interface of EXPO2014. The indexing procedure revealed a triclinic unit cell with the volume of 860.2 Å3, which corresponds to two PZQ molecules per unit cell. Since the hemihydrate material was prepared from a racemic anhydrous PZQ, structure solution was attempted in a centrosymmetric P-1 space group. The structure was solved using the Simulated Annealing procedure implemented in EXPO2014[142]. The asymmetric unit contained one PZQ molecule and one oxygen atom corresponding to water molecule. Structure solution process involved a large number of randomized steps where translational (for both PZQ and water oxygen) and rotation (PZQ only) degrees of freedom were varied. In addition, intramolecular rotation around the flexible bonds was allowed. The PZQ fragment was given full occupancy, while the water oxygen occupancy was fixed at 0.5, reflecting the experimentally determined stoichiometry of the material. Rietveld refinement[178] of the structure was preformed in TOPAS Academic 4.1[143]. In addition to the translational, rotational and intramolecular degrees of freedom, zero-point shift, peak shape function and background polynomial were refined. The diffraction peak shape was described by a pseudo-Voigt function, while background was fitted with a 12-term Chebyshev polynomial function. The occupancy parameter of the water oxygen atom was allowed to refine, and the occupancy remained close to the expected value of 0.5. In the final refinement oxygen occupancy was once again constrained to 0.5, and two hydrogen atoms were inserted in the most probable positions, corresponding to the hydrogen bond directions towards the carbonyl oxygens of PZQ. The resulting structural model reveals that water molecule is disorder over an inversion center with a 50:50 probability.

Periodic DFT calculations Periodic DFT calculations were performed using the plane-wave DFT code CASTEP 16.1.[150]Crystal structures of three polymorphs of anhydrous PZQ, as well as the racemic hemihydrate structures were geometry-optimized with the aim of calculating relative stability of these crystal forms. The experimental crystal structures were converted in CASTEP format with the help of cif2cell[155] utility. The DFT calculations were performed using semi-local PBE[152] functional combined with a Grimme D2[179] semiempirical dispersion correction. The plane wave basis set was truncated at 700 eV cutoff, and the norm-conserving pseudopotentials were used to modify the Coulomb potential in the core regions of electron density. The electronic Brillouin zone was sampled with a 0.03 Å-1 Monkhorst-Pack k-point grid[156]. Geometry optimization involved variation of atom coordinates and unit cell parameters subject to the symmetry constraints of the corresponding space groups. The following convergence criteria were used: maximum energy change 10-5 eV per atom, maximum force on atom 0.01 eV Å-1, maximum atom displacement 0.001 Å and residual stress 0.05 GPa.

Modelling of SSNMR The optimized crystal structures were used for modelling solid-state NMR spectra. NMR parameters were calculated using the CASTEP implementation of GIPAW method[151]. The calculations used PBE semi-local functional, with a plane-wave basis set truncated at 1000 eV cutoff. Core regions of electron density were described using on-the-fly generated ultrasoft pseudopotentials[180]. The calculated chemical shieldings were converted into chemical shift using a reference shielding of 170 ppm. The spectral lines were drawn with Lorentzian curves with 1 ppm HWHM. The comparison between the experimental and the calculated spextra is reported in Figure 5.28.

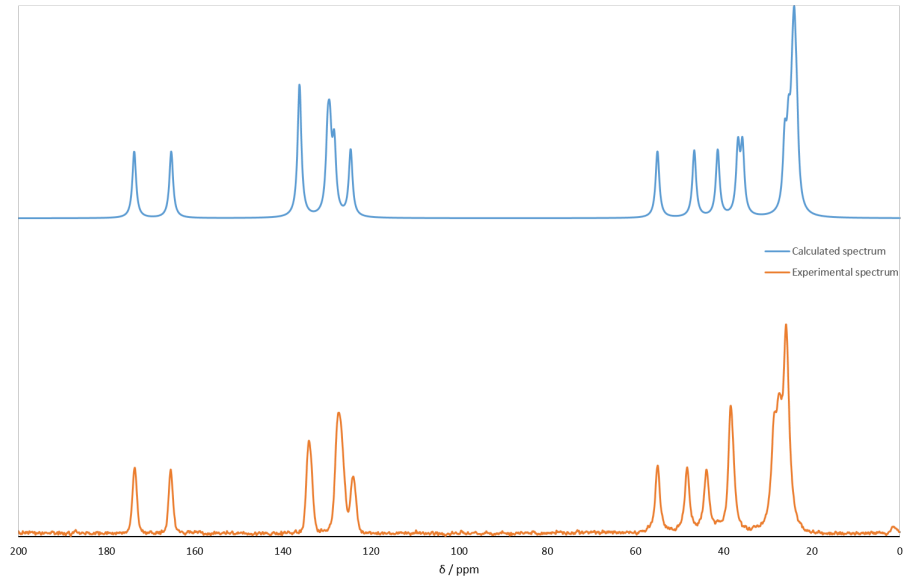

Figure 5.28: Comparison between the experimental and calculated ^{13}C SSNMR spectra.

Chapter 6

Other cogrinding strategies and formulation technologies

The last chapter of this thesis will focus on other cogrinding approaches and formulation strategies that have been applied to PZQ: the first one involves the use of mesoporous silica, since there are limited data in literature regarding the milling of API with this kind of excipient (as it will be later described), followed by different sugar esters both during neat and LAG experiments. Subsequently, the promising Form B previously described, one cryocoground sample and the corresponding physical mixture will be then included in microparticles to enhance PZQ biopharmaceutical properties. At the end, an interesting approach towards the amelioration of PZQ taste will be proposed by co-grinding with selected natural and artificial sweeteners.

6.1 Cogrinding PZQ with mesoporous silica

6.1.1 Introduction

The application of mesoporous silica in the pharmaceutical field is not a new technique, being frequently used carriers for drug delivery, both in case of simple molecules as ibuprofen, or more complex systems as anticancer drugs or DNA and proteins.The large use is due to various peculiar characteristics. First of all they are not-toxic and biocompatible, and also, they can be engineered different ways, creating films, fiber, spherical particles, rods and core-shell materials[181, 182]. Silica excipients are characterized by a high surface area and the presence of numerous high volumetric pores: the presence of these pores is of a critical importance on the drug load capacity, diffusion, stability and in its physical state. In fact, the drug, when confined in the pores, remains in the amorphous form, as it was demonstrated in literature[183]. Moreover, it is possible to tune the pore size in order to create different materials, classified as mesoporous by IUPAC when having a pore size between 2 and 50 μm. In addition, the silica surface is covered by silanol groups that represent places of interaction and absorption, able to

create both weak or covalent interactions (when functionalized) that are fundamental to immobilize the drug. In fact the H-bond donor nature of the silanol group can favor the formation of links when in contact with H-bond acceptor atoms, while the layering of the drug on silica surface can be attributed mostly to hydrophobic interactions[182, 184]. Moreover, there is the theoretical possibility of creating self-interacting matrix in highly hydroxylated sufaces, with the silanol oxygen acting as a H-bond acceptor. In the system composed of ibuprofen:silica the only interacting group of the drug was the carboxylic group, creating a cyclic H-bonds network with 3 silanol groups, while in aspirin three silanol are connected to the carboxylic group and another one to the ester carbonyl[185]. Obviously, the density, type the possible functionalization of the silanol groups are significative variables not only in the interaction strenght, but also in the final release of the drug during dissolution. Drug loading into mesoporous silica can be performed in different ways as adsorption from organic solution[181], spray drying[186, 187], melt[188], microwave[189] and many other methods[190]. However, very few works reported the use of grinding, as for the system with indomethacin [191, 192], which provided amorphous samples stable for 3-6 months at 40 °C and 75% RH. This section will investigate the effect of grinding PZQ with different grades of mesoporous silica, starting with a general screening by means of PXRD, DSC, HPLC for drug recovery. Then one of the system will be selected for further analysis, comprehending stability tests and the evaluation of the activity *in vitro* of the most promising samples against *S. mansoni*. Morever, since the formation of silica:API systems demonstrated to be effective in the enhancement of drug dissolution rate[184, 193, 194], this aspect will be evaluated for the silica system with PZQ. Future studies will investigate the type of incorporation/dispersion/absorption of PZQ with the sylica excipient, for the moment we refer to the interaction as PZQ amorphisation.

6.1.2 Materials and Methods

Materials

Praziquantel (PZQ, (11bRS)-2-(Cyclohexylcarbonyl)-1,2,3,6,7,11b-hexahydro-4-H -(pyrazino[2,1-a]isoquinolin-4-one)) was of Ph. Eur. grade and kindly donated by Fatro S.p.a. (Bologna, Italy). Syloid 244-FP, Syloid 74-FP and Syloid Al-1FP were a gigt from Alltech Italia s.r.l. - Grace Division (Columbia, USA) and the main characteristics are reported in Table 6.1. The HiPersolv Chromanorm methanol used for the HPLC analysis was of Ph. Eur. grade and purchased from VWR Chemicals (BHD PROLABO® Milano, Italy).

Methods

Preparation of the physical mixtures and coground samples The physical mixtures were prepared by mixing PZQ in an agate mortar (3 minutes) with each silica grade in a 1:1 weight ratio. The coground samples were obtained by milling using a vibrational mill Retsch MM400 (Retsch, Germany), zirconium oxide jars (35 mL) each one with 2 milling media (ϕ=10 mm). The total amount of the powder in the

Table 6.1: Main characteristics of the non-ordered mesoporous silica grades used.

Property	Syloid 74FP	Syloid 244FP	Syloid Al-1FP
Average particle size (μm)	5.9-7.5	2.5-3.7	6.5-8.1
Surface area (m^2/g)	340	310	700
Average pore volume (ml/g)	1.2	1.6	0.4
Average pore diameter (A)	150	200	-
Bulk density (g/cm^3)	0.26	0.11	0.90
pH (5% acqueous suspension)	6.0-8.0	6.0-8.0	4.0-6.0

jars was 4.50, 2.25 or 1.15 mL corresponding to a loading volume in each jar of 15.8, 9.4 and 6.3 % respectively, since the total volume of the milling media was 1.04 mL. The frequency of milling was varied between 15, 20 and 25 Hz and the time of milling was from 15 to 180 minutes, with withdrawing every 15/30 minutes. For comparison, all the Syloid grades were ground by themselves using a total loading of 9.4%. After preparation, the samples were stored in a desiccator in the dark at room temperature.

Differential Scanning Calorimetry Each sample was analyzed using a Mettler DSC TA 4000 (Greifensee, Switzerland) connected to a calorimetric cell Mettler DSC20 and using STARE software version 9.30 for data analysis. Prior to analysis the instrument was calibrated with Indium, Zinc and Lead for the temperature and with Indium for the enthalpy quantification; each sample, containing about 2 mg of PZQ exactly weighted, was placed in a 40 μm aluminum pan with perforated lid and heated from 30 to 200 °C (10 °C/min) under air atmosphere.

Powder X-ray Diffraction The sample were analyzed by powder X-ray diffraction using a Bruker AXS D5005 X-ray diffractometer with Ni-filtered Cu Kα radiation (wavelength=1.5418 A). The preparation of the samples consisted in pressing about 20-30 mg of powder over a glass slide to have a flat surface. The data were collected in a 2θ range of 3-35 degree, 0.5° every 2 sec. These analyses were performed thanks to the collaboration with prof. V. Lughi of the Department of Engineering and Architecture, University of Trieste, Italy.

FT-IR spectroscopy FT-IR analyses were performed using a Perkin Elmer System 2000 FT-IR; the samples were mixed with KBr in an agate mortar and then pressed with an hydraulic press for 2 minutes at 10 Ton to obtain homogeneous and transparent discs. The analysis was conducted in the range from 400 to 4000 cm^{-1} with a resolution of 4 cm^{-1} and total scan number of 3.

HPLC-UV The content of PZQ was assayed by means of a reverse-phase HPLC-UV by adapting a method already reported in literature[91][1]; the system had two delivery pumps (LC-10 ADVP, Shimadzu, Japan), an autosampler (SIL-20A, Shimadzu, Japan) a UV-vis detector (SPD-10Avp, Shimadzu, Japan) and the data were acquired at a fixed wavelength of 220nm using an interface (SCL-10Avp, Shimadzu, Japan) and analyzed with Ez-Star software; the column used was a Kinetex 5 um c18 (150 x 4.60mmm, Phenomenex, Bologna). The mobile phase used was a mixture of Methanol:water (65:35 v/v), purged at 1 ml/min. PZQ retention time was 5.5 min while the total run time for each sample was set at 12 min. Prior to analysis, a linear calibration curve with r^2=0.99996 was obtained for PZQ under these conditions using different concentrations of the drug from 0.3 to 10 mg/mL. Each day, a standard solution (with a concentration of 2.5 mg/L) was prepared by dissolving about 10 mg of PZQ accurately weighted in Methanol of HPLC grade (20 mL) and diluting the solution 1:200 with the mobile phase. Moreover, two additional calibration curve were obtained respectively for the relative impurity indicated in the Eur. Ph. (Ed. 8.0)[32], impurity A (r^2=0.9993) and impurity B (r^2=0.9994), which were identified at the retention time of 3.45 min and 11.2 min. The reference solution did not report any of these impurities.

Environmental Scanning Electron Microscopy Selected samples were observed using a ESEM Quanta 200 under low vacuum (minor/equal to 1.5 Torr), using an electron beam of 20 kV.

Dissolution studies The dissolution studies were performed in 1000 mL of water thermostated at 37±0.5 ° and stirred at 100 rpm using a paddle apparatus (Erweka DT800, Heusenstamm, Germany). The sample was added to the vessel according to the solubility value, in order to ensure the sink conditions. Withdrawals of 2 ml were performed at specific times with a 8μm filter and analyzed by HPLC using the method previously described to assess the PZQ content. Each time, the withdrawals were replaced with the same volume of thermostated fresh dissolution media. The dissolutions were performed at least three times and the mean±SD was considered aas the final value.

Sample stability Selected sample were analyzed in their physical and chemical stability over time using DSC, PXRD and HPLC.

Efficacy in *in vitro* The *in vitro* tests were performed at the Swiss Tropical and Public Health Insitute (Switzerland, thanks to the collaboration with prof. J. Keiser). The samples were tested in their efficacy against adult *S. mansoni* by preparing different concentrations, ranging from 0.021 to 0.33 μg/L in which adult Schisosomes

[1] In collaboration with proff. N. Passerini and B. Albertini of the Department of Pharmacy and Biotechnologies, University of Bologna, Italy, as well as for the dissolution and solubility studies.

were incubated for up to 72 hours. By using an inverse microscope (Carl Zeiss, Germany, magnification 80x) all the alterations of morphology, motility and viability were observed and the IC_{50} value was calculated with CompuSyn software.

6.1.3 Results and Discussion-1

The characterization of the obtained samples will be now presented in two sections: the first one reports the results obtained with Syloid 74FP and 244FP, while the second one with Al-1FP, due to its peculiar otcomes.

Coground samples with Syloid 74FP and 244FP

PZQ was ground with the silica excipients at the three frenquency, withdrawing samples every 15-30 minutes, which were immediately analyzed by DSC. Generally, after only 15 minutes grinding a dramatic reduction in PZQ enthalpy was noticed, even when working at a low frequency such as 15 Hz, passing from about 107 J/g to 12 J/g and 6 J/g respectively per Syloid 74FP and 244FP. When grinding at 20 Hz the amorphisation was reached after only 15 minutes grinding, highlighting the extraordinary efficacy of this kind of excipients, comparing to other experiences previously reported, where longer times or other techniques (i.e. cryogrinding) were necessary to have the same results. As reported in Figure 6.1, the more was the frequency and milling time, the more the amorphisation of the drug.

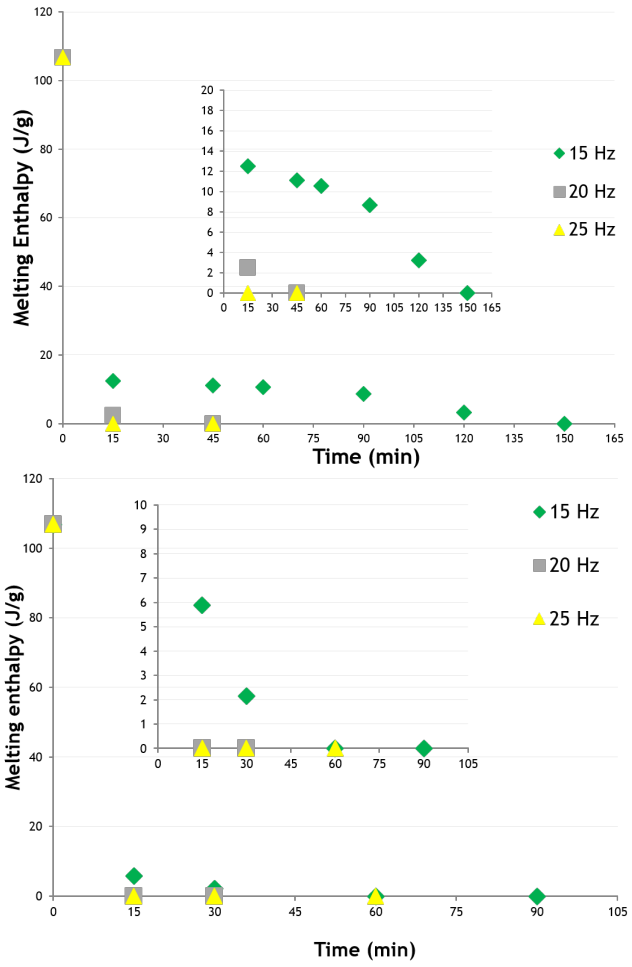

Figure 6.1: Graphics representing the melting enthalpy of the sample ground for different times, with Syloid 74-FP (top) and with Syloid 244-FP (bottom). The detail in the box.

In particular, the DSC trace of PZQ is characterized by the melting peak at about 142 °C, followed by an exothermic degradation with a maximum at about 185 °C which are represented also in the physical mixture together with the dehydration endotherm of the excipient (Figure 6.2). Interestingly, the dramatic reduction of the melting enthalpy could not be attributed to the dilution effect of the excipient, but to the specific interaction between the components. Also, an exothermic transition (at about 167-170 °C) was noticed in the physical mixture and in the coground samples. In the coground samples the melting endotherm of PZQ disappeared, sign of drug amorphisation, except for the samples ground at 20 Hz with Syloid 74-FP, where a reduction of the temperature and also of the melting enthalpy was noticed. This effect was attributed to the reduction in drug crystallinity and the presence of nanocrystalline phases, according to the Gibbs-Thomson effect as reported by Hasa and coworkers[107].

The exothermic event could be attributed to a degradation phenomenon, that in the case of the raw drug seemed to be more gradual, while in the binary systems is represented by a real peak. The reduction in the temperature range of this exotherm could be attributed to the de-structuration of the crystal lattice and the enhanced surface area that favoured drug degradation. These facts were confirmed by the DSC analyses of the excipient as a raw material and after grinding, which did not show any exothermic event. Additional thermial analyses were conducted under nitrogen atmosphere[2]: in the case of the physical mixture, the exothermic event disappeared (meaning the need of an oxidizing atmosphere for the thermodegradation), while in the coground sample was still evidenced. The possibility of a crystallization of the drug on Syloid surface was also analyzed, since the exothermic shape resembled this transition, but even when heating the sample till 300 °C or performing a controlled cooling and subsequent heating, no additional melting events were noticed. Another hypothesis relies on the breaking of the surface/inclusion interaction between PZQ and Syloid when heating at high temperatures. Silica excipients have been widely used as pharmaceutical carrier, but no evidence of similar behaviour upon grinding have been found in literature and only the system studied were based on Indomethacin[191, 192, 195, 196]. We tried for comparison a system based on Ibuprofen and no exothermic events were found.

[2]DSC PerkinElmer 6 (PerkinElmer, Beaconsfield, UK, software Pyris), under nitrogen atmosphere (20mL/min). 7-8 mg of the sample were analyzed in the temperature range of 30-210 °C at 10°C/min.

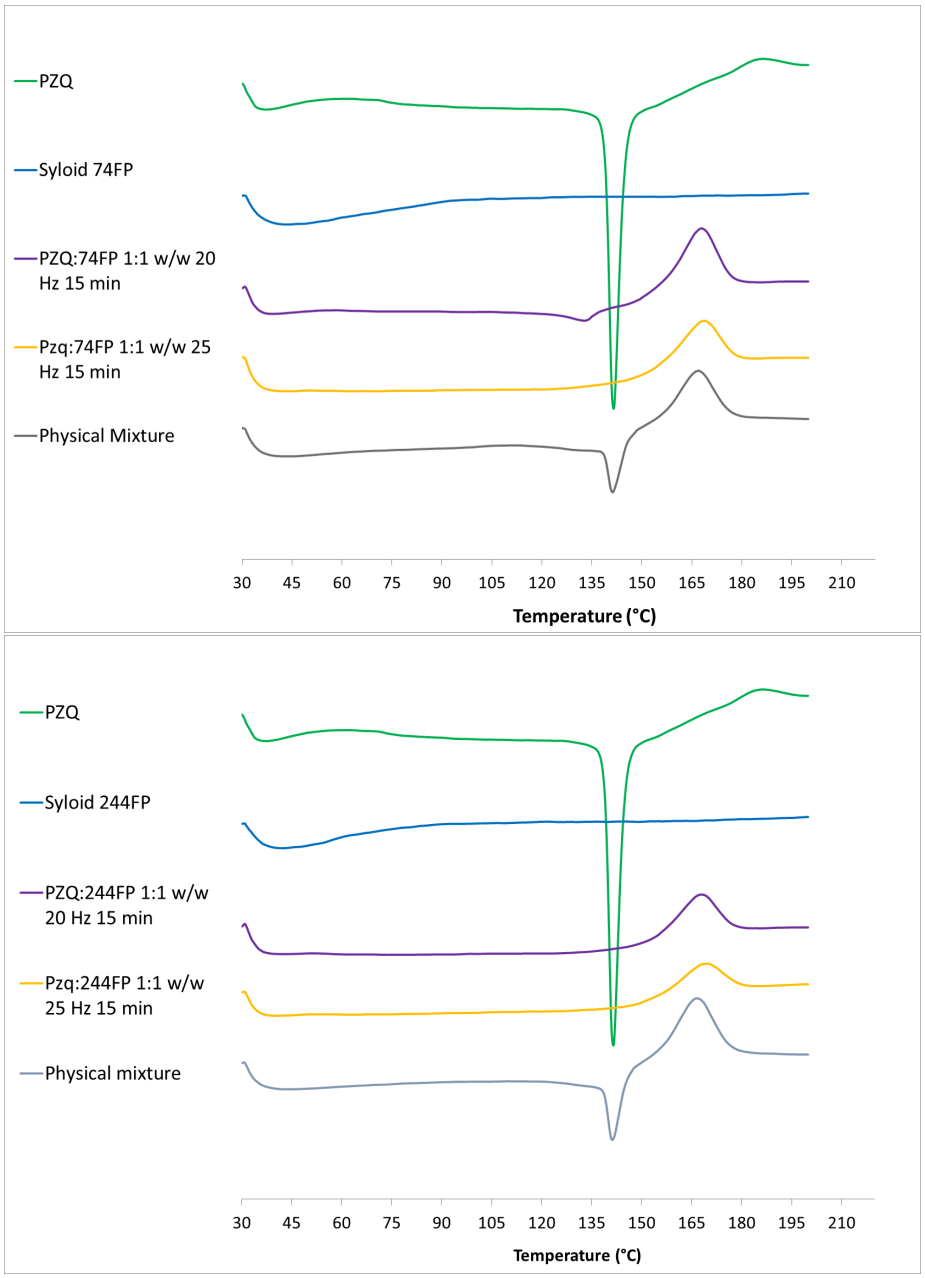

Figure 6.2: DSC traces of the coground samples with Syloid 74FP (top) and with Syloid 244FP (bottom).

The mechanochemical activation of PZQ was confirmed by the PXRD analyses: the excipients were characterized by an halo pattern without any sign of crystallinity, the physical mixtures evidenced the presence of PZQ in a partially broad spectrum due to the effect of Syloid as well as the reduction in the intensity of the peaks. The coground samples were characterized by an halo pattern with the disappearance of the PZQ signal as the first very intense peak at 4° of 2θ. In the case of Syloid 74FP ground at 20 Hz very little PZQ reflections were notice, signs of residual PZQ crystallinity (Figure 6.3). In all the binary samples a certain shift of the characteristic PZQ peaks was noticed, which could be related to the interaction of the two components, even in the physical mixture (data not shown) and also to the difficulties found in sample preparation. Contrariwise, no new solid forms were formed since no evidence of new peaks was noticed.

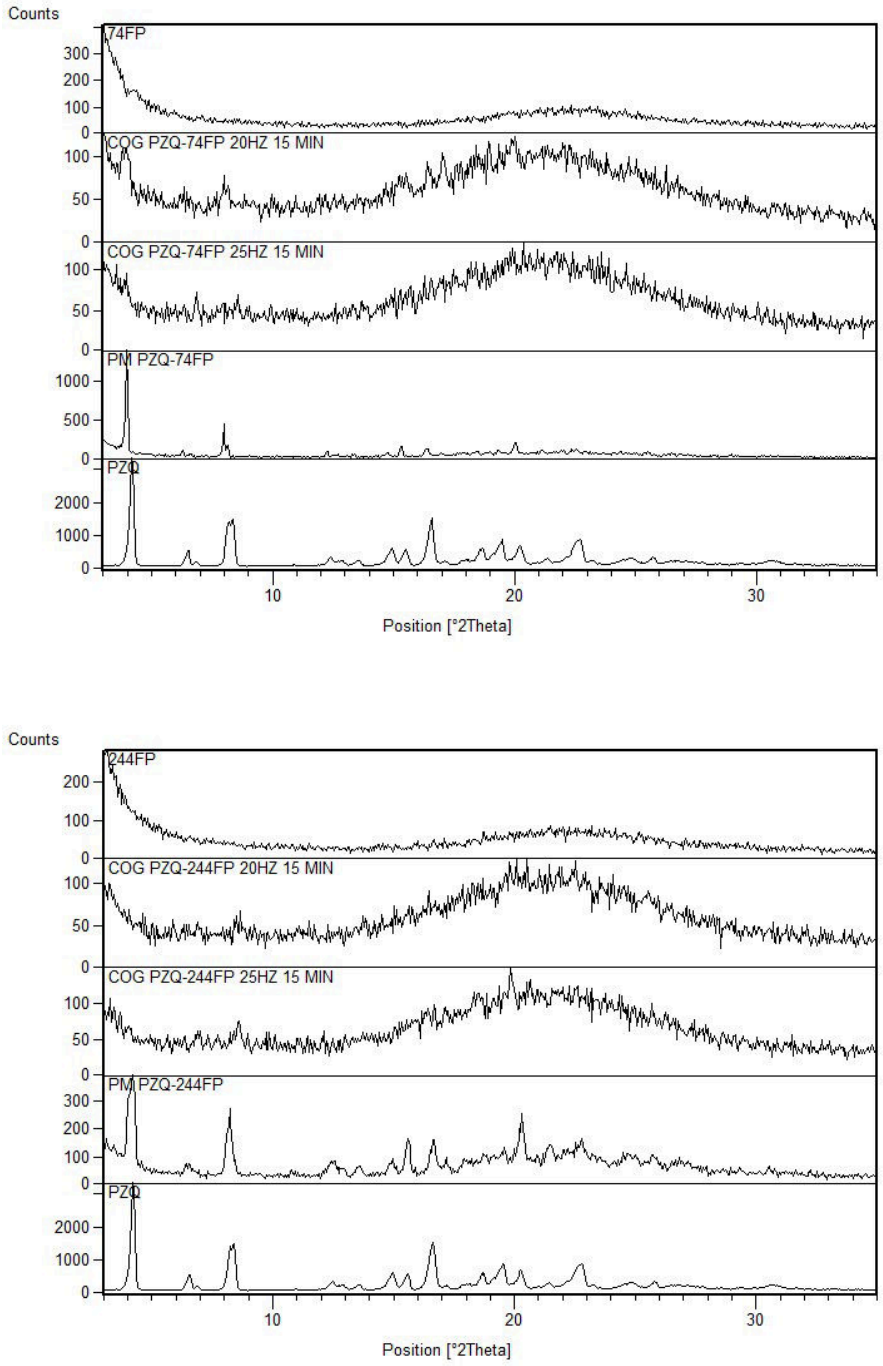

Figure 6.3: PXRD patterns of the coground samples with Syloid 74FP (top) and with Syloid 244FP (bottom).

In the FT-IR spectra of Syloid (Figure 6.4) the main bands identified were the asymmetric stretching of the Si-O-Si bonds at 1100 cm^{-1}, the bending of the sylanol group and the OH band at 3450 cm^{-1}, while the characteristic FT-IR bands of PZQ has been already described (section 4.1). In the physical mixture the most relevant region, the one of the carbonyl group, is superimposable with the raw drug, while in the case of the coground samples the two characteristic peaks of PZQ are replaced by a broad band, as it was also noticed in the amorphous solid dispersion with PVP and CROSPVP (section 4.1).

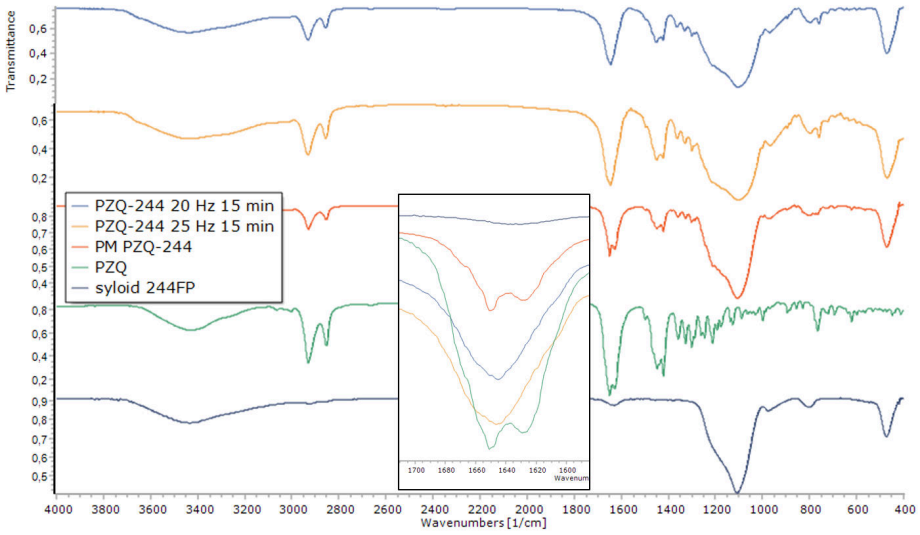

Figure 6.4: FT-IR spectrum of the sample coground with Syloid 244-FP, zoom detail in the box.

Coground samples with Syloid Al1-FP

The second part of the results and discussion is focused on the peculiar results of the PZQ:Syloid Al1-FP system. First of all, to achieve a certain grade of amorphisation longer times were necessary, comparing to the other silica grade. Moreover, when grinding for 90 minutes at 25 Hz or 180 minutes at 20 Hz an weak endothermic event was found at about 100 °C, not attributable to raw PZQ melting (Figure 6.5). This fact was particularly interesting since it has been reported that by selecting the silica excipient with an appropriate pore dimension, it is possible to control the polymorphic outcome[197]. In this case the melting point suggested the selective crystallization of part of the sample to PZQ Form C (previously described (paragraph 4.3)), while the other part remained in the amorphous state.

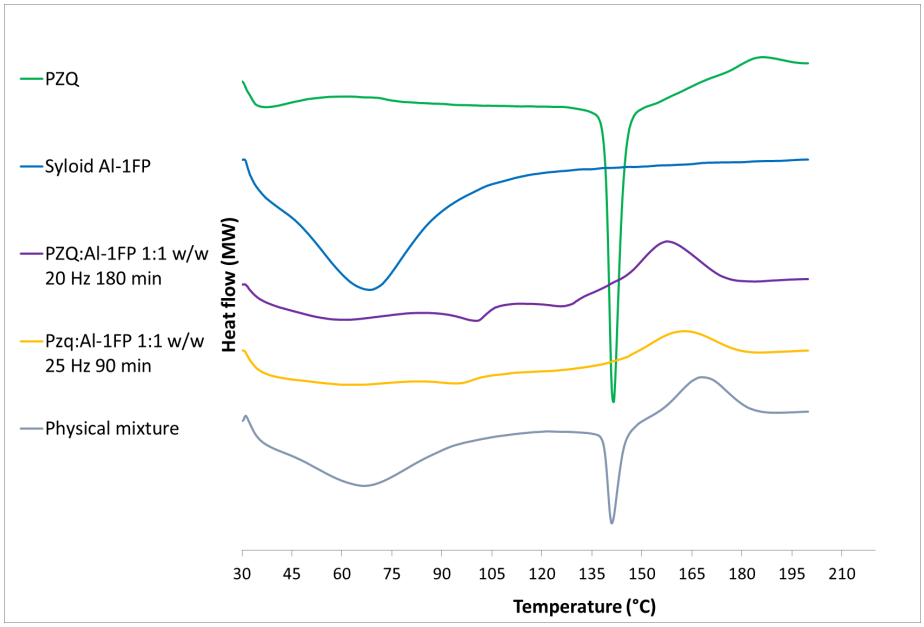

Figure 6.5: DSC traces of the coground samples with Al-1FP.

To confirm this hypothesis, PXRD and FT-IR analyses were conducted. In the physical mixture the characteristic reflections of PZQ were identified, even if with a reduced intensity and little shift in the 2θ position, while in the coground samples the PXRD peaks, surrounded by a conspicuous background noise, were more likely to be the ones of Form C, but certainly there were no resemblance of raw PZQ, as shown in Figure 6.6.

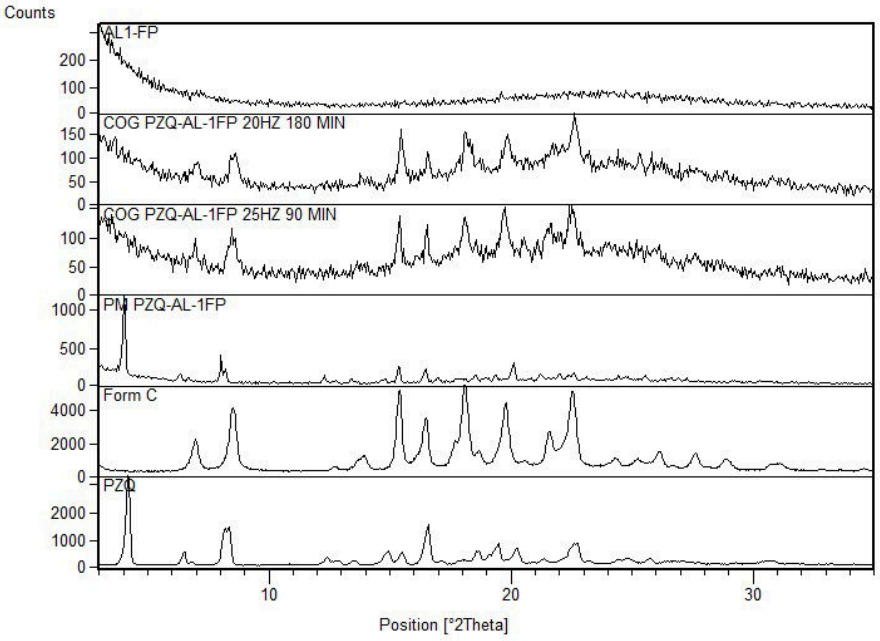

Figure 6.6: PXRD patterns of Al1-FP, coground sample for 180 at 20 Hz, coground sample for 90 minutes at 25 Hz, physical mixture, Form C and raw PZQ.

The FT-IR analysis confirmed the presence of a polymorphic form, due to the correspondence of the peaks in the carbonyl region, differently from raw PZQ, as reported in Figure 6.7. Nevertheless, this analysis could not discriminate between Form B and Form C due to their identical FT-IT spectra (section 4.3).

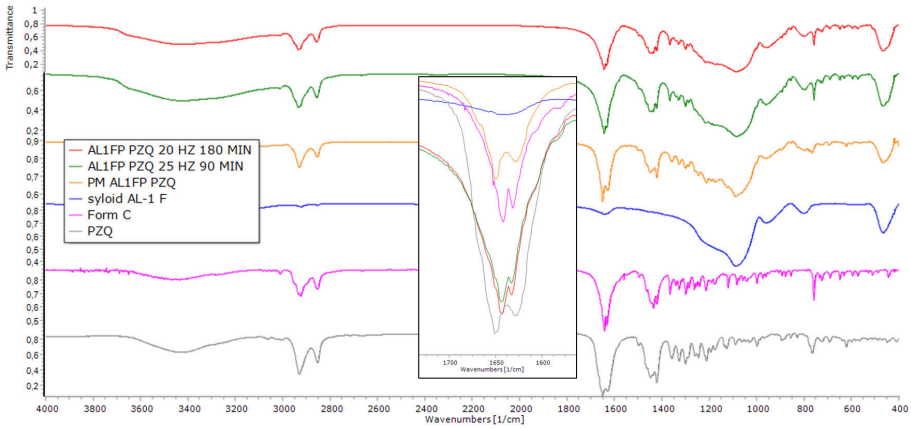

Figure 6.7: Detail of the FT-IR spectra of the coground samples with Al1-FP, the polymorphic forms and raw PZQ.

The surface confinement of the silica excipient was considered the main reason for the crystallization of the polymorphic form, and also, the very little pore volume in Syloid Al1- FP could favour the crystallization of structures with a smaller volume than raw PZQ, as in the case of both the polymorphic forms. The selective crystallization in Form C without any evidence of the presence also of form B was not surprisingly, since among all the experiments conducted on PZQ, the coexistence of both the two polymorphic form was never found. The samples were subjected to DSC analysis after two months, evidencing the slow crystallization of raw PZQ, as similarly observed for Form C physical stability (section 4.3).

In general two consideration regarding sample preparation arised from this screenig: when the jar loading was 9.4 % (2.25 mL of powder) the results were more repeatable and also the products were more activated and easier to be removed from the jars. Morever, by using a frequency of 15 Hz the worst performances were achieved, suggesting the use of 20/25 Hz for further characterization.

So, the three different binary coground systems were analyzed by HPLC-UV to determine the drug content and analyze possible degradation derived from the mechanochemical process or from the interaction with the excipients. The samples analyzed were ground with each silica grade for 60 minutes at 25 Hz obtaining PZQ recovery values of 95.68% (Al-1FP), 95.25 % (74FP) and 98.48% (244FP), in which, besides PZQ Pharmacopoeia related compound[32], the amount of other impurities was less than 0.14%. This analysis confirmed once more that mesoporous silica is a promising excipient.

6.1.4 Conclusions-1

PZQ has been previously combined with various excipients, from povidone and derivatives to different types of cyclodextrins and many others, but none of them was as effective as the mesoporous silica, as demonstrated in this first screening. The grinding experiments led to very interesting products, with highly grade or even complete amorphisation after only 15 minutes of process when using Syloid 74FP and 244FP in a 1:1 weight ratio with PZQ. In the case of the coground samples with Al-1FP the presence of PZQ Form C was noticed, but after only two months the original form of PZQ started to crystallize. Nevertheless the activation of the drug was remarkable in every case and for this reason a more deeply investigation will be now presented for the system composed of Syloid 244FP, comprehending the study of different process/formulation variables and stbaility and efficacy tests.

6.1.5 Results and Discussion-2

After the preliminary screening on the effect of cogrinding PZQ with different mesoporous silica grades, further investigations were performed on the system composed of Syloid 244-FP. The application of mechanochemistry on systems based on PZQ and Syloid 244-FP have previously demonstrated to be very effective in amorphisizing the drug when in a 1:1 weight ratio with short process time (15 min). The aim of this part was to evaluate the effect of PZQ:Syloid ratio on drug amorphisation and physical stability.

The materials and the method analysis for this section were the same as the previously reported ones (paragraph 6.1) not reported here for the sake of brevity. Differently, in this case, the trials were planned with an experimental design using Nemrodw[90]: the weight ratio between PZQ and Syloid (1:1, 1:0.75, 1:0.50, 1:0.25) and the time of milling (15 or 30 minutes) were selected as the variables for a factorial experimental design which was conducted in a randomized order to reduce the systematic order. The list of the experiments is reported in Table 6.2. The total amount of powder in each experiments was 1.012 g and all the trials were conducted in double.

Table 6.2: Details of the experimental design used.

Experiment	PZQ:Syloid	Milling time
1	1:0.25	15
2	1:0.25	30
3	1:0.50	15
4	1:0.50	30
5	1:0.75	15
6	1:0.75	30
7	1:1	15
8	1:1	30

The general trend observed was that the more was the excipient, the more was the amorphisation of the drug as reported in Figure 6.8, while in the physical mixtures the melting peak of PZQ was still visible, even though with a reduced endotherm (Figure 6.9). Also, the efficiency of the mesoporous silica in amorphisazing the drug was dramatically evident even after 15 minutes, and no significant advantages were derived from prolonged grinding.

The DSC traces were totally similar to the previously reported ones, with the same exothermic band evidenced both in the physical mixtures and in the coground samples at about 160-185 °C.

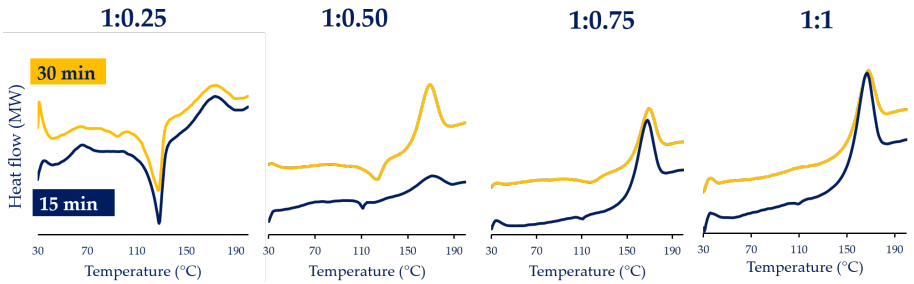

Figure 6.8: DSC of the coground samples for 15 and 30 minutes at the different PZQ:Syloid weight ratio.

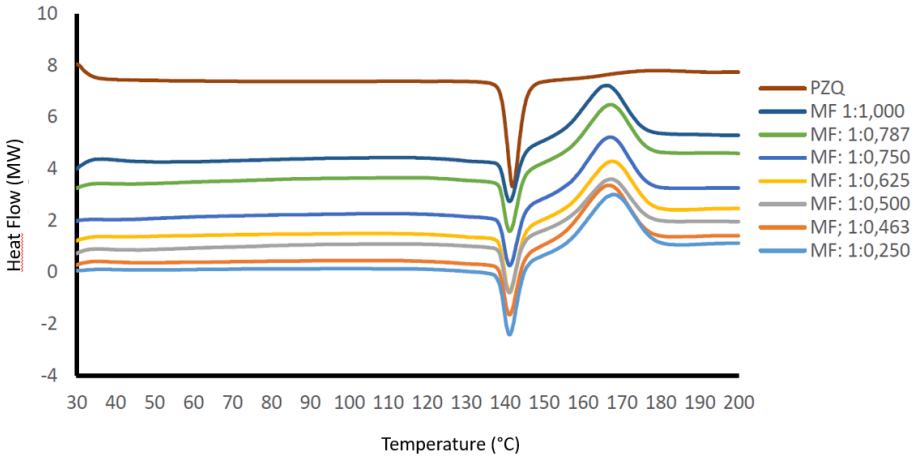

Figure 6.9: DSC of the different ratios physical mixtures of the PZQ:Syloid 244 FP system.

The dramating change of PZQ when in the Syloid matrix was confirmed by the SEM analysis: in fact, while in the physical mixture the needles of PZQ and the irregular agglomerates of silica maintained their integrity (Figure 6.11, a), in the coground samples, both for 15 and 30 min, the silica particles are covered by very small whiskers, evidencing the closed interaction between the components (Figure 6.11).

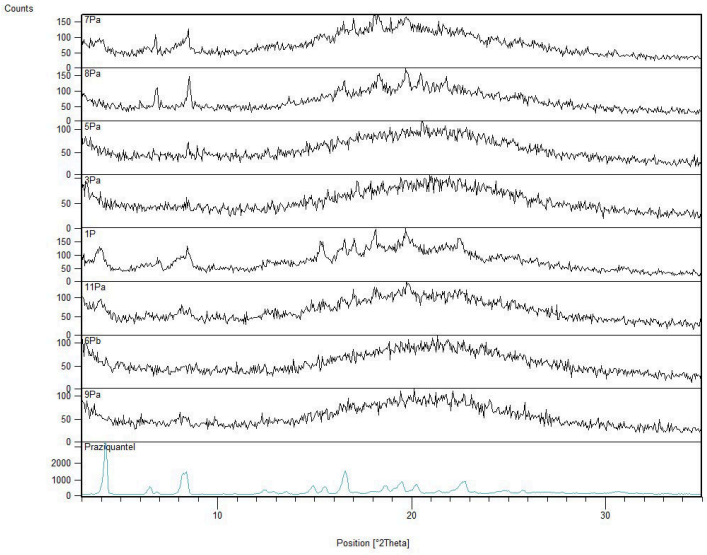

Figure 6.10: PXRD patterns of the coground samples. The pattern name refers to Table 6.2.

The PXRD pattern collected for all the samples are reported in Figure 6.10: when PZQ was in a 1:1 weight ratio with the excipient, a lack of reflections was evidenced, confirming the DSC results concerning drug amorphisation. When decreasing the Syloid content in the samples, the PXRD pattern presented a general halo resemblance, where very weak reflections were noticed, corresponding to PZQ polymorphic phases. This hypothesis was confirmed also by DSC analyses were very weak endotherms were found either around 94 or 110 °C, attributed to the activation of the drug and formation of nanocrystalline polymorphic phases, as reported in literature[107]. Nevertheless, the amorphisation of the drug was incredibly impressing considering the very low milling time and the possibility of lowering the Syloid:PZQ wt ratio. Worth of notice is the first part of each pattern starting at high intesity due to the effect of the syloid reflections at lower angles, as reported in literature[198].

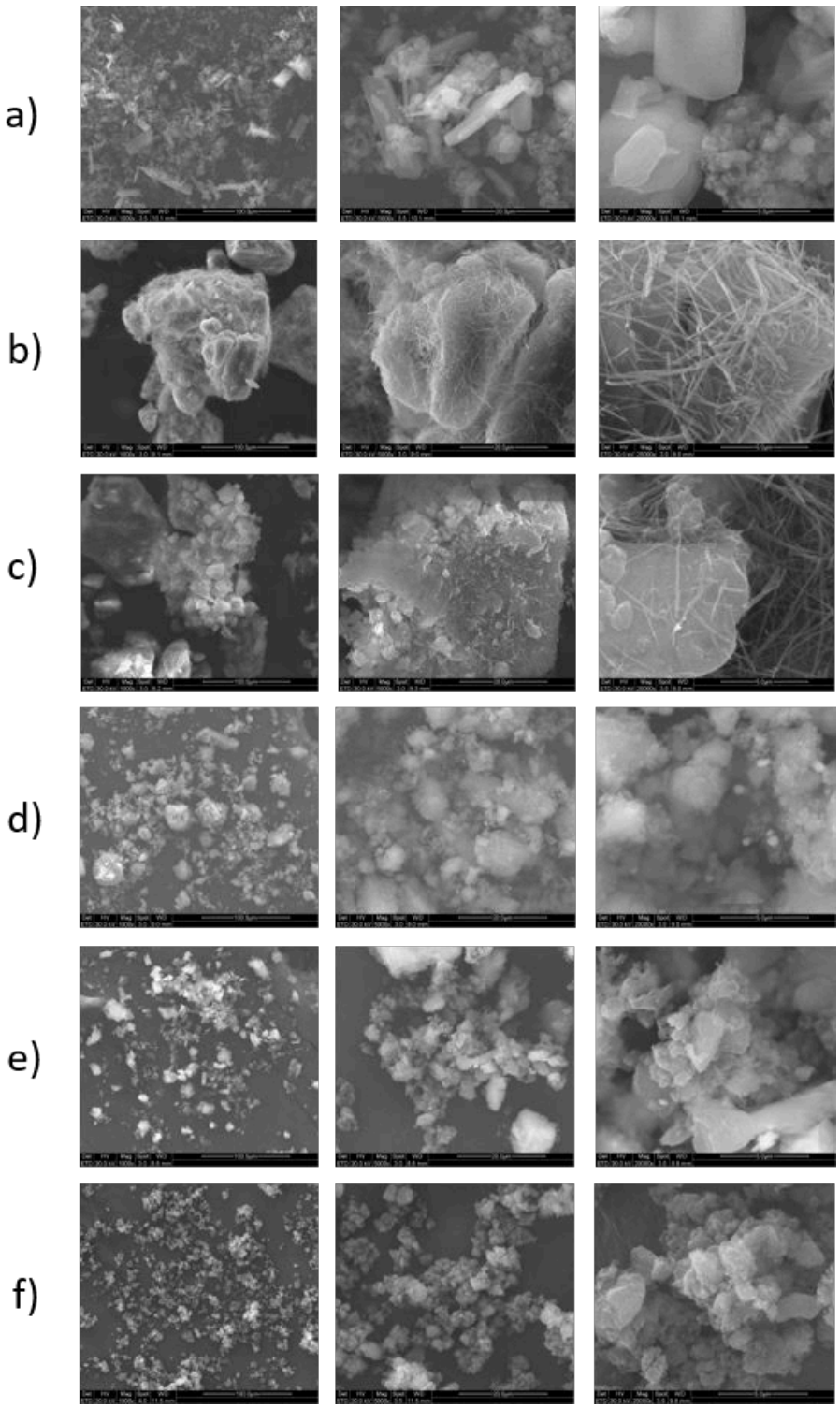

Figure 6.11: SEM images of a) PM PZQ:Syloid (1:1), b) Coground sample for 15 min, c) Coground sample for 30 min, d) Syloid ground for 30 min, e) Syloid ground for 15 min, f) Syloid raw.

The FT-IR analyses was a further confirmation of the previous assumptions (Figure 6.12): an overall amorphisation of the samples was observed in each trial with a broad signal in the PZQ carbonyl region. In some cases the presence of a polymorphic form was noticed by very hardly visible signals of either Form B/C, but as for the previous section, the discrimination between the polymorphs could be only hypothesized from the PXRD/DSC analysis, since the FT-IR spectra of Form B and C are identical. Differently, the PM spectra were the superimposition of PZQ and syloid bands (Figure 6.13).

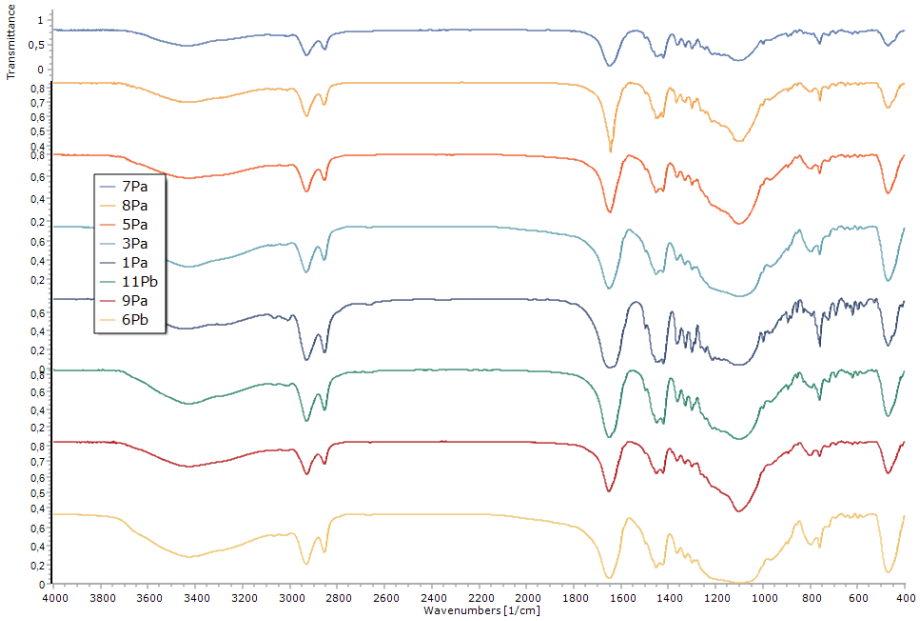

Figure 6.12: FT-IR spectra of the PZQ:syloid samples, from up to down: 1:0.250 15 min, 1:0.250 30 min, 1:0.500 15 min, 1:0.500 30 min,1:0.750 15 min, 1:0.750 30 min,1:1 15 min, 1:1 30 min.

Since the mechanochemical activation of PZQ with syloid was highly efficient, one fundamental aspect should be assessed: the possible degradation of the API, as it was observed for coground samples with polymers (chapter 2 and also by other authors[192]. The content of PZQ of the most amorphisized samples, 7 and 8, corresponding to the 1:1 PZQ:Syloid ratio ground for 15 and 30 minutes respectively was assessed by HPLC. In both cases drug recovery was highly acceptable, with a value of 96.12% in the case of sample 7, and 96.08% for sample 8.
The next step comprehended the evaluation of drug release. In fact, it is well known that the drug release from a silica matrix can sometimes be not complete, due to the different interactions activing between the components, the pore diameter and many other reason. All of these effect are reported related to other drug loading technology, rather than from the mechanochemical activation[184]. For this reason drug dissolution tests were performed on selected samples (Figure 6.14), resulting in a dramatic

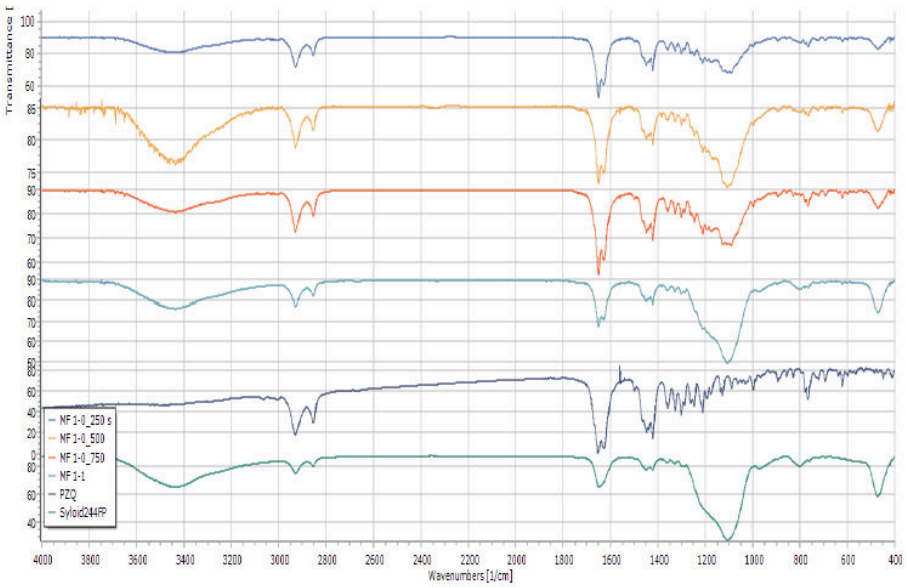

Figure 6.13: FT-IR spectra of the physical mixtures compared to the raw drug.

increase of drug dissolution, almost triplicate after 10 minutes in the case of sample 8, achieving the 90% of release after only 20 minutes comparing to raw PZQ (36%). Similar observation could be done for sample 7, and, interestingly, even in the case of the physical mixture, drug release was double than raw PZQ after 20 minutes and reached a maximum value of 91% after 60 minutes, compared to the 54% of PZQ. Therefore, the PZQ:syloid activated samples demonstrated an optimal capability of drug release, even in the simple physical mixture or very short grinding (15 min).

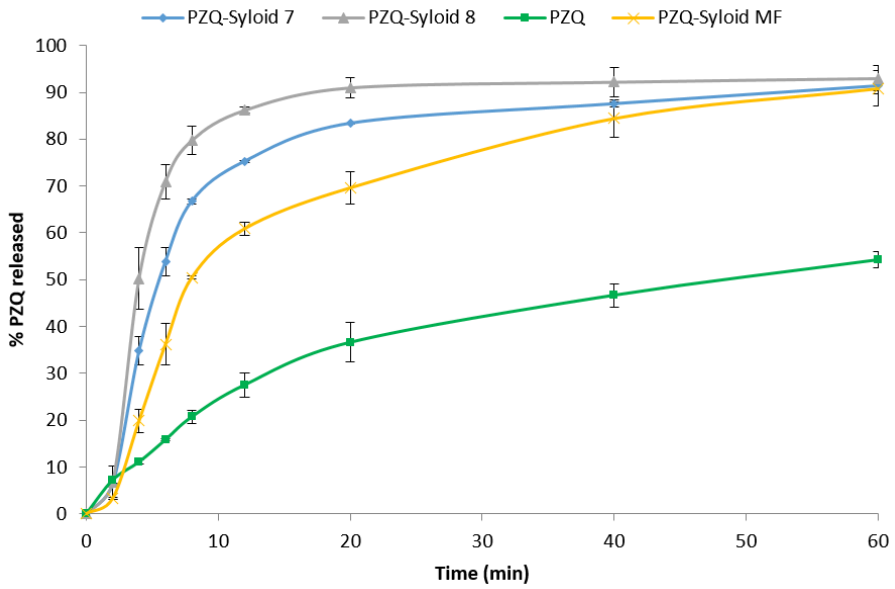

Figure 6.14: Drug release over time of sample 7 and 8.

The samples were analyzed in the physical stability over time for up to 5 months, by means of DSC measurements: as reported from Figure 6.15 to Figure 6.22, the sample were stable for all the time, with no signs of any crystallization/physical variation in any trial, suggesting a great stabilizing properties of this silica excipient. Also, in the sample with a 1:1 wt ratio the traces were completely superimposable and the corresponding figures report only the data of fresh samples and after 5 months storage. Another characteristic that was noticed for all the sample was the shift of the exothermic event at lower temperature range, possibily correlated to a weakening of the interaction between the components.

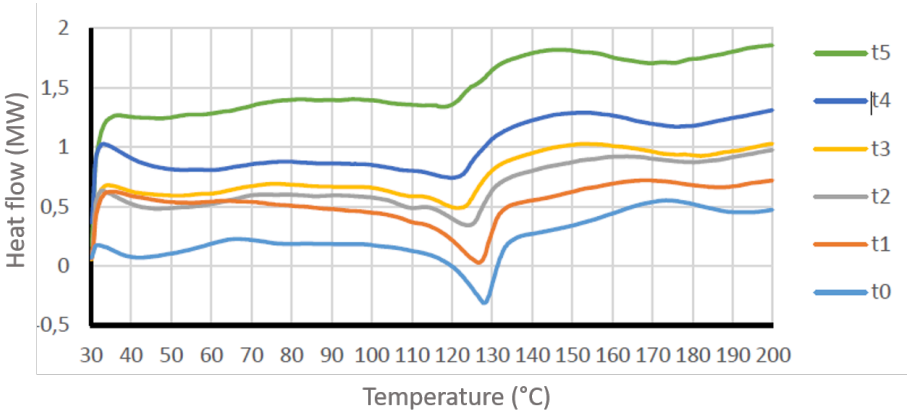

Figure 6.15: DSC traces of sample 1 (PZQ:Syloid 244FP 1:0.25, ground for 15 min) fresh and after 1, 2, 3, 4, and 5 months.

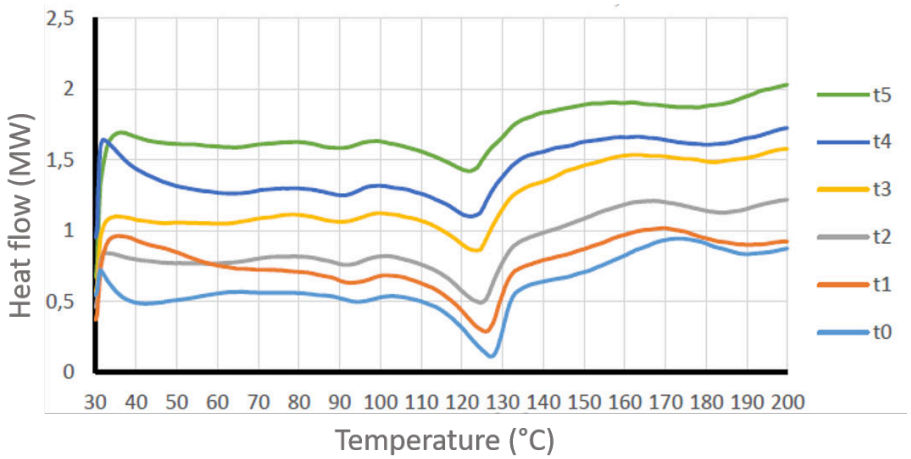

Figure 6.16: DSC traces of sample 2 (PZQ:Syloid 244FP 1:0.25, ground for 30 min) fresh and after 1, 2, 3, 4, and 5 months.

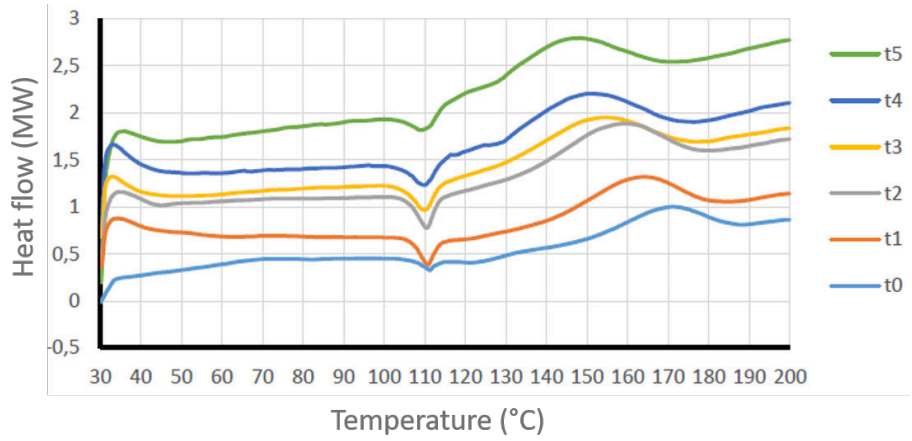

Figure 6.17: DSC traces of sample 3 (PZQ:Syloid 244FP 1:0.50, ground for 15 min) fresh and after 1, 2, 3, 4, and 5 months.

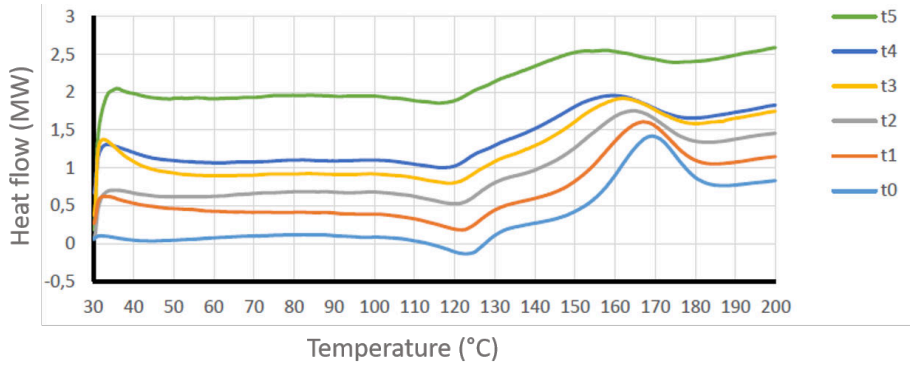

Figure 6.18: DSC traces of sample 4 (PZQ:Syloid 244FP 1:0.50, ground for 30 min) fresh and after 1, 2, 3, 4, and 5 months.

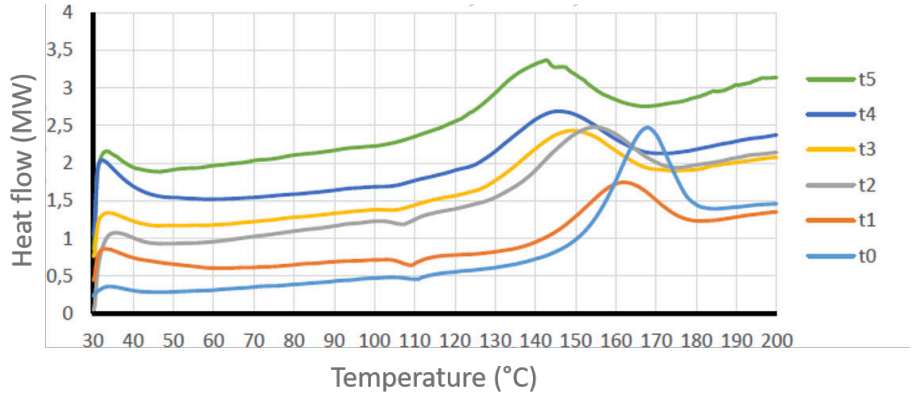

Figure 6.19: DSC traces of sample 5 (PZQ:Syloid 244FP 1:0.75, ground for 15 min) fresh and after 1, 2, 3, 4, and 5 months.

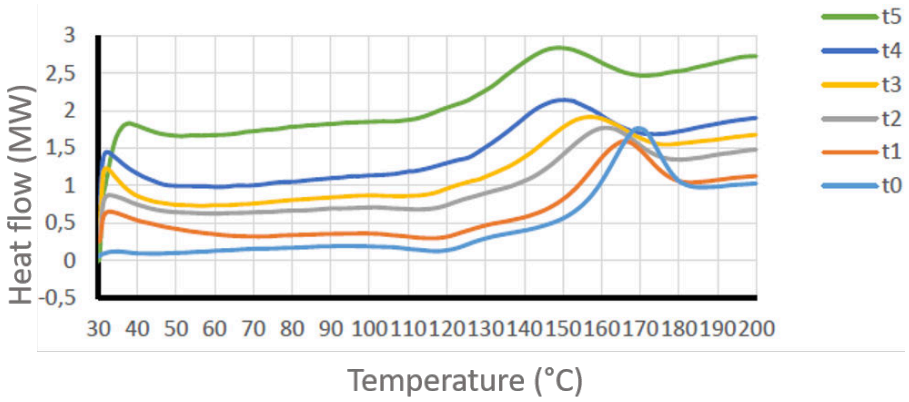

Figure 6.20: DSC traces of sample 6 (PZQ:Syloid 244FP 1:0.75, ground for 15 min) fresh and after 1, 2, 3, 4, and 5 months.

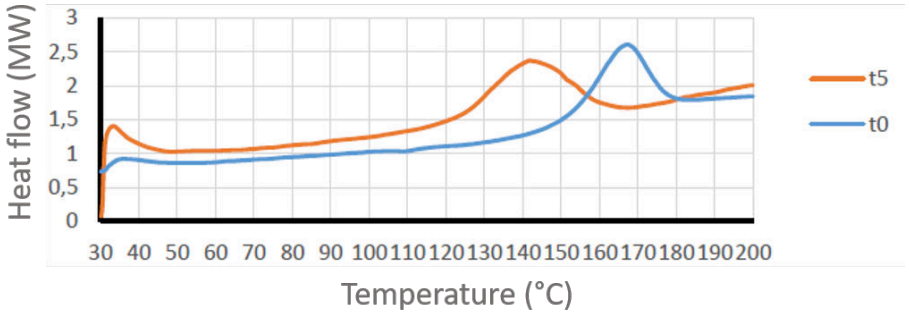

Figure 6.21: DSC traces of sample 7 (PZQ:Syloid 244FP 1:1, ground for 15 min) fresh and after 5 months. For the sake of brevity, only 2 analyses are reported.

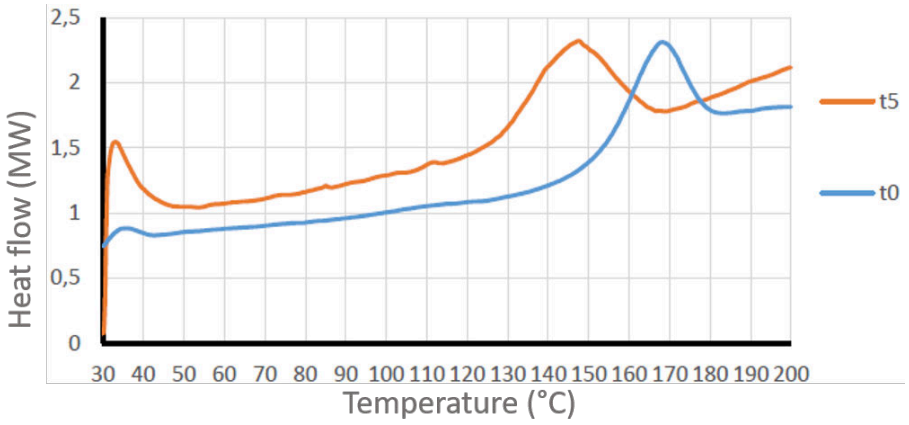

Figure 6.22: DSC traces of sample 8 (PZQ:Syloid 244FP 1:1, ground for 15 min) fresh and after 5 months. For the sake of brevity, only 2 analyses are reported.

Considering the high physical stability of the samples, the almost complete amorphisation and the high drug release, one can wonder if PZQ still maintained its efficacy: for this reason *in vitro* test were performed against *S. mansoni* at the Swiss Public and Tropical Health Institute of Basel. The samples analyzed were the one ground for 30 minutes containing PZQ:Syloid in 1:1 wt ratio and the correposnding physical mixture, which were compared to raw PZQ; also, the pure excipient was kept as a control. Table 6.3 reports the activity results: the coground sample maintained the activity as shown by comparable IC_{50} values with raw PZQ (0.134 VS 0.165 μg/ml), confirming a appropriate drug release from the formulation. For comparison, the physical mixture had an IC_{50} of 0.088 IC_{50}.

Table 6.3: *In vitro* activity against *S. mansoni*.

Sample	IC_{50}
PZQ	0.165 μM
PZQ:Syloid	0.42779 μM
PM PZQ:Syloid	0.28421 μM

One last point addressed the chemical stability: the HPLC analyses after 10 months form preparation attested a decrease on drug recovery, which was of 84.45% for sample 7 and 84.42% for sample 8. Nevertheless, these results were in accordance with the descrease of the melting enthalpy in the DSC analyses previously reported during time and to the tendency of drug degradation in API:silica systems found in literature[192].

6.1.6 Conclusions-2

Syloid 244-FP demonstrated to be a very interesting excipient for the PZQ-based system, both with high or low drug-to-polymer weight ratio. In fact, the samples in the 1:1 ratio were completely amorphous after only 15 minutes grinding, thanks to the extraordinary efficacy of silica, and even when using lower ratios drug amorphisation was considerable. Also, the samples were physically stable for at leas 5 months, as demonstrated by DSC analyses, proving the high stability capacity of the silica grade considered, that did not hinder drug activity, as reported for the *in vitro* analyses against *S. mansoni*, which remained comparable to raw PZQ. Worth of notice is the incredible dramatic increase in drug dissolution, which was even triplicate in the samples ground for 30 min after only 20 minutes. The coground samples reached the 90% of drug release, compared to the only 54% of the raw drug. Interestingly, even the simple physical mixture showed a double increased in drug release. This chapter proved the possibility of designing new PZQ formulations with mesoporous silica materials, with very short processes (as the grinding for 15 minutes), high drug amorphisation, still maintaining the antischistosomal activity. The future work will investigated the inner interaction between the component and the study of the kind of incorporation/dispersion/absorption of the drug on silica particles.

6.2 Cogrinding PZQ with selected sweeteners

6.2.1 Introduction

Having a look to the pharmaceutical compounds on the market, a large part of them is characterized by poor organoletic properties, which make them very unpleasant if not hidden with different taste masking agents or pharmaceutical technologies. It is well known that PZQ has a very bitter and disgusting taste, which makes its administration even more complicated than the large dose, since it can led to vomiting or gagging if chewed, especially in children, the main involved patients. Moreover, Meyer and collaborators reported an investigation on PZQ taste, revealing a less bitter taste in the active enantiomer (R-PZQ) respect to the racemic form[48], which is not surprinsing since the majority of the taste experiences are conditioned by the sterochemistry of the system involved[199]. Different taste-masking technologies has been tried on PZQ, from the simple addition of aromas or sugars, which was completely ineffective ([48]), up to more expensive and innovative technologies as microencapsulation or drug active coating in which PZQ was taken as a bitter model API (patents deposited[200, 201]). Among all the possible techniques in drug taste masking, the formation of solid dispersions can represent a possible valid option, as it was reported for dimenhydrinate with with polyvinyl acetate phthalate[202] or artemether with mono amino glycyrrhyzinate pentahydrate[203]. Also, the possibility of creating cocrystals between API and a sweetening agent was reported for hydrochlorothiazide with sucralose by solubilization and subsequent crystallization, which allowed the formation of fast disintegrating tablets [204]. Another example was reported by Wang and collaborators who reported the formation of a theophylline:acesulfame cocrystal with enhanced solubility compared to the raw drug[205]. Nevertheless, no literature data were found on the mechanochemical processing of API with sweetening agents to create advantageous solid dispersions, which is the aim of this chapter. In fact, as reported for the sugar-based confections, the sweeteners can be subjected to phase transitions upon processing and also during storage[206]. This means that even the mechanochemical activation may favour the formation of crystalline, partially crystalline or also amorphous systems. This fact suggests also a possible enhancement of the system solubility, when adequately formulated and processed and moreover, the smoothest mouthfell has been correlated with low crystal size[207]. In this chapter, six different sweeteners were selected to be ground with PZQ: four natural (xylitol, mannitol, maltitol and sorbitol) and two artificial (aspartame and sucralose), characterized by a very high sweetening power. All of them are actually used both in the pharmaceutical and food industry as sweetening agents and also as sweetening alternative to sucrose for dietary requirements[208]. A synthesis of the sweetening power and of the maximum daily intake is reported in Table 6.4.

Table 6.4: Synthesis of the sweetening power and of the maximum daily intake for the selected sweeteners used in this chapter (relative to a 10% sucrose solution)[209] and Center for Science in the Public Interest (US) for the daily intake.

Sweetener	Sweet. Power (sucrose=1)	Max intake (daily)
Sorbitol	0.6	70g
Mannitol	0.5–0.72	10-20g
Maltitol	0.5–0.9	30-50g
Xylitol	1.0	50g
Aspartame	180–200	40mg/Kg (WHO)
Sucralose	600	5mg/Kg (FDA)

6.2.2 Materials and Methods

Materials

Praziquantel (PZQ, (11bRS)-2-(Cyclohexylcarbonyl)-1,2,3,6,7,11b-hexahydro-4-H -(pyrazino[2,1-a]isoquinolin-4-one)) was of Ph. Eur. grade and kindly donated by Fatro S.p.a. (Bologna, Italy). Mannitol (MAN), xylitol (XYL), maltitol (MAL), sorbitol (SOR), sucralose (SUC) and aspartame (ASP) were a gift from Galeno srl (Carmignano, PO,Italy). The HiPersolv Chromanorm methanol used for the HPLC analysis was of Ph. Eur. grade and purchased from VWR Chemicals (BHD PROLABO® Milano, Italy).

Preparation of the samples Each selected sweetener was ground in a 1:1 molar ratio with PZQ for 30 minutes at 25 Hz using a Retsch MM400 vibrational mill (Retsch, Germany) and two zirconium oxide jars (35 mL) and two zirconium oxide balls (ϕ= 10 mm). After grinding the samples were collected and stored in a desiccator in the dark at ambient temperature.

Differential Scanning Calorimetry Each sample was analyzed using a Mettler DSC TA 4000 (Greifensee, Switzerland) connected to a calorimetric cell Mettler DSC20 and using STARE software version 9.30 for data analysis. Prior to analysis the instrument was calibrated with Indium, Zinc and Lead for the temperature and with Indium for the enthalpy quantification; each sample, containing about 2 mg of PZQ exactly weighted, was placed in a 40 μl aluminum pan with perforated lid and heated from 30 to 200 °C (10 °C/min) under air atmosphere. When the analyzed sample contained aspartame, the DSC was ended at 160 °C to avoid its decomposition, reported in literature by Goguta and coworkers[210].

Powder X-ray Diffraction The sample were analyzed by powder X-ray diffraction using a Bruker AXS D5005 X-ray diffractometer with Ni-filtered Cu K(α) radiation (λ=1.5418 A). The preparation of the samples consisted in pressing about 20-30 mg of powder over a glass slide to have a flat surface. The data were collected in a 2θ range of 3-35 degree. These analyses were performed thanks to the collaboration with prof. V. Lughi of the Department of Engineering and Architecture, University of Trieste, Italy.

Hot-stage Microscopy A Reichert Biovar microscope with a micro ocular MD-300 (Webcam Companion software) was used, connected to a Perkin Elmer hot-stage sample holder for the heating and observation.

FT-IR spectroscopy FT-IR analyses were performed using a Perkin Elmer System 2000 FT-IR on the raw samples, coground samples and the physical mixtures. Each time the sample was mixed with KBr in an agate mortar and then pressed with an hydraulic press for 2 minutes at 10 Ton to obtain homogeneous and transparent

discs. The analysis was conducted form 400 to 4000 cm-1 with a resolution of 4 cm^{-1} and total scan number of 3.

Solubility and intrinsic dissolution rate The solubility of the samples was analyzed by preparing saturated solutions of each samples in deionized water, which were kept under agitation in the dark for 48 hours. Then, the solutions were filtered (pore size 0.45 μm) and diluted 1:200 with the mobile phase prior injection in the HPLC system. The HPLC used was an Agilent HPLC-UV 1260 Infinity II with a EC-C18 Poroshell 120 A column of 4 μm and dimensions of 4.6 x 10 mm. The mobile phase was composed of 65% methanol and 35% of deionized water (MilliQ filtered) and the flux used was of 0.750 mL/min. The instrument was set at 25 °C and with a fixed wavelength of 220 nm for recording the absorbances. The external standardization method was used for the quantification of the integrated peaks. The PZQ retention peak was found at 7.7 minutes in a total run time of 10 minutes and the calibration curve obtained in the range of 0.5-10 mg/L had r^2=0.9988. Each analysis was conducted in triplicate and the average was reported. For the intrinsic dissolution rate determinations, about 150 mg of the samples were inserted in the sample holder and pressed using an hydraulic press (PerkinElmer, Norwalk, USA) for 1 min at 1 ton. The sample surface area obtained was of 0.785 cm^2 and the entire sample holder with the compressed powder was immersed in a vessel containing 1 L of distilled water kept at 37 °C. The system used was a Hanson Research SR8 Plus dissolution test station and the paddle were positioned at 3.5 cm from the tablet surface, with a rotation speed of 100 rpm. About 2 ml of the dissolution medium were withdrawn every ten minutes till 60 min and immediately replaced with an equal amount of thermo-stated distilled water. The aliquots were then diluted 1:20 with the mobile phase and analyzed by HPLC using the same above mentioned method. The analyses were performed in triplicate and for each point the mean, with SD (%) and RSD (%) were calculated. The amount of the dissolved drug per unit area over time was indicated by the slope of the curves, obtained through a linear regression method.

Physical stability The samples were subjected to DSC and PXRD analysis after one year storage to check the physical stability.

6.2.3 Results and Discussion

The grinding of PZQ with the selected sweeteners was very successful since after only 30 minutes of process at 25 Hz different solid dispersion were formed: as reported from Figure 6.23 to Figure 6.27, the PXRD spectra of the coground samples were quite broad: the intensity of the characteristic reflections of the sweeteners were very reduced, comparing to the raw high crystalline nature, while the PZQ peaks were missing. This fact was not due to a dilution effect since in the PXRD patterns of the physical mixtures both the drug and the sweeteners reflections were well visible. An exception of this trend was found in the coground samples with xylitol, which will

be described separately. In the physical mixtures, the reflections were found slightly shifted to lower 2θ angles, due to the difficulties in sample preparation.

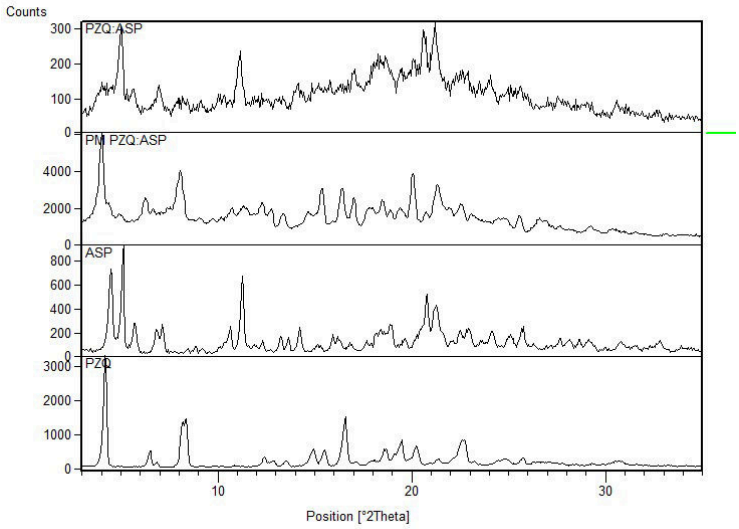

Figure 6.23: PXRD patterns of the PZQ:aspartame system, from the top: coground sample, physical mixture (due to the unavailability of the instrument, performed in collaboration with Dr. M. Lusi of the University of Limerick (UK)), aspartame and raw PZQ.

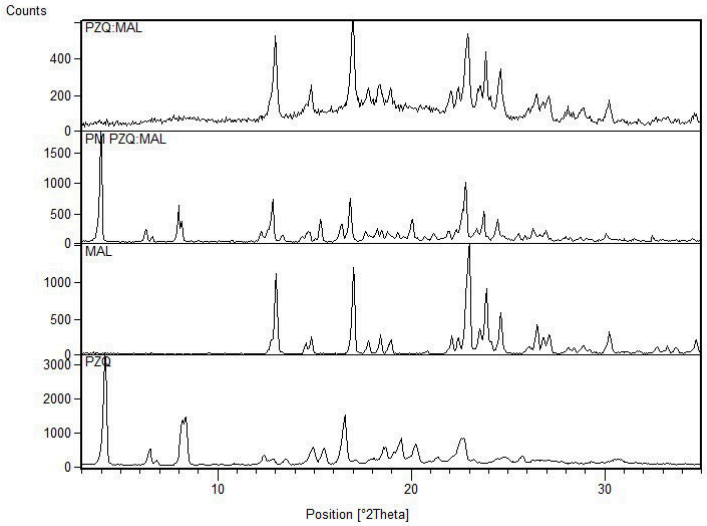

Figure 6.24: PXRD patterns of the PZQ:maltitol system, from the top: coground sample, physical mixture, maltitol and raw PZQ.

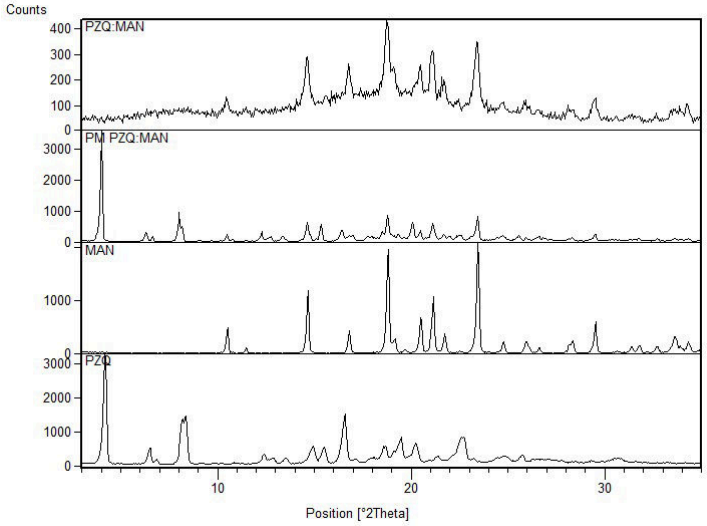

Figure 6.25: PXRD patterns of the PZQ:mannitol system, from the top: coground sample, physical mixture, mannitol and raw PZQ.

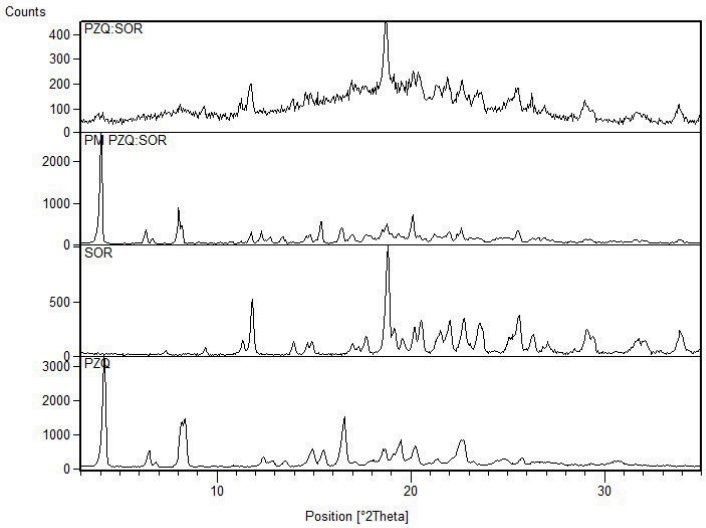

Figure 6.26: PXRD patterns of the PZQ:sorbitol system, from the top: coground sample, physical mixture, sorbitol and raw PZQ.

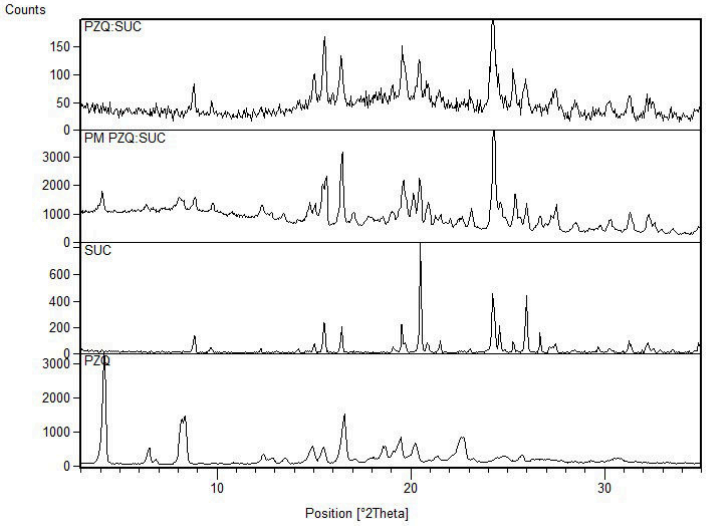

Figure 6.27: PXRD patterns of the PZQ:sucralose system, from the top: coground sample, physical mixture (due to the non-availability of the instrument, performed in collaboration with Dr. M. Lusi of the University of Limerick (UK), sucralose and raw PZQ.

The DSC traces confirmed the same observations: in the physical mixtures the melting peaks of the sweeteners and of PZQ were found in the same raw temperature range, but with a reduced enthalpy, while in the coground samples, PZQ was almost amorphous and the sweetener events even smaller. For the sake of brevity, only but one comparison of the DSC traces is reported in Figure 6.28 for the PZQ:SOR system.

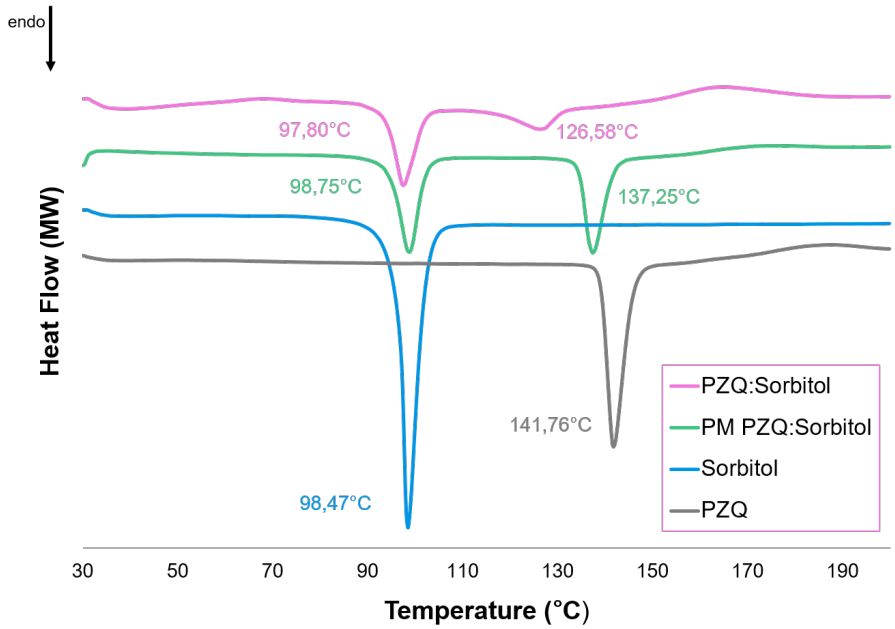

Figure 6.28: DSC traces of the PZQ:Sorbitol system: coground (a), physical mixture (b), sorbitol (c) and raw PZQ (d).

In the FT-IR analyses of the cogrounds samples (on example in Figure 6.29), the stretching vibration of PZQ carbonyl group, typically represented by two nearly overlapped peaks at about 1600 cm^{-1} in raw PZQ, was replaced by one large peak, similarly to other solid dispersion previously described in the coground samples with the polymers, pointing out once again the amorphous phase of PZQ in these coground samples.

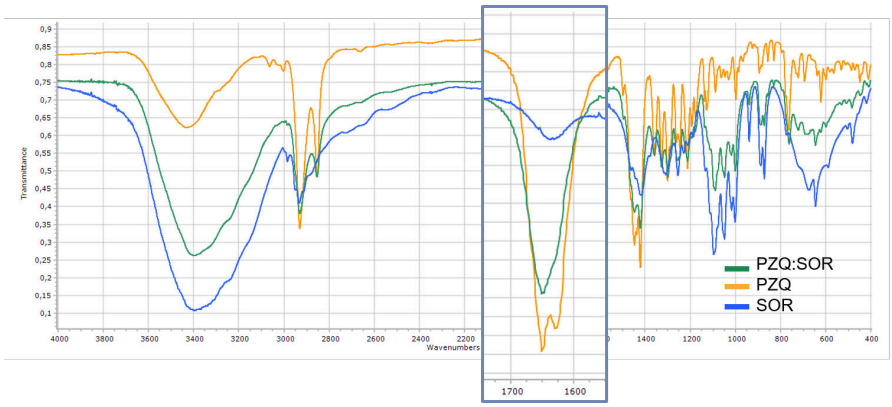

Figure 6.29: FT-IR spectra of PZQ:SOR (green), sorbitol (blue) and raw PZQ (orange).

Differently, in the PXRD spectrum of the coground sample made of PZQ and xylitol (reported in Figure 6.30), the reflections found were identified as the one of Form B, together with the ones of the sweetener, but no evidence of the presence of raw PZQ was found. In the thermal analysis (Figure 6.31) PZQ was found at about 106 °C and 123 °C, with very small endotherms, that can be identified respectively as PZQ polymorphic and raw form. The very small peak of Form B can be explained on one hand in part by the partial drug amorphisation (also confirmed by the slightly broad PXRD pattern), and from the other hand by to the close xylitol peak (at around 94 °C), which favors lowering of PZQ melting point. The peak of the raw drug at 123.42 °C can be referred to a partial recrystallization during the DSC process, or to a reduction of the PZQ crystal size (also compatible with the PXRD pattern recorded).

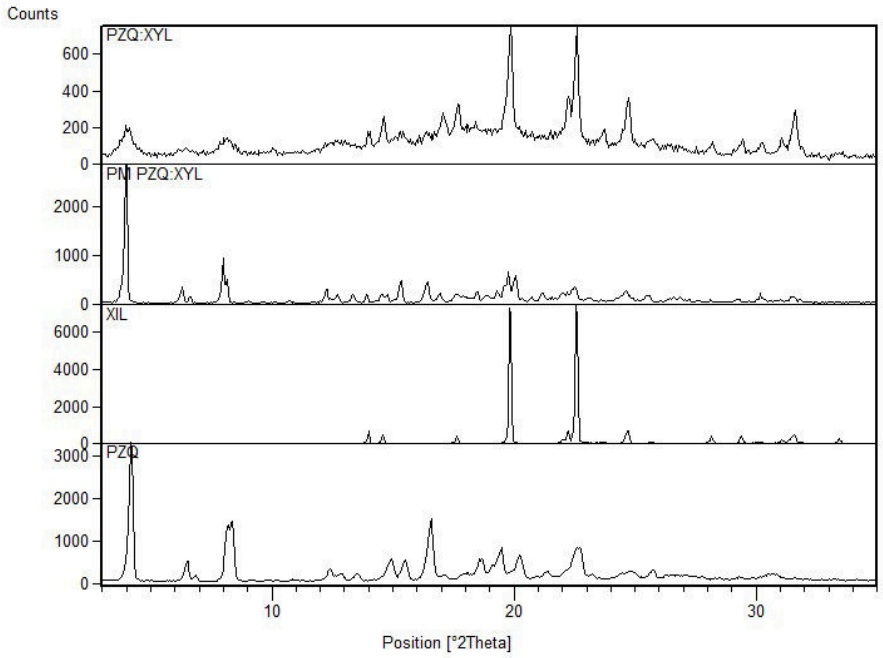

Figure 6.30: PXRD patterns of the PZQ:xylitol system: coground sample, physical mixture, xylitol and raw PZQ.

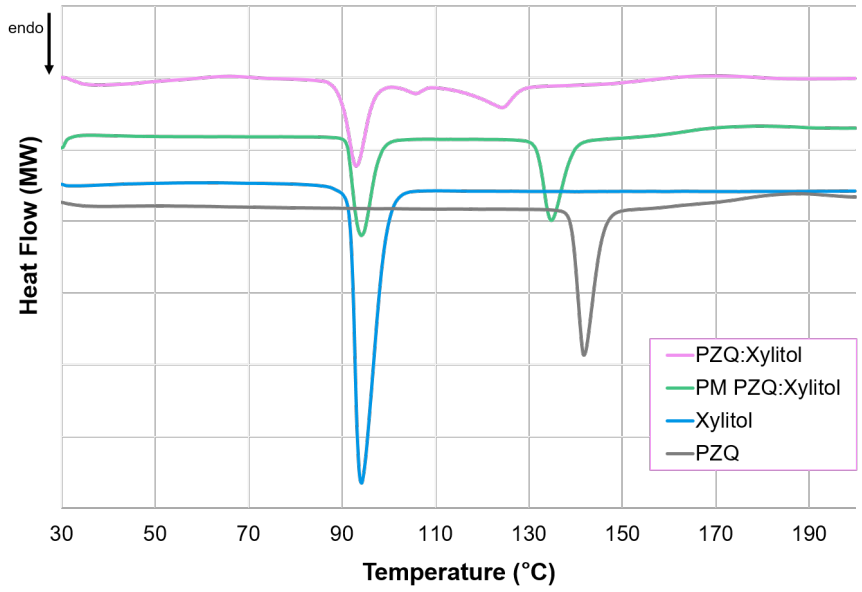

Figure 6.31: DSC traces of the PZQ:Xylitol system: coground sample, physical mixture, xylitol and raw PZQ.

Also, the FT-IR spectra of the ground PZQ:xylitol sample presented the same vibration peaks as the polymorphic form, confirming once again its identity by the superimposable shape and position of the asymmetric stretching of the PZQ carbonyl groups around 1650 cm^{-1} and at 750 cm^{-1}, shown in Figure 6.32.

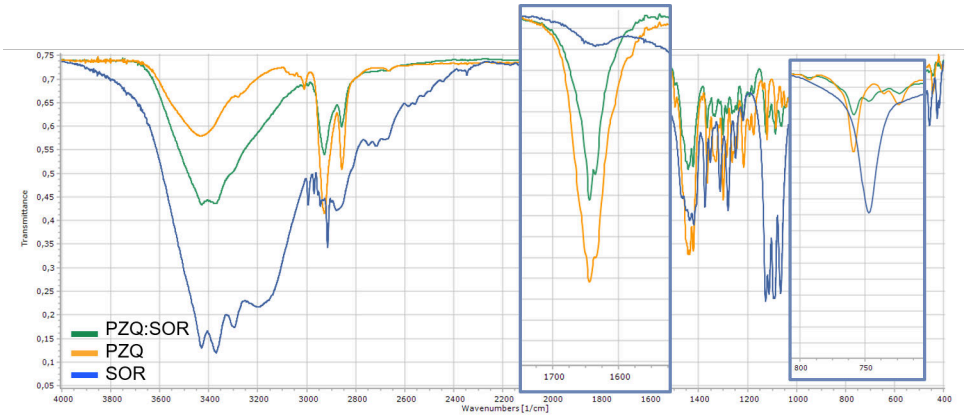

Figure 6.32: DSC traces of the PZQ:Xylitol system: coground sample (green), xylitol (blue) and raw PZQ (orange).

A possible explanation of the different oucomes obtained with XYL comparing to the other sweeteners can be found in the differences in the Tg of the sweeteners used, reported in Table 6.5, in fact, it is well known that molecular transformation are highly dependent on the working temperature, being dramatically reduced when staying well below the Tg of the system[14]. Xylitol has a Tg of -29 °C, while for PZQ is at about 37 °C (as analyzed in section 3.1), therefore we could expect a intermediate Tg for the coamorphous phase of the system, since a part of the sweetener still remained crystalline, as evident in the PXRD spectrum. It was not possible to calculate a precise Tg value with the Gordon-Taylor equation[211] since we had no indication of the mixture composition. As reported in a previous chapter (section 3.1), when grinding at 25 Hz for 30 minutes the temperature reached is in the range of 38-40 °C, certainly above the Tg of the coground system, thus promoting the polymorphic switch of PZQ, which has been previously amorphisized during grinding.

Table 6.5: Tg values of the natural sweeteners used in this chapter (asssuming all anhydrous)[212–214].

Sweetener	Tg (°C)
Sorbitol	-9
Xylitol	-29
Maltitol	39
Mannitol	12.6

After having characterized all the grinding outcomes, the coground samples were tested for their water solubility at 25 °C: as reported in Figure 6.33 all the tested sample had an enhanced solubility comparing to the raw drug of at least 2 folds. Also, the intrinsic dissolution rate was calculated for the following system: PZQ:ASP and PZQ:SUC for the enhanced solubility and high sweetening power[209], PZQ:XYL for the peculiar characteristic (i.e. presence of Form B). All the systems presented an intrinsic dissolution rate of about 2.6 times the one of raw PZQ, as shown in Figure 6.33. This fact could be attributed not only to the hydrotropism of the sweetener, but also to a change in the solid state. Moreover the presence of Form B in PZQ:XYL was also confirmed by the superimposable intrinsic dissolution rates(Figure 6.34).

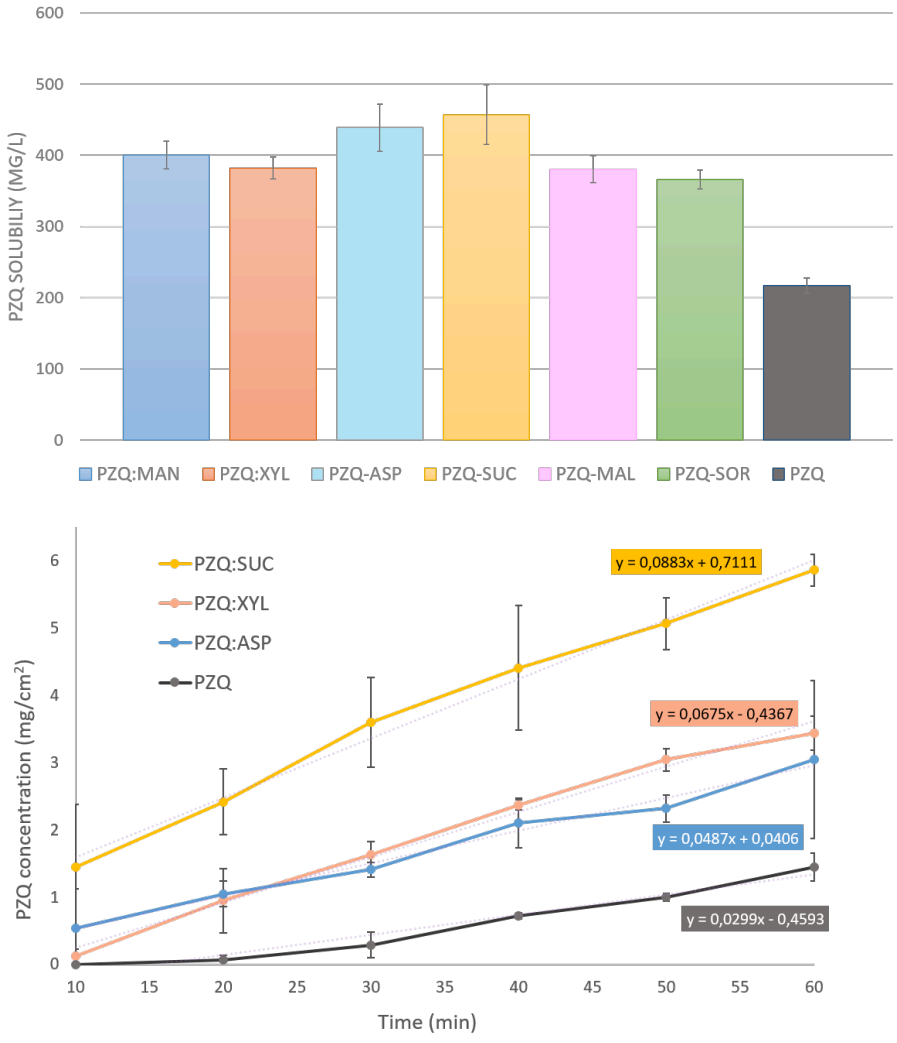

Figure 6.33: On the top, the solubility of the coground samples with the selected sweeteners and of raw PZQ. On the bottom: the intrinsic dissolution rate of selected systems compared to the raw drug.

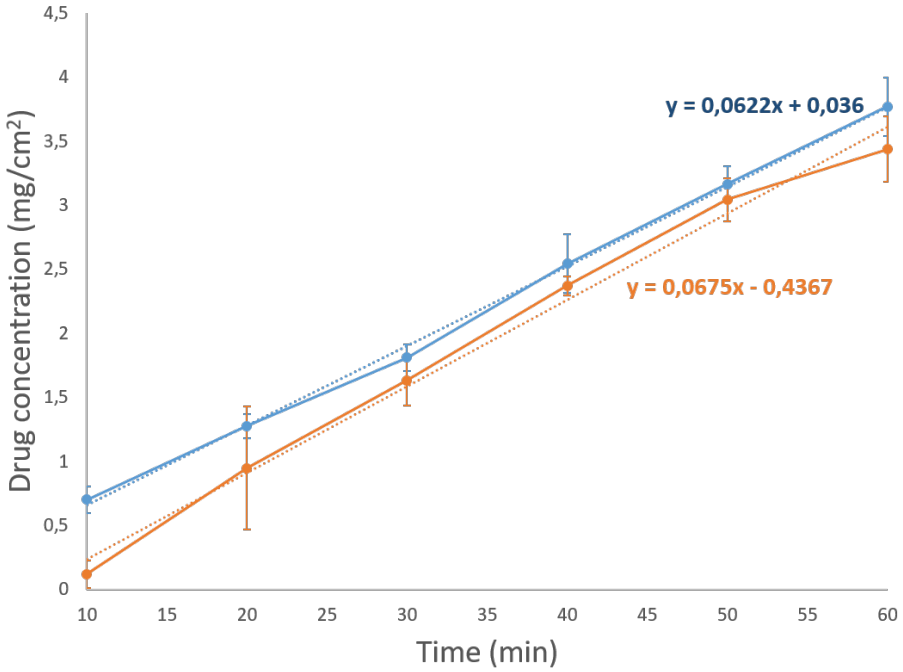

Figure 6.34: Comparison between the intrinsic dissolution rate of Form B and the coground sample composed of PZQ:XYL.

6.2.4 Conclusions

The grinding of PZQ with the selected sweeteners led to several very interesting products, with prevalent amorphous character, enhanced solubility and IDR comparing to the raw drug. All these promising characteristics put in light the possibility of ameliorate PZQ dosage forms, very likely to have a better taste and biopharmaceutical properties compared to the actual administered form. The following step will be represented by the taste evaluation of the coground samples, followed by the *in vivo* and *in vitro* evaluation of the maintainance of the antihelmintic activity. Worth of notice the peculiarity of the sample coground with xylitol, where the crystallization of Form B was seen and confirmed at the solid-state and biopharmaceutical characterization. This last observation combines not only the production of Form B in only 30 minutes grinding (compared to the 4 hours necessary by neat grinding), but also opens the doors for a very promising formulation based on an advantageous polymorphic form and a well known and effective sweetener.

6.3 Cogrinding PZQ with sucrose esters

6.3.1 Introduction

The sucrose esters (SEs) are a group of non-ionic surfactant, not toxic, biocompatible and highly biodegradable largely used in various field, from the pharmaceutical to the food industry, as well as in cosmetic preparations. In fact, they can act as solubilizing agents, lubricants, emulsifiers, pore forming agents and many other applications, depending on the esterification degree of the sucrose molecule or the nature of the esterified fatty acid. The most used SEs are derived from the lauric, myristic, palmitic, stearic, oleic, behenic and erucic acids and in Table 6.6 an indication of the pharmaceutical application depending on the HLB value is reported[215].

Table 6.6: Indication of the pharamceutical application of SEs depending on HLB values[215].

Application	HLB value
Emulsification	Low to high
Solubilization	High
Dissolution improvement	High
Controlled/sustained release	high
Absorption/penetration enhancement	High (especially with C12-14 fatty acids)
Lubrification	Low to medium
Disintegrant	High

SEs has been applied reported in many pharmaceutical reports: for drug stabilization, as in the case of amorphous cefditoren pivoxil in acqueous solution[216], microencapsulation of proteins[217], vescicle formation[218], transdermal delivery [219] and enhancement/modification of drug release and dissolution. In particular for this last application lots of works can be found in literature, involving different drugs, SEs and production techniques as it is extensively reported in the minireview by Szuts and coworkers[215]. For example the same group reported a study on the effect of meloxicam and diclofenac sodium on three SEs with different polarities, preparing binary samples via melt process and analyzing the changes in the structures and in drug release depending on the solid-state interaction[220]. Or, SEs have been used to tailor the rate of drug release in the case of etodolac[221], or to create ibuprofen microparticles in which the presence of the emulsifier was fundamental for microsphere formation and by increasing its concentration the particle size was decreased, favouring the increase of drug release properties[222]. Also, some examples on the use of SEs by grinding were reported: Otsuka and coworkers studied the effect of grinding phenytoin with different surfactants[223] and the physicochemical properties of coground and comelt

products made of glybuzole and various surfactants, obtaining and improvement in drug dissolution[223]. In this chapter two different applications of SEs to PZQ will be presented: the first includes the investigation of possible changes in the formation of PZQ hemihydrate by using SEs solutions during LAG, while the second will be focused on the results obtained by Neat-Neat grinding (i.e. milling PZQ by itself and subsequentely with the addition of SEs).

6.3.2 Materials and Methods

Materials

Praziquantel (PZQ, (11bRS)-2-(Cyclohexylcarbonyl)-1,2,3,6,7,11b-hexahydro-4-H -(pyrazino[2,1-a]isoquinolin-4-one)) was of Ph. Eur. grade and kindly donated by Fatro S.p.a. (Bologna, Italy). Four different sugar esters were used: Sucroester 15 (P1570), Surfhope SE cosme (C1816), Surfhope SE cosme (C1811), Surfhope SE cosme (C1807), all from Mitsubishi, Chemical Foods Corporation (Tokyo, Japan) and Ethanol $\geq$99.8% (Honeywell, Riedel-de-Haën - Germany).

Table 6.7 reports the main characteristics of the SEs used. The indication for the maximum potency refers to the FDA Inactive Ingredients Database for the maximum amount of inactive ingredient for each route/dosage form.

Methods

Preparation of the samples During the first part of study, each sucrose ester was solubilized in water (0.05% w/w) by heating at 75 °C under stirring (200 rpm) and cooled at room temperature. It is worth notice that the concentration selected was due to the impossibility to achieve clear solutions for all the SEs in higher concentrations. The conditions for the formation of PZQ hemihydrate were then reproduced: about 428 mg of PZQ were ground for 30 minutes at 25 Hz, then the SEs solution was added (24.6 μl) and the milling process was continued for other 60 minutes at 25 Hz. For the second part, PZQ was ground by itself for 30 minutes at 25 Hz and then the SEs were added in a 1:1 weight ratio in the solid state, for the subsequent milling for other 60 minutes at the same frequency. For all the analyses stainless steel jars (12 ml) and balls (2x7mm of diameter) were used. Physical mixtures of each SEs with PZQ were prepared by manually grinding in an agate mortar for 3 minutes in a 1:1 wt ratio. After preparation, all the samples were stored in a desiccator in the dark at room temperature.

Differential Scanning Calorimetry Each sample was analyzed using a Mettler DSC TA 4000 (Greifensee, Switzerland) connected to a calorimetric cell Mettler DSC20 and using STARE software version 9.30 for data analysis. Prior to analysis the instrument was calibrated with Indium, Zinc and Lead for the temperature and with Indium for the enthalpy quantification; each sample, containing about 2 mg of PZQ exactly weighted, was placed in a 40 μm aluminum pan with perforated lid and heated from 30 to 160 °C (10 °C/min) under air atmosphere.

Table 6.7: Main haracteristics of the SEs used.

SEs	Details	
C1807	Fatty acid	stearic acid
	Content in monoesters	40%
	HLB	7
	Melting temperature	60 °C
	Degradation temperature	233 °C
	Maximum potency[215]	31-44 mg
C1811	Fatty acid	stearic acid
	Content in monoesters	60%
	HLB	11
	Melting temperature	55 °C
	Degradation temperature	234 °C
	Maximum potency[215]	31-44 mg
C1816	Fatty acid	stearic acid
	Content in monoesters	75%
	HLB	16
	Melting temperature	56 °C
	Degradation temperature	237 °C
	Maximum potency[215]	31-44 mg
P1570	Fatty acid	palmitic acid
	Content in monoesters	70%
	Melting temperature	NA
	Degradation temperature	NA
	Maximum potency[215]	1%
	HLB	15

Powder X-ray Diffraction The sample were analyzed by powder X-ray diffraction using a Bruker AXS D5005 X-ray diffractometer with Ni-filtered Cu Kα radiation (wavelength 1.5418 A). The preparation of the samples consisted in pressing about 20-30 mg of powder over a glass slide to have a flat surface. The data were collected in a 2θ range of 3-40 degree. These analyses were performed thanks to the collaboration with prof. V. Lughi of the Department of Engineering and Architecture, University of Trieste, Italy.

FT-IR spectroscopy FT-IR analyses were performed using a Perkin Elmer System 2000 FT-IR; the samples were mixed with KBr in an agate mortar (RATIO) and then pressed with an hydraulic press for 2 minutes at 10 Ton to obtain homogeneous

and transparent discs. The analysis was conducted form 400 to 4000 cm^{-1} with a resolution of 4 cm^{-1} and total scan number of 3.

Scanning Electron Microscopy Selected samples were observed using a scanning electron microscope (Quanta250 SEM, FEI, Oregon, USA) operating in secondary electron detection mode, after beign sputtered with gold (Sputter Coater K550X, Emitech, Quorum Technologies Ltd, UK) in two subsequent steps of 30 sec. The working distance was adjusted in order to obtain the suitable magnification, the accelerating voltage was 30kV.

Efficacy in *in vitro* The *in vitro* tests were performed at the Swiss Tropical and Public Health Insitute (Basel, Switzerland, prof. Jennifer Keiser). The samples were tested in their efficacy by preparing different concentrations, ranging from 0.021 to 0.33 μg/L in which adult Schistosomes were incubated for up to 72 hours. By using an inverse microscope (Carl Zeiss, Germany, magnification 80x) all the alterations of morphology, motility and viability were observed and the IC_{50} value was calculated with CompuSyn software.

Drug recovery The content of PZQ was assayed by means of a reverse-phase HPLC.UV by adapting a method already reported in literature[91]; the system had two delivery pumps (LC-10 ADVP, Shimadzu, Japan), an autosampler (SIL-20A, Shimadzu, Japan) a UV-vis detector (SPD-10Avp, Shimadzu, Japan) and the data were acquired at a fixed wavelength of 220nm using an interface (SCL-10Avp, Shimadzu, Japan) and analyzed with Ez-Star software; the column used was a Kinetex 5 um c18 (150 x 4.60mmm, Phenomenex, Bologna). The mobile phase used was a mixture of Methanol:water (65:35 v/v), purged at 1 ml/min. PZQ retention time was 5.5 min while the total run time for each sample was set at 12 min. Prior to analysis, a linear calibration curve with r^2=0.99996 was obtained for PZQ under these conditions using different concentrations of the drug from 0.3 to 10 mg/mL. Each day, a standard solution (with a concentration of 2.5 mg/L) was prepared by dissolving about 10 mg of PZQ accurately weighted in Methanol of HPLC grade (20 mL) and diluting the solution 1:200 with the mobile phase. Moreover, two additional calibration curve were obtained respectively for the relative impurity indicated in the Eur. Ph. (Ed. 8.0)[32], impurity A (r^2=0.9993) and impurity B (r^2=0.9994), which were identified at the retention time of 3.45 min and 11.2 min. The reference solution did not report any of these impurities.

6.3.3 Results and Discussion

Following the method used for the preparation of PZQ hemihydrate (section 5.1), the SE solutions at 0.05% were added after 30 minutes of neat grinding of PZQ (25 Hz) and the milling process was continue for other 60 minutes at the same frequency. This was to evaluate the possible changes in the crystallinity and morphology of the samples, as it was reported by Hayama and collaborators[224]. The DSC traces were

similar to the one of PZQ hemihydrate, but with a more intense peak at about 75 °C and thinner signal of PZQ polymorph at about 112-113 °C, while the endotherm of raw PZQ was shifted a few degree higher, as shown in Figure 6.35.

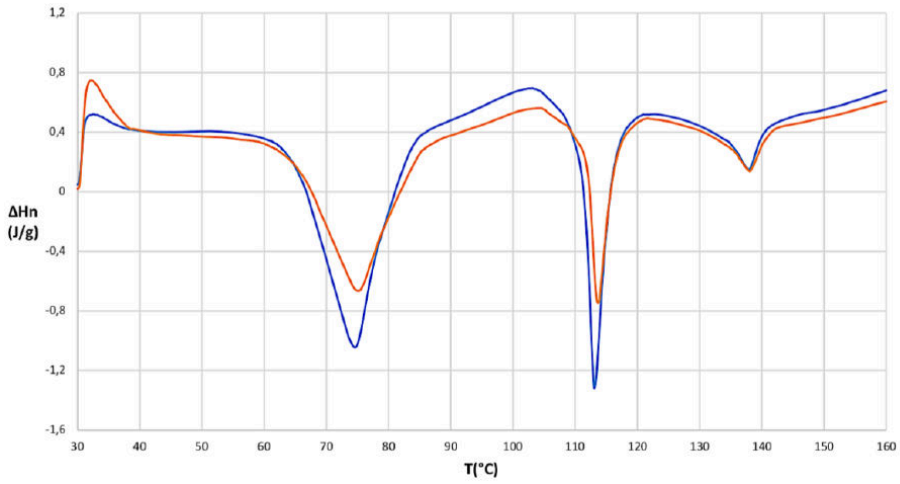

Figure 6.35: Example of the DSC traces of the PZQ hemihydrate (blue) and the results obtained when using the C1811 solution(orange).

Nevertheless, the low melting point of the excipients used could create bias in the endothermic curves at the DSC analysis, which was therefore discarded for this reason and replace by other solid-state characterization not requiring any heating of the sample. To assess the identity of the solid forms created, PXRD analysis was conducted: as reported in Figure 6.36, all the samples obtained with the SEs solutions evidenced the same characteristic peaks of the hemihydrated form previously reported (5.1.3), without any presences of the raw drug or other solid forms. Interestingly, the obtained hemihydrated forms exhibited a higher crystallinity, visible as the higher peak intensity in the PXRD analyses, respect to the previously reported form (Figure 6.37). This was in agreement with the higher melting enthalpy noticed in the DSC analysis previously shown (Figure 6.35).

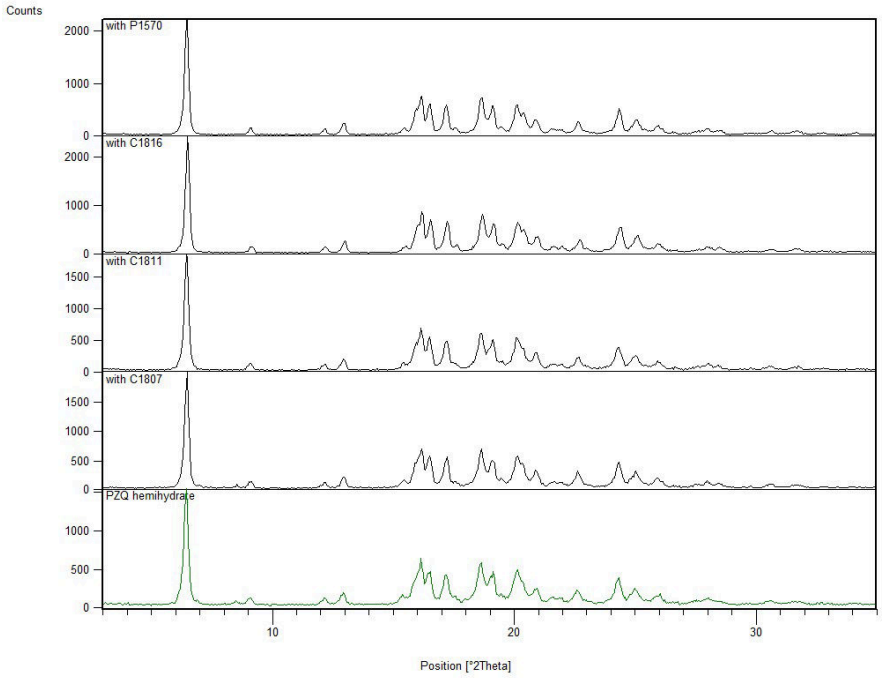

Figure 6.36: PXRD patterns of the products obtained using the SEs solutions compared to PZQ hemihydrate (green).

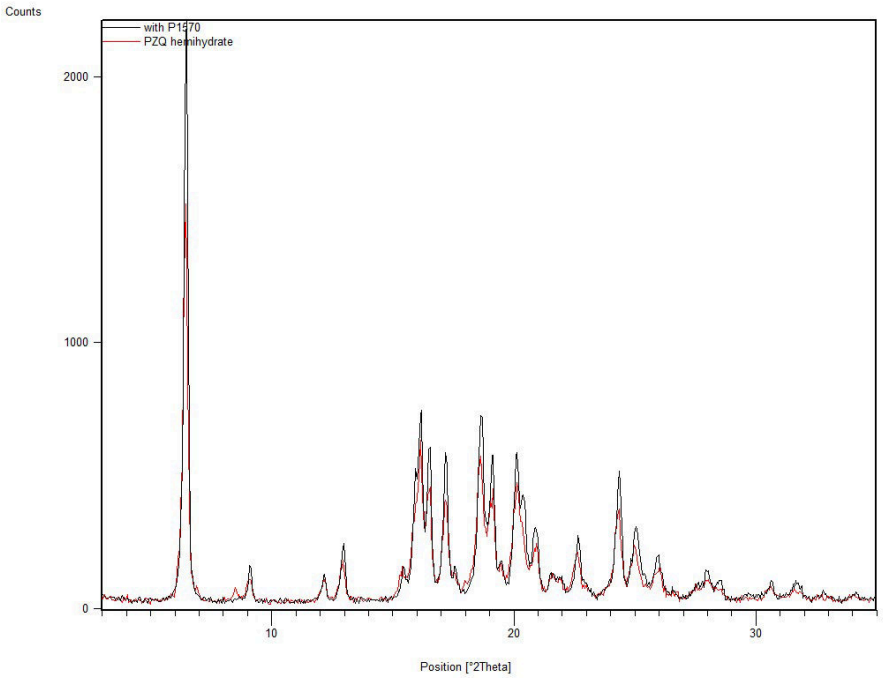

Figure 6.37: PXRD patterns of racemic PZQ hemihydrate (red) with the one obtained by LAG with a P1570 water solution.

Similarly, the FT-IR analyses of the 4 new hemihydrates were superimposable with the PZQ hemihydrate, one example is reported in Figure 6.38.

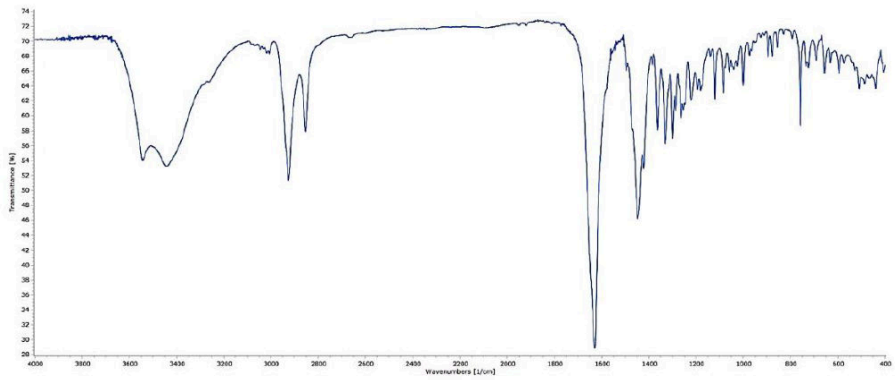

Figure 6.38: Example of the FT-IR spectra obtained when preparing PZQ hemihydrate using the surfactants solution. The pattern reported is for C1816.

The SEM analyses of the hemihydrates obtained with the surfactant solutions displayed a total change of the crystal habitus, comparing to RacH-PZQ (chapter 5.1): in fact, in place of the aggregates of large plate particles, very thin whiskers were found, which were similar between the 4 different samples, as reported in Figure 6.39. Thus, the presence of the surfactants in the acqueous solutions used for LAG led to the same PZQ hemihydrated form (equal to RacH-PZQ) as it was also reported for clathrate hydrate[225], but with a more pronunciated crystallinity and a complete new habitus. This behaviour could be attributed to the presence of the surfactant at the interface solid/liquid, where the nucleation of the hemihydrate is likely to begin, influencing the dimension and shape of the new crystallizing form. Similar observations were reported for the different morphologies of Clathrate Hydrate depending on water composition[226]. The reduction of the crystal dimensions could be related to the enhanced PZQ dispersion in water due to the presence of the surfactants, which avoided the formation of close nucleation centers and therefore big agglomerates.

Finally, it is worth noticed that these dramaticchanges were obtained using a very low sucrose ester concentration (0.05 %) and by grinding for only 60 minutes in the presence of water, attesting the great potentiality of the use of these surfactants in PZQ milling.

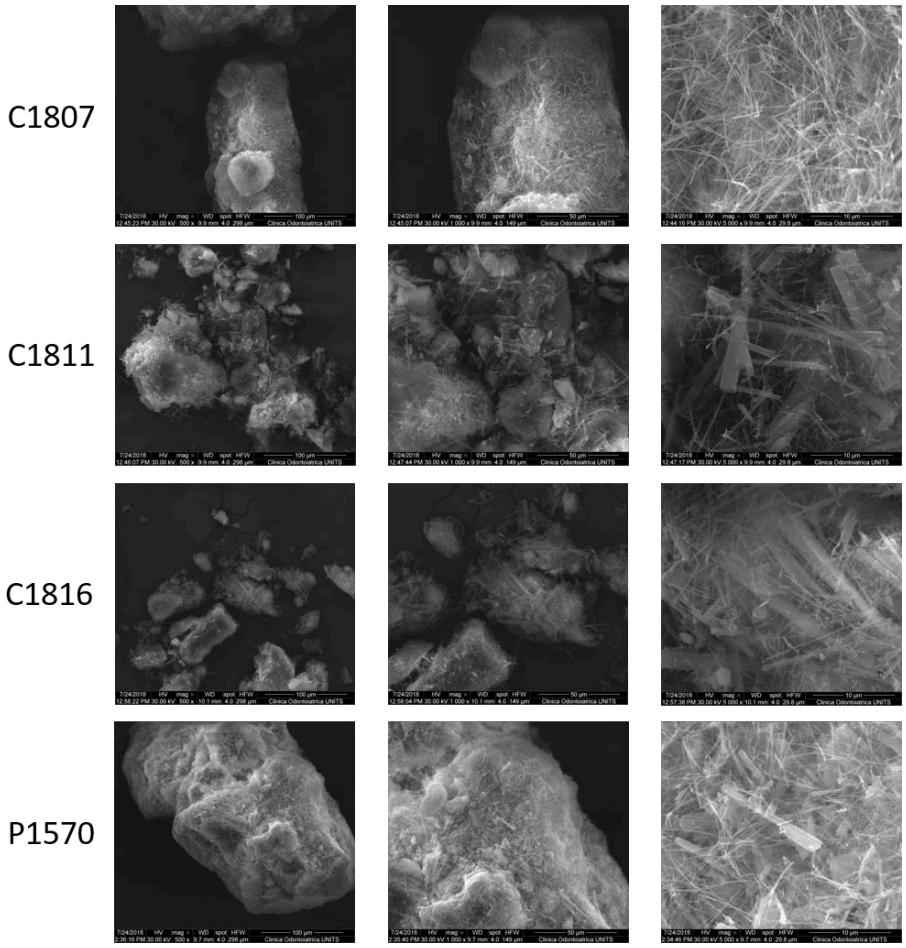

Figure 6.39: SEM images of the hemihydrates obtained with the water solutions with the surfactants. Magnification is 500x, 1000x and 5000x from left to right.

The second part of this section will present the investigation on PZQ behaviour when ground with the surfactants at the solid state. In particular, PZQ was ground for 30 minutes at 25 Hz, as previously, to achieve a partial amorphisation of the system; then, the surfactant was added in a 1:1 wt ratio and the milling was continued for other 60 minutes at 25 Hz. Due to the already reported degradation products upon grinding of PZQ (paragraph 2.4.3), the samples obtained were analyzed in the drug content (Table 6.8): the percentage of impurities/related products was generally less than 3%, similarly to the already reported experiences with other excipients.

Table 6.8: PZQ content of the samples obtained by neat-neat grinding

Sample	Drug content	SD
NNG C1807	44.45	0.39
NNG C1811	43.35	0.02
NNG C1816	47.47	0.01
NNG P1570	50.31	1.28

The PXRD analysis of the coground sample revealed a very interesting behavior: when using all the SEs derived from stearic acid, the application of the neat-neat grinding (i.e. passage through the partial amorphisation of the drug) led to the formation of PZQ polymorphs. Differently, in the case of P1570 (ester of palmitic acid) the pattern collected displayed the characteristic reflections of the starting materials immersed in an halo pattern, as visible in Figure 6.40.[3]

The FT-IR spectra confirmed the same observation, since the carbonyl region evidenced the close double peak typical of the *anti* conformation of PZQ polymorphs (at about 1624, 1634 cm^{-1}) respect to the *syn* conformation of raw PZQ (at about 1650, 1628 cm^{-1}), Figure 6.41 to Figure 6.43 . Nevertheless this analyses could not discriminate between Form B and C, due to the superimposable FT-IR spectra. The correspondence of the PXRD spectra allowed to attribute the formation of Form B when neat-neat grinding with C1807, and Form C with the other steraric acid SEs. In the case of P1570, the FT-IR spectrum confirmed the presence of the raw PZQ form, with the same characteristic bands as visible in Figure 6.44.

[3]PXRD patterns collected at the University of Limerick (thanks to the collaboration with Dr. M. Lusi), due to a problem in the diffractometer used before.

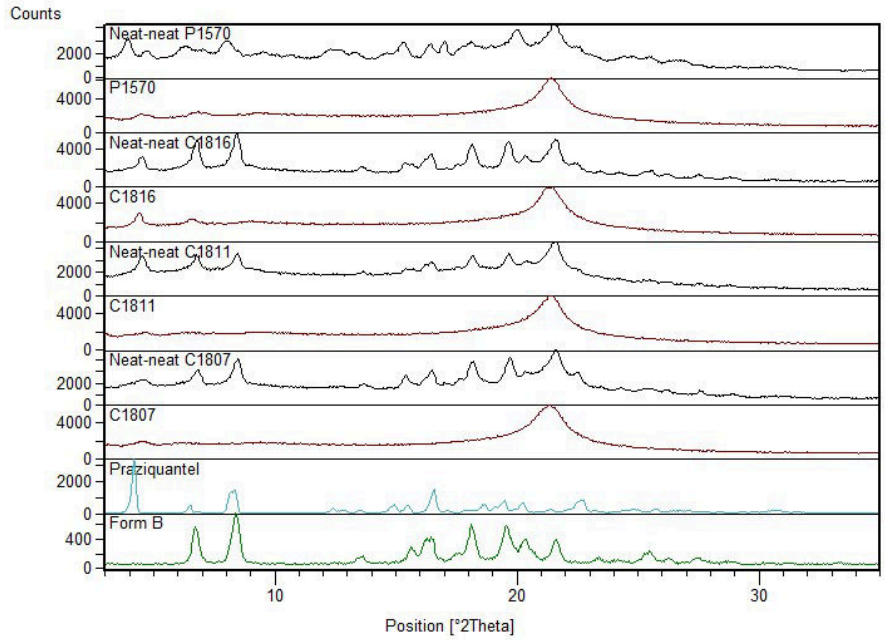

Figure 6.40: PXRD pattern of the neat-neat ground samples with each surfactant and the corresponding raw pattern. On the bottom From B and raw PZQ for comparison.

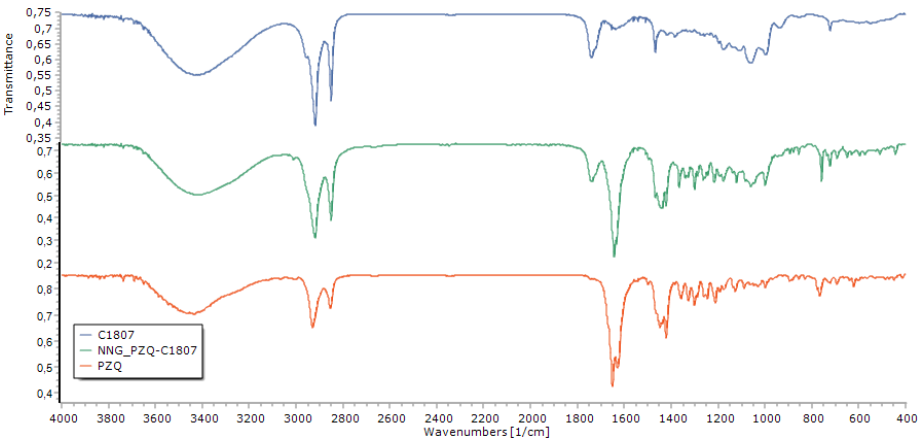

Figure 6.41: FT-IR spectra of C1807 (blue), neat-neat ground sample with C1807 (green) and raw PZQ (orange).

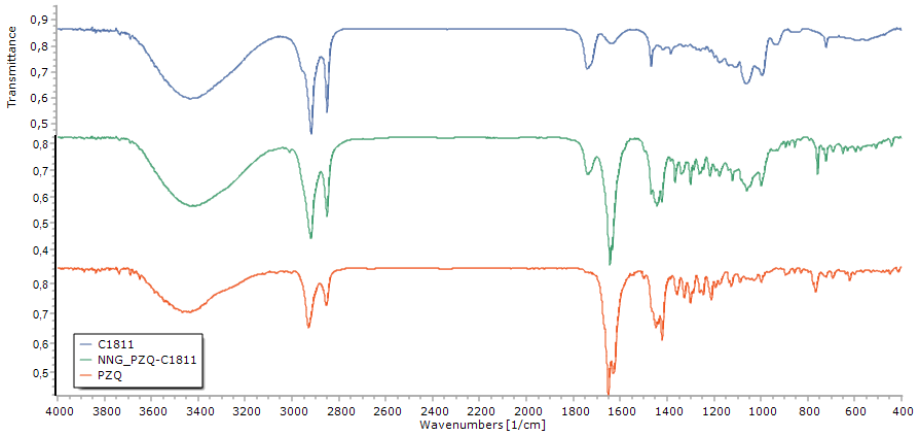

Figure 6.42: FT-IR spectra of C1811 (blue), neat-neat ground sample with C1811 (green) and raw PZQ (orange).

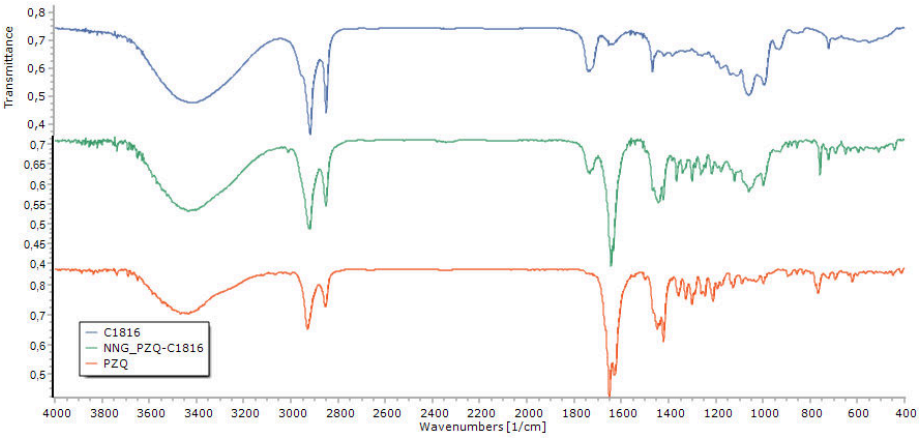

Figure 6.43: FT-IR spectra of C1816 (blue), neat-neat ground sample with C1816(green) and raw PZQ (orange).

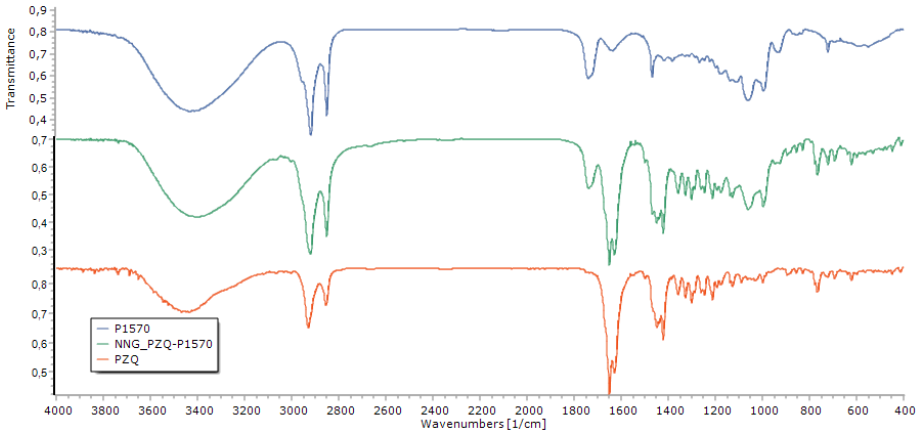

Figure 6.44: FT-IR spectra of C1570 (blue), neat-neat ground sample with C1570 (green) and raw PZQ (orange).

Figure 6.45 reports the SEM images of the raw excipient (left), the physical mixture with PZQ (centre) and the neat-neat coground sample (right) for each surfactant used. In all the physical mixtures the corresponding components could be easily identified: the surfactant is displayed as large particles, while PZQ as the typical needles. In all the neat-neat coground samples the habitus of the surfactant was dramatically changed with a certain correspondence with the PXRD results. When grinding with C1807 the sample showed the presence of very small whiskers covering and partially included in the surfactant particles. In the case of C1811 the whiskers are thinner and similar to the already reported habitus of Form B. With C1816, once again the characteristic whiskers of the polymorphic form were evidenced, covering the surfactant particles. In the case of P1570 no whiskers or needle-like particles were found, but large agglomerates with a smooth surface as reported in the last image of Figure 6.45, in agreement with previous findings.

Selected samples were tested *in vitro* against adult *S. mansoni*: the IC_{50} was 0.124 μg/ml, comparable to the already reported for PZQ (0.165 μg/ml), confirming the maintained antischistosomal activity.

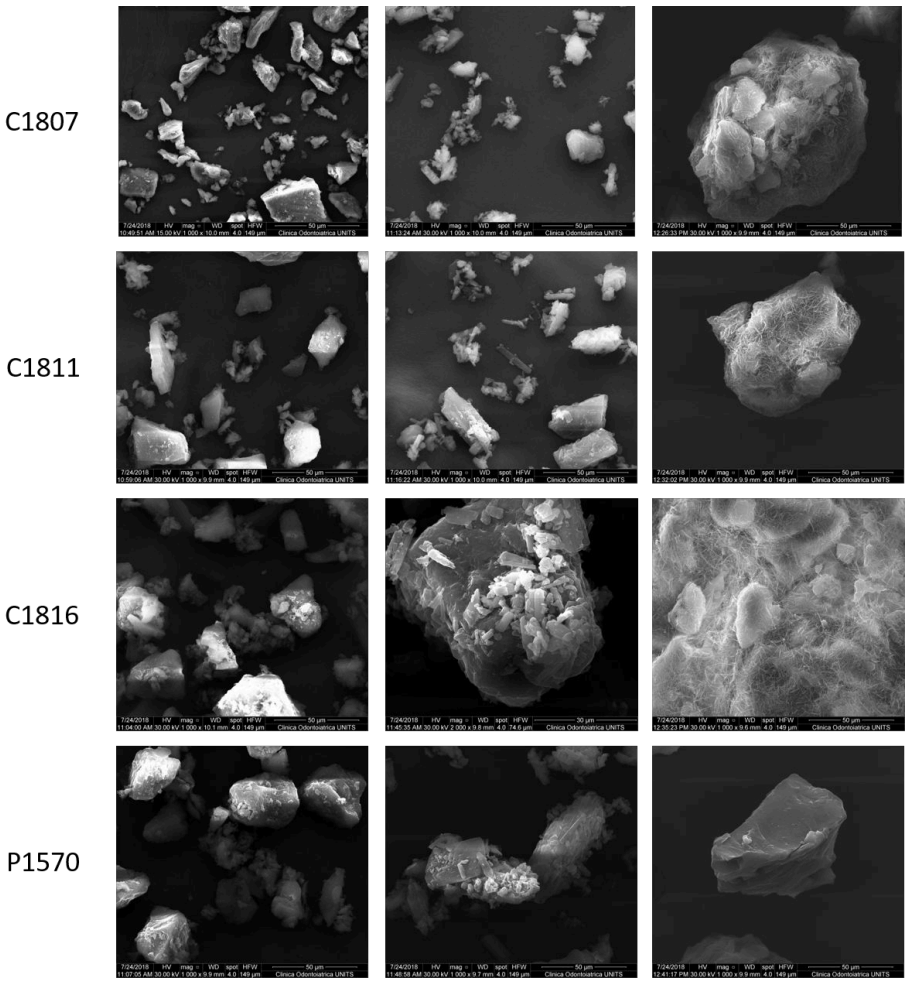

Figure 6.45: SEM images of the neat-neat coground samples. From left to righ: the raw surfactant, the physical mixture with PZQ and the neat.neat coground sample.

6.3.4 Conclusions

The use of SEs to prepare RacH-PZQ *via* liquid-assised grinding demonstrated to be effective in achieving the same solid form, but with an enhanced crystallinity and a complete different crystal habitus, by using a very limited concentration (0.05%s). The application of the neat-neat grinding process permitted the formation of PZQ polymorphic forms when using stearic SEs, in a total milling time of only 90 minutes, while the same behavior was not noticed in the case of P1570. Moreover, the samples obtained maintained the activity *in vitro* against *S. mansoni* The results presented in this section represent a good starting point for the investigation of further application of SEs in PZQ formulation and the future characterization of the biopharmaceutical properties, as drug solubility and dissolution rate.

6.4 Production and characterization of Praziquantel microparticles

6.4.1 Introduction

This chapter deals with a completely different approach to enhance PZQ dissolution rate, readily scalable and of low expense: the production of PZQ microparticles by spray congealing. This technique is based on the atomization of a melt liquid in a cooling chamber, which help the transformation of the molten droplets in solid particles. Differently from spray-drying, during spray-congealing no solvents and no post-processing are required (i.e. solvent evaporation); additionally, the particles obtained are spherical and dense, suitable for capsule filling or tabletting, where drug release can be controlled by the accurate selection of the carrier[227, 228] and drug can be taste-masked[229]. With all this advantages, combined with the easy scalable characteristics and short production time, spray congealing has been massively reported in literature and applied in the pharmaceutical industry. Actually, one example of a successfull product on the market prepared by spray-congealing is represented by Zmax® (Pfizer). In this formulation azithromycin dihydrate, glyceryl behenate and poloxomer 407 (ethylene oxide and propylene oxide blocks) are molten/dispersed by using an extruder and subsequentely atomized and congealed, forming microparticles with an optimized drug release. This production technology allows a reduced therapy duration by the administration of a single 2g dose, achieving also a good tolerability and taste-masking effect[230, 231]. As for the investigation of the process variables, many works were reported in literature[232, 233]: Maschke and coworkers used an experimental design to study the influence of the atomization pressure and spraying temperature on particle size and process yiels[234], while Passerini and collaborators reported various investigations on different aspects of the process, as the influence of the type/amount of the carrier on microparticles characteristics[235, 236], and the atomizer type[237]. In 2006, they reported also the evaluation of PZQ granules and microparticles produced by melt granulation and ultrasonic spray congealing as efficient techniques for drug dissolution rate enhancement[145]. The carrier selected for the spray congealing technique was Gelucire 50/13[4], the same presented in this chapter, which has already shown its ability of improving the biopharmaceutical properties of different active ingredients, as reported in literature for silybum Marianum dry extract[238], glibenclamide[239], carbamazepine[240] and also by Qui and coworkers in the case of piroxicam[115]. In this section, the same technique will be applied to the activated form of PZQ produced via mechanochemistry, Form B (chapter 4.1) and the cryo-coground sample with PVP (chapter 3.1), while raw PZQ and the corresponding physical mixture with the polymer will be also included in Gelucire 50/13 microparticles and analyzed for comparison. The research here presented was conducted in collaboration with proff. N. Passerini and B. Albertini of the Department

[4]Gelucire 50/13 is a low melting (50 °C) mixture of mono, di-, triglycerides and PEG-32 (MW 1500) mono-, diesters of palmitic and stearic acids having HLB=13

of Pharmacy and Biotechnology, University of Bologna (Italy).

6.4.2 Materials and Methods

Materials

Praziquantel (PZQ, (11bRS)-2-(Cyclohexylcarbonyl)-1,2,3,6,7,11b-hexahydro-4-H -(pyrazino[2,1-a]isoquinolin-4-one)) was of Ph. Eur. grade and kindly donated by Fatro S.p.a. (Bologna, Italy). PZQ impurity A (2-Benzoyl-1,2,3,6,7,11b-hexahydro-4-H- pyrazino[2,1-a]isoquinolin-4-one) and B (2-Cyclohexanecarbonyl-2,3,6,7-tetrahydro-pyrazino[2,1- a]isoquinolin-4-one) were Ph. Eur. grade and bought from Endotherm Gmbh (Saarbruecken, Germany). Gelucire 50/13 was gently donated by Gattefossè (Milan, Italy) and Povidone (Kollidon K30, PVP K30) was from by BASF (Ludwigshafen).

Methods

Preparation of the sample powders The powder samples for the microparticles formation were obtained by grinding: the first was PZQ Form B, produced following the method previously reported (chapter 4.1), consisting in 4 hours grinding of PZQ in a vibrational mill (MM400 Retsch, Germany) without interruption at 20 Hz. Then, the coground system obtained by cryo-grinding the drug with PVP, as previously described (chapter 3.1) for one hour at 20 Hz. The corresponding physical mixture was prepared by manually mixing the powders in a agate mortar for 3 minutes.

Preparation of the microparticles The particles were prepared using an external mix two-fluid atomizer (Wide Pneumatic Nozzle WPN, Figure 6.46) already reported in literature[241]. The carrier used was Gelucire 50/13 while the amount of activated material to be inserted was calculated in order to have a PZQ percentage of 15%. The carrier was heated about 10 °C above its melting point and then added with the powders under agitation, obtaining a solution/suspension ready to be sprayed by the spray-congealing system. The inlet air pressure of the nozzle was set at 3 bar and the suspension was kept at 60 °C. There was no need of specific cooling system since the droplets simply solidify while falling in the cooling chamber, left at room temperature. Once prepared, the microparticles were stored in closed bottles in the dark and at room temperature.

Determination of the drug content The content of PZQ and of the related impurities in the microparticles was assayed by means of a reverse-phase HPLC.UV by adapting a method already reported in literature[91]; the system had two delivery pumps (LC-10 ADVP, Shimadzu, Japan), an autosampler (SIL-20A, Shimadzu, Japan) a UV-vis detector (SPD-10Avp, Shimadzu, Japan) and the data were acquired at a fixed wavelength of 220nm using an interface (SCL-10Avp, Shimadzu, Japan) and analyzed with Ez-Star software; the column used was a Kinetex 5 um c18 (150 x 4.60mmm,

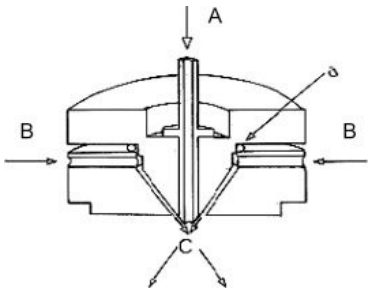

Figure 6.46: Scheme of the WPN (not in scale): material feeding (A), air inlet (B), atomization of the fluid (C), o-ring (a)[241].

Phenomenex, Bologna). The mobile phase used was a mixture of Methanol:water (65:35 v/v), purged at 1 ml/min. PZQ retention time was 5.5 min while the total run time for each sample was set at 12 min. Prior to analysis, a linear calibration curve with r^2=0.99985 was obtained for PZQ under these conditions using different concentrations of the drug from 0.4 to 40 mg/mL. Each day, a standard solution (with a concentration of 2.5 mg/L) was prepared by dissolving about 10 mg of PZQ accurately weighted in Methanol of HPLC grade (20 mL) and diluting the solution 1:200 with the mobile phase. Moreover, two additional calibration curve were obtained respectively for the relative impurities indicated in the Eur. Ph. (Ed. 8.0)[32], impurity A (r^2=0.9993) and impurity B (r^2=0.9994), which were identified at the retention times of 3.45 min and 11.2 min respectively. The reference solution did not report any of these impurities. Differently form the previous drug contet analyses reported in this thesis, 24 hour of agitation in the dark were necessary to complete the solubilization of the microparticles in methanol. The obtained solutions were then diluted 1:100 with the mobile phase, filtered with a 0.2 μm membrane and injected in the HPLC system using the method previously described. The drug recovery was considered as the PZQ % among all the peaks in the chromatogram (for the activated materials) and as the theoretical VS experimental drug loading for the microparticles, also expressed as the encapsulation efficiency. All the results were expressed as mean (n=3) ±SD.

Powder X-Ray Diffraction (PXRD) The raw and activated materials and the microparticles containing Form B and the coground sample together with their physical mixture were analyzed using a Bruker AXS D5005 X-Ray Diffractometer (Germany, Cu-kα=1.5418 A) in a range of 3-35° of 2θ, with a step size of 0.05° every 5 sec. These analyses were performed thanks to the collaboration with prof. V. Lughi of the Department of Engineering and Architecture, University of Trieste, Italy.

Environmental SEM Environmental SEM (ESEM) was performed to observed both the raw materials and the obtained microparticles, using a Quanta 200 FEI ESEM apparatus (FEI, company, Czech Republic) under low vacuum conditions.

Particle size determination Two different methods were used for the determination of the particle size. In the case of the microparticles, a vibrating shaker (Octagon Digital, Endecotts, London, UK) was used with 6 different sieves (Scientific Instrument, Milano, Italy) from 500 to 75 μm. Differently, the activated and raw materials were analyzed by laser light scattering (Malvern Masterisizer 2000, Malvern, UK) of the corresponding suspension in water with the 0.1% of polysorbate 80. If the sample contained PVP, a silicon oil (Silico DC 245 DOW Corning) was used as the dispersing agent. This analysis was conducted thanks to the collaboration with Dr. E. Franceschinis of the Department of harmaceutical and Pharmacological Sciences of the University of Padova, Italy.

FT-IR spectroscopy All the samples were analyzed with a Jasco FT-IR A-200 spectrophotometer, after being compressed with KBr in flat discs with an hydraulic press (Perkin Elmer, Norwalk USA), applying a force of 3 tons for 3 minutes. Data were collected between 650 and 4000 cm^{-1} with a resolution of 1 cm^{-1}.

Hot-stage microscopy The samples were observed using a Nikon eclipse E400 optical microscope connected to a Nikon Digital Camera DN100 for image acquisition and to a hot stage system from Mettler Toledo (Mettler Toledo s.p.a., Novate Milanese, Italy) to observe physical transformations during the heating process (25-200 °C at 10 °C/min).

Drug solubility and dissolution The solubility of all the samples and raw materials were analyzed following this method: saturated water solutions (10 mL) were kept under agitation in the dark at 25 °C for 48 hours, then centrifuged (10000 rpm for 20 minutes), filtered with a 0.2 μm membrane, diluted with the mobile phase (1:200) and injected in the HPLC system. Each sample was analyzed three times and the mean±SD was considered. The statistical assessment was performed using one way ANOVA, while comparison between means with t-Test. Statistically difference was considered with p values <0.01. The dissolution studies were performed under *sink* conditions, varying the quantity of the samples depending on their solubility and replacing the withdrawn amounts with thermo-stated dissolution medium. The apparatus used was a dissolution tester (Erweka DT800, Heusenstamm, Germany) with vessels containing 1000 mL of distilled water kept at 37±0.5 °C and under agitation with a paddle at 100 rpm. The withdrawals were performed at each sampling time by filtering 2 ml of the dissolution media (8 μm filter) which was subsequently subjected to HPLC analysis. Each sample was analyzed in triplicate and the mean±SD was considered.

Determination of the *in vitro* activity against *S. Mansoni* The activity of the microparticles containing Form B and the coground sample was tested in Newly Transformed Schistosomulae (NTS) and in adult *S. Mansoni*. For the first, concentrations of 1.23 μg/mL of each sample were used at 37 °C with three different testing times: after 24, 48 and 72 hours. At each one, the NTS were observed with

a microscope giving 3 grades of viability: 0 corresponded to the death, 1 to damages to the tegument and/or drastic reduction in the motility, 2 to some damages to the tegument and/or reduced motility and 3 to the absence of any changes in their motility. As negative controls, NTS under high DMSO concentrations were used. In the case of adult *S. Mansoni* the sample concentrations tested were 0.33, 0.11 and 0.037 μg/mL at 37 °C in the same time intervals (24, 48 and 72 hours) and the observation were conducted using the method previously described. The IC_{50} values for each test type were calculated using CompuSyn software.

Physical stability The physical stability of the selected microparticle system (MPsB) was studied over a period of 1 year by means of PXRD.

6.4.3 Results and Discussion

Prior to microparticles formation, the mechanochemically activated materials were characterized at the solid state similarly to the previously described methods, including DSC, PXRD, FT-IR, hot-stage Microscopy and SEM analyses.

Four different microparticles batches were prepared as reported in Table 6.9, containing raw PZQ, Form B, the physical mixture and the cryo coground sample. In particular, to calculate the precise quantity to be used for microparticle incorporation in the case of the binary system, the PZQ content was assayed resulting in about 46 % in the physical mixture as well as in the cryo coground sample.

Table 6.9: Composition of the microparticles and relative drug content (CG:CoGround, PM: Physical Mixture).

Microparticles	Name	Composition (%)			Drug content
		PZQ	PVP	Gelucire 50/13	%
CG PZQ:PVP	MPsA	15	15	70	13.75±0.14
Form B	MPsB	15	-	85	14.24±0.83
PM PZQ:PVP	MPsC	15	15	70	14.35±0.18
Raw PZQ	MPsD	15	-	85	15.16±0.11

During the microparticles formation an interesting behaviour was noticed: while in the case of MPsA, MPsC and MPsD the powder formed a suspension when mixed with the molten Gelucire, in the case of MPsB, the resulting solution was clear forming therefore a solid solution instead of a solid dispersion. The resulting microparticles displayed a drug loading comparable to the theoretical value of 15%, attesting an incapsulation efficiency of about 90%. The particle size analysis of the new products (Figure 6.47) showed a similar distribution between MPsA and MPsD with a Gaussian curve centered at 150-250 μm, while for MPsC the distribution was very broad due to the different composition of the physical mixture. In the case of MPsB the dimension of the almost totality of the particles was less than 250 μm. These differences were

accounted to the different viscosity of the solution/dispersion sprayed during the microparticles formation. In fact, at 60 °C the viscosity of the fluid followed the order MpsB<MpsD<MpsA<MpsC, depending on the amount of powder inserted (as also reported in literature[236]) and on particle size, shape and drug solid state in the fluid. In the particular case of Form B, even though its particle size mean distribution was bigger than the raw drug (54.89 μm VS 23.90 μm of $d_{0 \cdot 5}$), the viscosity of the fluid was the lowest, probably due to the major solubility evidenced by the formation of a clear solution.

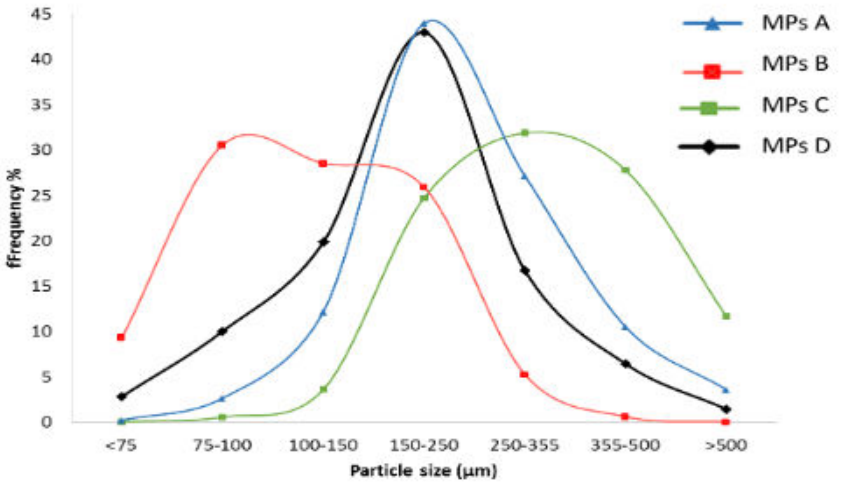

Figure 6.47: Size distribution of the microparticles formed.

The DSC analysis of the sample was discarded form the characterizing techniques due to the low melting point of Gelucire 50/13, which could create various bias in the curves interpretation. The thermal observation was performed by hot-stage microscopy, reported in Figure 6.48. When heating MPsD, at 48 °C the acicular crystal of PZQ could be easily recognized in the molten Gelucire, attesting the presence of the crystallize drug in the microparticles, without any solid-state modification by the spray-congealing process. The melting was then complete at about 110 °C. Similarly, in MPsB the presence of Form B could be observed even if as less and smaller spots, confirming the very fine dispersion of the polymorphic form in the molten Gelucire. The complete melting was observed at about 90 °C. In the case of MPsA, the cryocoground sample started its melting at 55 °C, completing the process only when heating till 150 °C, observing the rubbery state of the polymer and also the presence of PZQ in its nanocrystalline state. When observing the microparticles containing the physical mixture (MpsC), during Gelucire melting the nearly round particles of PVP and the needle crystals of PZQ were noticed. The PM started melting at about 50-60 °C, completing the process at 110 °C for PZQ and at higher temperatures (160 °C) for PVP. In all the cases presented, the melting of the drug was observed at lower

temperatures than expected, which could be explained by the effect of the low melting point of Gelucire.

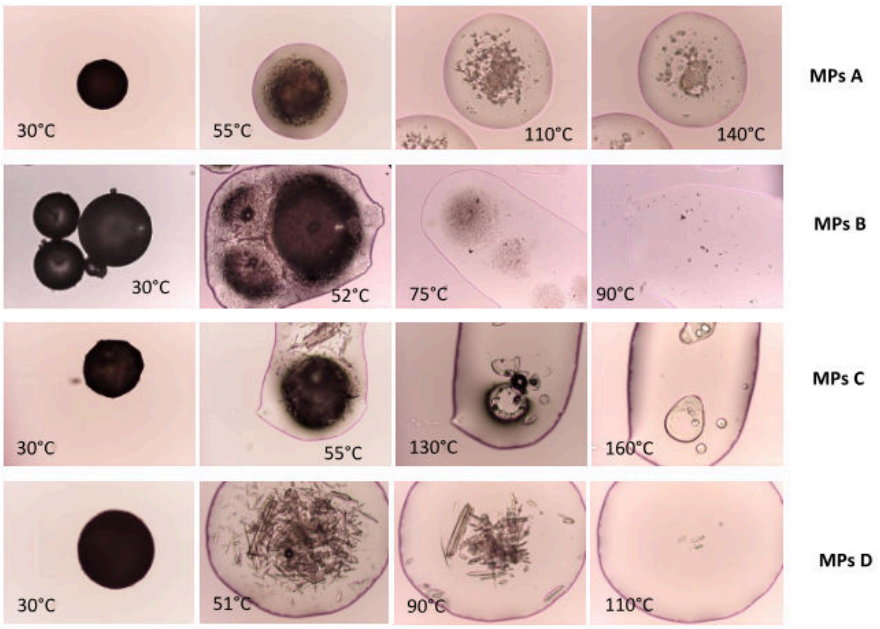

Figure 6.48: Hot-stage microscopy images of the microparticles formed (magnification=10x).

The PXRD patterns of the microparticles confirmed once again the presence of PZQ in its crystalline state, since the corresponding characteristic peaks could be noticed even if immersed in the broad pattern of the carrier, as shown by the arrow in Figure 6.49. The same reflections were more visible in the physical mixtures of the raw materials with Gelucire 50/13, even though with a reduced intensity due to the dilution in the linear polymer. In MPsB pattern, the signals attributable to Form B are very weak, but the polymorph is still recognizable and their intensity testifies a certain quote of drug amorphized/solved in Gelucire 50/13. The FT-IR analyses of the microparticles showed the characteristic bands of Gelucire, also reported by Brubach and collaborators[242], at about 1200-1100 cm^{-1} and the carbonyl stretching at 1715-1738 cm^{-1}; thus PZQ asymmetrich stretching of the carbonyl could be found at 1623 and 1646 cm^{-1} in MPsA, MPsC and MPsD, while at 1628 and 1640 cm^{-1} for Form B as already reported for the polymorphic form (chapter 4.1).

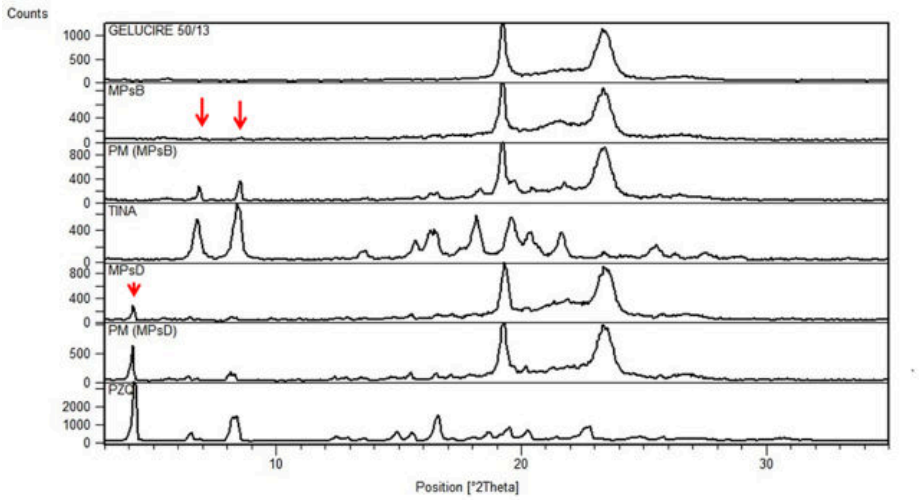

Figure 6.49: PXRD pattern of the microparticles comparing to the corresponding raw/activated materials and the corresponding physical mixture (PM) with Gelucire 50/13.

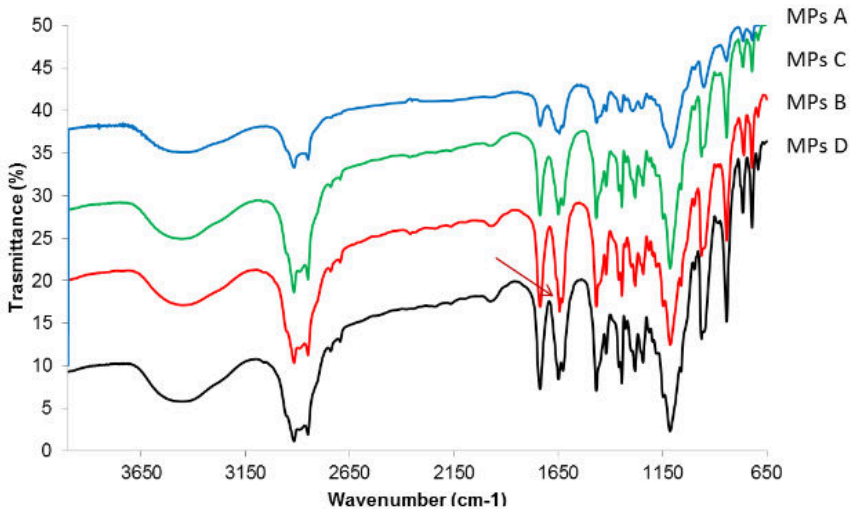

Figure 6.50: FT-IR spectra of the microparticles: MPsA (blue), MPsB (green), MPsC (red), MPsD (black). The arrow indicates the characteristic carbonyl group signal of Form B, still visible when loaded in the microparticle.

The microparticles containing raw PZQ and Form B were also studied in their surface morphology by ESEM, shown in Figure 6.51: MPsD were spherical non-aggregated microparticles with just a few elongated particles, while MPsB samples were highly spherical presenting groups of very small solidified droplets, thanks to the micronized particle of Form B.

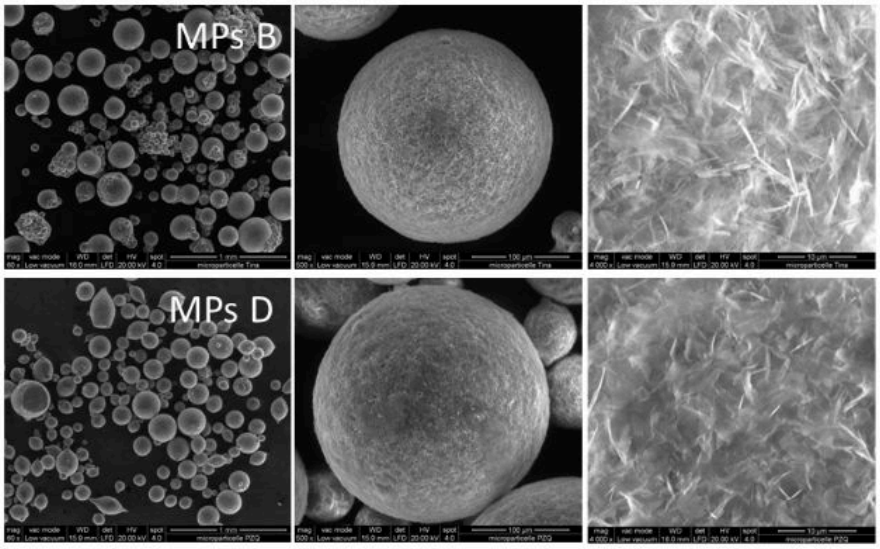

Figure 6.51: ESEM images of MPsB and MPsD: from left to righ: 60x, 500x and 4000x.

The main objective of this project was to study the effect of the incorporation of the raw drug and related activated materials in Gelucire-based microparticles to enhance drug solubility and dissolution. All the activated products and microparticles demonstrated a higher water solubility compared to the raw drug and in particular the combination of the mechanochemical activation and the spray congealing techniques in presence of the selfemulsifying agent led to products with a solubility of 651.28 mg/L, about five times greater than the raw drug (140.30 mg/L) in the case of the microparticles containing Form B. MPsA solubility was respectively two and four times higher than the raw drug and the activated cryo comilled sample. Also, when raw PZQ was included in the microparticles its solubility was triplicated. The enhancement of MPsB was significantly higher than MPsD, while among the other microparticles results there were no significative differences. A graphical representation of the results is reported in Figure 6.52.

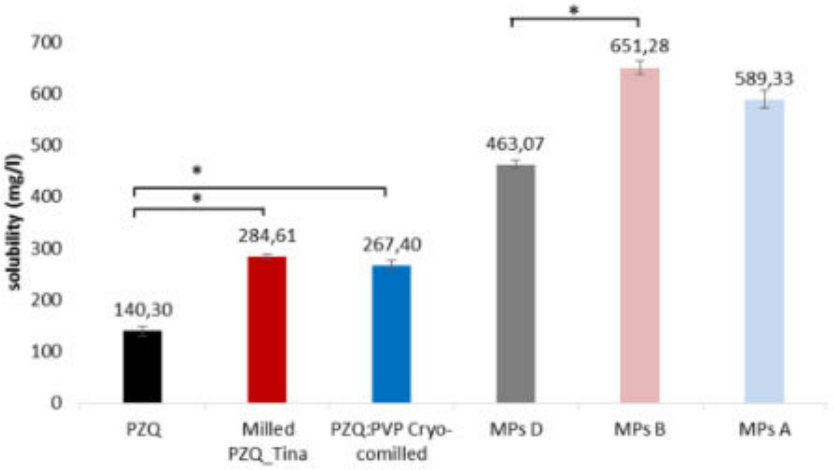

Figure 6.52: Water solubility at 20 °C of the microparticles together with the raw and activated materials. The $*$ indicates the statistical difference ($p<0.01$) between the corresponding solubility values.

The dissolution studies of the microparticles compared to raw PZQ are reported in Figure 6.53: all the samples exhibited an enhancement of drug dissolution due to the intrinsic properties of the formulation and to the higher solubility of the microparticles. In fact, Gelucire 50/13 can favour the formation of micelles to enhance the dissolution rate of drugs, thanks to its composition based on the mixture of mono-, di- or triglycerides with PEG1500 esters of stearic acid (HLB 13), as it was reported in the case of glibenclamide[239], carbamazepine[240] and Sylibum marianum dry extract [238]. Another mechanism reported was the one of Qi and collaborators[115], who studied the dissolution of microspheres containing piroxicam. The drug particles finely separated, enhanced the surface area and the wet phase, creating a lyotropic liquid crystalline phase that increased piroxicam dissolution. After one hour all the samples dissolved

about the 80% of the drug, and in particular in the case of MPsB (with Form B) and MPsA (with the coground sample) drug dissolution reached the 95-98% of drug dissolved after only 12 minutes. MPsC and MPsD, containing the physical mixture with PVP and the raw drug respectively, showed an increased dissolution comparing to the raw drug, even if less than the other microparticle formulation. Therefore the dissolution test evidenced the advantages of combining the mechanochemical process with the spray congealing, reaching higher PZQ dissolution in less time than the raw drug.

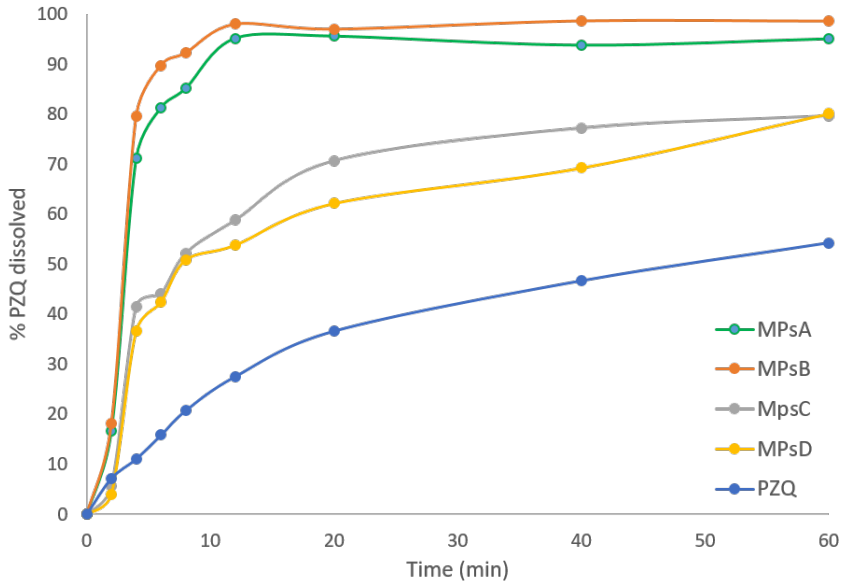

Figure 6.53: Dissolution kinetics of the microparticles compared to raw PZQ.

MPsB were tested in their physical stability after one year storage by PXRD: as visible in Figure 6.54, MPsB were highly stable, without any recrystallization/phase transformation occurring and a completely swuperimposable spectrum with the fresh one.

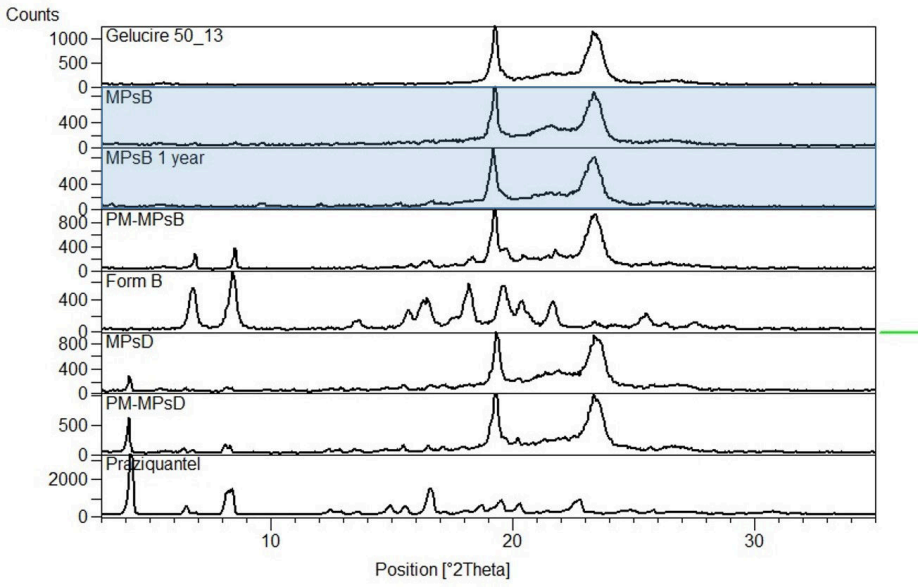

Figure 6.54: PXRD trace of MPsB after 1 year storage (3rd spectrum from the top) compared to the fresh one (2nd spectrum from the top).

Finally, due to the best performances exhibited, MPsB and the corresponding Form B were tested *in vitro* against NTS (newly transformed schistosomules) and adults *S. mansoni* worms comparing to the raw drug. The results are presented in Table 6.10: the microparticles and the activated Form B were active both against NTS and adult *S. mansoni*, though with little variations of the IC_{50}.

Table 6.10: Results of the *in vitro* analysis of the activity of MPsB, Form B and raw PZQ against NTS and adults *S. mansoni*.

Sample	IC_{50} NTS (μg/mL)	IC_{50} *S. mansoni* (μg/mL)
MpsB	3.16	0.48
Form B	2.40	0.23
Raw PZQ	2.58	0.13

6.4.4 Conclusions

The formation of mechanochemically activated PZQ forms, as Form B and cryo coground samples with PVP, has already demonstrated to be highly useful to increase drug solubility and dissolution in rthe previous chapters. In this one, the combination of the mechanochemical process and the spray-congealing technique permitted to further increase the solubility and the dissolution rate of PZQ, also representing a step forward the production of a advantageous dosage form of PZQ. In case of MPsB the results were highly positive, reaching a solubility of 651.28 mg/L, about five times greater than the raw drug (140.30 mg/L) and a dissolution of the 70 % of the drug after only 2 minutes. The promising MPsB formulation maintained also the *in vitro* activity against NTS (newly transformed schistosomules) and adults *S. mansoni* worms, with values comparable to the raw drug and Form B. Therefore, the production technique presented in this chapter represents a suitable way to enhance PZQ biopharmaceutical properties.

Final considerations

The research performed during the PhD course and reported in this thesis represents a comprehensive evaluation of Praziquantel (PZQ) behavior upon mechanochemical activation in a vibrational mill, with the aim of improving its poor biopharmaceutical properties. The results obtained were very positive and went far beyond the expectations: the amorphous solid dispersions obtained by cogrinding PZQ with various excipients (povidone, copovidone, sucrose esters, natural/synthetic sweeteners, non-ordered mesoporous silica) and in different conditions (including cryogenic milling) exhibited a significative increase in drug solubility, still maintaining the *in vitro* antischistosomal activity. Moreover, the samples ground with selected sweeteners were very interesting also for the possible amelioration of PZQ bitter and disgusting taste. The deep investigation of the mechanochemical process included also the identification of the degradation products forming during milling with polymers, which were not present with the drug by itself. The grinding of the drug on its own, which included also the application of a design of experiments, permitted the discovery of two new anhydrous solid-forms (Form B and Form C) with enhacenced solubility and dissolution rate. Also, Form B was stable for more than one year, showed a *in vitro/in vivo* activity and a pharmacokinetic profile comparable to the raw form and, when included in Gelucire 50/13 microparticles, drug biopharmaceutical properties were even more increased. When performing liquid-assisted grinding, other three solid forms of PZQ were discovered, namely one hemihydrate and two solvates, representing not only, once again, an improvement of the biopharmaceutical properties of the drug, but also another step towards a complete knowledge of PZQ propensity to cocrystal/solvate formation *via* mechanochemistry, widespreading the possibility of new discoveries and formulations. Therefore, all the systems studied in this thesis represent a viable contribution to the crystal structure, intermolecular interaction propensity, chemical, biopharmaceutical and bioactivity features of PZQ when subjected to mechanochemical activation both on its own and in combination of various pharmaceutical excipients.

In conclusion, this thesis combines several hot topics in the current chemical and pharmaceutical research, namely paediatric formulations, neglected tropical disease, crystal engineering, mechanochemistry, poor bioavailability issue and would seen to represent a new approach for the development of functional materials and suitable formulations.

Publications list and congress presentations

6.5 Research articles

- "An explorative analysis of process and formulation variables affecting comilling in a vibrational mill: The case of Praziquantel"
  B. Perissutti, N. Passerini, R. Trastullo, J. Keiser, **D. Zanolla**, G. Zingone, D. Voinovich, B. Albertini
  International Journal of Pharmaceutics, 2017, 553, 2, 402-412
  https://doi.org/10.1016/j.ijpharm.2017.05.053

- "Milling and comilling Praziquantel at cryogenic and room temperatures: Assessment of the process-induced effects on drug properties"
  D. Zanolla, B. Perissutti, N. Passerini, S. Invernizzi, D. Voinovich, S. Bertoni, C. Melegari, G. Milotti, B. Albertini
  Journal of Pharmaceutical and Biomedical Analysis, 2018 153, 82-89
  https://doi.org/10.1016/j.jpba.2018.02.018

- "A new soluble and bioactive polymorph of Praziquantel"
  D. Zanolla, B. Perissutti, N. Passerini, M. R. Chierotti, D. Hasa, D. Voinovich, L. Gigli, N. Demitri, S. Geremia, J. Keiser, P. Cerreia Vioglio, B. Albertini
  European Journal of Pharmaceutics and Biopharmaceutics, 2018, 127, 19-28
  https://doi.org/10.1016/j.ejpb.2018.01.018

- "Identification of degradation products of praziquantel during the mechano chemical activation"
  I. Sagud, **D. Zanolla**, B. Perissutti, N. Passerini, I. Skoric
  European Journal of Pharmaceutics and Biopharmaceutics, 2018, 159, 291-295
  https://doi.org/10.1016/j.jpba.2018.07.002

6.6 Oral presentation

"From bitter to sweet: towards a new patients-friendly Praziquantel dosage form"
D. Zanolla, E. Giron, B. Perissutti, N. Passerini, B. Albertini, D. Voinovich
12th A.It.U.N. Meeting: Medicines for older people, advances in drug delivery
10th-11th May 2018, Bologna (Italy)

6.7 Poster presentations

- "Preparation and characterization of a new soluble and bioactive polymorph of Praziquantel" B. Perissutti, N. Passerini, **D. Zanolla**, M. R. Chierotti, D. Hasa, D. Voinovich, J. Keiser, B. Albertini, 11t̂h CESPT Symposium 22nd-24th September 2016, Belgrade (Serbia)

- "New solid forms of Praziquantel through Liquid-Assisted Grinding" **D. Zanolla** B. Perissutti, D. Hasa, M. Arhangelskis, G. Rauber Schneider, D. Voinovich, W. Jones, 4th European Crystallographic School 2nd-7th July 2017, Warsaw (Poland) *Bursary winner*

- "Praziquantel Form B: preparation and characterization of the only ever-known anhydrous polymorph" **D. Zanolla**, B. Perissutti, N. Passerini, M.R. Chierotti, D. Hasa, D. Voinovich, L. Gigli, N. Demitri, J. Keiser, B. Albertini, 11th World Meeting on Pharmaceutics, Biopharmaceutics and Pharmaceutical Technology 19th-22nd March 2018, Granada (Spain)

- "Evaluation of praziquantel properties upon milling and comilling at room and cryogenic temperatures" **D. Zanolla**, B. Perissutti, S. Bertoni, S. Invernizzi, D. Voinovich, M. Moneghini, N. Passerini, B. Albertini
  11th World Meeting on Pharmaceutics, Biopharmaceutics and Pharmaceutical Technology 19th-22nd March 2018, Granada (Spain)

- "Crystal structure solution from PXRD and characterization of a new praziquantel polymorph (Form C)" **D. Zanolla**, B. Perissutti, D. Voinovich, N. Passerini, B. Albertini, L. Gigli, N. Demitri, P. Cerreia Vioglio, M. R. Chierotti 16th European Powder DIffraction Conference 1st-4th July 2018 Edinburgh (United Kingdom) *Bursary winner*

- "Combining mechanochemistry and spray congealing towards new praziquantel formulations" B. Albertini, B. Perissutti, S. Bertoni, **D. Zanolla**, E. Franceschinis, D. Voinovich, F. Lombardo, J. Keiser, N. Passerini 12th CESPT Symposium 20th-22nd September 2018, Szeged (Hungary)

Bibliography

1. Takacs, L. The mechanochemical reduction of AgCl with metals. *Journal of Thermal Analysis and Calorimetry* **90,** 81–84 (Oct. 2007).
2. Takacs, L. M. Carey Lea, the first mechanochemist. *Journal of Materials Science* **39,** 4987–4993 (Aug. 2004).
3. James, S. L., Adams, C. J., Bolm, C., Braga, D., Collier, P., Friščić, T., Grepioni, F., Harris, K. D. M., Hyett, G., Jones, W., Krebs, A., Mack, J., Maini, L., Orpen, A. G., Parkin, I. P., Shearouse, W. C., Steed, J. W. & Waddell, D. C. Mechanochemistry: opportunities for new and cleaner synthesis. *Chem. Soc. Rev.* **41,** 413–447 (1 2012).
4. Kaupp, G. Solid-state molecular syntheses: complete reactions without auxiliaries based on the new solid-state mechanism. *CrystEngComm* **5,** 117–133 (23 2003).
5. Kaupp, G., Schmeyers, J. & Hangen, U. D. Anisotropic molecular movements in organic crystals by mechanical stress. *Journal of Physical Organic Chemistry* **15,** 307–313.
6. Kaupp, G. Waste-free large-scale syntheses without auxiliaries for sustainable production omitting purifying workup. *CrystEngComm* **8,** 794–804 (11 2006).
7. Friščić, T. & Jones, W. Recent Advances in Understanding the Mechanism of Cocrystal Formation via Grinding. *Crystal Growth & Design* **9,** 1621–1637 (2009).
8. Tan, D., Loots, L. & Friščić, T. Towards medicinal mechano chemistry: evolution of milling from pharmaceutical solid form screening to the synthesis of active pharmaceutical ingredients (APIs). *Chemical Communications* **52,** 7760–7781 (50 2016).
9. Andersen, J. & Mack, J. Mechanochemistry and organic synthesis: from mystical to practical. *Green Chemistry* **20,** 1435–1443 (7 2018).

10. Delogu, F. & Cocco, G. Weakness of the "hot spots" approach to the kinetics of mechanically induced phase transformations. *Journal of Alloys and Compounds* **465,** 540–546 (2008).

11. Jones, W. & Eddleston, M. D. Introductory Lecture: Mechanochemistry, a versatile synthesis strategy for new materials. *Faraday Discussions* **170,** 9–34 (2014).

12. Colombo, I., Grassi, G. & Grassi, M. Drug Mechanochemical Activation. *Journal of Pharmaceutical Sciences* **98,** 3961–3986 (2009).

13. Kanaujia, P., Poovizhi, P., Ng, W. K. & Tan, R. B. H. Amorphous formulations for dissolution and bioavailability enhancement of poorly soluble APIs. *Powder Technology* **285.** Pharmaceutical Particle Technology, 2–15 (2015).

14. Descamps, M., Willart, J., Dudognon, E. & Caron, V. Transformation of pharmaceutical compounds upon milling and comilling: The role of Tg. *Journal of Pharmaceutical Sciences* **96,** 1398–1407.

15. Hsia, D. C., Kim, C.-K. & Kildsig, D. O. Determination of Energy Change Associated with Dissolution of a Solid. *Journal of Pharmaceutical Sciences* **66,** 961–965 (1977).

16. Hasa, D., Miniussi, E. & Jones, W. Mechanochemical Synthesis of Multicomponent Crystals: One Liquid for One Polymorph? A Myth to Dispel. *Crystal Growth & Design* **16,** 4582–4588 (2016).

17. Margetic, D. & Štrukil, V. *Mechanochemical Organic Synthesis* (Elsevier Science, 2016).

18. `https://www.micronanotools.com/products/planetary-ball-mill-4x100ml-two-year-warranty-vacuum-and-inert-gas-grinding-compatible`.

19. `https://www.retsch.com`.

20. Friščić, T., Halasz, I., Beldon, P. J., Belenguer, A. M., Adams, F., Kimber, S. A. J., V., H. & Dinnebier, R. E. Real-time and in situ monitoring of mechanochemical milling reactions. *Nature Chemistry* **5,** 66–73 (2013).

21. Do, J. L. & Friščić, T. Mechanochemistry: A Force of Synthesis. *ACS Central Science* **3,** 13–19 (2017).

22. Užarević, K., Halasz, I. & Friščić, T. Real-Time and In Situ Monitoring of Mechanochemical Reactions: A New Playground for All Chemists. *The Journal of Physical Chemistry Letters* **6,** 4129–4140 (2015).

23. Suryanarayana, C. Mechanical alloying and milling. *Progress in Materials Science* **46,** 1–184 (2001).

24. Shinozaki, M. & Senna, M. Effects of number and size of milling balls on the mechanochemical activation of fine crystalline solids. *Industrial & Engineering Chemistry Fundamentals* **20,** 59–62 (1981).

25. Chieng, N., Zujovic, Z., Bowmaker, G., Rades, T. & Saville, D. Effect of milling conditions on the solid-state conversion of ranitidine hydrochloride form 1. *International Journal of Pharmaceutics* **327,** 36–44. ISSN: 0378-5173 (2006).

26. Cioli, D., Pica-Mattoccia, L., Basso, A. & Guidi, A. Schistosomiasis control: praziquantel forever? *Molecular and Biochemical Parasitology* **195,** 23–29 (2014).

27. Vale, N., Gouveia, M. J., Rinaldi, G., Brindley, P. J., Gärtner, F. & Correia da Costa, J. M. Praziquantel for Schistosomiasis: Single-Drug Metabolism Revisited, Mode of Action, and Resistance. *Antimicrobial Agents and Chemotherapy* **61** (2017).

28. Mutapi, F., Maizels, R., Fenwick, A. & Woolhouse, M. Human schistosomiasis in the post mass drug administration era. *The Lancet infectious Diseases* **17,** PE42–E48 (2 2017).

29. `http://www.who.int/neglected_diseases/news/Egypt_leverages_domestic_funding_to_eliminate_schistosomiasis/en/`.

30. Gryseels, B., Polman, K., Clerinx, J. & Kestens, L. Human schistosomiasis. *The Lancet* **368,** 1106–1118 (2006).

31. Cioli, D., Pica-Mattoccia, L. & Archer, S. Antischistosomal drugs: Past, present and future? *Pharmacology & Therapeutics* **68,** 35–85 (1995).

32. *European Pharmacopoeia, 7th edition* ().

33. El-Subbagh, H. I. & Al-Badr, A. A. in *Analytical Profiles of Drug Substances and Excipients* (ed Brittain, H. G.) 463–500 (Academic Press, 1998).

34. Dömling, A. & Khoury, K. Praziquantel and Schistosomiasis. *Chem Med Chem* **5,** 1420–1434 (2010).

35. Andrews, P., Thomas, H., Pohlke, R. & Seubert, J. Praziquantel. *Medicinal Research Reviews* **3,** 147–200 (1983).

36. Da Silva, V. B. R., Campos, B. R. K. L., de Oliveira, J. F., Decout, J. L. & do Carmo Alves de Lima, M. Medicinal chemistry of antischistosomal drugs: Praziquantel and oxamniquine. *Bioorganic and Medicinal Chemistry* **25,** 3259–3277 (2017).

37. Groom, C. R., Bruno, I. J., Lightfoot, M. P. & Ward, S. C. The Cambridge Structural Database. *Acta Crystallographica Section B* **72,** 171–179 (2016).

38. Espinosa-Lara, J. C., Guzman-Villanueva, D., I., A.-G. J., Herrera-Ruiz, D., Rivera-Islas, J., Román-Bravo, P., Morales-Rojas, H. & Höpfl, H. Cocrystals of Active Pharmaceutical Ingredients-Praziquantel in Combination with Oxalic, Malonic, Succinic, Maleic, Fumaric, Glutaric, Adipic, And Pimelic Acids. *Crystal Growth & Design* **13,** 169–185 (2013).

39. Liu, Y., Wang, X., Wang, J. K. & Ching, C. B. Investigation of the phase diagrams of chiral praziquantel. *Chirality* **18,** 259–264.

40. El-Arini, S. K., Giron, D. & Leuenberger, H. Solubility Properties of Racemic Praziquantel and Its Enantiomers. *Pharmaceutical Development and Technology* **3,** 557–564 (1998).

41. Lim, B. G., Ching, C. B., Tan, R. B. H. & Ng, S. C. Recovery of (-)-praziquantel from racemic mixtures by continuous chromatography and crystallisation. *Chemical Engineering Science* **50,** 2289–2298 (1995).

42. Liu, Y., Wang, X., Wang, J. K. & Ching, C. B. Structural characterization and enantioseparation of the chiral compound praziquantel. *Journal of Pharmaceutical Sciences* **93,** 3039–3046 (2004).

43. Lim, B. G. & Ching, C. B. Characterization of Chiral Adsorbents on the Chromatographic Separation of Praziquantel Enantiomers. *Industrial and Engineering Chemistry Research* **35,** 169–175 (1996).

44. Woelfle, M., Seerden, J. P., de Gooijer, J., Pouwer, K., Olliaro, P. & Todd, M. H. Resolution of Praziquantel. *Plos-Neglected tropical diseases* **5,** 1260 (2011).

45. Sánchez-Guadarrama, O., Mendoza-Navarro, F., Cedillo-Cruz, A., Jung-Cook, H., Arenas-García, J. I., Delgado-Díaz, A., Herrera-Ruiz, D., Morales-Rojas, H. & Höpfl, H. Chiral Resolution of RS-Praziquantel via Diastereomeric Co-Crystal Pair Formation with l-Malic Acid. *Crystal Growth & Design* **16,** 307–314 (2016).

46. `https://www.pediatricpraziquantelconsortium.org/`.

47. Meister, I., Ingram-Sieber, K., Cowan, N., Todd, M., Robertson, M. N., Meli, C., Patra, M., Gasser, G. & Keiser, J. Activity of praziquantel enantiomers and main metabolites against Schistosoma mansoni. *Antimicrobial Agents and Chemotherapy* **58,** 5466–5472 (2014).

48. Meyer, T., Sekljic, H., Fuchs, S., Bothe, H., Schollmeyer, D. & Miculka, C. Taste, a new incentive to switch to (R)-Praziquantel in schistosomiasis treatment. *Plos-Neglected tropical diseases* **3,** 357 (2009).

49. Doenhoff, M. J., Cioli, D. & Utzinger, J. Praziquantel: mechanism of action, resistance ad new derivatives for Schistosomiasis. *Current Opinion in Infectious Diseases* **21,** 659–667 (2008).

50. Botros, S., Pica-Mattoccia, L., William, S., El-Lakkani, N. & D., C. Effect of praziquantel on the immature stages of Schistosoma haematobium. *International Journal for Parasitology* **35,** 1453–1457 (2005).

51. Coulibaly, J., Panic, G., Silue, K., Kovac, J., Hattendorf, J. & Keiser, J. Efficacy and safety of praziquantel in preschool-aged and school-aged children infected with Schistosoma mansoni: a randomised controlled, parallel-group, dose-ranging, phase 2 trial. *Lancet Global Health* **5,** 688–698 (2017).

52. Botros, S., El-Lakkany, N., Seif el-Din, S. H., Sabra, A. N. & Ibrahim, M. Comparative efficacy and bioavailability of different praziquantel brands. *Experimental Parasitology* **127,** 515–521 (2011).

53. Fallon, P. G., Sturrock, R. F., Capron, A., Niang, M. & Doenhoff, M. J. Short Report: Diminished Susceptibility to Praziquantel in a Senegal Isolate of Schistosoma mansoni. *The American Journal of Tropical Medicine and Hygiene* **53,** 61–62 (1995).

54. Ismail, M., Metwally, A., Farghaly, A., Bruce, J., Tao, L.-F. & Bennett, J. L. Characterization of Isolates of Schistosoma mansoni from Egyptian Villagers that Tolerate High Doses of Praziquantel. *The American Journal of Tropical Medicine and Hygiene* **55,** 214–218 (1996).

55. Fallon, P. G. & Doenhoff, M. J. Drug-Resistant Schistosomiasis: Resistance to Praziquantel and Oxamniquine Induced in Schistosoma Mansoni in Mice is Drug Specific. *The American Journal of Tropical Medicine and Hygiene* **51,** 83–88 (1994).

56. Cupit, P. M. & Cunningham, C. What is the mechanism of action of praziquantel and how might resistance strike? *Future Medicinal Chemistry* **7,** 701–705 (2015).

57. Aragon, A. D., Imani, R. A., Blackburn, V. R., Cupit, P. M., Melman, S. D., Goronga, T., Webb, T., Loker, E. S. & Cunningham, C. Towards an understanding of the mechanism of action of praziquantel. *Molecular and biochemical parasitology* **164,** 57–65 (Mar. 2009).

58. Olliaro, P., Delgado-Romero, P. & Keiser, J. The little we know about the pharmacokinetics and pharmacodynamics of praziquantel (racemate and R-enantiomer). *Journal of Antimicrobial Chemotherapy* **69,** 863–870 (2014).

59. Mandour, M. E., el Turabi, H., Homeida, M. M. A., el Sadig, T., Ali, H. M. M., Bennett, J. L., Leahey, W. J. & Harron, D. W. G. Pharmacokinetics of praziquantel in healthy volunteers and patients with schistosomiasis. *Transactions of the Royal Society of Tropical Medicine and Hygiene* **84 3,** 389–93 (1990).

60. Zhang, D., Wang, H., Ji, J., Nie, L. & Sun, D. A quantification method for determination of racemate praziquantel and R-enantiomer in rat plasma for comparison of their pharmacokinetics. *Journal of Chromatography B* **1048,** 64–69 (2017).

61. Watt, G., White, N. J., Padre, L., Ritter, W., Fernando, M. T. & Ranoa, C. P. Praziquantel Pharmacokinetics and Side Effects in Schistosoma japonicum-Infected Patients with Liver Disease. *The Journal of Infectious Diseases* **157,** 530–535 (1988).

62. Dayan, A. Albendazole, mebendazole and praziquantel. Review of non-clinical toxicity and pharmacokinetics. *Acta Tropica* **86,** 141–159 (2003).

63. Cioli, D. & Pica-Matoccia, L. Praziquantel. *Parasitology Research* **90,** S3–S9 (2003).

64. McManus, D., Dunne, D., Sacko, M., Utzinger, J., Vennervald, B. & Zhou, X.-N. Schistosomiasis. *Nature Reviews Disease Primers,* 4–13 (2018).

65. El-Lakkany, N., Seif el-Din, S. H. & Heikal, L. Bioavailability and in vivo efficacy of a praziquantel-polyvinylpyrrolidone solid dispersion in Schistosoma mansoni-infected mice. *European Journal of Drug Metabolism and Pharmacokinetics* **37,** 289–299 (Dec. 2012).

66. El-Arini, S. K. & Leuenberger, H. Dissolution properties of praziquantel-PVP systems. *Pharmaceutica Acta Helvetiae* **73,** 89–94 (1998).

67. Chaud, M. V., Lima, A. C., Vila, M. M. D. C., Paganelli, M. O., Paula, F. C., Pedreiro, L. N. & Gremiao, M. P. D. Development and evaluation of praziquantel solid dispersions in sodium starch glycolate. *Tropical Journal of Pharmaceutical Research* **12,** 163–168 (2013).

68. Marques, C. S. F., Rezende, P., Andrade, L. N., Mendes, T. M. F., Allegretti, S. M., Bani, C., Chaud, M. V., de Almeida, M. B., Souto, E. B., da Costa, L. P. & Severino, P. Solid dispersion of praziquantel enhanced solubility and improve the efficacy of the schistosomiasis treatment. *Journal of Drug Delivery Science and Technology* **45,** 124–134 (2018).

69. Trastullo, R., Dolci, L. S., Passerini, N. & Albertini, B. Development of flexible and dispersible oral formulations containing praziquantel for potential schistosomiasis treatment of pre-school age children. *International Journal of Pharmaceutics* **495,** 536–550 (2015).

70. De La Torre, P., Torrado, S. & Torrado, S. Preparation, Dissolution and Characterization of Praziquantel Solid Dispersions. *Chemical and Pharamceutical Bulletin* **47,** 1629–1633 (1999).

71. Costa, E. D., Priotti, J., Orlandi, S., Leonardi, D., Lamas, M. C., Nunes, T. G., Diogo, H. P., Salomon, C. J. & Ferreira, M. J. Unexpected solvent impact in the crystallinity of praziquantel/poly(vinylpyrrolidone) formulations. A solubility, DSC and solid-state NMR study. *International Journal of Pharmaceutics* **511,** 983–993 (2016).

72. Becket, G., Schep, L. J. & Tan, M. Y. Improvement of the in vitro dissolution of praziquantel by complexation with α-, β- and γ- cyclodextrins. *International Journal of Pharmaceutics* **179,** 65–71 (1999).

73. Rodrigues, S. G., Chaves, I. d. S., de Melo, N. F. S., de Jesus, M. B., Fraceto, L. F., Fernandes, S. A., de Paula, E., de Freitas, M. P. & Pinto, L. D. A. Computational analysis and physico-chemical characterization of an inclusion compound between praziquantel and methylβ -cyclodextrin for use as an alternative in the treatment of schistosomiasis. *Journal of Inclusion Phenomena and Macrocyclic Chemistry* **70,** 19–28 (2011).

74. De Oliveira, C. X., Ferreira, N. S. & Mota, G. V. S. A DFT study of infrared spectra and Monte Carlo predictions of the solvation shell of Praziquantel and β -cyclodextrin inclusion complex in liquid water. *Spectrochimica Acta Part A: Molecular and Biomolecular Spectroscopy* **153,** 102–107 (2016).

75. Arrúa, E. C., Ferreira, M. J. G., Salomon, C. J. & Nunes, T. G. Elucidating the guest-host interactions and complex formation of praziquantel and cyclodextrin derivatives by (13C) and (15N) solid-state NMR spectroscopy. *International Journal of Pharmaceutics* **496,** 812–821 (2015).

76. Mainardes, R. M., Gremiao, M. P. D. & Evangelista, R. C. Thermoanalytical study of praziquantel-loaded PLGA nanoparticles. *Revista Brasileira de Ciências Farmacêuticas* **42,** 523–530 (Dec. 2006).

77. Xie, S., Pan, B., Wang, M., Zhu, L., Wang, F., Dong, Z., Wang, X. & Zhou, W. Formulation, characterization and pharmacokinetics of praziquantel loaded hydrogenated castor oil solid lipid nanoparticles. *Nanomedicine* **5,** 693–701 (2010).

78. Yang, L., Geng, Y., Li, H., Zhang, Y., You, J. & Chang, Y. "Enhancement the oral bioavailability of praziquantel by incorporation into solid lipid nanoparticles". *Pharmazie* **64,** 86–89 (2009).

79. Amara, R. O., Ramadan, A. A., El-Moslemany, R. M., Eissa, M. M., El-Azzouni, M. Z. & El-Khordagui, L. K. *Praziquantel-lipid nanocapsules: an oral nanotherapeutic with potential Schistosoma mansoni tegumental targeting* in *International journal of nanomedicine* **13** (2018), 4493–4505.

80. Malhado, M., Pinto, D. P., Silva, A. C., Silveira, G. P., Pereira, H. M., Santos, J. G., Guilarducci-Ferraz, C. V., Viçosa, A. L., Nele, M., Fonseca, L. B., Pinto, J. C. C. & Calil-Elias, S. Preclinical pharmacokinetic evaluation of praziquantel loaded in poly (methyl methacrylate) nanoparticle using a HPLC-MS/MS. *Journal of Pharmaceutical and Biomedical Analysis* **117,** 405–412 (2016).

81. Cong, Z., Shi, Y., Peng, X., Wei, B., Wang, Y., Li, J., Li, J. & Li, J. Design and optimization of thermosensitive nanoemulsion hydrogel for sustained-release of praziquantel. *Drug Development and Industrial Pharmacy* **43,** 558–573 (2017).

82. Frezza, T. F., Gremiao, M. P. D., Zanotti-Magalhães, E. M., Magalhães, L. A., de Souza, A. L. R. & Allegretti, S. M. Liposomal-praziquantel: Efficacy against Schistosoma mansoni in a preclinical assay. *Acta Tropica* **128,** 70–75 (2013).

83. Cugovčan, M., Jablan, J., Lovrić, J., Cinčić, D., Galić, N. & Jug, M. Biopharmaceutical characterization of praziquantel cocrystals and cyclodextrin complexes prepared by grinding. *Journal of Pharmaceutical and Biomedical Analysis* **137,** 42–53 (2017).

84. Liu, H., Taylor, L. S. & Edgar, K. J. The role of polymers in oral bioavailability enhancement; a review. *Polymer* **77,** 399–415 (2015).

85. Baghel, S., H., C. & O'Reilly, N. O. Polymeric Amorphous Solid Dispersions: A Review of Amorphization, Crystallization, Stabilization, Solid-State Characterization, and Aqueous Solubilization of Biopharmaceutical Classification System Class II Drugs. *Journal of Pharmaceutical Sciences* **105,** 2527–2544 (2016).

86. Karagedov, G. & Lyakhov, N. Mechanochemical Grinding of Inorganic Oxides. *KONA Powder and Particle Journal* **21,** 76–87 (2003).

87. Lewis, G., Mathieu, D. & Phan-tan-luu, R. *Pharmaceutial Experimental Design* (CRC PRess, Dekker, New York, 1998).

88. Cela, R., Claeys-Bruno, M. & Phan-tan-luu, R. in *Comprehensive chemometrics* (eds D., B. S., R., T. & B., W.) 251–300 (Elsevier B. V., Amsterdam, The Netherlands, 2009).

89. Lundstedt, T., Seifert, E., Abramo, L., Thelin, B., Nyström, A., Pettersen, J. & Bergman, R. Experimental design and optimization. *Chemometrics and Intelligent Laboratory Systems* **42,** 3–40 (1998).

90. Mathieu, D., Nony, J. & Phan-Tan-Luu, R. NEMRODW (New Efficient Technology for Research using Optimal Desing) (ed Marseille:LPRAI) (2011).

91. Sun, Y. & Bu, S. J. Simple, cheap and effective high-performance liquid chromatographic method for determination of praziquantel in bovine muscle. *Journal of Chromatography B* **899,** 160–162 (2012).

92. Moutasim, S. I., Elfatih, K. I. A., Kamal, I. E. E., Babiker, A. M., Ahmed, S. E. M. & Ahmed, H. E. M. E. Photo-thermal stability of praziquantel. *Saudi Pharmaceutical Journal* **12,** 157 (2004).

93. Blagden, N., de Matas, M., Gavan, P. T. & York, P. Crystal engineering of active pharmaceutical ingredients to improve solubility and dissolution rates. *Advanced drug delivery reviews* **59,** 617–630 (July 2007).

94. Kaminska, E., Adrjanowicz, K., Kaminski, K., Wlodarczyk, P., Hawelek, L., Kolodziejczyk, K., Tarnacka, M., Zakowiecki, D., Kaczmarczyk-Sedlak, I., Pilch, J. & Paluch, M. A New Way of Stabilization of Furosemide upon Cryogenic Grinding by Using Acylated Saccharides Matrices. The Role of Hydrogen Bonds in Decomposition Mechanism. *Molecular Pharmaceutics* **10.** Pharmaceutical Particle Technology, 1824–1835 (5 2013).

95. Belenguer, A. M., Lampronti, G. I., Cruz-Cabeza, A. J., Hunter, C. A. & Sanders, J. K. M. Solvation and surface effects on polymorph stabilities at the nanoscale. *Chemical Science* **7,** 6617–6627 (11 2016).

96. Adrjanowicz, K., Kaminski, K., Grzybowska, K., Hawelek, L., Paluch, M., Gruszka, I., Zakowiecki, D., Sawicki, W., Lepek, P., Kamysz, W. & Guzik, L. Effect of Cryogrinding on Chemical Stability of the Sparingly Water-Soluble Drug Furosemide. *Pharmaceutical Research* **28,** 3220–3236 (2011).

97. Hashem, H., Ibrahim, A. E. & Elhenawee, M. A rapid stability indicating LC-method for determination of praziquantel in presence of its pharmacopoeial impurities. *Arabian Journal of Chemistry* **10,** S35–S41 (2017).

98. Čizmić, M., Ljubas, D., Ćurković, L., Škorić, I. & Babić, S. Kinetics and degradation pathways of photolytic and photocatalytic oxidation of the anthelmintic drug praziquantel. *Journal of Hazardous Materials* **323,** 500–512 (2017).

99. Shakhtshneider, T. Phase transformations and stabilization of metastable states of molecular crystals under mechanical activation. *Solid State Ionics* **101-103.** International Symposium on the Reactivity of Solids, 851–856 (1997).

100. Balasubramaniam, J., Rajesh, Y., Bindu, K., Tangi, H., Maroju, S. & Rao, V. U. Enhanced Dissolution and Bioavailability of Raloxifene Hydrochloride by Co-grinding with Different Superdisintegrants. *Chemical and Pharmaceutical Bulletin* **58,** 293–300 (2010).

101. Voinovich, D., Perissutti, B., Magarotto, L., Ceschia, D., Guiotto, P. & A.Bilia, R. Solid state mechanochemical simultaneous activation of the constituents of the Silybum marianum phytocomplex with crosslinked polymers. *Journal of Pharmaceutical Sciences* **98,** 215–228 (2009).

102. Hasa, D., D., V., B., P., A., B., M., G., E., F., S., D., M., S., J., P. & Invernizzi, S. Multidisciplinary approach on characterizing a mechanochemically activated composite of vinpocetine and crospovidone. *Journal of Pharmaceutical Sciences* **100,** 915–932 (2011).

103. Hasaand, D., Perissutti, B., Grassi, M., Chierotti, M., Gobetto, R., Ferrario, V., Lenaz, D. & Voinovich, D. Mechanochemical activation of vincamine mediated by linear polymers: Assessment of some "critical" steps. *European Journal of Pharmaceutical Sciences* **50,** 56–68 (2013).

104. Willart, J. F. & Descamps, M. Solid state amorphization of pharmaceuticals. *Molecular Pharmaceutics* **5,** 905–920 (2008).

105. Willart, J. F. & Descamps, M. Solid State Amorphization of Pharmaceuticals. *Molecular Pharmaceutics* **5,** 905–920 (2008).

106. Moneghini, M., Carcano, A., Zingone, G. & Perissutti, B. Studies in dissolution enhancement of atenolol. Part I. *International Journal of Pharmaceutics* **175,** 177–183 (1998).

107. Hasa, D., Voinovich, D., Perissutti, B., Grassi, G., Fiorentino, S., Farra, R., Abrami, M., Colombo, I. & Grassi, M. Reduction of melting temperature and enthalpy of drug crystals: Theoretical aspects. *European Journal of Pharmaceutical Sciences* **50,** 17–28 (2013).

108. Crowley K. J. and, Z. G. Cryogenic grinding of indomethacin polymorphs and solvates: Assessment of amorphous phase formation and amorphous phase physical stability. *Journal of Pharmaceutical Sciences* **91,** 492–507 (2008).

109. Otte, A. & Carvajal, M. T. Assessment of Milling-Induced Disorder of Two Pharmaceutical Compounds. *Journal of Pharmaceutical Sciences* **100,** 1793–1804 (2011).

110. Irwin, W. & Iqbal, M. Solid-state stability: the effect of grinding solvated excipients. *International Journal of Pharmaceutics* **75,** 211–218 (1991).

111. Suleiman, M. I., Karim, E. I. A., Ibraim, K. E. E., Ahme, B. M., Saeed, A. E. M. & Hamid, A. E. M. E. Photo-thermal stability of praziquantel. *Saudi Pharmaceutical Journal* **12,** 157–162 (2004).

112. Joshi, M., Tiwari, R. & Tiwari, G. Design and development of bilayer tablet for immediate and extended release of acarbose and metformin HCl. *Drug Development and Therapeutics* **5,** 93–108 (2014).

113. `https://pharmaceutical.basf.com/en/Drug-Formulation/Kollidon-CL-M.html`.

114. Ye, J. & Schoenung, J. Technical Cost Modeling for the Mechanical Milling at Cryogenic Temperature (Cryomilling). *Advanced Engineering Materials* **6,** 656–664.

115. Qi, S., Marchaud, D. & Craig, D. Q. M. An investigation into the mechanism of dissolution rate enhancement of poorly water-soluble drugs from spray chilled gelucire 50/13 microspheres. *Journal of Pharmaceutical Sciences* **99,** 262–274 (2010).

116. Otsuka, M., Matsumoto, T. & Kaneniwa, N. Effect of Environmental Temperature on Polymorphic Solid-State Transformation of Indomethacin during Grinding. *Chemical and Pharmaceutical Bulletin* **34,** 1784–1793 (1986).

117. Shakhtshneider, T. P., Danède, F., Capet, F., Willart, J. F., Descamps, M., Paccou, L., Surov, E. V., Boldyreva, E. V. & Boldyrev, V. V. Grinding of drugs with pharmaceutical excipients at cryogenic temperatures, Part II: Cryogenic grinding of indomethacin-polyvinylpyrrolidone mixtures. *Journal of Thermal Analysis and Calorimetry* **89,** 709–715 (Sept. 2007).

118. Oguchi, T., Kazama, K., Yonemochi, E., Churimaworapan, S., Choi, W. S., Limmatvapirat, S. & Yamamoto, K. Specific complexation of ursodeoxycholic acid with guest compounds induced by co-grinding. *Physical Chemistry Chemical Physics* **2,** 2815–2820 (12 2000).

119. Guinet, Y., Paccou, L., Danède, F., Willart, J. F., Derollez, P. & Hèdoux, A. Comparison of amorphous states prepared by melt-quenching and cryomilling polymorphs of carbamazepine. *International Journal of Pharmaceutics* **509,** 305–313. ISSN: 0378-5173 (2016).

120. Niwa, T., Nakanishi, Y. & Danjo, K. One-step preparation of pharmaceutical nanocrystals using ultra cryo-milling technique in liquid nitrogen. *European Journal of Pharmaceutical Sciences* **41,** 78–85 (2010).

121. Shakhtshneider, T. P., Danède, F., Capet, F., Willart, J. F., Descamps, M., Myz, S. A., Boldyreva, E. V. & Boldyrev, V. V. Grinding of drugs with pharmaceutical excipients at cryogenic temperatures, Part I: Cryogenic grinding of piroxicam-polyvinylpyrrolidone mixtures. *Journal of Thermal Analysis and Calorimetry* **89,** 699–707 (Sept. 2007).

122. Kang, K., Lee, J., Choi, J. N., Mao, C. & Lee, E. H. Cryomilling-induced solid dispersion of poor glass forming/poorly water-soluble mefenamic acid with polyvinylpyrrolidone K12. *Drug Development and Industrial Pharmacy* **41,** 978–988 (2015).

123. Adrjanowicz, K., Kaminski, K., Grzybowska, K., Hawelek, L., Paluch, M., Gruszka, I., Zakowiecki, D., Sawicki, W., Lepek, P., Kamysz, W. & Guzik, L. Effect of Cryogrinding on Chemical Stability of the Sparingly Water-Soluble Drug Furosemide. *Pharmaceutical Research* **28,** 3220–3236 (Dec. 2011).

124. *JMP* version 4.1. Cary, North Carolina: SAS Institute Inc., 2007.

125. Hüttenrauch, R., Fricke, S. & Zielke, P. Mechanical Activation of Pharmaceutical Systems. *Pharmaceutical Research* **2,** 302–306 (Nov. 1985).

126. Hasa, D., Perissutti, B., Cepek, C., Bhardwaj, S., Carlino, E., Grassi, M., Invernizzi, S. & Voinovich, D. Drug salt formation via mechanochemistry: The case study of vincamine. *Molecular Pharmaceutics* **10,** 211–224 (2013).

127. Hasa, D., Schneider, G., Voinovich, D. & Jones, W. Cocrystal Formation through Mechanochemistry: From Neat and Liquid-Assisted Grinding to Polymer-Assisted Grinding. *Angewandte Chemie-International Edition* **54,** 7371–7375 (2015).

128. Hasa, D., Carlino, E. & Jones, W. Polymer-Assisted Grinding, a Versatile Method for Polymorph Control of Cocrystallization. *Crystal Growth & Design* **16,** 1772–1779 (2016).

129. Trask, A. V., Shan, N., Motherwell, W. D. S., Jones, W., Feng, S., Tan, R. B. H. & Carpenter, K. J. Selective polymorph transformation via solvent-drop grinding. *Chem. Commun.* 880–882 (7 2005).

130. Fischer, F., Scholz, G., Benemann, S., Rademann, K. & Emmerling, F. Evaluation of the formation pathways of cocrystal polymorphs in liquid-assisted syntheses. *CrystEngComm* **16,** 8272–8278 (35 2014).

131. Trask, A. V., Motherwell, W. D. S. & Jones, W. Solvent-drop grinding: green polymorph control of cocrystallisation. *Chem. Commun.* 890–891 (7 2004).

132. Leung, S. S., Padden, B. E., Munson, E. J. & Grant, D. J. W. Solid-State Characterization of Two Polymorphs of Aspartame Hemihydrate. *Journal of Pharmaceutical Sciences* **87,** 501–507 (1998).

133. Lefebvre, C., Guyot-Hermann, A. M., Draguet-Brughmans, M., Bouché, R. & Guyot, J. C. Polymorphic Transitions of Carbamazepine During Grinding and Compression. *Drug Development and Industrial Pharmacy* **12,** 1913–1927 (1986).

134. Otsuka, M., Otsuka, K. & Kaneniwa, N. Relation Between Polymorphic Transformation Pathway During Grinding and the Physicochemical Properties of Bulk Powders for Pharmaceutical Preparations. *Drug Development and Industrial Pharmacy* **20,** 1649–1660 (1994).

135. Kaneniwa, N. & OTSUKA, M. Effect of Grinding on the Transformations of Polymorphs of Chloramphenicol Palmitate. *Chemical & Pharmaceutical Bulletin* **33,** 1660–1668 (1985).

136. Madusanka, N., Eddleston, M. D., Arhangelskis, M. & Jones, W. Polymorphs, hydrates and solvates of a co-crystal of caffeine with anthranilic acid. *Acta Crystallographica Section B* **70,** 72–80 (Feb. 2014).

137. Lausi, A., Polentarutti, M., Onesti, S., Plaisier, J. R., Busetto, E., Bais, G., Barba, L., Cassetta, A., Campi, G., Lamba, D., Pifferi, A., Mande, S. C., Sarma, D. D., Sharma, S. M. & Paolucci, G. Status of the crystallography beamlines at Elettra. *The European Physical Journal Plus* **130,** 43 (Mar. 2015).

138. Hammersley, A. P., Svensson, S. O., Hanfland, M., Fitch, A. N. & Hausermann, D. Two-dimensional detector software: From real detector to idealised image or two-theta scan. *High Pressure Research* **14,** 235–248 (1996).

139. Xiao, S. H., Keiser, J., Chollet, J., Utzinger, J., Dong, Y., Endriss, Y., Vennerstrom, J. L. & Tanner, M. In vitro and in vivo activities of synthetic trioxolanes against major human Schistosome species. *Antimicrobial Agents and Chemotherapy* **51,** 1440–1445 (2007).

140. Cedillo-Cruz, A., Aguilar, M. I., Flores-Alamo, M., Palomares-Alonso, F. & Jung-Cook, H. A straightforward and efficient synthesis of praziquantel enantiomers and their 4-hydroxy derivatives. *Tetrahedron: Asymmetry* **25,** 133–140 (2014).

141. Shakhtshneider, T. Phase transformations and stabilization of metastable states of molecular crystals under mechanical activation. *Solid State Ionics* **101-103,** 851–856 (1997).

142. Altomare, A., Cuocci, C., Giacovazzo, C., Moliterni, A., Rizzi, R., Corriero, N. & Falcicchio, A. *EXPO2013*: a kit of tools for phasing crystal structures from powder data. *Journal of Applied Crystallography* **46,** 1231–1235 (Aug. 2013).

143. A.A. Coelho. *TOPAS-Academic* version 4.1. Brisbane, Australia: Coehlo Software, 2007.

144. Spek, A. L. Structure validation in chemical crystallography. *Acta Crystallographica Section D* **65,** 148–155 (Feb. 2009).

145. Passerini, N., Albertini, B., Perissutti, B. & Rodriguez, L. Evaluation of melt granulation and ultrasonic spray congealing as techniques to enhance the dissolution of praziquantel. *International Journal of Pharmaceutics* **318,** 92–102 (2006).

146. Borrego-Sánchez, A., Viseras, C., Aguzzi, C. & Sainz-Díaz, C. I. Molecular and crystal structure of praziquantel. Spectroscopic properties and crystal polymorphism. *European Journal of Pharmaceutical Sciences* **92,** 266–275 (2016).

147. Borrego-Sánchez, A., Hernández-Laguna, A. & Sainz-Díaz, C. I. Molecular modeling and infrared and Raman spectroscopy of the crystal structure of the chiral antiparasitic drug Praziquantel. *Journal of Molecular Modeling* **23,** 106 (Mar. 2017).

148. Ferreira, S. L., dos Santos, W. N., Quintella, C. M., Neto, B. B. & Bosque-Sendra, J. M. Doehlert matrix: a chemometric tool for analytical chemistry-review. *Talanta* **63,** 1061–1067 (2004).

149. *Biltricide, data sheet* `https://www.accessdata.fda.gov/drugsatfda_docs/label/2014/018714s013lbl.pdf`.

150. Clark, S. J., Segall, M. D., Pickard, C. J., Hasnip, P. J., Probert, M. J., Refson, K. & Payne, M. C. First principles methods using CASTEP. *Zeitschrift für Kristallographie* **220.** Reproduced with permission from the publisher., 567–570 (2005).

151. Pickard, C. J. & Mauri, F. All-electron magnetic response with pseudopotentials: NMR chemical shifts. *Phys. Rev. B* **63,** 245101 (24 May 2001).

152. Perdew, J. P., Burke, K. & Ernzerhof, M. Generalized Gradient Approximation Made Simple. *Phys. Rev. Lett.* **77,** 3865–3868 (18 Oct. 1996).

153. McNellis, E. R., Meyer, J. & Reuter, K. Azobenzene at coinage metal surfaces: Role of dispersive van der Waals interactions. *Phys. Rev. B* **80,** 205414 (20 Nov. 2009).

154. Hasnip, P. J., Refson, K., Probert, M. I., Yates, J. R., Clark, S. J. & Pickard, C. J. Density functional theory in the solid state. *Philosophical transactions. Series A, Mathematical, physical, and engineering sciences* **372,** 20130270. (2014).

155. Björkman, T. CIF2Cell: Generating geometries for electronic structure programs. *Computer Physics Communications* **182,** 1183–1186 (2011).

156. Monkhorst, H. J. & Pack, J. D. Special points for Brillouin-zone integrations. *Phys. Rev. B* **13,** 5188–5192 (12 June 1976).

157. Harris, R. K., Hodgkinson, P., Pickard, C. J., Yates, J. R. & Zorin, V. Chemical shift computations on a crystallographic basis: some reflections and comments. *Magnetic Resonance in Chemistry* **45,** S174–S186.

158. Reddy, G. N. M., Huqi, A., Iuga, D., Sakurai, S., Marsh, A., Davis, J. T., Masiero, S. & Brown, S. P. Co-existence of Distinct Supramolecular Assemblies in Solution and in the Solid State. *Chemistry* **23,** 2315–2322 (2017).

159. Macrae, C. F., Edgington, P. R., McCabe, P., Pidcock, E., Shields, G. P., Taylor, R., Towler, M. & van de Streek, J. *Mercury*: visualization and analysis of crystal structures. *Journal of Applied Crystallography* **39,** 453–457 (June 2006).

160. Shan, N., Toda, F. & Jones, W. Mechanochemistry and co-crystal formation: effect of solvent on reaction kinetics. *Chem. Commun.* 2372–2373 (20 2002).

161. Friščić, T., Childs, S. L., Rizvi, S. A. A. & Jones, W. The role of solvent in mechanochemical and sonochemical cocrystal formation: a solubility-based approach for predicting cocrystallisation outcome. *CrystEngComm* **11,** 418–426 (3 2009).

162. Karki, S., Friščić, T., Jones, W. & Motherwell, W. D. S. Screening for Pharmaceutical Cocrystal Hydrates via Neat and Liquid-Assisted Grinding. *Molecular Pharmaceutics* **4,** 347–354 (2007).

163. Karki, S., Friščić, T. & Jones, W. Control and interconversion of cocrystal stoichiometry in grinding: stepwise mechanism for the formation of a hydrogen-bonded cocrystal. *CrystEngComm* **11,** 470–481 (3 2009).

164. Weyna, D. R., Shattock, T., Vishweshwar, P. & Zaworotko, M. J. Synthesis and Structural Characterization of Cocrystals and Pharmaceutical Cocrystals: Mechanochemistry vs Slow Evaporation from Solution. *Crystal Growth & Design* **9,** 1106–1123 (2009).

165. Healy, A. M., Worku, Z. A., Kumar, D. & Madi, A. M. Pharmaceutical solvates, hydrates and amorphous forms: A special emphasis on cocrystals. *Advanced Drug Delivery Reviews* **117,** 25–46 (2017).

166. Khankari, R. K. & Grant, D. J. W. Pharmaceutical hydrates. *Thermochimica Acta* **248.** Pharmaceuticals and Thermal Analysis, 61–79 (1995).

167. Franklin, S. J., Younis, U. S. & Myrdal, P. B. Estimating the Aqueous Solubility of Pharmaceutical Hydrates. *Journal of Pharmaceutical Sciences* **105,** 1914–1919 (2016).

168. Morris, K. R. in *Polymorphism in Pharmaceutical Solids* 125–181 (Marcel Dekker, 1999).

169. Tian, F., Qu, H., Zimmermann, A., Munk, T., Jørgensen, A. C. & Rantanen, J. Factors affecting crystallization of hydrates. *Journal of Pharmacy and Pharmacology* **62,** 1534–1546.

170. Allen, P. V., Rahn, P. D., Sarapu, A. C. & Vanderwielens, A. J. Physical Characterization of Erythromycin: Anhydrate, Monohydrate, and Dihydrate Crystalline Solids. *Journal of Pharmaceutical Sciences* **67,** 1087–1093 (1978).

171. Minkov, V. S., Beloborodova, A. A., Drebushchak, V. A. & Boldyreva, E. V. Furosemide Solvates: Can They Serve As Precursors to Different Polymorphs of Furosemide. *Crystal Growth & Design* **14,** 513–522 (2014).

172. Surov, O. V., Voronova, M. I., Smirnov, P. R., Mamardashvili, N. Z. & Shaposhnikov, G. P. Polymorphism of 4-tert-butylcalix[4]arene upon formation of n-hexane and acetonitrile complexes and thermal desolvation. *CrystEngComm* **14,** 533–536 (2 2012).

173. Rocco, W. L., Morphet, C. & Laughlin, S. M. Solid-state characterization of zanoterone. *International Journal of Pharmaceutics* **122,** 17–25 (1995).

174. Bhattacharya, S. & Saha, B. K. Polymorphism through Desolvation of the Solvates of a van der Waals Host. *Crystal Growth & Design* **13,** 606–613 (2013).

175. Braun, D. E., Gelbrich, T., Kahlenberg, V., Tessadri, R., Wieser, J. & Griesser, U. J. Stability of Solvates and Packing Systematics of Nine Crystal Forms of the Antipsychotic Drug Aripiprazole. *Crystal Growth & Design* **9,** 1054–1065 (2009).

176. Caira, M. R., Bettinetti, G. & Sorrenti, M. Structural relationships, thermal properties, and physicochemical characterization of anhydrous and solvated crystalline forms of tetroxoprim. *Crystal Growth & Design* **91,** 467–481 (2002).

177. Aulton, M. & Taylor, K. *Aulton's Pharmaceutics: The Design and Manufacture of Medicines* (Churchill Livingstone/Elsevier, 2013).

178. Rietveld, H. M. A profile refinement method for nuclear and magnetic structures. *Journal of Applied Crystallography* **2,** 65–71 (June 1969).

179. Grimme, S. Semiempirical GGA-type density functional constructed with a long-range dispersion correction. *Journal of Computational Chemistry* **27,** 1787–1799.

180. Yates, J. R., Pickard, C. J. & Mauri, F. Calculation of NMR chemical shifts for extended systems using ultrasoft pseudopotentials. *Phys. Rev. B* **76,** 024401 (2 July 2007).

181. Rosenholm, J. M. & Lindén, M. Towards establishing structure-activity relationships for mesoporous silica in drug delivery applications. *Journal of Controlled Release* **128,** 157–164. ISSN: 0168-3659 (2008).

182. Juère, E. & Kleitz, F. On the nanopore confinement of therapeutic drugs into mesoporous silica materials and its implications. *Microporous and Mesoporous Materials* **270,** 109–119 (2018).

183. Van Speybroeck, M., Barillaro, V., Do Thi, T., Mellaerts, R., Martens, J., Van Humbeeck, J., Vermant, J., Annaert, P., Van Den Mooter, G. & Augustijns, P. Ordered Mesoporous Silica Material SBA 15: A Broad-Spectrum Formulation Platform for Poorly Soluble Drugs. *Expert Opinion on Drug Delivery* **98,** 2648–2658 (2009).

184. Maleki, A., Kettiger, H., Schoubben, A., Rosenholm, J. M., Ambrogi, V. & Hamidi, M. Mesoporous silica materials: From physico-chemical properties to enhanced dissolution of poorly water-soluble drugs. *Journal of Controlled Release* **262,** 329–347 (2017).

185. Delle Piane, M., Corno, M. & Ugliengo, P. Does Dispersion Dominate over H-Bonds in Drug-Surface Interactions? The Case of Silica-Based Materials As Excipients and Drug-Delivery Agents. *Journal of Chemical Theory and Computation* **9,** 2404–2415 (2013).

186. Takeuchi, H., Nagira, S., Yamamoto, H. & Kawashima, Y. Solid dispersion particles of amorphous indomethacin with fine porous silica particles by using spray-drying method. *International Journal of Pharmaceutics* **293,** 155–164 (2005).

187. Shen, S. C., Ng, W. K., Chia, L., Dong, Y. C. & Tan, R. B. Stabilized Amorphous State of Ibuprofen by Co-Spray Drying With Mesoporous SBA 15 to Enhance Dissolution Properties. *Journal of Pharmaceutical Sciences* **99,** 1997–2007 (2010).

188. Mellaerts, R., Jammaer, J. A. G., Van Speybroeck, M., Chen, H., Humbeeck, J. V., Augustijns, P., Van den Mooter, G. & Martens, J. A. Physical State of Poorly Water Soluble Therapeutic Molecules Loaded into SBA-15 Ordered Mesoporous Silica Carriers: A Case Study with Itraconazole and Ibuprofen. *Langmuir* **24,** 8651–8659 (2008).

189. Hussain, T., Waters, L. J., Parkes, G. M. & Shahzad, Y. Microwave processed solid dispersions for enhanced dissolution of gemfibrozil using non-ordered mesoporous silica. *Colloids and Surfaces A: Physicochemical and Engineering Aspects* **520,** 428–435 (2017).

190. Limnell, T., Santos, H. A., Mäkilä, E., Heikkilä, T., Salonen, J., Murzin, D. Y., Kumar, N., Laaksonen, T., Peltonen, L. & Hirvonen, J. Drug Delivery Formulations of Ordered and Nonordered Mesoporous Silica: Comparison of Three Drug Loading Methods. *Journal of Pharmaceutical Sciences* **100,** 3294–3306 (2011).

191. Watanabe, T., Hasegawa, S., Wakiyama, N., Kusai, A. & Senna, M. Comparison between polyvinylpyrrolidone and silica nanoparticles as carriers for indomethacin in a solid state dispersion. *International Journal of Pharmaceutics* **250,** 283–286 (2003).

192. Bahl, D. & Bogner, R. H. Amorphization of Indomethacin by Co-Grinding with Neusilin US2: Amorphization Kinetics, Physical Stability and Mechanism. *Pharmaceutical Research* **23,** 2317–2325 (Oct. 2006).

193. McCarthy, C. A., Ahern, R. J., Dontireddy, R., Ryan, K. B. & Crean, A. M. Mesoporous silica formulation strategies for drug dissolution enhancement: a review. *Expert Opinion on Drug Delivery* **13,** 93–108 (2016).

194. Biswas, N. Modified mesoporous silica nanoparticles for enhancing oral bioavailability and antihypertensive activity of poorly water soluble valsartan. *European Journal of Pharmaceutical Sciences* **99,** 152–160 (2017).

195. Watanabe, T., Hasegawa, S., Wakiyama, N., Kusai, A. & Senna, M. Prediction of apparent equilibrium solubility of indomethacin compounded with silica by 13C solid state NMR. *International Journal of Pharmaceutics* **248,** 123–129 (2002).

196. Watanabe, T., Wakiyama, N., Usui, F., Ikeda, M., Isobe, T. & Senna, M. Stability of amorphous indomethacin compounded with silica. *International Journal of Pharmaceutics* **226,** 81–91 (2001).

197. Choi, K. M. & Kuroda, K. Polymorph Control of Calcium Carbonate on the Surface of Mesoporous Silica. *Crystal Growth & Design* **12,** 887–893 (2012).

198. Lu, J., Liong, M., Zink, J. I. & Tamanoi, F. Mesoporous Silica Nanoparticles as a Delivery System for Hydrophobic Anticancer Drugs. *Small* **3,** 1341–1346.

199. Koenig, W. A. in *Chirality in Natural and Applied Science* (eds Lough, W. J. & Wainer, I. W.) 261–284 (Blackwell Science Ltd, 2002).

200. Bellimghausen, R., Steinbeck, M., Zank, J., Weis, M., Behrend, O., Rudhardt, D., Ridder, F. & Stiphout, U. V. *Patent* US 7062320 (DE). `https://worldwide.espacenet.com/publicationDetails/biblio?DB=EPODOC&locale=en_EP&FT=D&date=20070628&CC=DE&NR=102005062270A1&KC=A1#`(2007).

201. Mattern, C. & Berger, A. *Patent* EP1362583 (A1). `https://worldwide.espacenet.com/publicationDetails/biblio?DB=EPODOC&locale=en_EP&FT=D&date=20031119&CC=EP&NR=1362583A1&KC=A1`(2003).

202. Damini, N. & Tsau, J. *Patent* EP0212641 (EU) (1987).

203. Shah, P. P. & Rajashree, C. M. Development and evaluation of artemether taste masked rapid disintegrating tablets with improved dissolution using solid dispersion technique. *AAPS PharmSciTech* **9,** 494–500 (2 2008).

204. Arafa, M. F., El-Gizawy, S. A., Osman, M. A. & El Maghraby, G. M. Sucralose as co-crystal co-former for hydrochlorothiazide: development of oral disintegrating tablets. *Drug Development and Industrial Pharmacy* **42,** 1225–1233 (2016).

205. Wang, L., Luo, M., Li, J., Wang, J., Zhang, H. & Deng, Z. Sweet Theophylline Cocrystal with Two Tautomers of Acesulfame. *Crystal Growth & Design* **15,** 2574–2578 (2015).

206. Hartel, R. W., Ergun, R. & Vogel, S. Phase/State Transitions of Confectionery Sweeteners: Thermodynamic and Kinetic Aspects. *Comprehensive Reviews in Food Science and Food Safety* **10,** 17–32.

207. Jeffery, M. S. Grained and Ungrained Confections, The Basics. *The Manufacturing Confectioner* **73,** 97–98 (2001).

208. *Sweeteners and Sugar Alternatives in Food Technology* (ed Kay O'Donnell, M. K.) (Wiley-Blackwell, Oxford, United Kingdom, 2012).

209. Chattopadhyay, S., Raychaudhuri, U. & Chakraborty, R. Artificial sweeteners-a review. *Journal of Food Science and Technology* **51,** 611–621 (2014).

210. Guguta, C., Meekes, H. & de Gelder, R. The hydration/dehydration behavior of aspartame revisited. *Journal of Pharmaceutical and Biomedical Analysis* **46,** 617–624 (2008).

211. Gordon, M. & Taylor, J. S. Ideal copolymers and the second-order transitions of synthetic rubbers. i. non-crystalline copolymers. *Journal of Applied Chemistry* **2,** 493–500.

212. Ergun, R., Lietha, R. & Hartel, R. W. Moisture and Shelf Life in Sugar Confections. *Critical Reviews in Food Science and Nutrition* **50,** 162–192 (2010).

213. Shirke, S., Takhistov, P. & Ludescher, R. D. Molecular Mobility in Amorphous Maltose and Maltitol from Phosphorescence of Erythrosin B. *The Journal of Physical Chemistry B* **109,** 16119–16126 (2005).

214. Yu, L., Mishra, D. S. & Rigsbee, D. R. Determination of the Glass Properties of D-Mannitol Using Sorbitol as an Impurity. *Journal of Pharmaceutical Sciences* **87,** 774–777 (1998).

215. Szüts, A. & Szabó-Révész, P. Sucrose esters as natural surfactants in drug delivery systems-A mini-review. *International Journal of Pharmaceutics* **433,** 1–9 (2012).

216. Yokoi, Y., Yonemochi, E. & Terada, K. Effects of sugar ester and hydroxypropyl methylcellulose on the physicochemical stability of amorphous cefditoren pivoxil in aqueous suspension. *International Journal of Pharmaceutics* **290,** 91–99 (2005).

217. Youan, B.-B. C., Hussain, A. & Nguyen, N. T. Evaluation of sucrose esters as alternative surfactants in microencapsulation of proteins by the solvent evaporation method. *AAPS PharmSci* **290,** 123–131 (2 2003).

218. Mollee, H., De Vrind, J. & De Vringer, T. Stable Reversed Vesicles in Oil: Characterization Studies and Encapsulation of Model Compounds. *Journal of Pharmaceutical Sciences* **89,** 930–939 (2000).

219. Thevenin, M., Grossiord, J. & Poelman, M. Sucrose esters/cosurfactant microemulsion systems for transdermal delivery: Assessment of bicontinuous structures. *International Journal of Pharmaceutics* **137,** 177–186 (1996).

220. Szüts, A., Makai, Z., Rajkó, R. & Szabó-Révész, P. Study of the effects of drugs on the structures of sucrose esters and the effects of solid-state interactions on drug release. *Journal of Pharmaceutical and Biomedical Analysis* **48,** 1136–1142 (2008).

221. Abd-Elbary, A., Tadros, M. I. & Alaa-Eldin, A. A. Sucrose Stearate-Enriched Lipid Matrix Tablets of Etodolac: Modulation of Drug Release, Diffusional Modeling and Structure Elucidation Studies. *AAPS PharmSciTech* **14,** 656–668 (June 2013).

222. Perumal, D., Dangor, C. M., Alcock, R. S., Hurbans, N. & Moopanar, K. R. Effect of formulation variables on in vitro drug release and micromeritic properties of modified release ibuprofen microspheres. *Journal of Microencapsulation* **16,** 475–487 (1999).

223. Otsuka, M., Ofusa, T. & Matsuda, Y. Dissolution improvement of water-insoluble glybuzole by co-grinding and co-melting with surfactants and their physicochemical properties. *Colloids and Surfaces B: Biointerfaces* **10,** 217–226 (1998).

224. Hayama, H., Mitarai, M., Mori, H., Verrett, J., Servio, P. & Ohmura, R. Surfactant Effects on Crystal Growth Dynamics and Crystal Morphology of Methane Hydrate Formed at Gas/Liquid Interface. *Crystal Growth & design* **16,** 6084–6088 (2016).

225. Okutani, K., Kuwabara, Y. & Mori, Y. H. Surfactant effects on hydrate formation in an unstirred gas/liquid system: An experimental study using methane and sodium alkyl sulfates. *Chemical Engineering Science* **63,** 183–194 (2008).

226. Watanabe, S., Saito, K. & Ohmura, R. Crystal Growth of Clathrate Hydrate in Liquid Water Saturated with a Simulated Natural Gas. *Crystal Growth & Design* **11,** 3235–3242 (2011).

227. Dixit, M., Kini, A. G. & Kulkarni, P. K. Preparation and characterization of microparticles of piroxicam by spray drying and spray chilling methods. *Research in pharmaceutical sciences* **5,** 89–97 (2010).

228. Cordeiro, P., Temtem, M. & Winters, C. Spray congealing: applications in the Pharmaceutical Industry. *Powder Technologies & processing* **31,** 69–72 (2013).

229. Yajima, T., Umeki, N. & Itai, S. Optimum spray congealing conditions for masking the bitter taste of clarithromycin in wax matrix. *Chemical and Pharmaceutical Bulletin - Tokyo* **47,** 220–225 (1999).

230. lo, J. B., Appel, L. E., Herbig, S. M., McCray, S. B. & Thombre, A. G. Formulation design and pharmaceutical development of a novel controlled release form of azithromycin for single-dose therapy. *Drug Development and Industrial Pharmacy* **35,** 1522–1529 (2009).

231. Curatolo, W. Interdisciplinary science and the design of a single-dose antibiotic therapy. *Pharmaceutical research* **28,** 2059–2071 (Sept. 2011).

232. Oh, C. M., Guo, Q., Heng, P. W. S. & Chan, L. W. Spray-congealed microparticles for drug delivery - an overview of factors influencing their production and characteristics. *Expert Opinion on Drug Delivery* **11,** 1047–1060 (2014).

233. Martins, R. M., Siqueira, S. & Freitas, L. A. P. Spray Congealing of Pharmaceuticals: Study on Production of Solid Dispersions Using Box-Behnken Design. *Drying Technology* **30,** 935–945 (2012).

234. Maschke, A., Becker, C., Eyrich, D., Kiermaier, J., Blunk, T. & Göpferich, A. Development of a spray congealing process for the preparation of insulin-loaded lipid microparticles and characterization thereof. *European Journal of Pharmaceutics and Biopharmaceutics* **65,** 175–187 (2007).

235. Passerini, N., Perissutti, B., Albertini, B., Voinovich, D., Moneghini, M. & Rodriguez, L. Controlled release of verapamil hydrochloride from waxy microparticles prepared by spray congealing. *Journal of Controlled Release* **88,** 263–275 (2003).

236. Albertini, B., Passerini, N., González-Rodríguez, M. L., Perissutti, B. & Rodriguez, L. Effect of Aerosil®on the properties of lipid controlled release microparticles. *Journal of Controlled Release* **100,** 233–246 (2004).

237. Passerini, N., Qi, S., Albertini, B., Grassi, M., Rodriguez, L. & Craig, D. Q. Solid lipid microparticles produced by spray congealing: Influence of the atomizer on microparticle characteristics and mathematical modeling of the drug release. *Journal of Pharmaceutical Sciences* **99,** 916–931 (2010).

238. Passerini, N., Perissutti, B., Albertini, B., Franceschinis, E., Lenaz, D., Hasa, D., Locatelli, I. & Voinovich, D. A new approach to enhance oral bioavailability of Silybum Marianum dry extract: Association of mechanochemical activation and spray congealing. *Phytomedicine* **19,** 160–168 (2012).

239. Albertini, B., Di Sabatino, M., Melegari, C. & Passerini, N. Formulation of spray congealed microparticles with self- emulsifying ability for enhanced glibenclamide dissolution performance. *Journal of Microencapsulation* **32,** 181–192 (2015).

240. Passerini, N., Perissutti, B., Moneghini, M., Voinovich, D., Albertini, B., Cavallari, C. & Rodriguez, L. Characterization of Carbamazepine-Gelucire 50/13 Microparticles Prepared by a Spray-congealing Process Using Ultrasounds. *International Journal of Pharmaceutics* **91,** 699–707 (2002).

241. Albertini, B., Passerini, N., Pattarino, F. & Rodriguez, L. New spray congealing atomizer for the microencapsulation of highly concentrated solid and liquid substances. *European Journal of Pharmaceutics and Biopharmaceutics* **69,** 348–357 (2008).

242. Brubach, J. B., Ollivon, M., Jannin, V., Mahler, B., Bourgaux, C., Lesieur, P. & Roy, P. Structural and Thermal Characterization of Mono- and Diacyl Polyoxyethylene Glycol by Infrared Spectroscopy and X-ray Diffraction Coupled to Differential Calorimetry. *The Journal of Physical Chemistry B* **108,** 17721–17729 (2004).